LOAN DOCUMENT

PHOTOGRAPH THIS SHEET

DTIC ACCESSION NUMBER

LEVEL

INVENTORY

0

EPA-600/R-98-037

DOCUMENT IDENTIFICATION

APR 98

DISTRIBUTION STATEMENT A
Approved for Public Release
Distribution Unlimited

DISTRIBUTION STATEMENT

ACCESSION FOR

NTIS GRA&I ☐

DTIC TRAC ☐

UNANNOUNCED ☐

JUSTIFICATION

BY

DISTRIBUTION/

AVAILABILITY CODES

DISTRIBUTION	AVAILABILITY AND/OR SPECIAL	
A-1		

DISTRIBUTION STAMP

DATE ACCESSIONED

DATE RETURNED

19990609 035

DATE RECEIVED IN DTIC

REGISTERED OR CERTIFIED NUMBER

PHOTOGRAPH THIS SHEET AND RETURN TO DTIC-FDAC

HANDLE WITH CARE

DTIC FORM 70A JUN 90

DOCUMENT PROCESSING SHEET

PREVIOUS EDITIONS MAY BE USED UNTIL STOCK IS EXHAUSTED.

LOAN DOCUMENT

United States
Environmental Protection
Agency

EPA-600/R-98-037
April 1998

PP309

EPA

Research and Development

TRANSPORT PROPERTY
MEASUREMENTS OF HFC-236ea

Prepared for

Strategic Environmental Research and
Development Program

Prepared by

National Risk Management
Research Laboratory
Research Triangle Park, NC 27711

FOREWORD

The U.S. Environmental Protection Agency is charged by Congress with protecting the Nation's land, air, and water resources. Under a mandate of national environmental laws, the Agency strives to formulate and implement actions leading to a compatible balance between human activities and the ability of natural systems to support and nurture life. To meet this mandate, EPA's research program is providing data and technical support for solving environmental problems today and building a science knowledge base necessary to manage our ecological resources wisely, understand how pollutants affect our health, and prevent or reduce environmental risks in the future.

The National Risk Management Research Laboratory is the Agency's center for investigation of technological and management approaches for reducing risks from threats to human health and the environment. The focus of the Laboratory's research program is on methods for the prevention and control of pollution to air, land, water, and subsurface resources; protection of water quality in public water systems; remediation of contaminated sites and groundwater; and prevention and control of indoor air pollution. The goal of this research effort is to catalyze development and implementation of innovative, cost-effective environmental technologies; develop scientific and engineering information needed by EPA to support regulatory and policy decisions; and provide technical support and information transfer to ensure effective implementation of environmental regulations and strategies.

This publication has been produced as part of the Laboratory's strategic long-term research plan. It is published and made available by EPA's Office of Research and Development to assist the user community and to link researchers with their clients.

E. Timothy Oppelt, Director
National Risk Management Research Laboratory

EPA REVIEW NOTICE

EPA-600/R-98-037
April 1998

TRANSPORT PROPERTY MEASUREMENTS OF HFC-236ea

by

J.-Y. Lin
M.B. Pate
Iowa State University
Ames, IA 50011

EPA Cooperative Agreement No. CR 820755-01-4

Project Officer:

Theodore G. Brna
U.S. Environmental Protection Agency
National Risk Management Research Laboratory
Air Pollution Prevention and Control Division
Research Triangle Park, NC 27711

Prepared for:

U.S. ENVIRONMENTAL PROTECTION AGENCY
OFFICE OF RESEARCH AND DEVELOPMENT
WASHINGTON, DC 20460

ABSTRACT

CFC-114 has been used as a working refrigerant in shipboard and submarine chiller units. Because CFC-114 is one of the designated phase-out refrigerants, alternatives for CFC-114 in shipboard and submarine chiller units are being sought by the U.S. Navy with the assistance of the Environmental Protection Agency (EPA). Presently, one of the leading candidates to replace CFC-114 is HFC-236ea (hexafluoropropane), which was identified by EPA. This study, one part of the EPA/Navy program, is an evaluation of transport properties of HFC-236ea. Liquid viscosity and thermal conductivity of HFC-236ea are the two main transport properties of interest in this study.

This study used a novel method for simultaneously measuring viscosity and thermal conductivity by using inline property sensors in series with a heat transfer measurement system. For this purpose, a test system with inline viscosity measurements and a single-phase heat transfer test facility was established in the Refrigeration Laboratory at Iowa State University. In this approach, viscosity was measured with an inline torsional oscillation viscometer, while the thermal conductivity was determined from the knowledge of the single-phase heat transfer characteristics of a heated test section.

The resulting viscosity and thermal conductivity of CFC-114 by the current measuring method were compared with ASHRAE (American Society of Heating, Refrigerating and Air-Conditioning Engineers) data with a difference within ±5% in thermal conductivity and ±2% in viscosity. For HFC-236ea, the measured data were compared with predictions of REFPROP, a theoretical package developed by the NIST (National Institute of Standards and Technology), with an average deviation within +15% in thermal conductivity and −5% in viscosity.

The properties of HFC-236ea mixed with a lubricant (Castrol oil SW68) were also investigated. The results showed that the thermal conductivity increased with lubricant concentration in a low temperature range, but decreased with the mixture in a high temperature range. However, there was no significant difference of thermal conductivity of refrigerant/lubricant mixtures for mixtures of various lubricant concentrations at high temperatures. For the viscosity of HFC-236ea/lubricant mixtures, the results showed a significant increase at the higher lubricant concentrations and lower temperature ranges. In addition, the specific heat and density of refrigerant/lubricant mixtures were also determined in this study.

This report was submitted in partial fulfillment of CR 820755-01-4 by Iowa State University under the sponsorship of the U.S. Environmental Protection Agency with funding from the Department of Defense's Strategic Environmental Research and Development Program (SERDP). This report covers a period from October 1992 to May 1995.

CONTENTS

Contents (continued)

Contents (continued)

LIST OF FIGURES

List of Figures (continued)

List of Figures (continued)

LIST OF TABLES

List of Tables (continued)

LIST OF ABBREVIATIONS AND SYMBOLS

ABBREVIATIONS

A	-- total heat transfer area, m^2
A_o	-- outer insulation surface area, m^2
A_i	-- the i-th subsection heat transfer area, m^2
a	-- thermal diffusivity of fluid, m^2/s
a,b	-- exponential power constants for correlation curve-fitting
a^e,b^e	-- exponential power constants for measured data curve-fitting
C	-- coefficient of correlation curve-fitting
C^e	-- coefficient of measured data curve-fitting
CF	-- calibration function
Cp	-- constant pressure specific heat, $kJ/(kg \cdot K)$
C_v	-- constant volume specific heat, $kJ/(kg \cdot K)$
C_w	-- heat capacity of wire, J/k
D	-- inside tube diameter, m
d	-- hard-sphere diameter or thickness of fluid layer, m
f	-- friction factor
F	-- function
g	-- gravity acceleration, m/s^2
Gr	-- Grashof number
$\bar{h}$	-- average heat transfer coefficient inside tube, $W/(m^2 \cdot K)$
h_x	-- local heat transfer coefficient, $W/(m^2 \cdot K)$
$\bar{h}_o$	-- average heat transfer coefficient outside tube, $W/(m^2 \cdot K)$
k	-- thermal conductivity, $W/(m \cdot K)$
$kapp$	-- apparent thermal conductivity, $W/(m \cdot K)$
k_m	-- thermal conductivity of refrigerant and oil mixture, $W/(m \cdot K)$
k_o	-- thermal conductivity of oil, $W/(m \cdot K)$
k_r	-- thermal conductivity of refrigerant, $W/(m \cdot K)$
k_s	-- thermal conductivity of copper tube, $W/(m \cdot K)$
k_a	-- absorption coefficient, m^{-1}

Abbreviations (continued)

L	-- mean free path or tube length, m or cm
l	-- length of cylinders, m
Δl_i	-- length of i-th section, m or cm
M	-- molecular weight, $g/mole$
$\dot{m}$	-- mass flow rate, kg/s
m	-- mass of molecule, g
$\overline{Nu}_D$	-- Nusselt number based on diameter D
n	-- refractive index or number of molecules in a unit volume
P	-- pressure, Pa
P_c	-- critical pressure, Pa
ΔP	-- differential pressure, Pa
P_{vp}	-- vapor pressure, Pa
ΔP_r	-- differential reduced pressure, $(P - P_{vp})/P_c$
Pr	-- Prandtl number
P_r	-- reduced pressure, P/P_c
$\dot{Q},\dot{q}$	-- heat rate, W
$\dot{Q}_t,\dot{Q}_r$	-- total, radiation heat rate, W
$\dot{Q}_{conv}$	-- heat transfer by convection, W
$\dot{Q}_{cond}$	-- heat transfer by conduction, W
q''	-- heat flux, W/m^2
q''_{loss}	-- loss heat flux, W/m^2
q''_{net}	-- net heat flux, W/m^2
q''_{tot}	-- total heat flux, W/m^2
q_{loss}	-- heat loss rate of test section, W
q_{net}	-- net heat input rate to test section, W
q_{tot}	-- total heat loss rate of test section, W
R	-- radiation parameter, $r \cdot k_a$, Equation 4.19
Ra	-- Rayleigh number, $Gr \cdot Pr$
r	-- radius of line source, m
r_i	-- radial distance of point i from a line source, $i = 0, 1, 2, \ldots, m$
Re_D	-- Reynolds number based on diameter D
r_0	-- wire radius, μm
r_1	-- inside radius of tube, m
r_2	-- radius at the point where thermocouple heads are buried, m

Abbreviations (continued)

SS	-- sum of square quantity
T_a	-- ambient temperature, °C
T_b	-- boiling temperature, °C
T_r	-- reduced temperature
T_s	-- static temperature or outer insulation temperature, °C
T_t	-- total temperature, °C
T_{wi}	-- subsection wall temperature, °C
T_0	-- equilibrium temperature of the test fluid, °C
$\overline{T}_i$	-- average inlet temperature of the test section, °C
$\overline{T}_o$	-- average outlet temperature of the test section, °C
$\overline{T}_f$	-- average fluid temperature of the test section, °C
$\overline{T}_s$	-- average outer insulation surface temperature, °C
$\overline{T}_w$	-- average wall temperature of the test section, °C
$\overline{T}_\infty$	-- average ambient temperature, °C
$\Delta\overline{T}_{wf}$	-- average temperature difference between , $\overline{T}_w$ and $\overline{T}_f$, °C
ΔT_{id}	-- ideal temperature rise in transient hot-wire method, °C
ΔT_{wf_i}	-- the i-th subsection local average temperature difference, $\overline{T}_{w_i} - \overline{T}_{f_i}$, °C
ΔT^*	-- dimensionless temperature group in test-tube, $(\overline{T}_o - \overline{T}_i) / (\overline{T}_w - \overline{T}_f)$
$\overline{T}_{i,\infty}$	-- temperature at a radial distance i from a line source, °C
$T_{r,1}$	-- temperature at r_1, °C
$T_{r,2}$	-- temperature at r_2, °C
t or t_i	-- time or time i, sec
Ur_{dk}	-- uncertainty percentage of k by the Dittus-Boelter correlation
Ur_{pk}	-- uncertainty percentage of k by the Petukhov and Popov correlation
Ur_{gk}	-- uncertainty percentage of k by the Gnielinski correlation
V,v	-- velocity, *m/s*
V_s	-- speed of sound, *m/s*
Δx	-- distance between two parallel plates, *m*

Superscripts

e	-- experimental
c	-- correlation
*	-- nondimensional quantity

Subscripts

a	-- air or absorption
app	-- apparent quantity
D	-- diameter based
f	-- fluid
i	-- inside or inlet
net	-- net quantity
o	-- outside or outlet
∞	-- uniform stream
0	-- equilibrium quantity
r	-- radiation or reduced property
s	-- surface
sat	-- saturation state
t or tot	-- total quantity
w	-- wall

Greek Symbols

α	-- volumetric thermal expansion coefficient of fluid, K^{-1}, or thermal diffusivity, m^2/s
ε	-- emissivity of surface
ε_i	-- emissivity of surface i, i = 1,2, ... etc.
$\varepsilon_{1,2}$	-- emissivity of surface 1 to 2
μ	-- viscosity, $N \cdot s/m^2$ or cp (centipoises = 10^{-3} $N \cdot s/m^2$)
ρ	-- density, kg/m^3
σ_s	-- Stefan-Boltzmann constant, 5.6697 x 10^{-8}, W/m^2K^4
ϕ	-- nondimensional apparent thermal conductivity group, Equation 4.18
ω	-- acentric factor

ACKNOWLEDGMENTS

This work was sponsored by the United States Environmental Protection Agency (EPA) under cooperative agreement CR-820755-01-4 with funding provided by the Strategic Environmental Research and Development Program, a joint program of the Department of Defense, the Department of Energy, and the Environmental Protection Agency. The United States Navy cooperated with the EPA in the program seeking a non-ozone-depleting alternative to CFC-114 for its shipboard chillers. The authors would like to thank the EPA and the Navy for their assistance and support of this work. Special thanks are given to the project officer, Theodore G. Brna, with the EPA.

The authors also would like to thank the Heat Transfer Laboratory and Department of Mechanical Engineering of Iowa State University for their support and provision of resources. Finally, the assistance of the co-workers in the Heat Transfer Laboratory is also greatly appreciated.

CHAPTER 1

INTRODUCTION

Chlorofluorocarbon refrigerants (CFCs) have been widely used as working fluids in refrigeration and air-conditioning applications. In the past few decades, CFC refrigerants have been used as refrigerants due to their excellent thermal performance, stable chemical properties, and low toxicity. However, because of the problems with CFCs that were exposed in the early 1970's, CFC refrigerant production ends on December 31, 1995 under the Montreal protocol and its amendments. In addition, through usage regulation and prohibition, the CFC refrigerants are to be totally phased-out in the next few years [1,2]. Since the CFC problems surfaced, people have sought CFC alternatives to take the place of existing refrigerants. So far, several alternatives have been found for some banned refrigerants, such as HFC-134a for CFC-12 and HCFC-123 for CFC-11.

A cooperative project has been initiated by the United States Navy and the Environmental Protection Agency (EPA). The U.S. Navy currently uses CFC-114 ($CClF_2CClF_2$) as the working refrigerant in shipboard chiller units. Because CFC-114 performs well in shipboard chillers, which use sea water as the heat sink fluid on the condenser side, CFC-114 has served as a good working fluid in the past. However, CFC-114 is one of the banned refrigerants. With the mandatory phase-out program of CFCs as stipulated by the Montreal Protocol, it is an urgent task for the U.S. Navy under national policy to find a new refrigerant alternative which is non-ozone depleting and has acceptable thermal characteristics for replacing CFC-114. Some points of concern for the Navy in switching refrigerant to an acceptable alternative are: 1. safety (non-flammable, non-toxic) in application; and 2. easy to exchange with the present refrigerant (CFC-114) in the field with only minor equipment modifications.

HFC-236ea (CF_3CFHCF_2H), a new refrigerant, has already been selected as one of the candidates for CFC-114 alternatives. There are several reasons that this refrigerant shows promise to replace CFC-114. Firstly, the thermophysical properties were investigated and found to be similar to those of CFC-114 [3,4]. Secondly, according to simulation results, the performance of HFC-236ea is similar in the performance to CFC-114. Thus, it is a retrofit candidate. This latter characteristic is attractive for the shipboard or submarine chiller's refrigerant transition. Other preliminary test results, such as flammability, material compatibility, and toxicity, are also favorable. The EPA, which identified HFC-236 isomers as promising non-ozone depleting refrigerants, has been cooperating with the Navy in evaluating HFC-236ea (and HFC-236fa as well) as an alternative to CFC-114 for shipboard chillers. The EPA effort has included property measurements, performance modeling, and small-scale engineering tests.

PROPERTIES OF INTEREST

Some of the general steps for refrigerant replacements include property evaluations, heat transfer characterization studies, design evaluation for retrofit application, and field tests. The property evaluations of interest include thermodynamic properties, solubility and miscibility characteristics, and transport properties. Some of the properties, such as viscosity, thermal conductivity, and specific heat, are important properties in any heat transfer study.

Today these properties are known for numerous fluids; however, there are still potentially useful fluids whose properties need to be measured. Among these fluids are new refrigerants, refrigerant mixtures, and the refrigerant/lubricant mixtures. This study focuses on the transport property evaluations of the alternative refrigerant HFC-236ea. The transport properties of interest in this study include thermal conductivity and viscosity of pure HFC-236ea and mixtures of HFC-236ea with lubricant.

LUBRICANTS OF INTEREST

Lubricants are required for the proper operation of the mechanical compressor in refrigeration systems. However, the use of lubricants will cause changes in a refrigerant's properties, such as viscosity, miscibility, and solubility, and eventually affect heat transfer characteristics [5]. Finally, mixing lubricants with refrigerants could affect material compatibilities [6].

The mineral, naphthenic, paraffinic, and synthetic lubricants usually used with CFC refrigerants are not miscible in the HFC refrigerants [7,8]. Several lubricant alternatives are presently considered as suitable with HFCs. These lubricants, which include polyol ester lubricants (POEs), alkylbenzenes, and polyalkylene glycols (PAGs), are currently being tested by compressor manufacturers and lubricant suppliers for a wide range of characteristics, such as miscibility, lubricity, and material compatibility. Recent research shows that the POEs and PAGs are more favorable, due to good miscibility and stability when subjected to a wide range of operating conditions, for new HFC refrigerants such as HFC-236ea [9]. According to the solubility and miscibility test results, Icematic Castrol SW68 lubricant was shown to be compatible with HFC-236ea [9] and was selected for property measurements in this study. Various concentrations of lubricant which cover a possible range of concentrations in a vapor compression refrigeration system were mixed with HFC-236ea. Measurements were performed on the refrigerant/ lubricant mixtures in order to understand the effect of lubricant concentration on selected properties.

OBJECTIVES

Refrigerant properties, such as thermodynamic properties and transport properties, provide important information as to the acceptability of a refrigerant for use as a working fluid in a refrigeration cycle. Thermal conductivity and viscosity are especially important in any heat transfer analysis as applied to refrigeration cycle

performance studies. Because HFC-236ea is a new refrigerant, there are very limited property data published for this potential refrigerant. As a result, the objectives of this research focus on measuring the transport properties for HFC-236ea. The transport properties of interest are liquid thermal conductivity and viscosity. The lubricant's effects on the transport properties of HFC-236ea were also investigated.

METHODOLOGY

Because of the limitation in accurately predicting transport properties (such as thermal conductivity) by using theory, experimental measurement is the only reliable method of obtaining viscosity and thermal conductivity. There are a number of ways to measure viscosity such as: the capillary viscometer [10,11], the vibrating principle viscometer [12], and the torsional oscillation viscometer [13-16]. For thermal conductivity, the vertical coaxial cylinder method [17,18], transient hot-wire method [19-23], and transient hot-strip method [24] are the usual measurement methods employed.

As can be seen from the above list of methods, each property is measured by using a method independent of the other properties. In this study, a new approach is adopted for simultaneously measuring these properties [25,26]. This approach uses an inline viscometer and a heat transfer test section to dynamically measure viscosity and thermal conductivity at the same time. Viscosity is measured by a torsional oscillation inline viscometer, while thermal conductivity is measured from knowledge of the single-phase heat transfer characteristics of a heated test section. In addition, by placing a mass flow meter and densimeter in series with the viscometer and heat transfer test section, density and specific heat can also be determined.

RESEARCH PROGRAM

The main goal of this study is to measure transport properties of HFC-236ea with and without lubricant (Castrol oil SW68) by using a new methodology [25,26]. Measured data for pure refrigerant were compared with other theoretical data sources (e.g., REFPROP [27]). The test facility was calibrated by using the well-known properties of HCFC-22, CFC-12, and CFC-113, and the methodology was verified by using the properties of CFC-114.

SCOPE

The scope of this study was as follows:

- Design and construct a test rig for measuring transport properties, such as thermal conductivity by using an approach based on the knowledge of single-phase heat transfer.
- Install a viscometer in series with a heat transfer test section for simultaneously measuring viscosity and thermal conductivity.

- Calibrate heat transfer and heat loss characteristics of the test section by using refrigerants of known properties.
- Verify the accuracy of the viscometer with fluids of known viscosity.
- Measure the viscosity and thermal conductivity of CFC-114 and compare them with the ASHRAE (American Society of Heating, Refrigerating and Air-Conditioning Engineers) standard handbook data.
- Measure the viscosity and thermal conductivity of HFC-236ea and compare them with theoretically predicted data (i.e., REFPROP).
- Measure the viscosity and thermal conductivity of HFC-236ea with lubricant.
- Develop prediction equations from measured properties.

In this study, density (ρ) and specific heat (C_p) of the refrigerants of interest are also measured and discussed.

CHAPTER 2

CONCLUSIONS

This study uses a new approach for simultaneously measuring several thermophysical properties, such as thermal conductivity, viscosity, specific heat, and density. This approach uses single-phase in-tube heat transfer knowledge to obtain thermal conductivity. Viscosity is measured by a viscometer placed in-line with the heat transfer test section. There are two approaches; Approach 1: the Nusselt number (Nu) method and Approach 2: the Prandtl number (Pr) method. The uncertainty analysis was presented in this study. Approach 2 seems to have less uncertainty than Approach 1 and T_i and ΔT do not significantly affect the uncertainties. However, ΔT_{wf} is a significant parameter that affects the uncertainties.

In Approach 1, the determination of a calibration function (CF) by experiments using fluids with known properties is shown to be important for accurate thermal conductivity measurements. Three different Nusselt number correlations were used for calculating thermal conductivity in this study, and they have been examined and discussed herein. Four refrigerants, HCFC-22, CFC-12, CFC-113, and CFC-114, were used for calibration and verification purposes. These refrigerants cover the Pr range from 3 to 9 and Re_D range from 8,000 to 180,000. Based on the calibration results, the CF functions were found for three different correlations which were examined in this study. In Approach 2, bypassing the Nusselt number, the thermal conductivity was found from Pr which is directly related to Re_D and non-dimensional temperature, ΔT^*. This approach was shown to be more accurate and convenient to use because less variables were involved. A theoretical uncertainty analysis also showed this approach to have less uncertainty than Approach 1. The measured results were also compared and discussed for both approaches, and consistency was shown between them.

Viscosity was measured by a torsional oscillation inline viscometer. The accuracy of the viscosity measurement was verified with CFC-113, CFC-12, and pure water, and shown to be within ±2% when compared with the ASHRAE data. The measured properties included specific heat, density, viscosity, and thermal conductivity. They were also examined for CFC-114, compared with ASHRAE data, and shown to be matched closely within ±5% for thermal conductivity, ±3% for specific heat, and within ±1% for density. For HFC-236ea property measurements, REFPROP-4.0 data were used as a comparison with the measured data. The deviations of measured properties from REFPROP-4.0 are +4.8% for specific heat, -5.0% for viscosity, ±1% for density, and +15% for thermal conductivity.

A lubricant (Castrol oil SW68) was selected to mix with HFC-236ea. Properties were measured for five lubricant concentrations over a temperature range of -10 to 50°C. Thermal conductivity effects due to the lubricant seemed to be more significant at low temperatures than at high temperatures. For example, at a low temperature (-10°C) the thermal conductivity of the mixture was found to increase by 40% as the mixture concentration changed from 0.0% oil concentration to 7.4%. At a high temperature (50°C), this decrease of thermal conductivity was found to be less than 15% at a for oil concentration changing from 0% to 7.4%. Viscosity was obviously affected by lubricant concentration, especially at a low temperature and high lubricant concentration at the low temperature. It increased over 50% as the lubricant concentration went from 0% to 7.4% at the low temperature while it increased nearly 100% at the high temperature. Curve fit equations for both one variable (temperature) and two variables (temperature and lubricant concentration) were provided for convenient use. Other properties, such as density, specific heat, thermal diffusivity, and Prandtl number, were also calculated.

Transport properties are important for the evaluation of refrigerant alternatives. The method developed in this study shows that several properties can be quickly and simultaneously measured. Today refrigerant alternatives are being screened and tested for application. The methods developed in this study can provide a quick way for obtaining these properties.

CHAPTER 3

RECOMMENDATIONS

The following are suggestions for further improvement of the current study and possible extended future research using the current test facility and methodology:

1. The Prandtl number (*Pr*) and Reynolds number (*Re*) ranges of calibration can be further extended by testing more fluids of known properties to extend the ranges of application for the adopted methodology in this study so that wider range of properties can be further evaluated.
2. The accuracy of the thermal conductivity and viscosity measurements can be further improved by using more accurate sensors.
3. Property correlations for HFC-236ea with lubricant can be further developed if more data are taken and accumulated.
4. Although properties are the primary interest in this study, the single-phase heat transfer and flow characteristics of lubricant/refrigerant mixtures can be further investigated by the current test facility.
5. An obvious extension of this study would be to use other potential lubricants mixed with HFC-236ea, subjected to a wide range of temperatures. A study of partly-miscible lubricant-refrigerant mixtures would be another interesting study.

CHAPTER 4

REVIEW OF EXPERIMENTAL METHODS FOR THE DETERMINATION OF TRANSPORT PROPERTIES

This chapter will review the theory surrounding transport properties and the experimental methods used to determine transport properties. Several traditional methods of measuring transport properties will be reviewed. Existing error sources of each method will also be discussed. Finally, the advantages and disadvantages of each traditional method will also be compared.

REVIEW OF THEORY OF TRANSPORT PROPERTIES

The elementary model of a molecule assumes that the shape of the molecule is like a rigid sphere of diameter, d. When molecules move randomly at a mean velocity, v, they collide and transfer momentum or energy assuming velocity or temperature gradients exist. These momentum or energy transfers will cause an exchange of momentum or energy flux as the molecules try to reach an equilibrium status. The momentum or energy flux was found to be proportional to the velocity or temperature gradient. The corresponding constants of proportionality for the momentum and energy flux equations are known as transport properties. Viscosity is associated with the velocity gradient while thermal conductivity is proportional to the temperature gradient. These coefficients are also proportional to $vL/3$ according to kinetic theory [28-31], where v is the average molecular speed and L is the mean free path between molecular collisions. The relations between these properties are usually described by the following equations for low density gas:

$$Momentum\ flux = -\mu\frac{dv}{dz} = -\frac{vL}{3}nm\frac{dv}{dz} \tag{4.1}$$

$$Energy\ flux = -k\frac{dT}{dz} = -\frac{vL}{3}C_v n\frac{dT}{dz} \tag{4.2}$$

where n is the number of molecules in a unit volume, m is the mass of the molecule, and C_v is the specific heat under constant volume. The term nmv is often called the momentum density while $C_v nT$ is the energy density. The above equations define the transport properties in the momentum and energy flux equations, which are

viscosity, μ, and thermal conductivity, k, respectively. However, if the average speed is proportional to $(RT/M)^{1/2}$ and the mean free path to $(nd^2)^{-1}$, where R is the gas constant, M is the molecular weight, and T is the temperature, then the viscosity and thermal conductivity can be rewritten as:

$$\mu = \frac{m\rho vL}{3} = (constant)\frac{T^{1/2}M^{1/2}}{d^2} \tag{4.3}$$

$$k = \frac{vLC_v n}{3} = (constant)\frac{T^{1/2}}{M^{1/2}d^2} \tag{4.4}$$

where ρ is the mass density. Another theoretical equation for the thermal conductivity of liquids, which was also based on a rigid sphere model, was proposed by Bridgman in 1923 and later modified by Powell et al. [31]. The resulting equation, which has been used for pure substances, is:

$$k = 2.8\left(\frac{N}{V}\right)^{2/3}\sigma Vs \tag{4.5}$$

where N is Avogadro's number, V is the molar volume, σ is the Boltzmann's constant, and Vs is the speed of sound.

The above equations are based on ideal models which neglect an interaction force that might exist between molecules. As a result, a rigid sphere model which neglects forces between molecules is no longer acceptable and must be modified. For different molecules, the modification will be different.

Although a number of prediction rules were developed, there is still no universal principle which can be used to cover every group of fluids, especially when applied to mixtures. Baroncini et al. (1981) developed a general correlation for organic liquid thermal conductivity [32]. Although it provided useful information for some existing materials, it still needs further study for new fluids or refrigerant mixtures. Kandlikar et al. (1975) also published a paper to theoretically predict viscosity and thermal conductivity for HCFC-22 and CFC-12 mixtures [33]. Later, Levy (1981) used a modified Maxwell-Eucken equation to calculate thermal conductivity for two component solution mixtures [34]. Ely and Hanley (1983) used a corresponding state method to predict the viscosity and thermal conductivity of mixtures [35].

Although the above studies provide useful information, they still have some limitations in actual use, especially for multi-component mixtures. This is because the interaction force between molecules is still not fully understood, and some correlations need semi-empirical data from experiments to modify the models. However, one of the mixing rules has been widely used in past studies [36,37]. This rule is described by the equation shown below:

$$k_m = k_r(1-C) + k_o C - 0.72\,(k_o - k_r)(1-C)\,C \tag{4.6}$$

where C represents the lubricant concentration.

Lin and Pate (1992) used thermodynamic property data and the speed of sound of the mixture to predict the thermal conductivity of refrigerant mixtures by using Bridgman and Powell's equation (Equation 4.5) to develop a mixing rule [38]. However, this method needs modified coefficients which requires calibrations and numerous tests with known fluid properties.

Although some theoretical prediction methods and limited experimental data for obtaining properties of new pure refrigerants and refrigerant mixtures have been published [39-43], there are still very limited experimental data for verification, especially for lubricant/refrigerant mixtures. Therefore, experimental methods for obtaining the required data become vital in the current CFC transition.

EXPERIMENTAL METHODS FOR THE DETERMINATION OF THERMAL CONDUCTIVITY

Thermal conductivity can be measured by experimental methods [44,45] by using Fourier's law. The methods developed for measuring thermal conductivity can be divided into the following two categories: steady-state methods and unsteady-state methods. The following is a brief review of these methods.

Steady-State Methods

Steady-state methods differ primarily in the different geometries used in the apparatus. In addition, all steady-state methods require careful experimentation to minimize errors for heat losses and to prevent the onset of any convective motion in the fluid.

1. Horizontal Flat-Plate Method--

In this method, the heat passes through a layer of fluid located between two circular horizontal metal plates. With a suitable design along with radiation and convection corrections in the measurement, the thermal conductivity accuracy can be optimized. This method measures the temperature difference across the fluid layer and the heat flow rate with known geometric dimensions. The accuracy of thermal conductivity measurement by using this method depends on the precision of the temperature measurement and the accuracy of the geometric dimensions of the cell.

2. The Vertical Coaxial Cylinder Method--

In this method, two coaxial, vertical cylinders form a test cell. Fluid fills the annulus of the cylinders, and heat is generated in the center of the inner cylinder. By measuring the heat passing through the test fluid and the temperatures at the inner and outer surfaces of the two cylinders, the thermal conductivity can be determined. Again, the experimental uncertainty needs to be minimized for improving accuracy.

3. Hot-Wire Method–

The hot-wire method is in principle a special case of the coaxial cylinder method in which the inner cylinder is replaced by a thin wire. The wire not only performs as a heater, but also performs as an internal thermometer. The temperature of the outer surface of the fluid-filled annulus can be evaluated from the dimensions heat flow rate, thermal conductivity of test fluid, and the outer surface temperature of the outer cylinder. The heat flow generated in the wire is determined from the electric power added to wire. Correction for the heat loss is required for an accurate heat flow determination. The thermal conductivity is determined from the measured quantities and the dimensions of the cell.

4. Concentric Sphere Method–

In this method, two concentric spheres make up the test cell. The test fluid is contained in the volume between the spheres. A heater located in the cavity of the inner sphere generates heat that is conducted radially outward to a concentric spherical shell. Temperatures on the inner and outer surfaces of the spheres are measured by sensors embedded in the surface walls. With known dimensions, the heat generated in the inner sphere, and temperature measurements, the thermal conductivity can be obtained.

Unsteady Methods

The establishment of steady state in an apparatus of considerable mass is a slow process, and measurements may be rather time consuming. It is therefore natural to explore the possibility of employing transient techniques in which the same information may be obtained while the fluid system is subjected for a short time to the influence of a transient temperature field.

1. Continuous Line Source--

A transient heat transfer characteristic of a line source with an infinite length and a constant energy generation in an extended isotropic fluid can be used to determine the fluid thermal conductivity. From the measurement of the temperatures at a fixed radial distance at two different times, the thermal conductivity can be determined by the following equation:

$$k = \frac{Q}{4\pi} \cdot \frac{ln\,(t_2/t_1)}{(T_{2,\infty} - T_{1,\infty})} \tag{4.7}$$

where Q is the total heat added to the line source between times t_1 and t_2 , and $T_{1,\infty}$ and $T_{2,\infty}$ are the measured fluid temperatures at a fixed radial distance from the heat-dissipated line source at two different times, t_1 and t_2, respectively. A plot of temperature versus the natural logarithm of time should result in a straight line. The

unique feature of the solution from this method is that it yields thermal conductivity, k, directly. Recently, the transient hot-wire method has been applied to the measurement of liquid thermal conductivity[46-50]. This method uses a very thin wire as a line source in which heat is generated electrically. The thermal conductivity, k, of the test liquid is determined by measuring heat input, temperature rise of the wire, and the time of heating. The equation [51,52] is given as follows:

$$\Delta T_{id} = \frac{q}{4\pi k} ln \left[\frac{4at}{r_0^2 C} \right] \tag{4.8}$$

in which q is the heat input per unit length of the wire, k is the liquid thermal conductivity surrounding the wire, t is the time of heating, r_0 the wire radius, and C a numerical constant ($C = e^{\gamma}$), $\gamma = 0.5772157\cdots$, Euler's constant). The symbol a represents the thermal diffusivity of the liquid surrounding the wires.

2. Cylindrical, Spherical, and Plane Sources--

A different approach from that used in the transient hot-wire method is based on a cylindrical, spherical, or plane source taking the place of the line source (wire). In these methods, heat is generated electrically for a short period of time in a relatively large solid body of a simple geometry (cylinder, sphere, plane). After the temperature of this body has been raised by a few degrees above that of the heat receiving body, which is assumed to remain at a constant temperature in its isothermal surroundings, heating is discontinued. Heat is now conducted through the narrow, fluid-filled gap between the two geometrically similar bodies and the change of temperature with time is recorded. The thermal conductivity is then calculated using the equations which describe the transient heat transfer characteristics for different geometries.

ERROR SOURCES FOR EXPERIMENTAL METHODS FOR THE DETERMINATION OF THERMAL CONDUCTIVITY

Despite precautions and sophistication in the test system's design and of the sensors, it is impossible to completely eliminate all sources of error for the measured quantities. There are several error sources which exist in the methods mentioned above; however, two sources of error, namely radiation and convection, are the major contributors affecting the energy transfer through the fluid film.

Radiation Effect in Parallel Plates or Cylinders

Thermal radiation in partly transparent fluids affects the heat transfer in two ways: first, the energy is directly absorbed and emitted by the test fluids, and second, the energy is absorbed and emitted by the walls or

surfaces of the test cell or gap. Thus, the radiation heat transfer affects the conduction heat exchange determined from Fourier's Law which is the basis for the thermal conductivity measurement methodology. Since Fourier's Law does not account for radiation, the thermal conductivity measurement needs to be corrected for radiation heat transfer. The temperature distribution depends not only on the geometry of the cell system, but also on the temperature of the surfaces surrounding the test fluid.

Leidenfrost analyzed the thermal radiation effects on the thermal conductivity measurement in both vertical and horizontal parallel plate cells [53]. Leidenfrost calculated the ratio of the heat transferred by radiation to the total heat transfer and found that this ratio was strongly related to emissivity. Table 4.1 was obtained from the calculated results shown in Figure 10 of Leidenfrost's publication [53].

TABLE 4.1. RADIANT PERCENTAGE BETWEEN PARALLEL WALLS

Temperature, K	Emissivity, $\varepsilon = 0.1$	Emissivity, $\varepsilon = 1.0$
273	0.1%	1.0%
383	0.2%	2.0%
483	0.5%	4.1%
600	1.0%	8.8%
example for toluene at $\Delta T = 5$ K		

From the radiant heat transfer percentages shown in Table 4.1, it was noted that the radiation heat flow affects, the heat conduction which, in turn, affects the accuracy of the thermal conductivity measurement. The higher the temperature and emissivity, the larger the radiant heat exchange. At a temperature of 600 K for toluene, the radiation heat transfer ratio can even reach 8.8% if black bodies are used. This result suggests that if no corrections for radiant heat exchange are applied to the measurements, then the values of thermal conductivity will be too high by the same percentages.

As a further step in understanding how radiation affects conduction in flat plate and concentric cylinder cells, a theoretical analysis is performed below. The situation is one in which the test fluid is completely transparent to radiation of all wavelengths. For this situation, the heat transferred by radiation can be calculated as follows.

1. Parallel Flat Plate Case--

The equations governing the radiation and conduction heat transfer between two parallel flat plates are given as:

$$\dot{Q}_r = \varepsilon_{1,2}\sigma_s A \left(T_1^4 - T_2^4\right) \tag{4.9}$$

where $\varepsilon_{1,2}$ is the radiation interchange factor, σ_s is the Stefan-Boltzmann constant, A is the heat transfer area, and T_1, T_2 represent the surface temperatures of these two flat plates. For two parallel walls, $\varepsilon_{1,2}$ is given as:

$$\frac{1}{\varepsilon_{1,2}} = \frac{1}{\varepsilon_1} + \frac{1}{\varepsilon_2} - 1 \tag{4.10}$$

However, the total heat transferred by conduction, which is the quantity used to calculate thermal conductivity in this apparatus, is based on Fourier's Law and expressed as:

$$\dot{Q}_t = \frac{kA\,(T_1 - T_2)}{\Delta x} \tag{4.11}$$

where k is thermal conductivity of test fluid and Δx is the normal distance between emitter and receiver plates or the distance of test cell gap. The ratio of the radiation heat transfer to the total heat transfer is then calculated by dividing these two equations, which is:

$$\frac{\dot{Q}_r}{\dot{Q}_t} = \frac{\sigma_s \left(T_1^4 - T_2^4\right) \Delta x}{K\,(T_1 - T_2)\left(\frac{1}{\varepsilon_1} + \frac{1}{\varepsilon_2} - 1\right)} \tag{4.12}$$

It is of interest to calculate this ratio in order to determinate the significance of the radiation heat transfer in relation to the total heat transfer. For this example CFC-114 was selected as the test fluid. Figure 4.1 plots the radiant heat transfer ratio versus temperature for this case. As shown in the figure, the radiation heat transfer is quite significant at high temperatures and high emissivities of the plates. This ratio, for example, can even reach +15%. In other words, the thermal conductivity measured under this situation will be 15% higher than the true value. Viskanta and Grosh (1962) calculated the simultaneous conduction and radiation in an absorbing medium between parallel flat plates [54]. The calculated results showed that the radiation effect, which depend on the distance between the two plates, was of the same order of magnitude as the conduction.

2. Concentric Cylinder Case--

The equation which governs the radiation heat transfer in between two long concentric cylinders is given as:

$$\dot{Q}_r = \varepsilon_{1,2}\sigma_s 2\pi l \left(T_1^4 - T_2^4\right) \tag{4.13}$$

where, again, $\varepsilon_{1,2}$ is the radiation interchange factor, σ_s is the Stefan-Boltzmann constant, l is the length of each cylinder, r_1 is the center radius of the inner cylinder, and r_2 is the inner radius of the outer cylinder ($r_1 < r_2$). For this case, $\varepsilon_{1,2}$ is given as:

$$\frac{1}{\varepsilon_{1,2}} = \frac{1}{\varepsilon_1} + \frac{r_1}{r_2}\left(\frac{1}{\varepsilon_2} - 1\right) \tag{4.14}$$

In this case, the total heat transferred by conduction is expressed as:

$$\dot{Q}_t = \frac{2\pi k l\,(T_1 - T_2)}{ln\left(\frac{r_2}{r_1}\right)} \tag{4.15}$$

The ratio of radiation to the total conduction heat transfer is then calculated by dividing these two equations (Equations 4.13 and 4.15), resulting in

$$\frac{\dot{Q}_r}{\dot{Q}_t} = \frac{\sigma_s r_1 \left(T_1^4 - T_2^4\right) ln\,(r_2 / r_1)}{k\,(T_1 - T_2)\left[\frac{1}{\varepsilon_1} + \frac{r_1}{r_2}\left(\frac{1}{\varepsilon_2} - 1\right)\right]} \tag{4.16}$$

This ratio was calculated by using CFC-114 as a test fluid. Figure 4.2 shows the percentage of the ratio of radiant heat transfer to total heat transfer versus temperature for CFC-114 in the concentric cylinder case. Compared with the parallel flat plate case shown in Figure 4.1, the radiant ratio for the concentric cylinder case is quite similar. Again, the radiant heat transfer is quite significant at high emissivities and high temperatures.

In summary, the errors in thermal conductivity measurements introduced by radiant heat exchange in both parallel flat plate and concentric cylinder cells should not be assumed to be negligibly small until verified. In order to achieve the desired accuracy, corrections should be made and the material selected for the test cell walls should be appropriate so that the errors can be minimized.

Radiation Effect on Hot-Wire Cell

In the transient hot-wire method, the essential relationship is that of the temperature rise of the thin wire immersed in the fluid as a function of time following the stepwise initiation of a heat flux within it. There have been a number of attempts to carry out an analysis of the process of simultaneous conduction and radiation in an absorbing fluid for the transient hot-wire instrument [55-57]. Menashe and Wakeham analyzed the combined radiation and conduction heat exchange in a transient hot-wire cell in 1982 [56]. They theoretically calculated the apparent thermal conductivity measured by this method and drew the conclusion that the apparent thermal conductivity ratio, *kapp / k*, is proportional to the equilibrium temperature, T_0,

$$kapp / k \propto T_0^3 \tag{4.17}$$

They also calculated the *kapp / k* for n-undecane at 348 K and found that the apparent thermal conductivity of the fluid was as much as 2.5% greater than the true value.

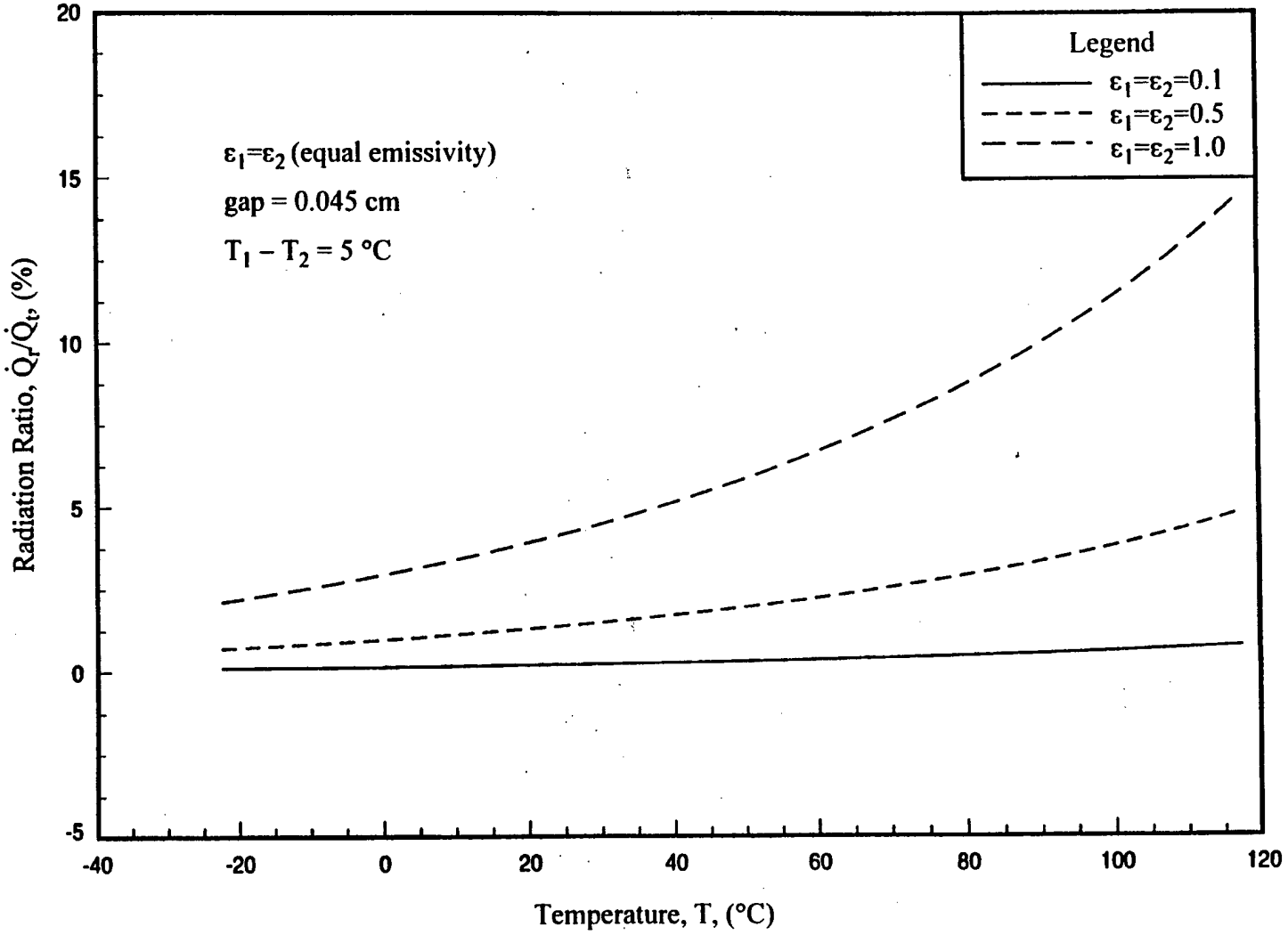

Figure 4.1: Radiant heat transfer percentage in two parallel flat plates using CFC-114 as the test fluid.

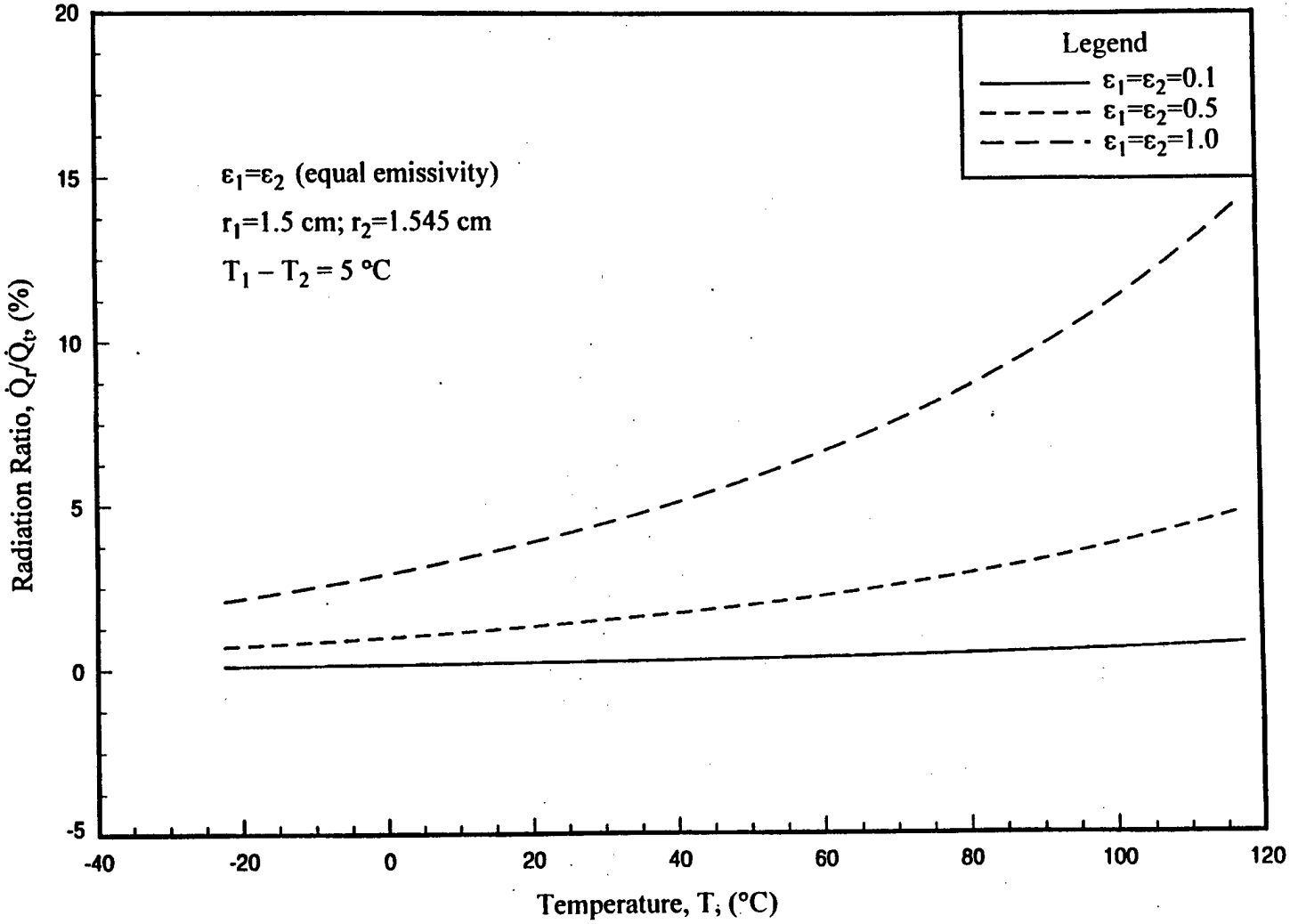

Figure 4.2: Radiant heat transfer percentage in concentric cylinder cell using CFC-114 as the test fluid.

Saito and Venart analyzed the radiation effect on a transient line source measurement by a theoretical approach [57]. They analyzed the ratio of apparent thermal conductivity (radiation involved) to true thermal conductivity and found it was a function of radiation properties such as emissivity and refractivity plus equilibrium temperature and geometric parameters, such as the radius of the line source. The results are tabulated in Table 4.2 (values were cited from Figure 6 of Reference [57]).

TABLE 4.2: ϕ VALUES[a] FOR APPARENT THERMAL CONDUCTIVITY RATIO

ε	R = 0.01	R = 0.075	R = 0.001
ε = 0.2	2.750	2.125	0.750
ε = 0.4	3.188	2.500	1.250
ε = 0.6	3.625	3.000	1.750
ε = 0.8	4.063	3.500	2.313
ε = 1.0	4.500	4.000	2.813

ϕ is defined in Equation 4.18 and R is defined in Equation 4.19
[a] values were cited from Figure 6 of Reference [57]

In Table 4.2, the non-dimensional group (ϕ) as a function of apparent thermal conductivity ratio is defined as:

$$\phi = \left(kapp / k - 1 \right) \frac{\pi k}{16 r_1 \sigma_s n^2 T_0^3} \tag{4.18}$$

$$R = r_1 \cdot k_a \tag{4.19}$$

where r_1 is the radius of line source, n is the index of refraction, and k_a is absorption coefficient, m^{-1}.

Table 4.2 shows the ϕ values (read from Figure 6 of Ref. [57]) for various ε and R. Because ϕ is proportional to *kapp / k*, an increasing tendency of *kapp / k* with larger ε and R was obtained from Table 4.2. These results, as expected, have the same trends for both the parallel flat plate and the concentric cylinder arrangements.

In Equation 4.18, the equilibrium temperature, T_0, is another quantity that affects the radiation strength. A plot of *kapp / k* versus T_0 is interesting to view. Applying Equation 4.18 to a test condition, the *kapp / k* ratio can be shown. Figures 4.3 through 4.5 show plots of *kapp / k* versus k for various T_0 values at ε = 0.2, ε = 0.6, and ε = 1.0, respectively.

As shown in these figures, the ratio of *kapp / k* generally increases with increasing temperature, T_0, at the smaller k values. In addition, in the lower thermal conductivity range, this ratio becomes more significant than it is at the higher thermal conductivity ranges. Figure 4.6 shows the *kapp / k* versus k at a high temperature of T_0 = 120°C for various emissivities. As expected in this case of higher emissivity, radiation heat transfer contributes more

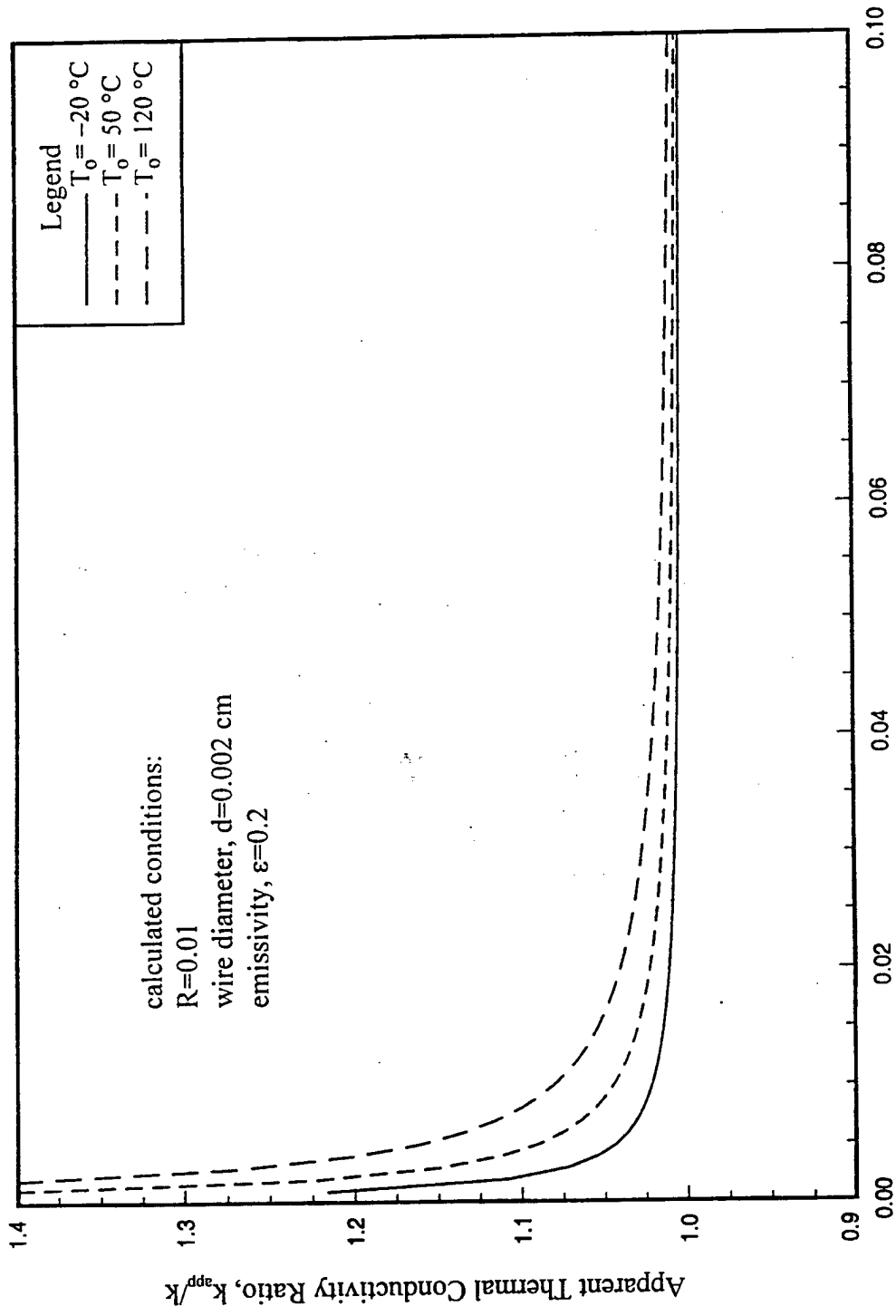

Figure 4.3: *kapp / k* ratio as a function of *k* for various temperatures at ε = 0.2 case.

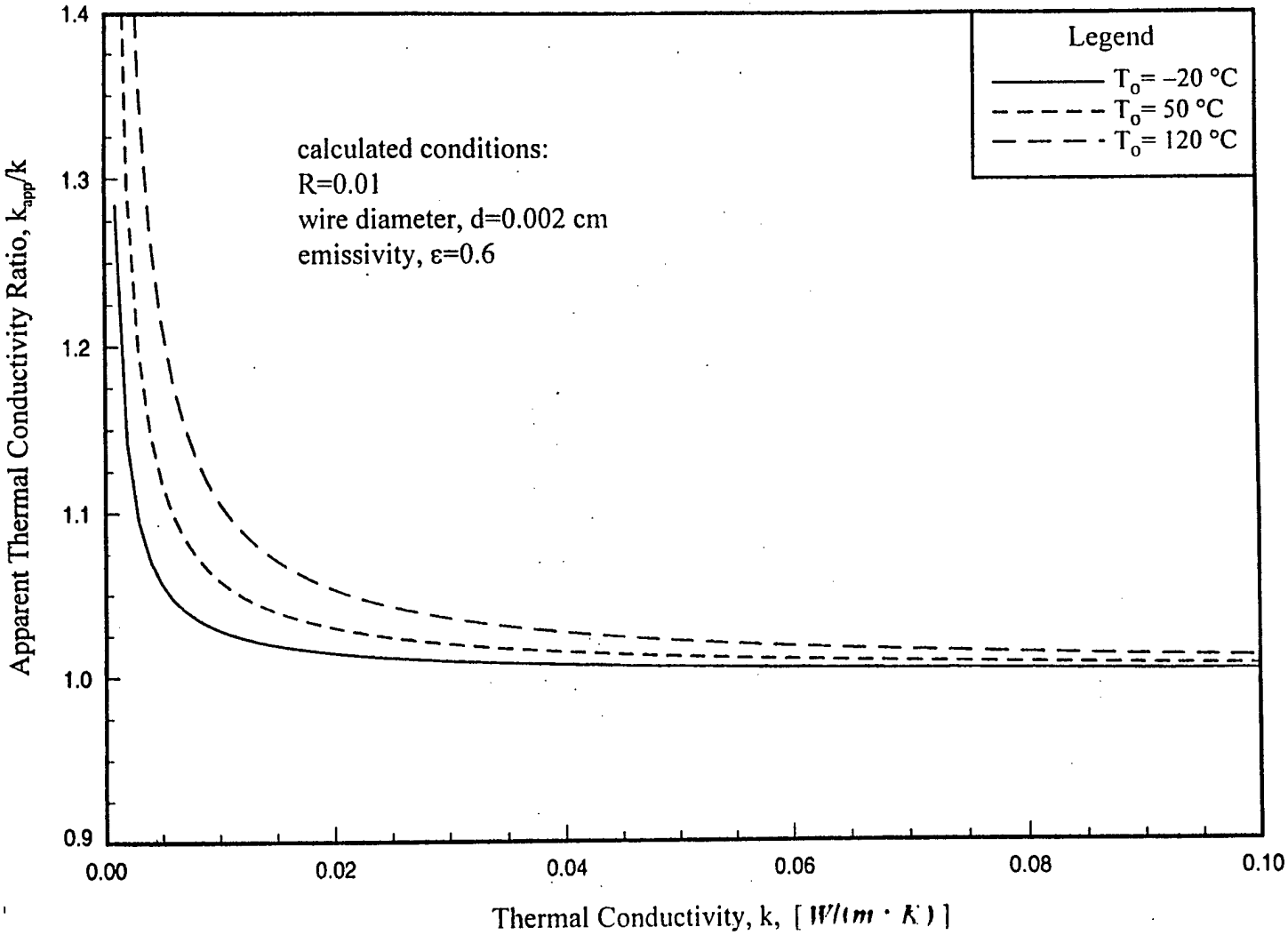

Figure 4.4: ***kapp / k*** **ratio as a function of** ***k*** **for various temperatures at ε = 0.6 case.**

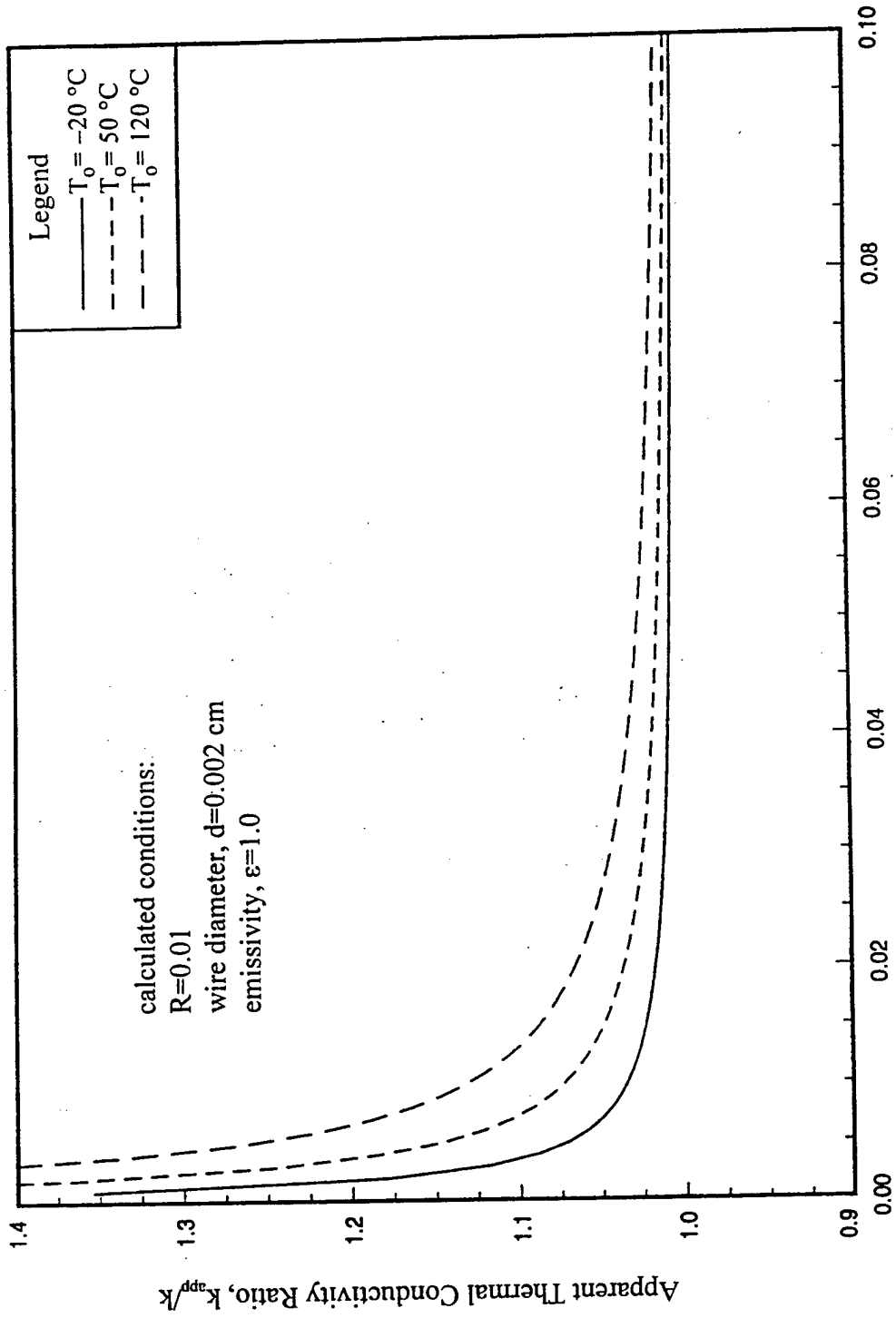

Figure 4.5: ***kapp / k*** **ratio as a function of *k* for various temperatures at ε = 1.0 case.**

to the total conduction heat transfer so that the ratio, *kapp / k*, becomes higher. Figure 4.7 shows the *kapp / k* versus temperature at $\varepsilon = 1.0$ for different thermal conductivity ranges. It indicates that the higher the temperature, the higher the ratio, and for low thermal conductivity fluids, this tendency would be more significant. These results show that in the transient hot-wire method the temperature and emissivity of the wire are two important factors affecting the thermal conductivity measurement. C.A. Nieto de Castro et al. (1991) [58] stated that the contribution of radiative heat transfer to thermal conductivity was found to range between 2 and 50%.

C.A. Nieto de Castro et al. investigated toluene and dimethylphthalate liquid thermal conductivity [59]. They indicated that the radiant effect in determining the thermal conductivity using the transient hot-wire method is quite significant without any corrections. Gross et al. (1992) [60] measured the thermal conductivities of refrigerants HFC-134a, HFC-152a, and CFC-123 using the hot-wire transient method. Although the accuracy was claimed within ±1.6 to ~2.0% with proper corrections, the uncertainties were attributed to limitations in the ideal mathematical model of a line source in infinite space and the effects of convection and radiation.

Another factor which affects the thermal conductivity measurement error is the wire diameter. From Saito's apparent thermal conductivity ratio equation, Equation 4.18, the apparent thermal conductivity ratios were dominated by the diameter ($2r_1$) of the thin wire used. Table 4.3 indicates how the ratio was affected by the wire diameter used.

TABLE 4.3: RATIO OF APPARENT THERMAL CONDUCTIVITY TO ACTUAL THERMAL CONDUCTIVITY

diameter ($2r_1$), μm	*kapp / k*
5.0	1.003
10.0	1.006
50.0	1.030
100.0	1.060

1. *kapp / k* was calculated by Equation 4.18
2. Cases for toluene with the following parameters:
   equilibrium temperature, $T_0 = 360\ K$
   $R = 0.01$
   thermal conductivity, $k = 0.1137\ W/(m \cdot K)$
   refractive index, $n = 1.4961$
   Stefan-Boltzmann constant, $\sigma_s = 5.6697 \times 10^{-8}\ W/(m^2 \cdot K^4)$

As shown in Table 4.3, the radiation effect is affected by the wire diameter and is never completely eliminated although minimized by using a thin wire. However, the experimental uncertainty of the smaller diameter wire would be larger than that for a larger diameter wire. Therefore, an appropriate wire diameter must be selected in order to achieve optimal accuracy by this method.

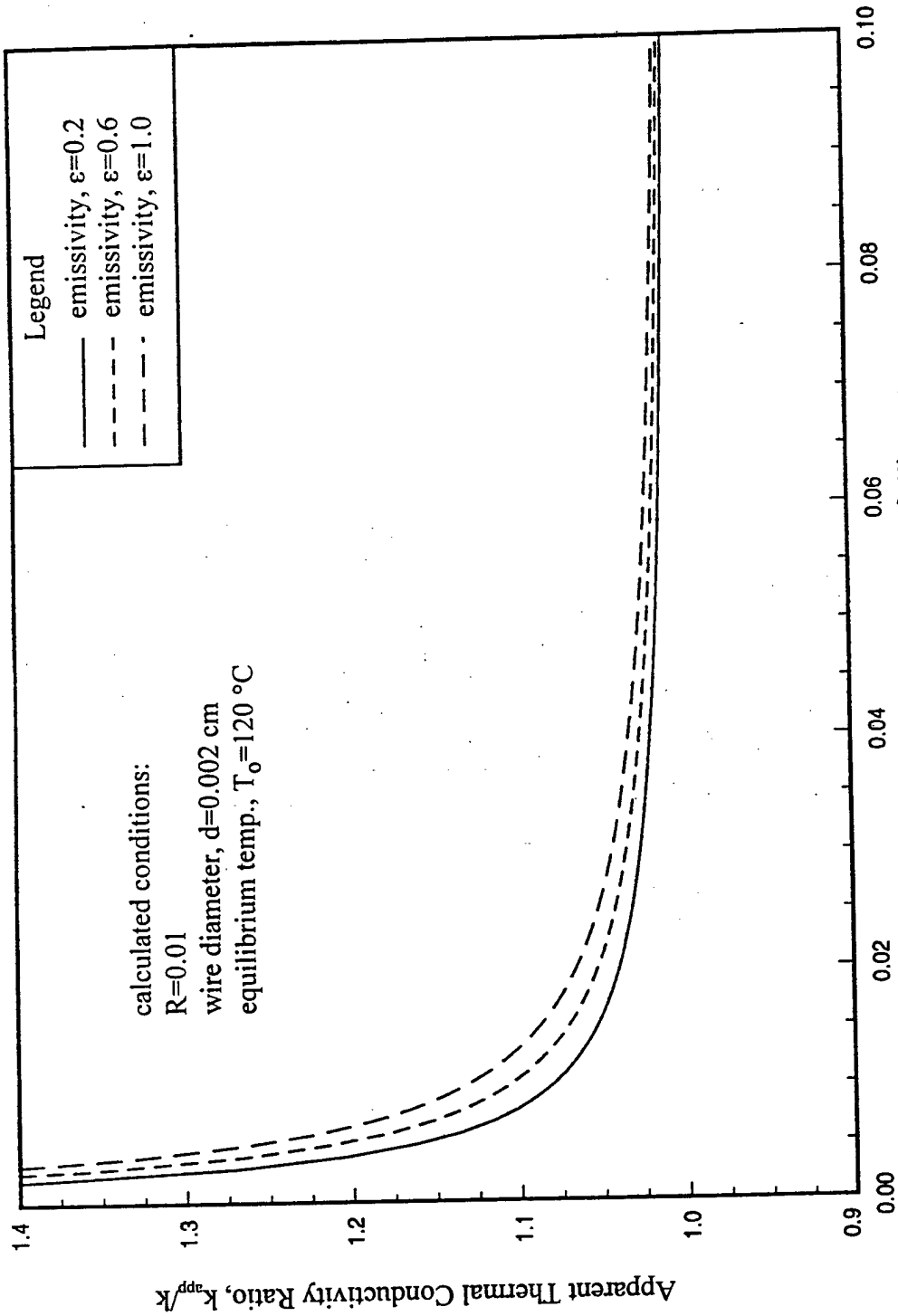

Figure 4.6: ***kapp / k*** **ratio as a function of *k* for various ε at high temperature case.**

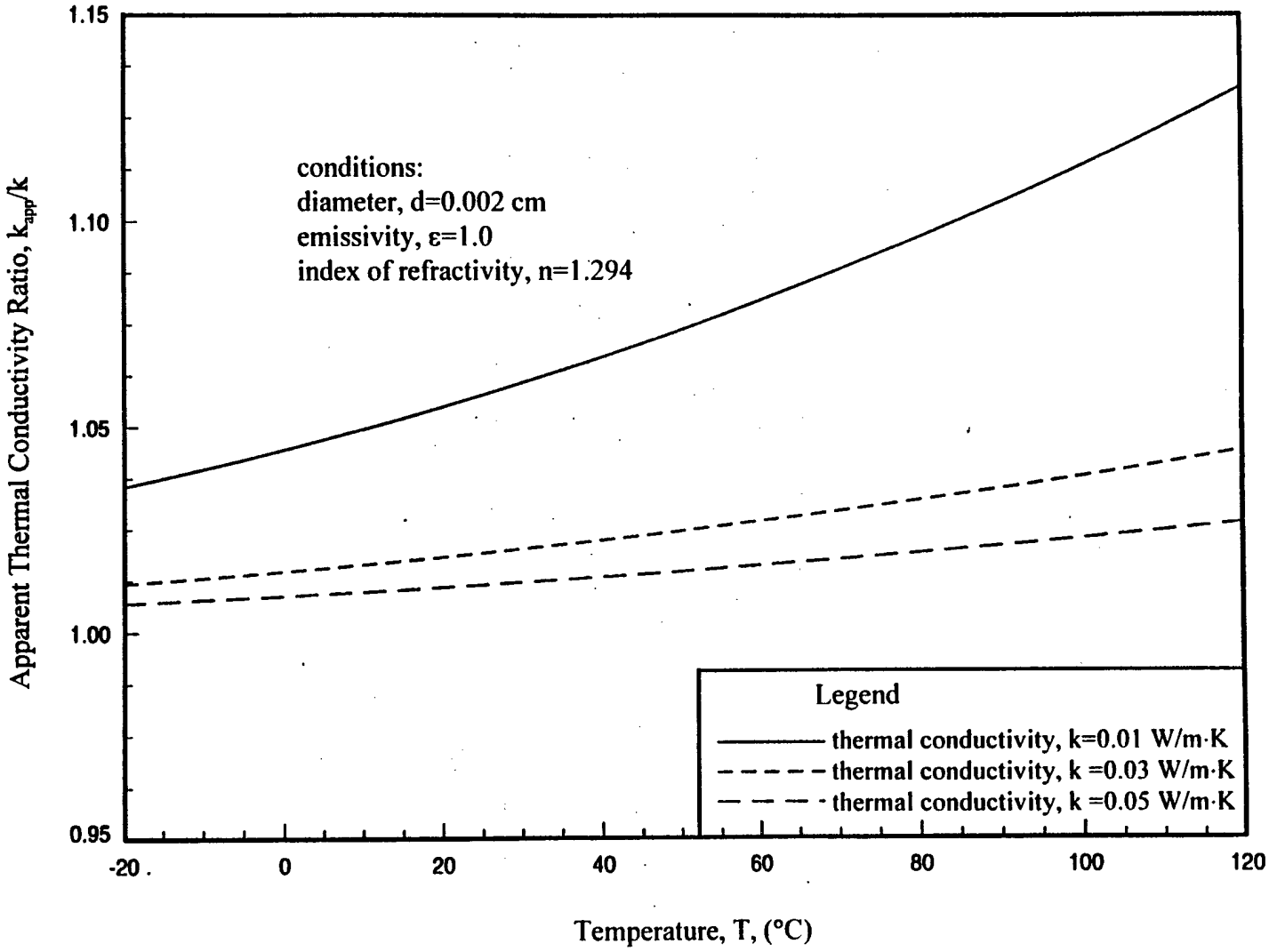

Figure 4.7: *kapp / k* ratio as a function of temperature for different thermal conductivity ranges.

Convection Effects on Thermal Conductivity Measurement

The design of an experimental apparatus for the determination of the thermal conductivity of a liquid should preclude the possibility of free convection [61,62]. Tsederberg [45] mentioned Kraussold's study of the conditions at which free convection occurs for various liquids located between two concentric cylinders when the thermal conductivity of the fluids was known. Kraussold found that free convective heat transfer arises when $(Gr \cdot Pr) \geq 1000$. Kraussold, indicating that both horizontal and vertical placements of the tube were similar, analyzed the apparent thermal conductivity ratio for concentric cylinders and developed the following correlation:

$$\frac{kapp\,/\,k}{k} = 0.11\,(Gr \cdot Pr)^{0.29} \tag{4.20}$$

This equation is only valid for $3.8 \leq (Gr \cdot Pr) \leq 6.0$. Instead of Kraussold's equation, Equation 4.20, Wakeham et al. [51] used a different equation to estimate the heat transfer by convection, which for a cylindrical geometry is:

$$\frac{\dot{Q}_{conv}}{\dot{Q}_{cond}} = \frac{dRa}{720l} \tag{4.21}$$

where d is the thickness of the fluid layer, l the length of the internal cylinder, and $Ra = (Gr \cdot Pr)$ is the Rayleigh number. Results from using Equation 4.21 are shown in Table 4.4.

TABLE 4.4: AN EXAMPLE OF CONVECTION EFFECTS ON CONDUCTION IN CYLINDRICAL GEOMETRY

Apparent thermal conductivity ratio (based on $l = 120$ mm)		
$Ra = Gr \cdot Pr$	$\dot{Q}_{conv} / \dot{Q}_{cond}$ ($d = 0.2$ mm)	$\dot{Q}_{conv} / \dot{Q}_{cond}$ ($d = 0.5$ mm)
1000	0.0023	0.0058
5000	0.0116	0.0289
10000	0.0231	0.0579

From Table 4.4, it is noted that the significance of free convection depends on the Rayleigh number, Ra. For large Ra, the convection effect would be large if the fluid layer, d, is large. Therefore, control of Ra is necessary in order to decrease the effect of free convection on total heat transfer. However, the measured thermal conductivity still needs to be corrected for free convection effects. For a non-steady method, such as the transient hot-wire method, Tye [44] mentioned and suggested that there might be a corresponding pseudo-steady state, and convection would be

expected to occur when the pseudo-steady state temperature reaches a critical value defined by $Ra \equiv Gr \cdot Pr \geq 1000$ [44]. A criterion for the onset of convection in a non-steady hot-wire cell was suggested:

$$\left(\frac{g\alpha\rho\dot{Q}r_1^3}{4\pi k C_w}\right) T^* \left(e^{0.5T^*} - 1\right)^3 \leq 1000 \qquad (4.22)$$

where $T^* = 4\pi k T_\infty / \dot{Q}$, μ is dynamic viscosity of liquid, C_w is the wire heat capacity, T_∞ is fluid temperature, $\dot{Q}$ is the heat input, and α is thermal diffusivity. A plot of t^* ($= 4\, C_w / r_0^2$) against T^* ($e^{0.5T^*} - 1$) can be used to determine the true time, t, for the onset of convection, and the necessary error correction can be made.

Summary of Thermal Conductivity Measuring Methods

The methods mentioned above for experimental thermal conductivity determination are summarized as: the steady-state method and the non-steady-state method. The main difference between the steady-state and unsteady method is the amount of time consumed. The steady-state method requires more time to reach steady state, which affects the accuracy of measurement because the mathematical model is based on the real steady-state conditions, whereas the unsteady-state method allows prompt measurements to be taken. Both methods demand careful experimentation to minimize corrections for heat losses and to prevent the onset of convective motion in the fluids. However, other effects such as time counting deviation, geometric errors, temperature sensor errors, and constant surface temperature controlling scheme also contribute to the overall uncertainty in values of thermal conductivity for both methods. Table 4.5 is a brief discussion of those steady-state methods mentioned above, and Table 4.6 describes the advantages and disadvantages for unsteady-state methods.

The uncertainty sources are generally known for all of these methods. Typically, the main uncertainties have been catalogued into two sources: radiation error and convection error. Table 4.7 shows the errors of these main sources.

TABLE 4.5: SUMMARY OF ADVANTAGES AND DISADVANTAGES OF STEADY-STATE METHODS OF THERMAL CONDUCTIVITY MEASUREMENTS

method	horizontal, flat-plate and vertical, coaxial cylinder method	hot-wire method	concentric sphere method
advantages	• static fluid - no flow • less fluid properties related	• static fluid - no flow • simplicity and ease of construction • less fluid properties related	• static fluid - no flow • no other properties related
disadvantages	• difficulties in eliminating convection perturbation along the edges of the heated plates • difficulties in controlling isothermal conditions on the surfaces of the plates • radiation effect not negligible • real steady state attainment • time consuming	• axial conduction effect of the wire • precise determination of the wire and tube diameters • accurate coaxial alignment of the wire in the tube	• difficulty in apparatus's construction and accurate alignment • effect of convection • difficulty in real surface temperature measurement
approximate error range	±1.0% ~ ±15%	±1.0% ~ ±18%	±1.0% ~ ±15%

TABLE 4.6: SUMMARY OF ADVANTAGES AND DISADVANTAGES OF UNSTEADY-STATE METHODS OF THERMAL CONDUCTIVITY MEASUREMENTS

method	hot-wire cell - line source	cylindrical, spherical source
advantages	• less time consuming • no thermal-resistance layer	• less time consuming • simple construction
disadvantages	• effect of finite length (originally assumed as infinitely long) • effect of heat capacity depending on temperature • effect of bounding wall • onset of convection effect ($Ra \geq 1000$) - when time going • radiation effect never completely eliminated - correction is difficult	• difficulty in apparatus's construction and accurate alignment • effect of heat capacity • effect of thermal boundary layer • onset of convection effect ($Ra \geq 1000$) • radiation effect never completely eliminated - correction is difficult
approximate error range	±1.0% ~ ±18%	±1.0% ~ ±15%

TABLE 4.7: SUMMARY OF TYPICAL UNCERTAINTIES FOR EXPERIMENTAL THERMAL CONDUCTIVITY MEASUREMENTS

method	radiation	convection	total error
steady state: parallel flat plates or concentric cylinders	emissivity and temperature dependent - low temp.: ±0.1% ~ ±1.0% (ε = 0.1 ~ 1.0) high temp.: ±1.0% ~ ±8.8% (ε = 0.1 ~ 1.0)	negligible for $Ra \leq 1000$ ±0.3% ~ ±4.2% Ra: 1000 ~ 10,000	±0.4% ~ ±13%
non-steady state: transient hot- wire method	emissivity, wire size, and temp. depending on - ε effect: ±1.0% ~ ±10% wire diameter: ±0.3% ~ ±6% temp. effect: ±1% ~ ±10%	less than ±1%	±3% ~ ±26%

EXPERIMENTAL METHODS FOR VISCOSITY MEASUREMENT

Some methods usually used for the viscosity measurements include the capillary tube [10,11,63,64,65], falling cylinder [66,67], rolling ball [68,69], vibrating-wire method [12], and torsional oscillation method [14-16]. The following is a brief introductory review of these methods.

Capillary Viscometer

The capillary viscometer [10,11] uses the flowing fluid characteristics in a capillary tube of a certain length. The viscosity is related to the following quantities: volumetric flow rate, pressure drop, density of fluid, thermal expansion coefficient of the capillary, kinetic energy correction factor, and the capillary constant. The capillary constant is determined using a known viscosity fluid, usually pure water. The viscosity is calculated from a modified Hagen-Poiseuille equation.

Vibrating-Wire Viscometer

The vibrating-wire viscometer [12] is used for Newtonian fluids. A circular-section beam of constant length with both ends clamped at fixed points is subjected to a working fluid. The beam is set into oscillation in a single mode within a plane containing the axis of the beam and perpendicular to it by means of an initial displacement at time $t = 0$ in an initially stationary fluid of constant viscosity and density. The viscosity is determined by the relationship between the frequency and the magnitude of the oscillation of the beam or wire in a fluid. A correction is required for the specific wire.

Torsional Oscillation Viscometer

This kind of viscometer uses the principle of surface loading, that is, a vibrating surface in contact with a liquid experiences a force which is a function of viscosity [14]. The oscillatory surface may be spherical, cylindrical, or planar. The wave propagation is created outward by the oscillating surface. To eliminate the complexity of the counter-reflected wave effects, the container size must be large enough so that no disturbance reaches the walls. The viscosity can be found from the relationship between the frequency of the oscillation and the shear rate.

The viscosity measurement in the current study was measured by this kind of viscometer.

Summary of Experimental Investigations of Liquid Viscosity of Refrigerants

Table 4.8 is a summary of previous experimental investigations for the viscosity of liquid refrigerants [65].

TABLE 4.8: LIST OF PREVIOUS INVESTIGATIONS OF LIQUID REFRIGERANT VISCOSITY MEASUREMENTS

Investigator	Year	Refrig.	Temp. (K)	Pressure	Method	Accuracy (%)	Ref.
Benning and Markwood	1939	CFC-11	243-333	sat.	roll. ball	-	[68]
		CFC-12	243-332	sat.	roll. ball	-	
		HCFC-22	240-318	sat.	roll. ball	-	
		CFC-113	243-333	sat.	roll. ball	-	
		CFC-114	242-332	sat.	roll. ball	-	
Lilios	1957	CFC-12	243-332	sat.	capillary	2.2	[69]
			213-243	sat.	roll. ball	-	
		R-13b1	203-218	sat.	roll. ball	-	
		CFC-113	243-293	sat.	roll. ball	-	
Gordon et al.	1969	CFC-11	245-347	sat.	capillary	-	[63]
		CFC-12	245-305	sat.	capillary	-	
		HCFC-22	246-312	sat.	capillary	-	
		R-13b1	246-301	sat.	capillary	-	
Phillips and Murphy	1970	CFC-11	209-352	sat.	capillary	-	[64]
		CFC-12	202-312	sat.	capillary	-	
		HCFC-22	201-299	sat.	capillary	-	
		R-152a	200-318	sat.	capillary	-	
Kumagai and Takahashi	1990	11 kinds of refrig.	273-353	sat. sat.	capillary	±9 ~13 for HFC-134a	[65]
Okubo and Nagashima	1992	CFC-123	233-418	20 MPa	capillary	±1.2	[10]
		HFC-134a	213-423	30 MPa	capillary	±1.3	
Assael et al.	1992	liquids	270-370	300 MPa	vibrating	±3	[12]
Diller et al.	1993	HFC-134a	175-320	sat.	torsional crystal	±3-8 compared to others	[13]
		CFC-123	170-320	sat.	torsional crystal	±7-12 compared to others	
		R-141b	175-320	sat.	torsional crystal	less than ±12 compared to others	

Note: "-" accuracy not reported, "sat." saturation state

CHAPTER 5

EXPERIMENTAL APPARATUS AND OPERATION

This chapter describes the details and designs of the experimental facility. The construction of the test rig is described and shown. Sensors and test section calibration are also presented. Finally, the experimental procedures are discussed for proper operation of this test facility.

EXPERIMENTAL FACILITY CONSTRUCTION

The experimental test rig was established for the purpose of measuring liquid transport properties of refrigerant, refrigerant mixtures, or refrigerant/lubricant mixtures. Each experiment measures the single-phase heat transfer coefficients of liquids by a surface temperature method.

Heat Transfer Test Facility

The test section is a 0.9525-cm (3/8-inch) inside diameter by 2-m long smooth copper tube. The measured quantities are tube wall temperature, inlet/outlet fluid temperatures, absolute and differential pressures, dynamic viscosity, and the mass flow rate. A schematic of this test rig is shown in Figure 5.1, while a photograph is shown in Figure 5.2.

Eleven T-type thermocouples are installed on the outer wall of the tube at equal distances of 0.2 m, starting from the inlet point and ending at the outlet point, along the 2-m long test section. In order to get more average temperature measurements at the inlet and outlet locations, two additional thermocouples were placed 0.1 m from the inlet and the outlet points on the outer tube wall. Moreover, one thermocouple is placed on the outer insulated wall surface for measuring the temperature there. Also, one thermocouple is used for measuring the room temperature. The thermocouple for measuring room temperature is located in a wooden box which is wrapped with aluminum foil on the outer surfaces to insure the measurement of a radiation, and convection-free temperature. Figure 5.3 shows the details of the test section configuration. A picture of the test section is also shown in Figure 5.4. Two RTDs were placed right at the inlet and outlet points of the test section to measure the respective fluid temperatures. All thermocouples and RTDs were calibrated to ±0.05°C.

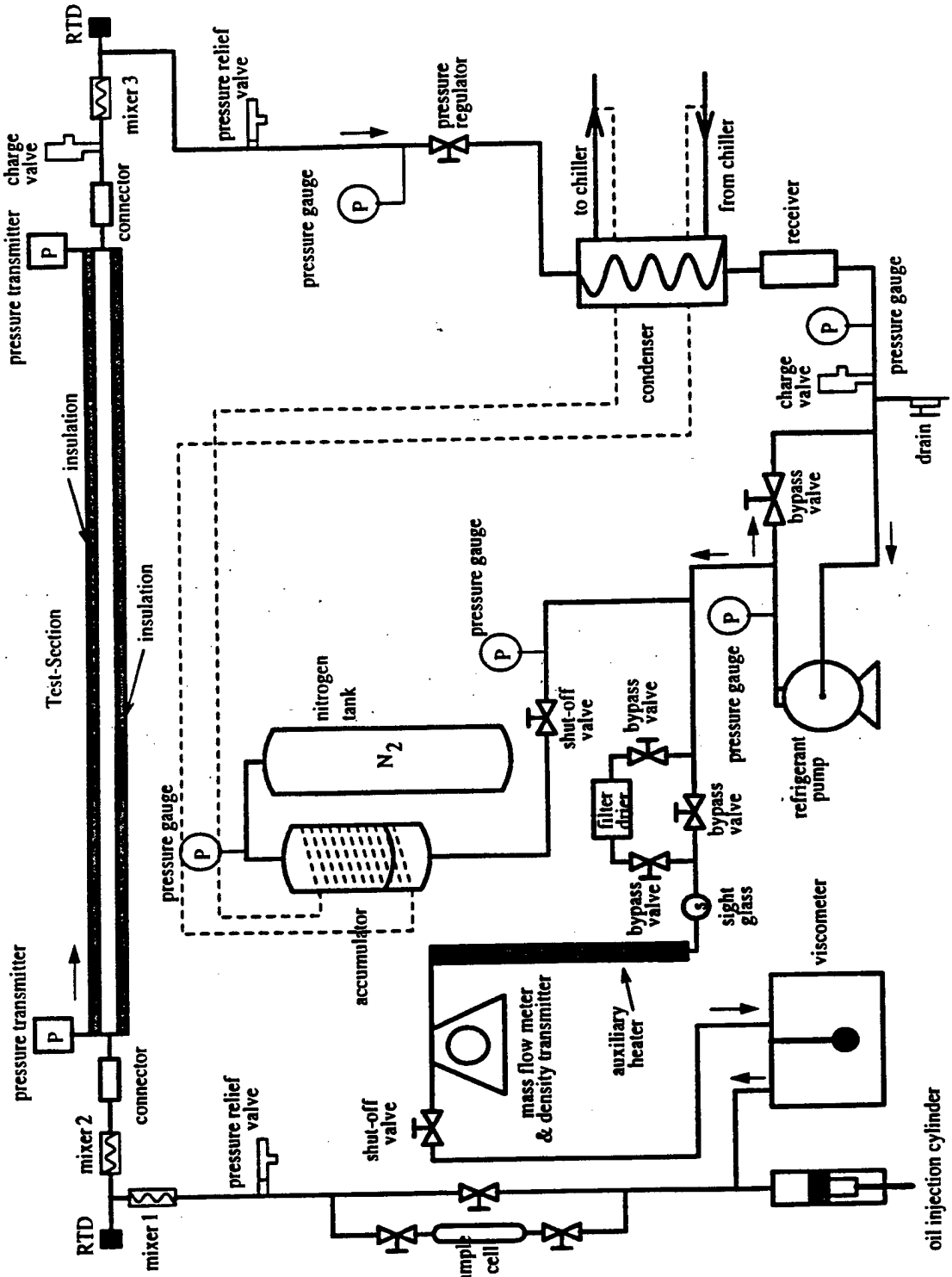

Figure 5.1: Schematic diagram of test facility.

Figure 5.2: Photograph of test facility.

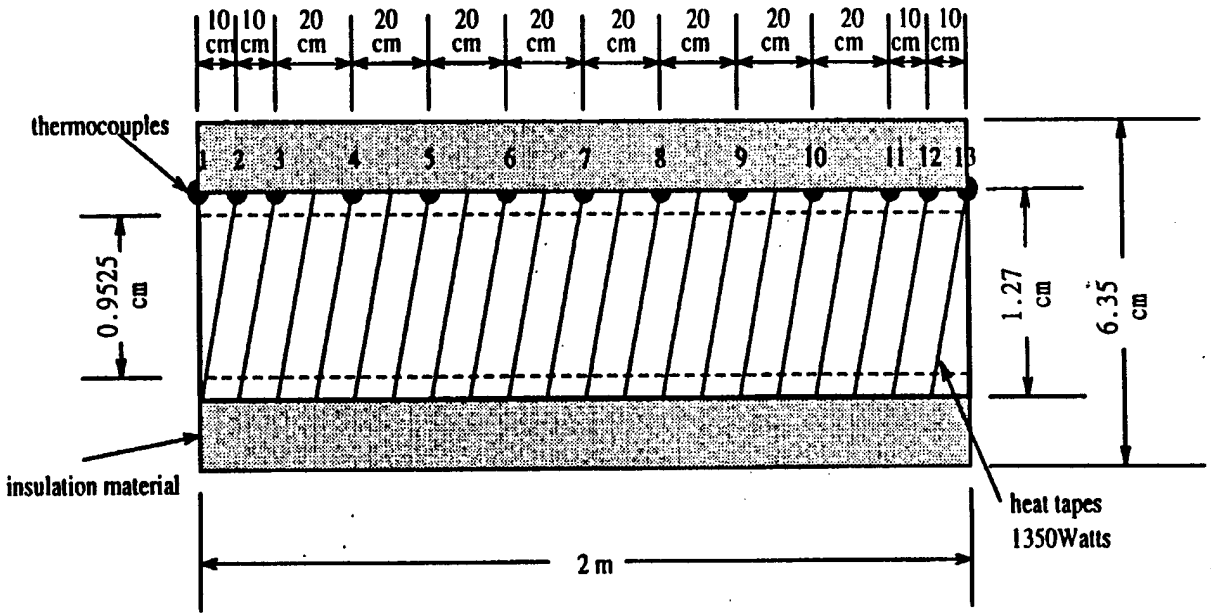

Figure 5.3: Test section configuration.

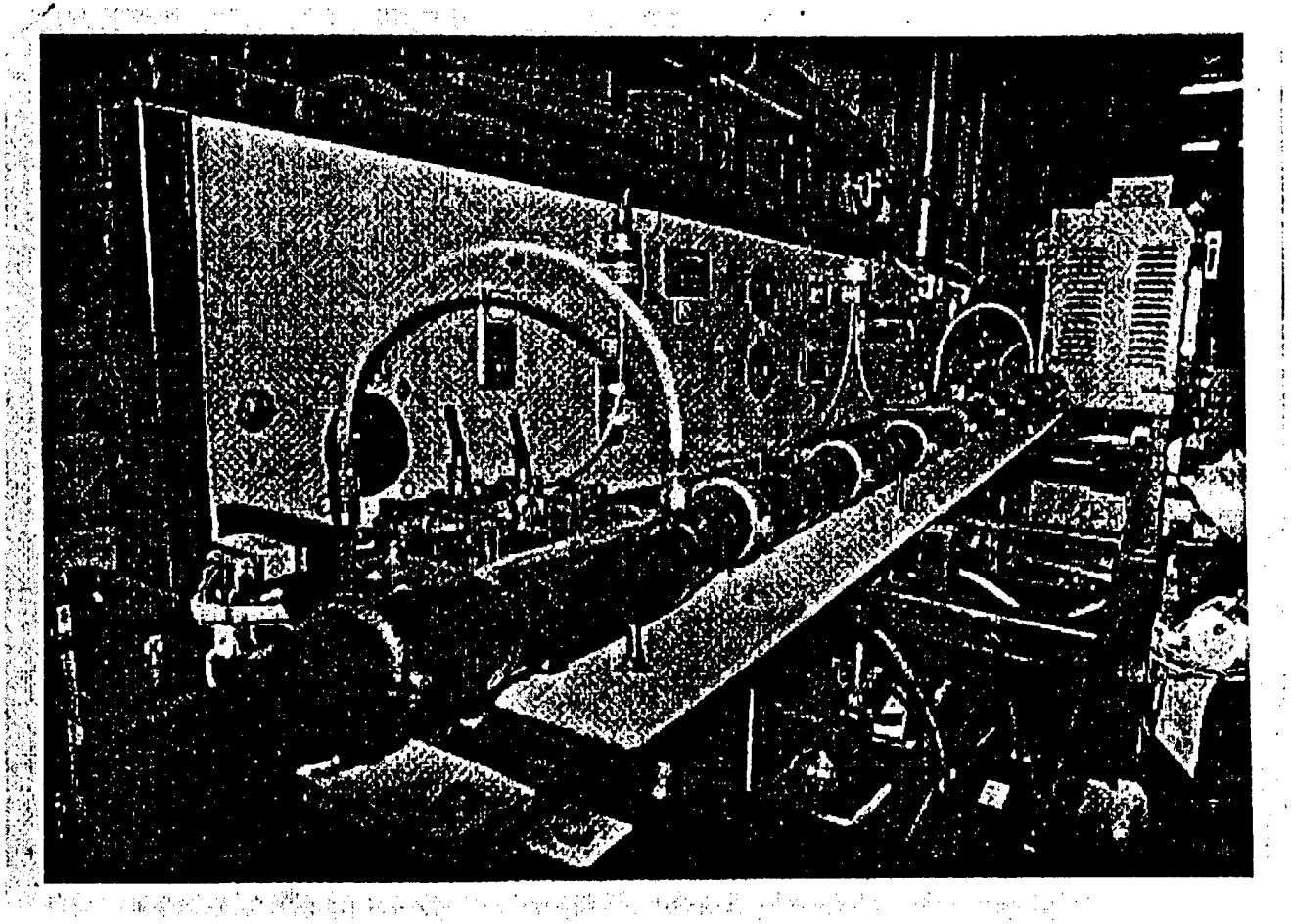

Figure 5.4: Photograph of test section.

In order to get more accurate inlet and outlet temperatures, three plastic mixers were installed inside the tube for the purpose of determining a more accurate average fluid temperature. The first one was located vertically just prior to the tube elbow of the inlet portion, the second one was horizontally placed between the test section and the tube elbow, and the third one was installed horizontally immediately after the outlet of the test section.

Two plastic tube connectors which served as heat insulators were placed at both the inlet and outlet of the test section in order to prevent axial heat loss from the ends of the test-tube. One was placed right before the inlet point of the test-tube, while the other was placed just after the outlet point of the test-tube. The test section pressure was monitored by an absolute pressure gauge and a differential pressure transmitter which measured the test section inlet and differential pressures across the test-tube, respectively.

The system pressure was controlled by an accumulator which was connected to a nitrogen vessel. Pressure, therefore, was regulated by the nitrogen pressure. The system mass flow rate was adjusted by a variable-speed controlled motor pump assembly. The system heating control was achieved by two parallel power connected heat tapes of 675 watts each. The heating capacity was controlled by adjusting the power regulator which was connected to a watt transducer with an accuracy of ±0.2% of reading. The heat tapes were uniformly wrapped along the test section; thus, constant heat flux was expected and assumed.

After the heated test section, two condensers were placed between the outlet of the test section and the inlet of the pumps for removing the heat that was added in the test section. Two pumps were installed in a parallel arrangement with each of the condensers in order to enable a wide operating range of mass flow rates. The cooling capacity could also be controlled by adjusting the chiller water flow rate as shown in Figure 5.1.

All of the measurement signals were connected to a HP3457A switch and control unit and a HP3488A multimeter. Data acquisition and measuring process control were driven by a personal computer.

Viscometer

Viscosity is simultaneously measured with other measurements in the test system. In this study, the viscosity is measured by an inline viscometer installed at the inlet portion of the test section. Viscosity can be dynamically measured at the same time along with the other measurements. This viscometer uses the torsional oscillation principle which is the principle of "surface load." A vibrating surface is in contact with a liquid which experiences a force that is a function of the viscosity [14]. This type of viscometer measures the product of dynamic viscosity and density. The range of this instrument can vary from a low viscosity range of 0.1 $cp \cdot g / cm^3$ to a high viscosity range of 500 $cp \cdot g / cm^3$, which covers most of the pure refrigerants, refrigerant mixtures, and even refrigerant/ lubricant mixtures with low lubricant concentrations. The accuracy of the viscosity measurement is ±2% of reading. The fluid is controlled by a bypass valve which regulates flow through a sample cell in which the sensor of the viscometer is mounted. The temperature of the fluid at the sample cell is also measured by a calibrated RTD with an accuracy of ±0.05°C. To determine viscosity, density is required. In this test rig, density is directly

measured by a densimeter of the vibrating-wire type which is installed in series with the viscometer. A schematic diagram is shown in Figure 5.5. A photograph of the viscometer sample cell is shown in Figure 5.6.

SENSOR CALIBRATIONS

The physical quantities measured directly by this test rig include temperature, mass flow rate, viscosity, pressure, and power input. The temperature measurements include inlet and outlet temperatures, test-tube wall temperatures, insulated wall temperature, and the ambient temperature. The inlet and outlet temperatures are measured by RTD sensors while the other temperatures are determined with thermocouples. All the RTD and thermocouple sensors were calibrated by a standard thermometer with an accuracy of ±0.05°C.

The other measurement devices such as for mass flow rate, viscosity, pressure, and power were calibrated at the factory. The uncertainty of each sensor is listed in Table 5.1.

TABLE 5.1: SENSOR UNCERTAINTY

measured quantity	unit	uncertainty
mass flow rate	*kg/s*	±0.15% of reading
pressure	psi	±0.2% of reading
viscosity · density	$cp \cdot g/cm^3$	±2% of reading
density	kg/m^3	±0.15% of reading
power	W	±0.2% of reading
temperature (RTD, thermocouples)	°C	±0.05°C

TEST SECTION HEAT LOSS CALIBRATION

The energy balance principle can not only be applied to estimate the heat loss of the test section for fluids with known specific heats, but it can also be applied in reverse to obtain the heat loss for fluids of unknown specific heats. However, to get accurate specific heat measurements, heat loss calibrations using several fluids with known specific heats are required. It should be noted that the heat loss estimation will be dependent on the specific test section with its own geometric and insulating characteristics. In other words, the heat loss is only valid for the test section being used for calibration and cannot be applied to other test sections or any situations changed from the original.

The heat loss of the test section was obtained from the calibration of previously tested refrigerants which are HCFC-22, CFC-12, and CFC-113. The accuracy of the heat loss calibration was tested using CFC-114. Then, the net heat input of the test section was used to calculate the specific heat of the test fluids. Figure 5.7 shows the logarithmic function of the test section heat loss associated with the logarithmic function of the temperature difference between the average outer insulated surface temperature, T_s, and average ambient temperature, T_a.

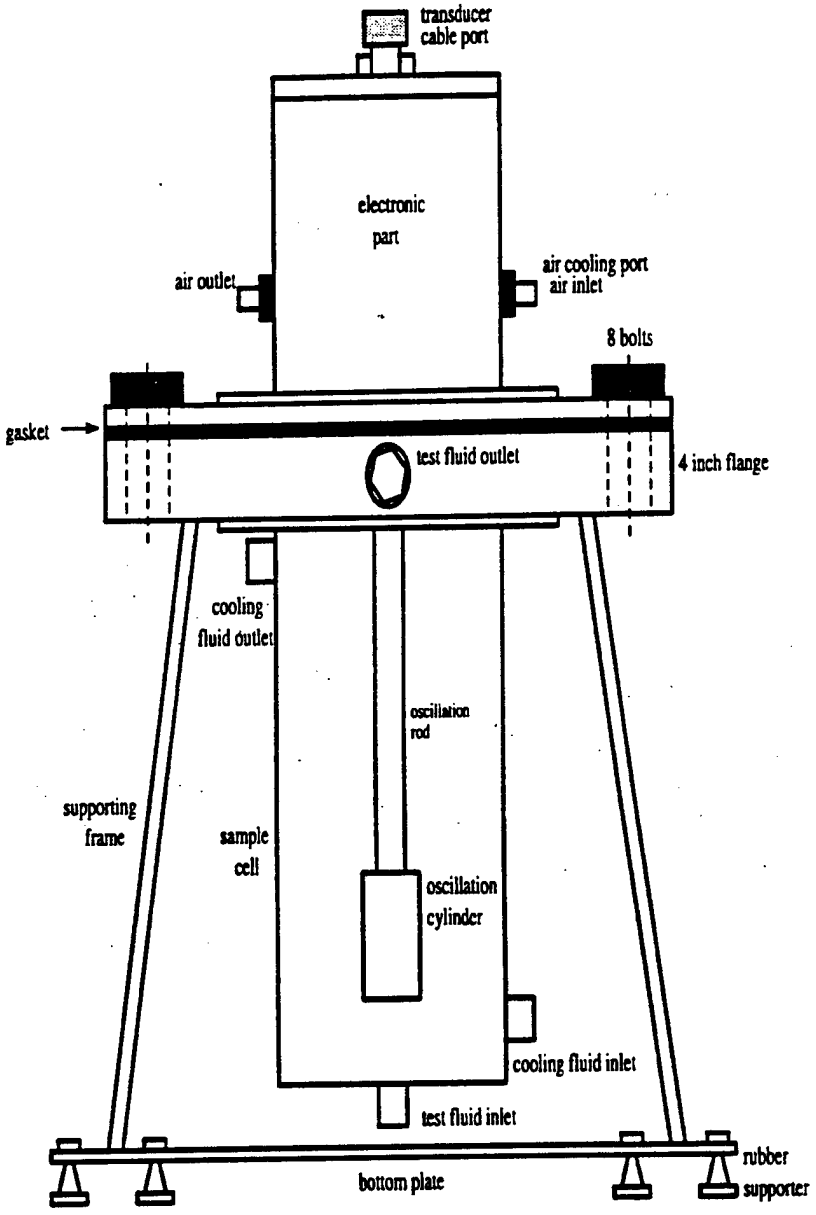

Figure 5.5: Viscometer construction.

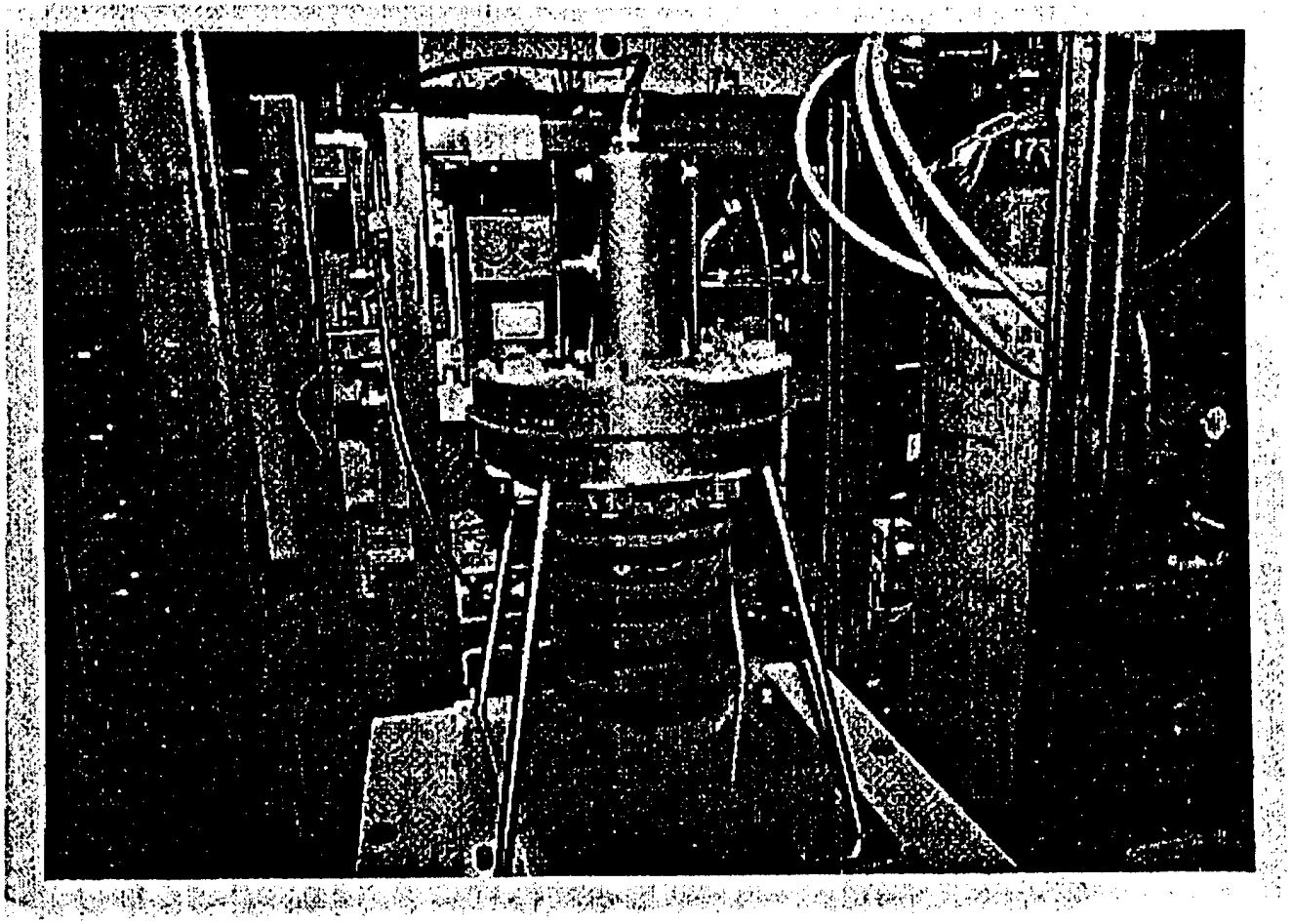

Figure 5.6: Photograph of viscometer sample cell.

The curve fit equation of the heat loss, $\dot{Q}_{loss}$ (in watts), associated with the $ln\ (T_s - T_a)$ is shown below:

$$ln\ (\dot{Q}_{loss}) = 0.612 + 1.33\ ln\ (T_s - T_a) \tag{5.1}$$

It should be noted that this equation will be only applicable to this particular test section as constructed including the particular insulation. For any other construction, the heat loss must be redetermined and the heat loss equation must also be reformulated.

ACCURACY VERIFICATION OF DENSIMETER

Although the accuracy of the densimeter was claimed to be ±0.15% within 1300 kg/m^3, it was necessary to verify the accuracy with refrigerants of known density. The verified refrigerants used were HCFC-22, CFC-12, CFC-113, and CFC-114, which were also the refrigerants for properties measured by using the current methodology and facility. Figure 5.8 shows the plot of measured density versus the ASHRAE reported density. As indicated in the deviation band in this figure, the deviation was within ±2%. However, it is necessary to mention that some of the measured densities were higher than 1300 kg/m^3, which is considered the upper level with highest accuracy for the densimeter used. Moreover, all the densities measured were under a compressed liquid state rather than a saturation state. As it can be seen, most densities were measured within ±1%.

ACCURACY VERIFICATION OF VISCOMETER

Viscosity is measured by an inline torsional oscillation viscometer. This type of instrument measures the product of kinematic viscosity and density. The accuracy was verified using CFC-12, CFC-114, CFC-113, and pure water. Figure 5.9 shows the plot of the measured viscosity of CFC-12 versus temperature compared with ASHRAE data. The deviation percentage plot is shown in Figure 5.10. As the plots show, the measured viscosity matches the ASHRAE data within ±2%. The measured viscosity of CFC-114 and its deviation compared with the ASHRAE data are shown in Figures 5.11 and 5.12, respectively, while the measured viscosity of CFC-113 and its deviation compared with the ASHRAE data are shown in Figures 5.13 and 5.14, respectively. The repeatability of the measurements was tested by CFC-114, which began with the temperature around room temperature and went down to nearly 0°C. The temperature then went up to nearly 50°C and back to room temperature. Finally, the measured repeatability of viscosity was verified with pure water. This test measured the viscosity of pure water at room temperature for nearly 17 hours. The measured viscosity of pure water and its deviation with the Chemistry/ Physics Handbook (CPH) data [70] are shown in Figures 5.15 and 5.16, respectively. As can be seen, the measured accuracy was within ±2%.

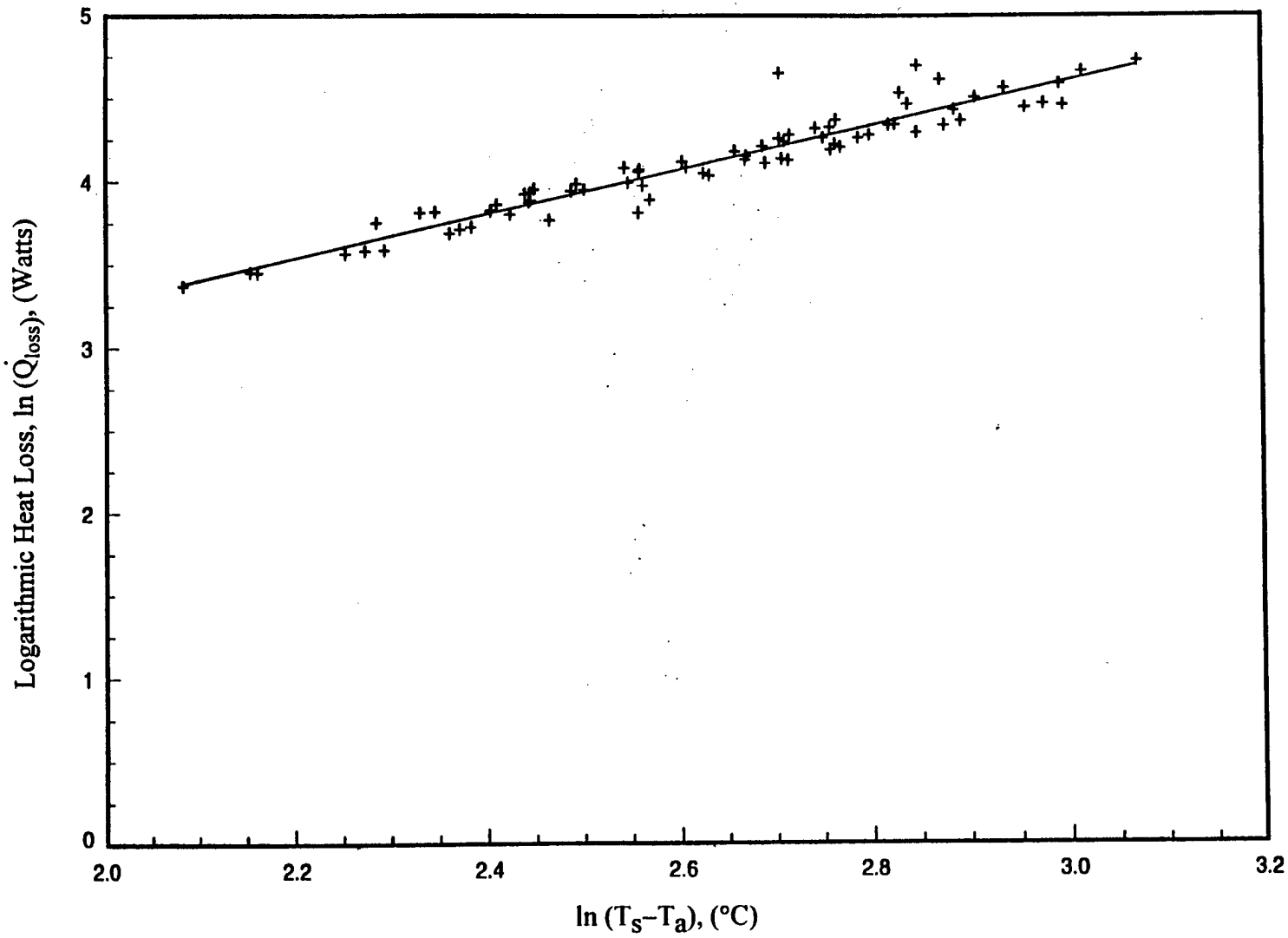

Figure 5.7: Heat loss estimation as a function of wall-fluid temperature difference.

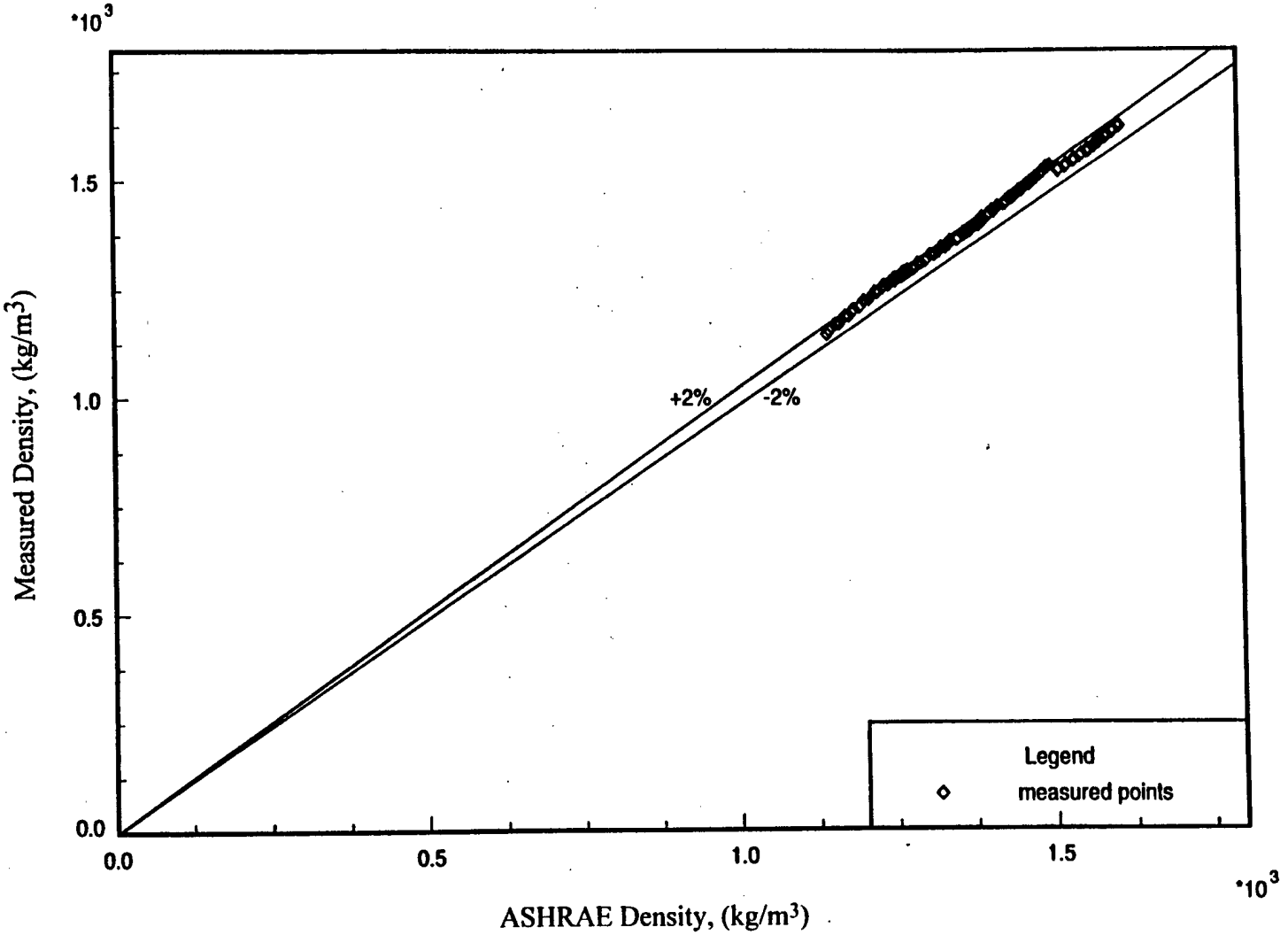

Figure 5.8: Comparison of measured densities and ASHRAE densities.

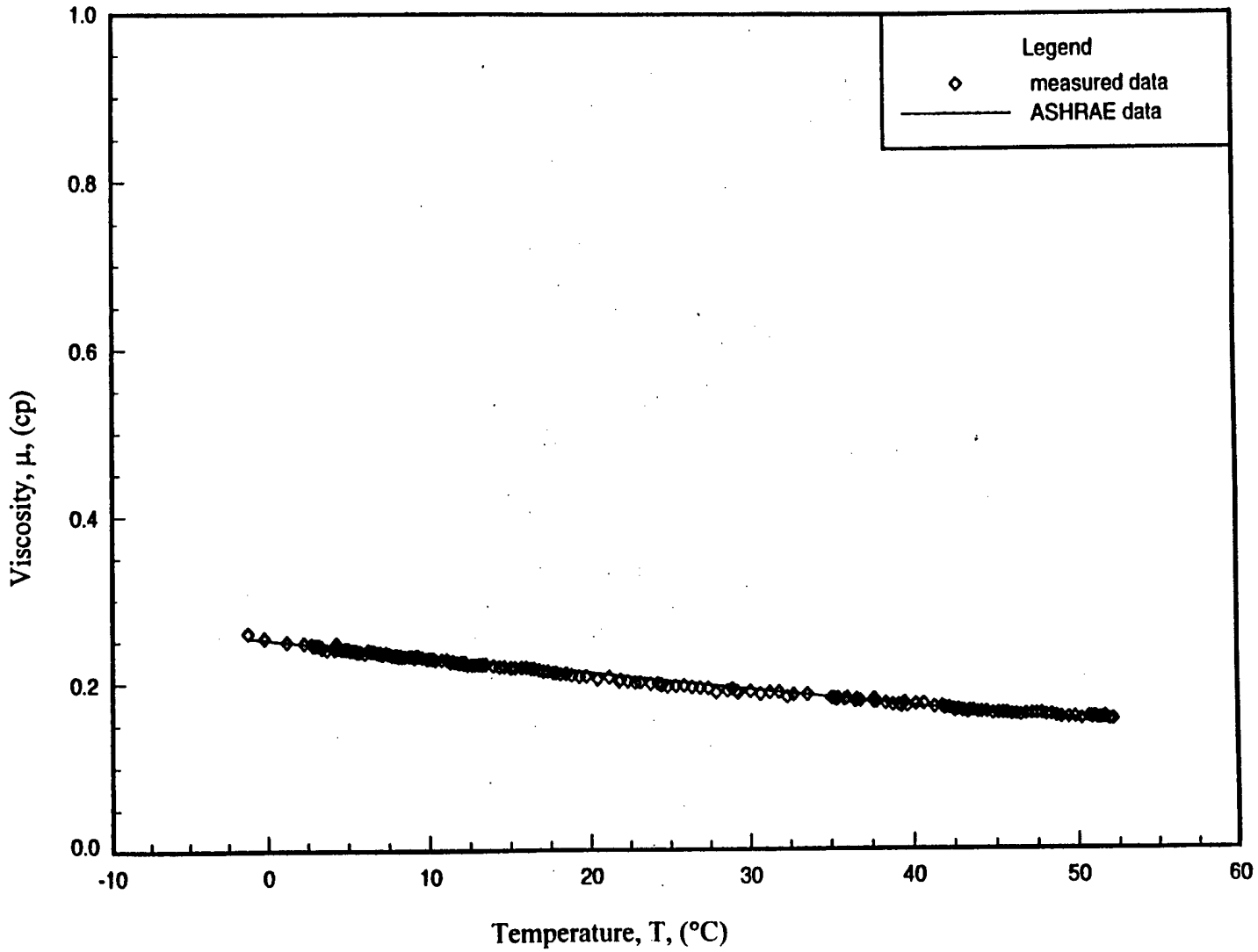

Figure 5.9: Measured viscosity CFC-12 as a function of temperature.

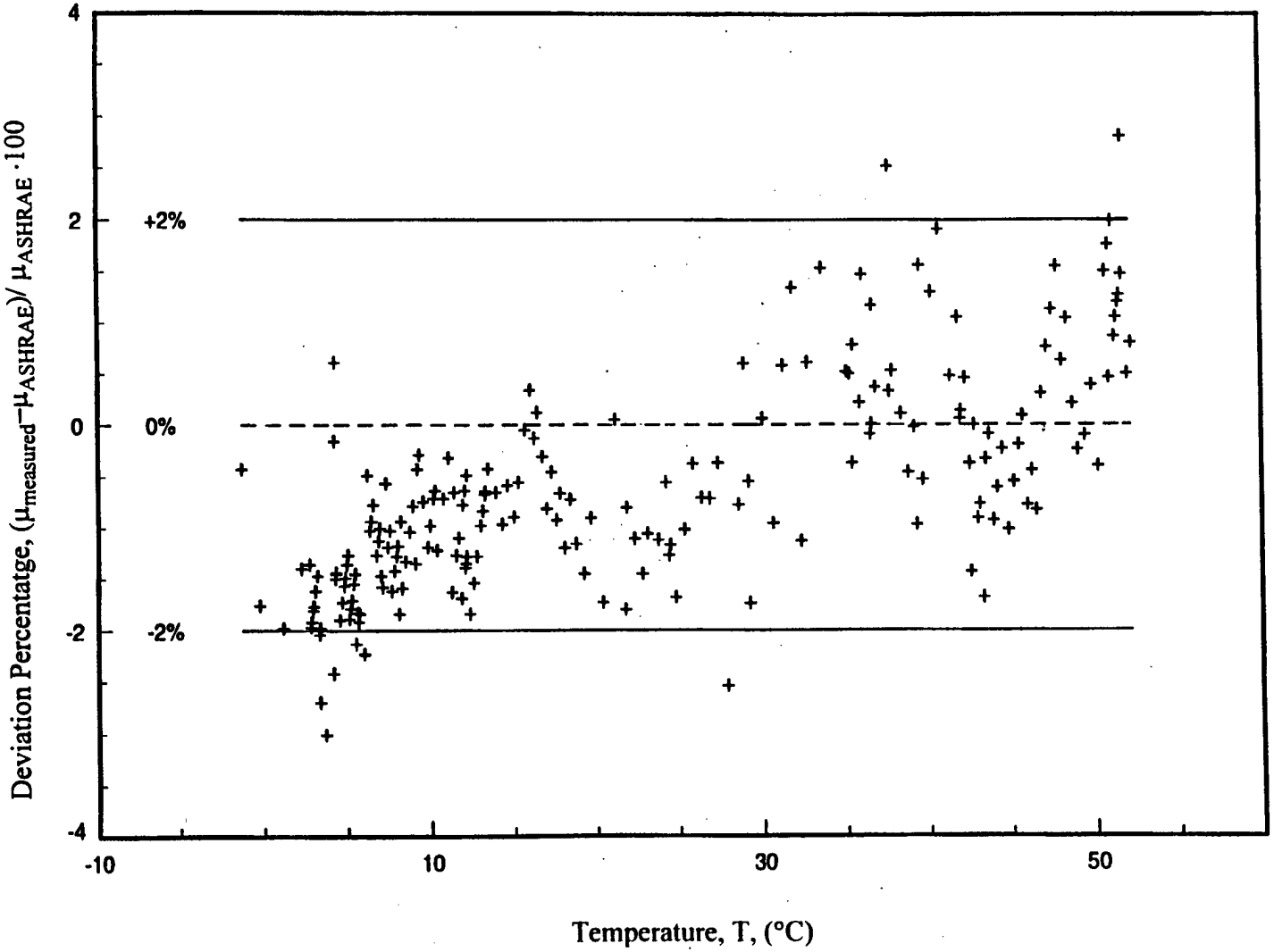

Figure 5.10: Deviation of CFC-12 measured viscosity compared with ASHRAE data.

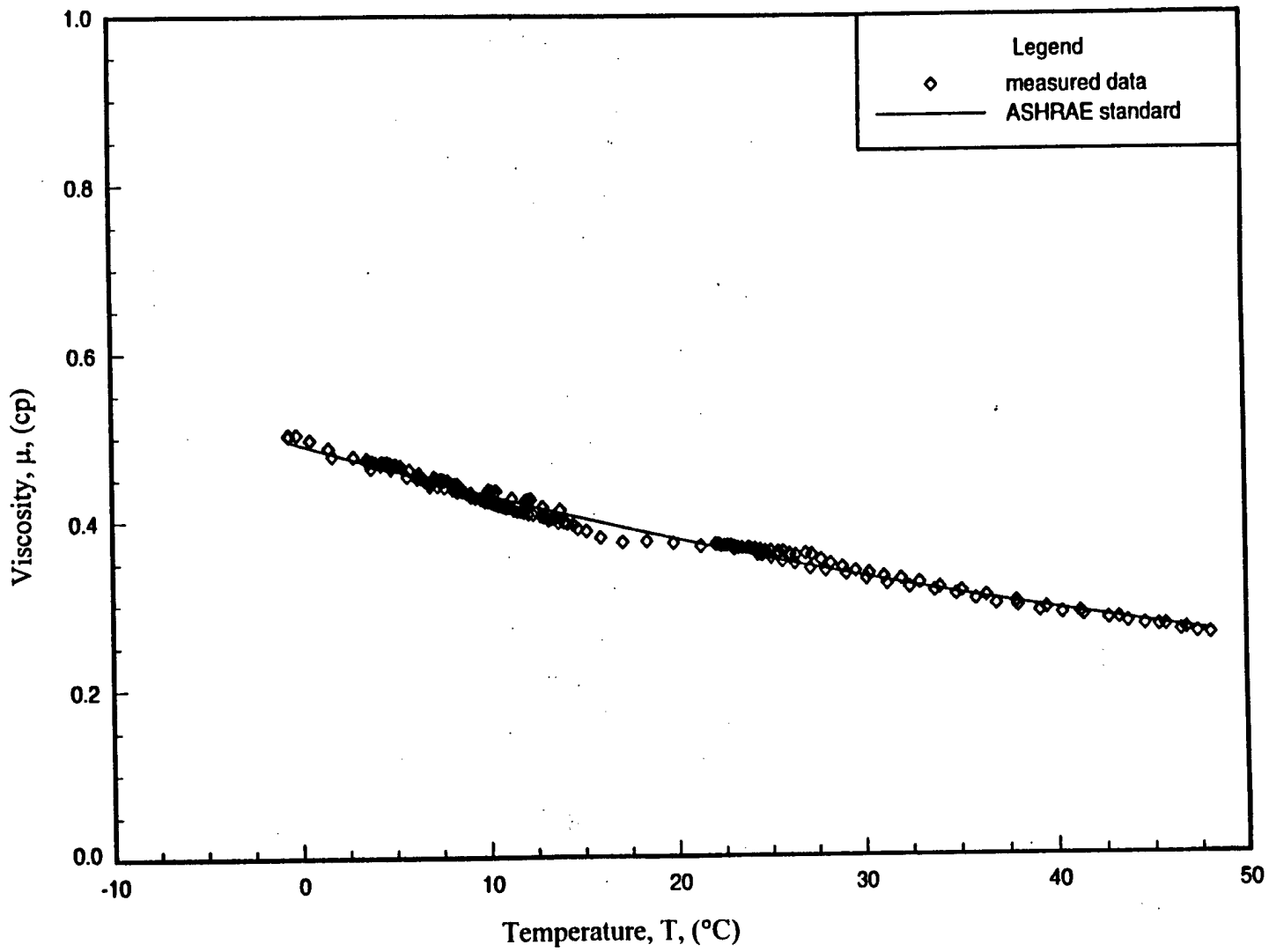

Figure 5.11: CFC-114 measured viscosity as a function of temperature.

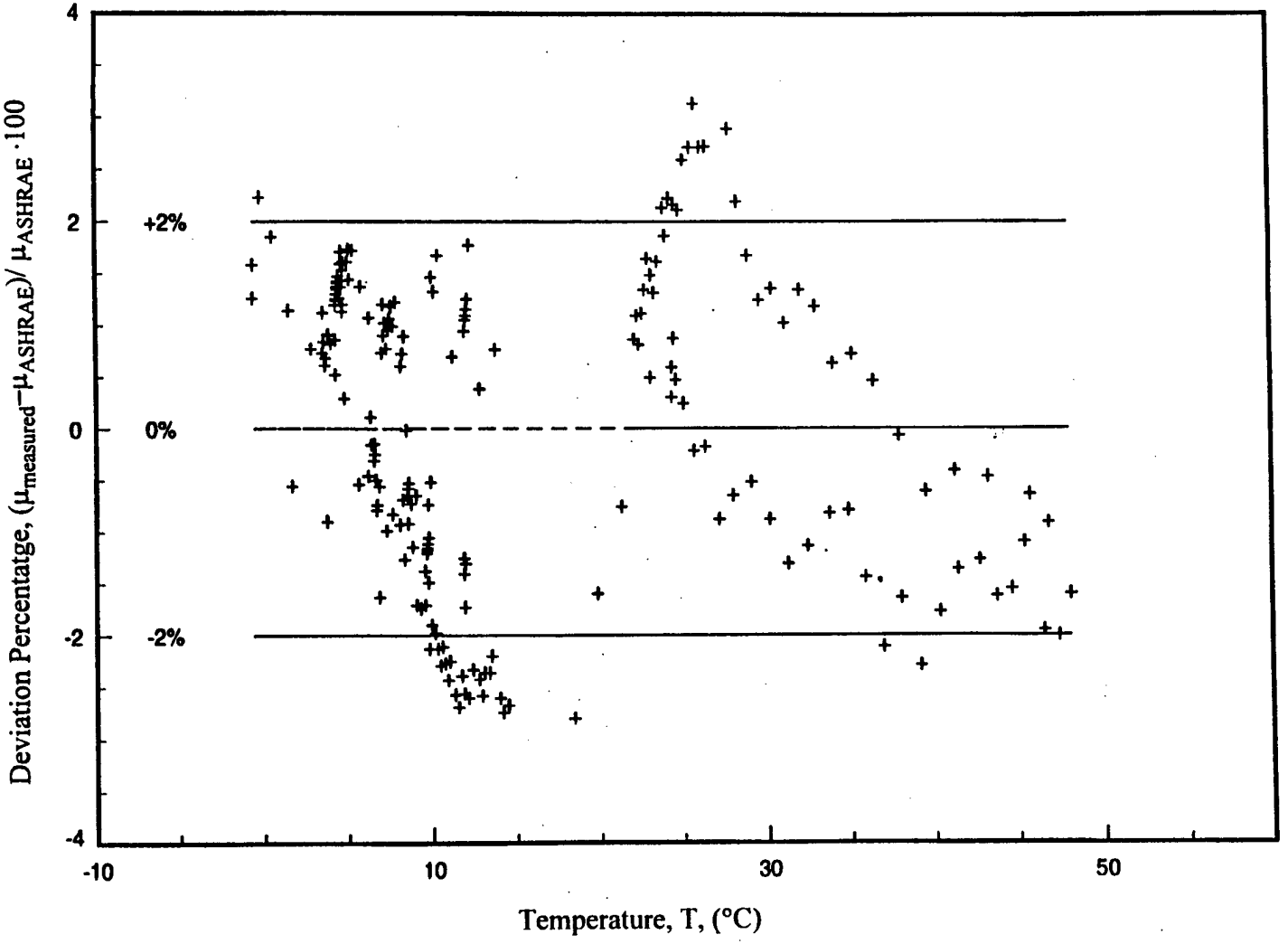

Figure 5.12: Deviation of measured and ASHRAE-listed viscosity for CFC-114.

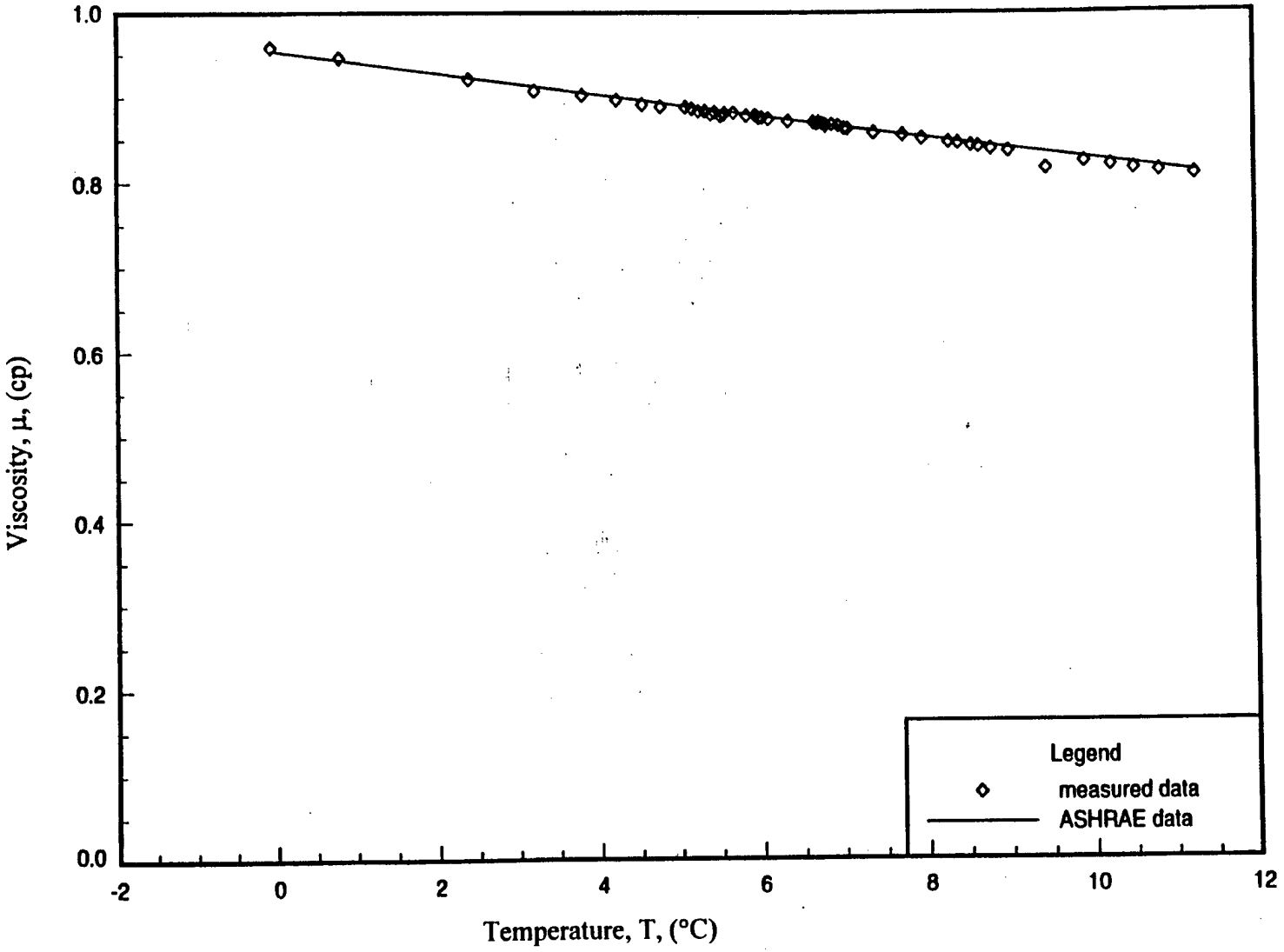

Figure 5.13: CFC-113 measured viscosity as a function of temperature.

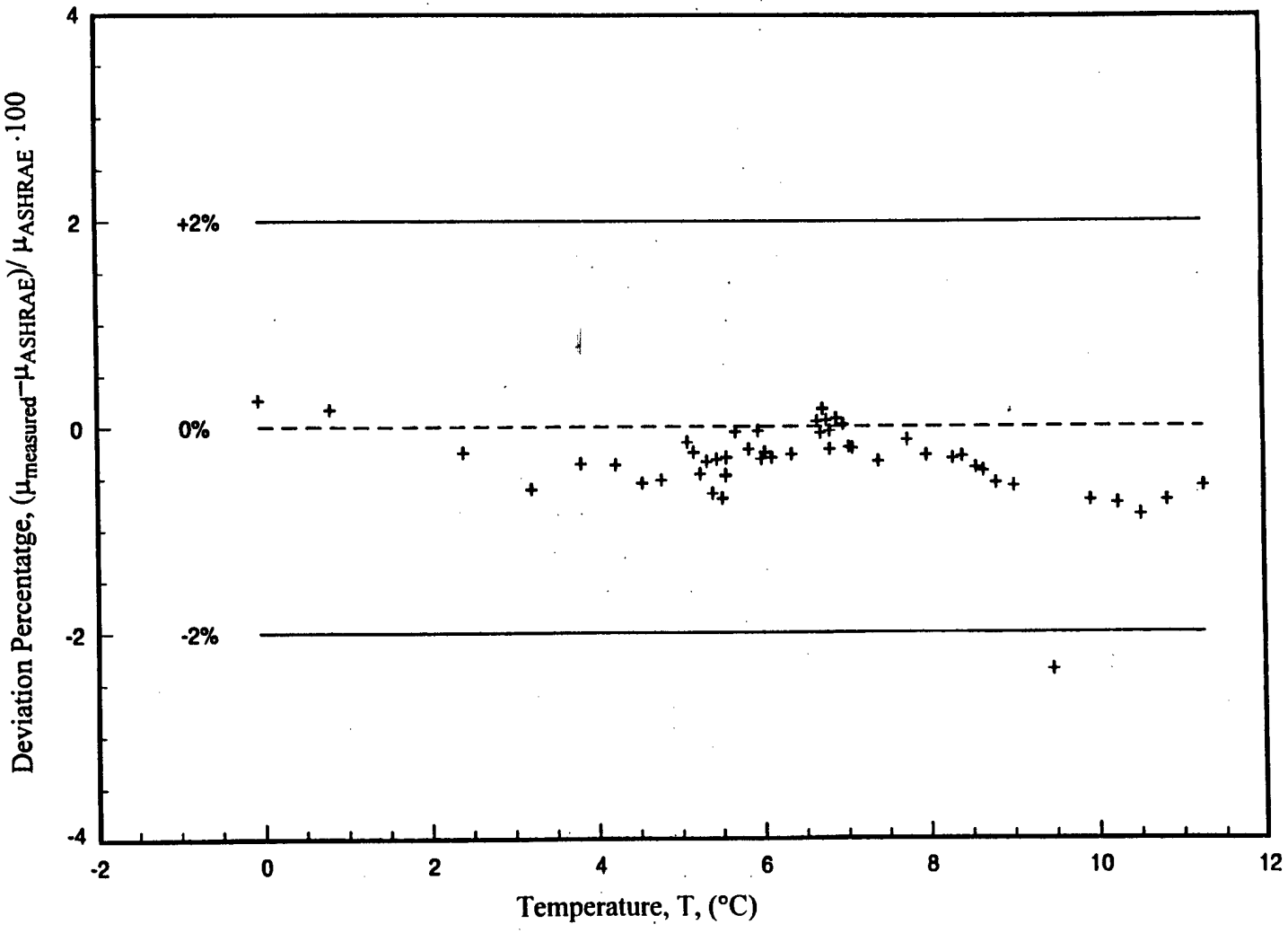

Figure 5.14: Deviation of measured and ASHRAE-listed viscosity for CFC-113.

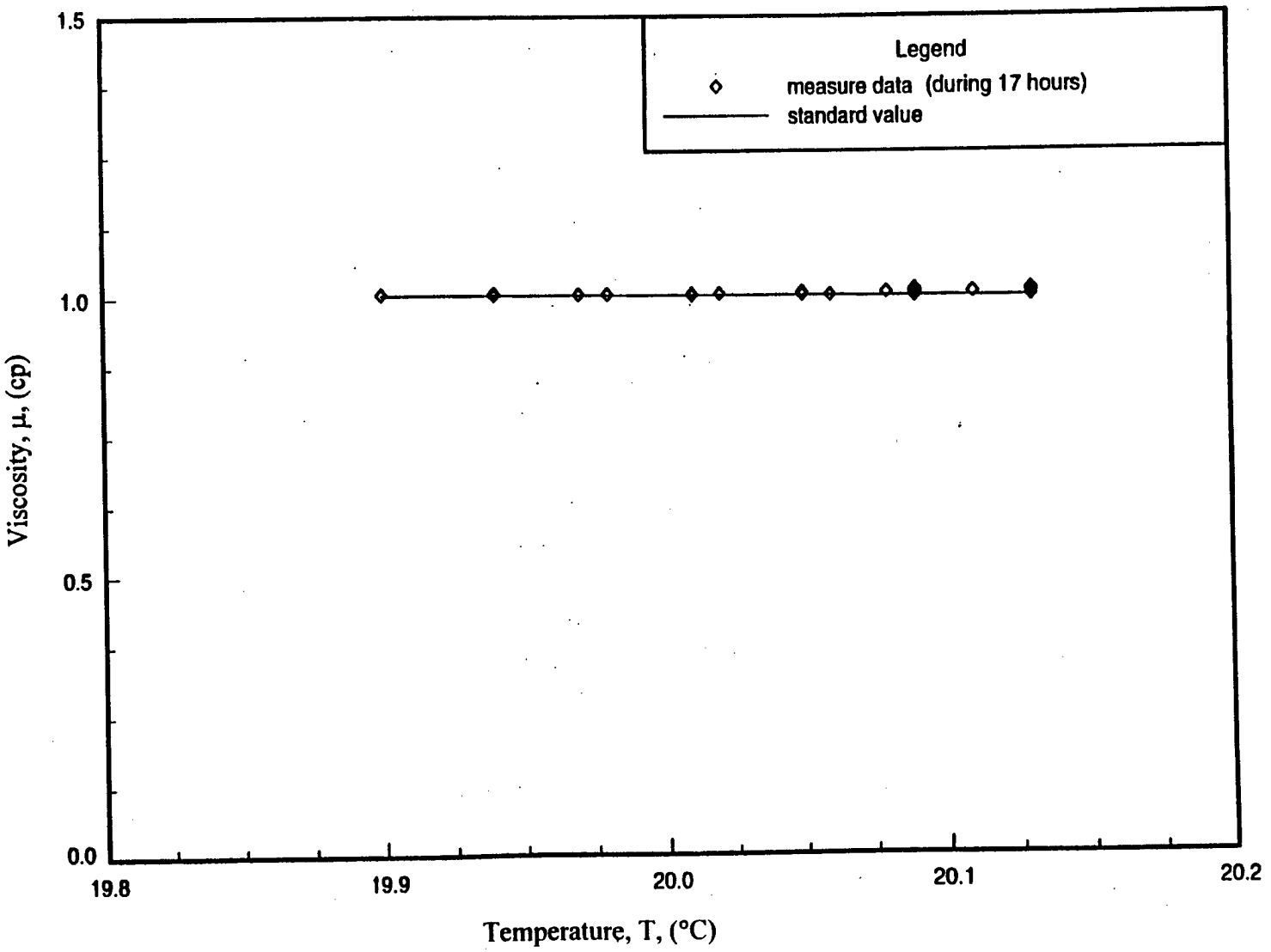

Figure 5.15: Pure water measured viscosity as a function of temperature.

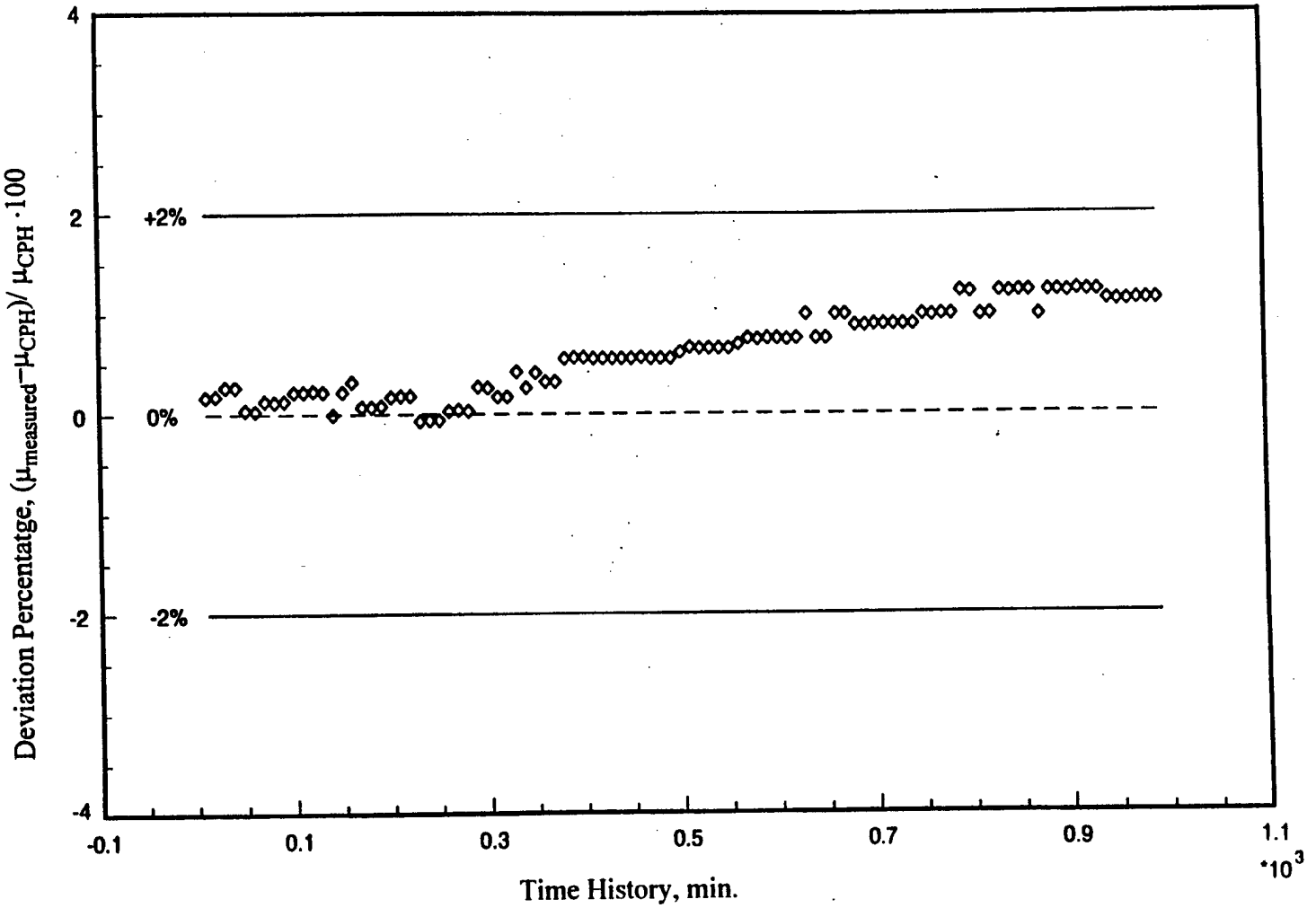

Figure 5.16: Pure water measured viscosity deviation for stability test.

EXPERIMENTAL OPERATION

This section describes the operation of the test rig and the experimental procedures. In order to obtain reliable test data, the test system should be operated under specific procedures. Based upon operational experiences, these procedures must be followed by the operator in order to achieve success. The test procedures are outlined in the following discussion.

Test System Preparation

Before charging the facility with refrigerant, the test system should be evacuated. A system pressure less than 2.76 *kPa* is considered to be evacuated enough and ready for charging refrigerant. The chiller can be turned on and the chiller working fluid can be circulated through the heat exchangers while the pressure approaches 2.76 *kPa*. Meanwhile, the refrigerant to be used can be pre-heated in order to increase the pressure which eases transfer into the system. During this time, the data acquisition system is monitoring the status of the system.

Some potential problems can occur if proper preparations are not made. These are:

- Check the material compatibility of refrigerant test system materials with refrigerants in all wet parts (seals). Elastomer material, such as pressure relief valve seals, accumulator bladder, and pump diaphragm could be eroded by refrigerants due to incompatibility.
- Leakage of the system could cause a loss of refrigerant or an intake of atmospheric air. This could cause problems if non-condensable gases were to exist in the system, and an adequate system evacuation could be difficult to achieve. Leaks should be detected and fixed for losses of 14 *kPa* (or more) in a 24-hour period.
- In order to store more refrigerant in the accumulator, chiller glycol must be circulated around the accumulator in order to keep the refrigerant cool and ease charging the accumulator. In addition, the bladder of the accumulator should be pre-charged to a pressure up to 276 *kPa* in order to control the space for receiving the refrigerant. Failure to do this will result in improper functioning of the accumulator.
- Check all the valves to make sure they are appropriately opened or closed.
- Monitor the system status to see if its properties are in the desired range (pressures and temperatures).
- Ensure that a refrigerant cylinder is used as a buffer for overcharged refrigerant, this is required by the facility for reclaiming extra refrigerant due to density changes (temperature fluctuations). This cylinder should be properly evacuated when hooked up to the system.

Viscometer Preparation

The type of viscometer used measures the oscillation frequency of a cylinder sensor which is immersed in the refrigerant in a sample cell. There are eight bolts surrounding the flange to connect the transmitter portion and the sample cell. The torque balance of the bolts is very sensitive to the frequency output which is converted to a digital current output to the DAS (data acquisition system). The following procedures are required for viscometer preparation:

- Carefully lift up the viscometer sensor and carefully clean the sensor surface with a soft tissue to make sure no impurities are deposited on the surface.
- Check the gasket material and inspect for any damage. Replace it if it is necessary.
- Carefully place the sensor into the sample cell while lining up all the bolts.
- Tighten each of the eight bolts to a torque of 45 $lb_f - ft$.
- Eliminate all possible vibration sources in order to avoid any effects on the measured frequency.
- Adjust the potentiometer of the viscometer console to zero voltage output at a current at 4 mA when the sensor is subjected to complete evacuation (no material). If this is not properly done, an inaccuracy could be introduced in the measurement.

Charging Refrigerants

The following steps outline the procedures for charging refrigerants:

- Make sure the system is evacuated at a proper pressure and the chiller glycol-water mixture is circulating in the heat exchangers.
- Slowly open the valve and let refrigerant flow into the system.
- Watch the sight-glass to make sure refrigerant is flowing into the system.
- Make sure the liquid refrigerant fills the housings of the refrigerant pumps. Then, turn on the pumps and operate at a low speed.
- Release the nitrogen gas inside the accumulator to allow proper space for the storage of liquid refrigerant.
- Continue charging refrigerant until the refrigerant is seen to fully fill the plastic tubes at the highest point of the system. Then close the refrigerant valve.
- When the refrigerant is properly charged, glycol circulating around the accumulator could be disconnected. Charge nitrogen pressure into the accumulator to the desired pressure.
- When charging a non-azeotropic refrigerant mixture, because of the influence of composition on the mixture's properties, a liquid mixture must be charged to the test system. Vapor charging should be avoided. In addition, to prevent the composition from changing, the use of distilled refrigerants should also be avoided.

System Operation and Data Acquisition

Data are taken under steady-state conditions. The following steps control steady-state operation:

- Apply power to the heat tape and adjust power to desired wattage by the Variac.
- Apply pressure by adjusting the nitrogen regulation valve of the supply tank.
- Adjust the pump speed controller to control the refrigerant mass flow rate.
- Adjust the controlling valve of the glycol-water mixture to a desired flow rate as indicated by the rotameter.
- Steady-state in the test section has been achieved when the heat input equals the heat removed. Repeat any of the above steps as required for reaching steady-state.
- Steady-state is considered to be reached by monitoring the inlet and outlet temperature change of the test section within ±0.05°C between two scans (approximately one minute). Then, a data point is determined as the average value of 20 consecutive scans.
- Another test point may be taken by repeating the above procedures for a different inlet temperature, mass flow rate of refrigerant, or mass flow rate of chiller glycol.

Injecting Lubricant and Sampling Lubricant Concentration

Lubricant concentration is an important quantity for understanding the lubricant's effects on properties. There are a number of methods which could have been adopted in the current study, such as the light absorption method [71], vibrating U-tube densimeter sensor and ultrasonic acoustic sensor [72,73], viscometer lubricant concentration sensor [74], and sampling mass method. In the current study, the last method was adopted over the other methods due to their limited availability.

The injection of lubricant into the test system is achieved by an oil-injection piston with a 15.24-cm stroke. The lubricant concentration sample cell is in line with the injection cylinder. This assembly is placed at the inlet portion of the test section. The schematic diagram is shown in Figure 5.17. A picture of the oil-injection assembly and oil-sample device is shown in Figure 5.18. The operational procedures are described as follows.

Oil Injection--

- Evacuate the dead space of the piston cylinder assembly and fully close the valve at the oil outlet after completing evacuation.
- Evacuate the upper volume of the cylinder above the piston and fully close the upper valve after finishing the evacuation.
- Suck oil into the cylinder from the lower oil outlet by slowly opening the needle valve while preventing air from leaking into the cylinder.
- Close the lower needle valve when finished charging the oil.

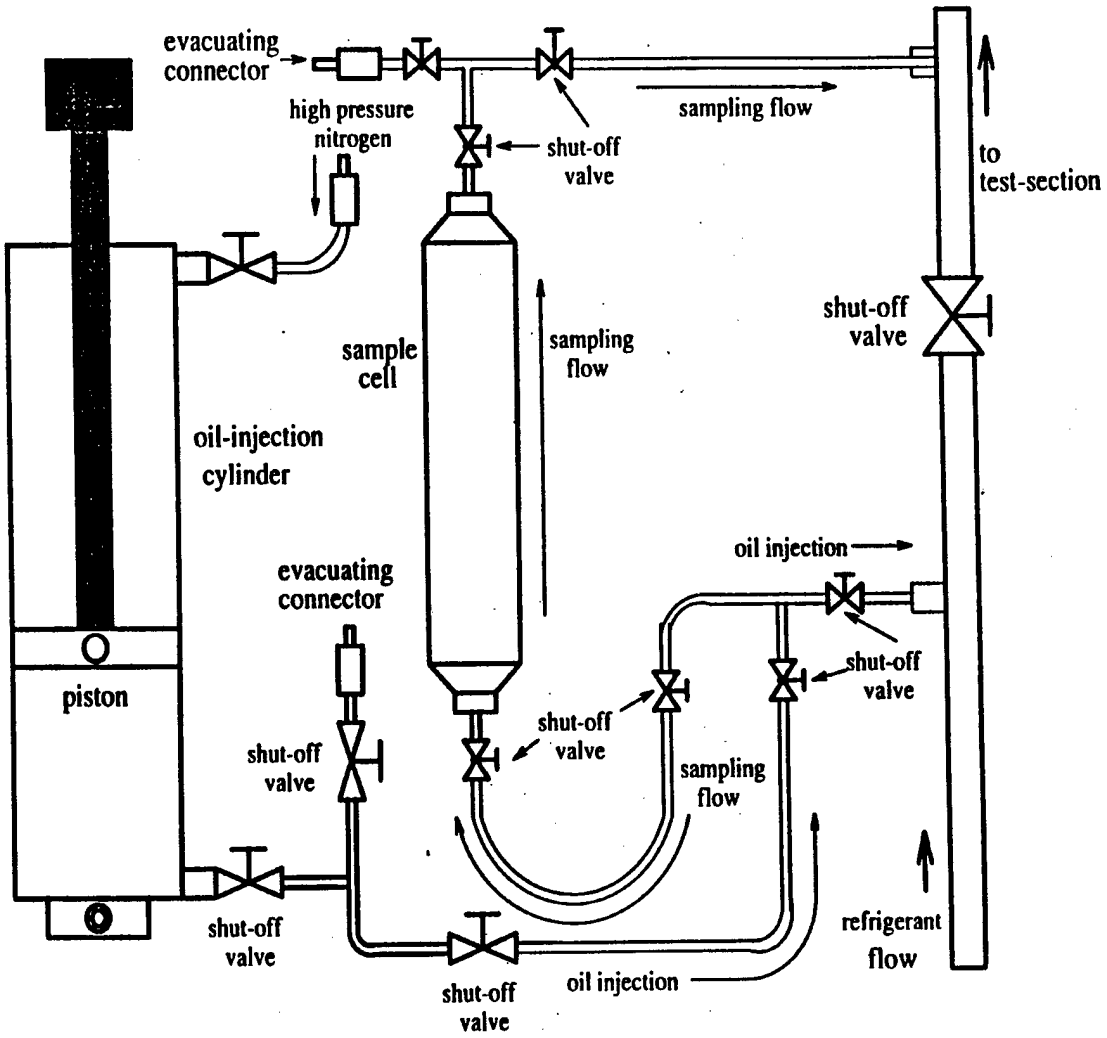

Figure 5.17: Schematic diagram of oil injection and sampling devices.

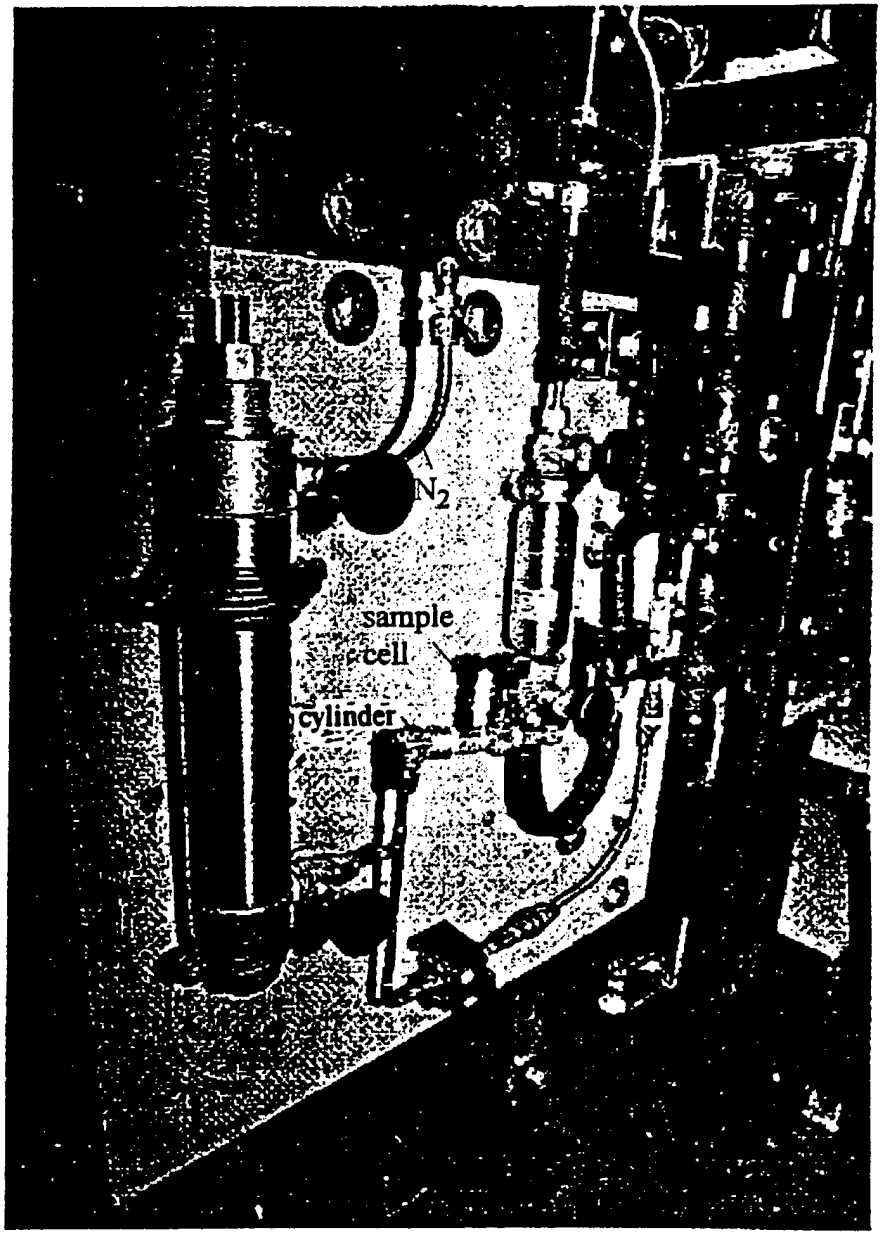

Figure 5.18: Photograph of oil injection and sample cell.

- Place the cylinder up-side-down and evacuate gases from the cylinder top by hooking up an evacuating hose to remove the residual air remaining or dissolved in the oil.
- Install the cylinder at the position for oil injection.
- Open the valves connected to the test system and apply high pressure nitrogen at the top of the piston.
- Inject oil into the system until the desired amount of oil is injected.
- Circulate refrigerant while the oil is being injected and continuously circulate for at least 10 hours to insure the oil is uniformly mixed with the refrigerant. Finally, sample the lubricant concentration in the refrigerant.

Lubricant Concentration Sampling--

- Close the valves of the sample cell to isolate it from the system.
- Remove the sample cell and weigh the total mass of the cell including the refrigerant and lubricant.
- Slowly open the top valve of the sample cell to allow the refrigerant to evaporate from the cell. An oil absorber hooked up to the cell can be used when the vacuum pump is operated.
- Weigh the cell and oil inside the cell and record until the weight remains constant.
- Calculate the oil concentration by dividing the net oil weight (oil in the cell + oil in the oil-absorber) by the total mixture weight (refrigerant + oil).

CHAPTER 6

THEORY OF THERMAL CONDUCTIVITY MEASUREMENT

In this chapter, the theory of thermal conductivity measurement will be described. Two methods were developed in this study, which will be referred to as Approach 1: The Nusselt number method, and Approach 2: The Prandtl number method. In Approach 1, the heat transfer characteristics of the test section and Nusselt number correlations were used to obtain the thermal conductivity, while in Approach 2, the thermal conductivity was directly related to the Reynolds number, Re_D, and the temperature characteristics of the test-tube. The detailed mathematical approaches are described below.

APPROACH 1: THE NUSSELT NUMBER METHOD

In this method, the thermal conductivity is obtained from heat transfer characteristics of a heated test-tube. From experimental measurements, an average heat transfer coefficient for single-phase conditions in the test-tube can be determined. Meanwhile, the heat loss from the test-tube can also be measured for a specific test-tube. The average Nusselt number was calculated from the heat transfer measurements, and the thermal conductivity was then calculated from the Nusselt number. Details of the measuring principles are described as follows.

Heat Transfer Measurement

The average heat flux is calculated from the following equation:

$$q'' = \bar{h}\,(\bar{T}_w - \bar{T}_f) \tag{6.1}$$

Thus, the average heat transfer coefficient can be written as:

$$\bar{h} = \frac{q''}{(\bar{T}_w - \bar{T}_f)} \tag{6.2}$$

where $\bar{T}_w$ and $\bar{T}_f$ are the average tube wall temperature and fluid temperature, respectively. The quantity $\bar{T}_w - \bar{T}_f$ can be calculated from either the individual average wall temperature, $\bar{T}_w$, and fluid temperature, $\bar{T}_f$, or the

quantity $\bar{T}_w - \bar{T}_f$, which is described in a later section. The net heat transfer rate, $\dot{q}_{net}$, to the fluid can be calculated from the total heat input from the power applied, $\dot{q}_{tot}$, and heat loss to the environment, $\dot{q}_{loss}$, as follows:

$$\dot{q}_{net} = \dot{q}_{tot} - \dot{q}_{loss} \tag{6.3}$$

The purpose of measuring heat loss from the test section, $\dot{q}_{loss}$, is to obtain the net heat input to the test section, $\dot{q}_{net}$. The heat loss is transferred to the environment around the test section by a combination of natural convection and radiation. For calculating the heat loss, the following equation is used:

$$\dot{q}_{loss} = \bar{h}_o A_o (\bar{T}_s - \bar{T}_a) \tag{6.4}$$

where $\bar{T}_s$ and $\bar{T}_a$ are the average outer insulation surface temperature over area, A_o, and the ambient room temperature, respectively, which can be obtained from experimental measurements. The average heat transfer coefficient for the heat loss of the test section, $\bar{h}_o$, can be determined and calibrated from experimental measurements with a fluid of known specific heat, *Cp*. This equation has already been shown in Chapter 5 as Equation 5.1. Once the heat loss characteristics of the test section are obtained, they can be applied to the *Cp* calculation for the other unknown fluids.

By knowing the test section heat loss characteristics, the $\dot{q}_{net}$, can be calculated from an energy balance for a working fluid. Then, *Cp* for an unknown fluid can be obtained as follows:

$$Cp = \frac{\dot{q}_{net}}{\dot{m}(\bar{T}_o - \bar{T}_i)} \tag{6.5}$$

where $\bar{T}_i$ and $\bar{T}_o$ are the mean inlet and outlet fluid temperatures, respectively, while $\dot{m}$ is the mass flow rate. This specific heat determination is important for new refrigerant mixtures and blends and for refrigerant/lubricant mixtures when non-ideal mixing occurs. In both cases, a theoretical calculation of *Cp* for the pure fluids (either the pure refrigerant or pure lubricant) will not result in an accurate specific heat value.

Nusselt Number Correlations

Heat transfer data are usually given by the Nusselt number which is defined as $\bar{h}D/k$. A number of single-phase Nusselt number correlations have been published for convection heat transfer. Some examples are the Dittus-Boelter correlation [75,76], the Petukhov and Popov correlation [77], and the Gnielinski correlation [78]. These three correlations are given below:

The Dittus-Boelter correlation (for heating):

$$\bar{N}u_D = 0.023 Re_D^{0.8} Pr^{0.4} \tag{6.6}$$

The Petukhov correlation:

$$\bar{N}u_D = \frac{(f/8)\, Re_D Pr}{1.07 + 12.7\,(f/8)^{1/2}\,(Pr^{2/3} - 1)} \tag{6.7}$$

The Gnielinski correlation:

$$\bar{N}u_D = \frac{(f/8)\,(Re_D - 1000)\, Pr}{1 + 12.7\,(f/8)^{1/2}\,(Pr^{2/3} - 1)} \tag{6.8}$$

where f is friction factor. For smooth tubes, expressions for f are:

Petukhov correlation,

$$f = (1.82 log_{10} Re_D - 1.64)^{-2} \tag{6.9}$$

Gnielinski correlation,

$$f = (0.79 ln Re_D - 1.64)^{-2} \tag{6.10}$$

In the above equations, Re_D and Pr are defined as:

$$Re_D = \frac{\rho \bar{V} D}{\mu} \tag{6.11}$$

$$Pr = \frac{\mu Cp}{k} \tag{6.12}$$

As mentioned previously, with $\bar{h}$ and $\dot{m}$ known, the thermal conductivity can be obtained from the equality by setting the Nusselt number, $\bar{h}D/k$, equal to the above correlations, Equations 6.6, 6.7, or 6.8.

Calibration Function

The method used to determine thermal conductivity involves applying the Nusselt number correlations and solving for the thermal conductivity. Therefore, an accurate Nusselt correlation is necessary in order to obtain an accurate value of thermal conductivity. Although some published Nusselt correlations have claimed good accuracy, their calibrations from the heat transfer data are still needed. This is because the correlations were obtained by curve fitting a large number of data with a wide range of Pr and Re_D, which might not apply to some specific fluids with a limited range of Pr and Re_D. Moreover, the thermal conductivity was originally used for obtaining those correlations. Now it will be obtained in a reversed manner. Therefore, in order to obtain an acceptable thermal conductivity, an accurate Nusselt correlation is required in the specific range of Pr and Re_D.

The method used for calibrating Nusselt number correlations assumes a calibrated function exists between the values of Nusselt number calculated from the correlations and definition. The calibration function will be denoted as *CF*. With this assumption, a set of *CF* values can be obtained from experimental data. Then, the CF correlations can be obtained by a curve fit for various *Pr* and Re_D. The mathematical procedures are interpreted as follows.

The definition of the average Nusselt number is:

$$\bar{N}u_D = \frac{\bar{h}D}{k} \tag{6.13}$$

The CF, therefore, exists between $\bar{N}u_D$ and correlations like

$$CF = \frac{\bar{N}u_{D_{experiment}}}{\bar{N}u_{D_{correlation}}} = F(Pr, Re_D) \tag{6.14}$$

The calibrated Dittus-Boelter correlation (for heating):

$$\bar{N}u_D = 0.023 Re_D^{0.8} Pr^{0.4} CF \tag{6.15}$$

The calibrated Petukhov correlation:

$$\bar{N}u_D = \frac{(f/8)\, Re_D Pr}{1.07 + 12.7\,(f/8)^{1/2}\,(Pr^{2/3} - 1)}\, CF \tag{6.16}$$

The calibrated Gnielinski correlation:

$$\bar{N}u_D = \frac{(f/8)\,(Re_D - 1000)\, Pr}{1 + 12.7\,(f/8)^{1/2}\,(Pr^{2/3} - 1)}\, CF \tag{6.17}$$

Regression of the Calibration Function

Because the Re_D and *Pr* are not of the same order of magnitude, a logarithmic transformation function is applied for convenience. Other types of transformations are possible. In the following equations, the superscript, *e*, denotes the curve fit equations obtained from measured data while the superscript, *c*, denotes curve fit equations obtained from correlations. Thus, Equation 6.14 becomes in natural logarithmic form:

$$\ln(\bar{N}u_D^e) = \ln \bar{N}u_D^c + \ln(CF) \tag{6.18}$$

or

$$\ln(CF) = \ln(\bar{N}u_D^e) - \ln \bar{N}u_D^c \tag{6.19}$$

A curve fit for $ln\ (CF)$ can then be obtained. A linear relationship between $ln\ (\bar{N}u_D / Pr^n)$ and $ln\ (Re_D)$ is well known from past knowledge. Therefore, an easy method to correlate these two logarithmic quantities is of the linear form:

$$ln\ (\bar{N}u_D / Pr^n) = A + B \cdot ln\ (Re_D) \tag{6.20}$$

where A, B, and n are the curve fit constants. Different constants were obtained from different applied correlations. The calibration function, CF, is therefore different for the various correlations and is denoted as:

$$CF = \frac{\bar{N}u_D^e}{\bar{N}u_D^c} \tag{6.21}$$

Once the calibration function, CF, is obtained as a function of Re_D and Pr, the modified Nusselt correlations can be used to determine thermal conductivity as shown in the following sections. With this assumption, a set of CF values can be obtained from experimental data and correlation calculations for different fluids. CF correlations can then be obtained by curve fitting CF with Pr and Re_D. The mathematical procedures are described below.

For heat transfer in tubes in this study, the following curve fit equations are used for experimentally measured Nusselt numbers, $\bar{N}u_D^e$, and correlation Nusselt numbers, $\bar{N}u_D^c$, respectively.

$$\bar{N}u_D^e = C^e Re_D^{a^e} Pr^{b^e} \tag{6.22}$$

$$\bar{N}u_D^c = CRe_D^a Pr^b \tag{6.23}$$

It should be noted that the Dittus-Boelter equation is already in this form while the other two in-tube equations (Equations. 6.7 and 6.8) must be curve fit into this form for consistent treatment. In addition, the magnitudes of Pr and Re are quite different. Again, a logarithmic function is recommended for convenient curve fitting. By dividing Equation 6.22 by Equation 6.23, CF can be expressed as:

$$CF = \frac{C^e}{C} Re_D^{(a^e - a)} \cdot Pr^{(b^e - b)} \tag{6.24}$$

Thermal Conductivity Calculations

After a calibrated $\dot{q}_{net}$ is obtained, the heat transfer coefficient can be calculated from an average $(\bar{T}_w - \bar{T}_f)$, which is measured. The Nusselt number will be obtained thereafter. Then, the thermal conductivity can be obtained from the calibrated Nusselt number correlations. However, the calibration function, CF, should be obtained from known property fluids. Once the calibration function, CF, is obtained as a function of Re_D and Pr, the thermal conductivity can be expressed in general form as follows.

$$k = \left[CF(Pr, Re_D)\left(\bar{N}u_{D_{correlation}}\right)\right]^{-1} \bar{h}^e D \tag{6.25}$$

where $\bar{h}^e$ denotes the average heat transfer coefficient from experimental measurements.

For each calibrated Nusselt number correlation, the k values are expressed as the following:

for Dittus-Boelter correlation:

$$k_d = \left[0.023\, Re_D^{0.8} Pr^{0.4} CF \right]^{-1} \bar{h} D \tag{6.26}$$

for Petukhov correlation:

$$k_p = \frac{1.07 + 12.7\,(f/8)^{1/2}(Pr^{2/3} - 1)}{CF\,(f/8)\,Re_D Pr}\,\bar{h} D \tag{6.27}$$

for Gnielinski correlation:

$$k_g = \frac{1 + 12.7\,(f/8)^{1/2}(Pr^{2/3} - 1)}{CF\,(f/8)\,(Re_D - 1000)\,Pr}\,\bar{h} D \tag{6.28}$$

For each of the three calibrated Nusselt correlations, the thermal conductivity equation is of a different form. The final equation for each correlation is presented below. It is important to note that the Prandtl number used in each theoretical correlation still contains the thermal conductivity, k. Each of the three correlations handles this problem differently.

- The k_d equation from the Dittus-Boelter correlation is:

$$k_d = \left[\frac{\bar{h}^e D}{C^e Re_D^{a^e} (\mu Cp)^{b^e}} \right]^{\frac{1}{b^e}} \tag{6.29}$$

- The Pr equation from the Petukhov and Popov correlation is:

$$Pr^{2/3} - \frac{C^e\,(f/8)^{1/2}\,Re_D^{(a^e - a + 1)}\,\mu Cp}{12.7\,C\bar{h}^e_D}\,Pr^{(b^e - b)} + \frac{1.07}{12.7\,(f/8)^{1/2}} - 1 = 0 \tag{6.30}$$

However, since k is implicit in Pr, k must be solved for by solving for Pr first from the above equation. In other words, k is divided into μCp to obtain Pr which is then treated as the unknown in the above equation. This equation is not an explicit linear type, but it can be solved by a numerical iteration such as the Newton-Raphson method. Once Pr is determined, the thermal conductivity, k, can be obtained from $\mu Cp / Pr$.

- The Pr equation from the Gnielinski correlation is:

As before, the k must be solved implicitly. The resulting Pr equation is:

$$Pr^{2/3} - \frac{C^e (f/8)^{1/2} Re_D^{(a^e - a)} (Re_D - 1000)\,\mu Cp}{12.7\,\bar{C}\bar{h}^e D} Pr^{(b^e - b)} + \frac{1}{12.7\,(f/8)^{1/2}} - 1 = 0 \qquad (6.31)$$

Again, Pr in this equation must be determined by a numerical iteration method.

APPROACH 2: THE PRANDTL NUMBER METHOD

In the previous section, the Nusselt number method was discussed for calculating thermal conductivity and the concept of the relative accuracy of the Nusselt number method by a calibration function. This section will follow similar concepts but bypass the Nusselt number to discuss the Prandtl method for thermal conductivity calculations. Unlike the hot-wire transient method for thermal conductivity measurements, this method has only recently been applied to thermal conductivity measurements. This method measures the Prandtl number, and the thermal conductivity is calculated by knowing the Prandtl number, viscosity, and specific heat. The mathematical approach follows.

Prandtl Number and Other Related Parameters

Based on past studies, the Nusselt number, $\bar{N}u_D^e$ in a turbulent channel flow was known as function of the Reynolds number, Re_D, and the Prandtl number, Pr. From the definition of Nusselt number, $\bar{N}u_D^e = \bar{h}D / k$ and the form of the Dittus-Boelter correlation, the following equation is rewritten to correlate heat transfer for a turbulent flow heated by the tube wall:

$$\frac{\bar{h}D}{k} = C \cdot Re_D^m \cdot Pr^n \qquad (6.32)$$

where $\bar{h}$ is the average heat transfer coefficient which equals $\dot{q}_{net} / A\Delta\bar{T}_{wf}$. By introducing $\dot{m}$, Cp, and the temperature difference of the fluid at the inlet and outlet, the above equation can be rearranged as:

$$\frac{\dot{m}Cp\,(\bar{T}_o - \bar{T}_i)\,D}{kA\,(\bar{T}_w - \bar{T}_f)} = C \cdot Re_D^m \cdot Pr^n \qquad (6.33)$$

After substituting the definitions of the Prandtl and Reynolds numbers, this equation can also be rewritten as:

$$Pr = \left[\frac{D}{4CL} Re_D^{(1-m)} \left(\frac{\bar{T}_o - \bar{T}_i}{\bar{T}_w - \bar{T}_f}\right)\right]^{\frac{1}{n-1}} \qquad (6.34)$$

In other words, the Prandtl number is expressed as a function of Re_D and a dimensionless temperature group, $(\bar{T}_o - \bar{T}_i) / (\bar{T}_w - \bar{T}_f)$. If this dimensionless temperature group is defined as ΔT^*, the relationship is expressed as:

$$Pr = F(Re_D, \Delta T^*) \qquad (6.35)$$

$$\Delta T^* = \frac{\bar{T}_o - \bar{T}_i}{\bar{T}_w - \bar{T}_f} \tag{6.36}$$

This is the relation for the measured *Pr*. It should be noted that all the quantities on the right hand side of Equation 6.34 can be obtained from experimental measurements. These involve $\dot{m}$, μ, $\bar{T}_w$, $\bar{T}_f$, $\bar{T}_i$, and $\bar{T}_o$. With the measurement of these quantities, the Prandtl number can be obtained. However, for fluids with known properties, the *Pr* can also be calculated from $\mu Cp / k$. Therefore, the thermal conductivity can then be calculated from *Pr*. This method is simpler than the Nusselt number calibration method.

Prandtl Number Expression

The *Pr* relationship has been shown in Equation 6.35 as a function of Re_D and ΔT^*. An expression for *Pr* in terms of Re_D and ΔT^* is required for easy use, and it requires calibration. This calibration for *Pr* is very important to the accuracy of the thermal conductivity measurement. The expression of Pr with Re_D and ΔT^* in a closed form is very difficult to obtain because it requires a number of test data. However, one of the represented approaches for this function is to directly express *Pr* as a function of Re_D and ΔT^* in a polynomial form. An example of a three-degree polynomial function is given as:

$$\begin{aligned} Pr = {} & a_0 + a_1 Re_D + a_2 \Delta T^* + a_3 Re_D^2 + a_4 (Re_D \cdot \Delta T^*) \\ & + a_5 \Delta T^{*2} + a_6 Re_D^3 + a_7 (Re_D^2 \cdot \Delta T^*) \\ & + a_8 (Re_D \cdot \Delta T^{*2}) + a_9 (\Delta T^{*3}) \end{aligned} \tag{6.37}$$

where the coefficients, a_i, can be fitted from measured data for fluids of known properties.

UNCERTAINTY ANALYSIS

This section describes the uncertainties in the thermal conductivity measurements by the methods of Approach 1 and Approach 2. A propagation-of-error method [79] is used to estimate the experimental uncertainties associated with each experimental measurement. The sensor and equipment uncertainties are listed in Table 6.1. The derivation of all related uncertainty equations is also presented in Appendix B, which includes the thermal conductivity uncertainty by Approach 1 (three correlations) and Approach 2, heat exchange rate uncertainty, Re_D uncertainty, friction factor (f) uncertainty, heat transfer coefficient ($\bar{h}$) uncertainty, ΔT^* uncertainty, and *Pr* uncertainty.

Sensor and Geometry Uncertainty

Based upon the uncertainties in the measured data (both sensor- and geometry-related), which is used to determine thermal conductivity, the uncertainty in k calculated from the three different correlations can be determined. Therefore, the uncertainty analysis for various ranges of Pr and Re_D was performed.

Sensor and geometry uncertainties are listed in Table 6.1.

TABLE 6.1: SENSOR AND GEOMETRY UNCERTAINTY

sources	uncertainty
length, L	0.1 *mm*
diameter, D, D_o	0.1 *mm*
mass flow rate, $\dot{m}$	0.15% in *kg/s*
temperature, $\bar{T}_i$, $\bar{T}_o$, $\bar{T}_w$	0.05°C
viscosity, μ	2.0% of measurement
specific heat at constant pressure, Cp	2.0% of measurement

Uncertainty Estimation and Comparison Between Approaches 1 and 2

Based upon the existing sensor and equipment uncertainties, the thermal conductivity uncertainties were estimated and compared. In Approach 1, the thermal conductivity calculated from the three different correlations was estimated for a typical operating condition. The results are tabulated in Table 6.2. Table 6.2 shows the uncertainty, presented as the percentage of measured thermal conductivity, by Approach 1 for the three Nusselt number correlations (see Appendix B). The uncertainty analysis was based upon the sensor and dimensional uncertainties listed in Table 6.1 for a particular operating condition listed at the bottom of Table 6.2. The uncertainty varies not only with the correlation used but also with various Re_D and Pr.

TABLE 6.2: THERMAL CONDUCTIVITY UNCERTAINTY PERCENTAGES FOR THREE NUSSELT NUMBER CORRELATIONS

case	Re_D	Pr	Ur_{dk}	Ur_{pk}	Ur_{gk}
at a small Pr	10000	1.0	6.75	6.43	6.35
	20000	1.0	6.79	7.42	6.97
	40000	1.0	6.92	8.61	7.81
	80000	1.0	7.29	10.29	9.13
	160000	1.0	8.29	13.33	11.67
at a moderate Re_D	80000	6.0	6.84	5.97	5.79
	80000	11.0	6.80	5.46	5.36
	80000	16.0	6.78	5.25	5.18
at a low Re_D	10000	1.0	6.75	6.43	6.35
	10000	6.0	6.73	5.08	5.24
	10000	11.0	6.73	4.90	5.09
	10000	16.0	6.73	4.82	5.01

operation conditions:
viscosity, μ: $2.0 \cdot 10^{-4}\ Pa \cdot s$
specific heat, Cp: $1.0\ kJ/(kg \cdot K)$
inlet temperature, T_i: 10°C
heat input rate, $\dot{q}$: $1\ kW$

From the uncertainty results shown in Table 6.2, it is learned that:

1. At a low Pr, when Re_D is higher, the uncertainty is larger. However, the uncertainty of k through the Dittus-Boelter correlation seems less affected by Re_D than the other two correlations.
2. At a moderate Re_D, Pr significantly affects the uncertainty of k for the Petukhov and Popov correlation and the Gnielinski correlation.
3. At a low Re_D, the uncertainty in k from these three correlations is not significant for a change in Pr.
4. From an overview of the uncertainty in k from these three correlations, the Dittus-Boelter correlation seems to be more stable than the other two correlations, even if these two correlations have smaller uncertainty values at some particular operating conditions.

Because CF is obtained from two Nusselt number ratios as mentioned earlier, the only uncertainty source of CF is from the Nusselt number curve fit, which will be dependent on the curve fit method used and how the data are fit.

It is interesting to compare the uncertainty differences between Approaches 1 and 2. From an overview, the variables involved in Approach 1, regardless of the correlation, are more complex than those in Approach 2. Therefore, it implies that the uncertainty of Approach 2 should be less than that in Approach 1. This point can be verified later. The thermal conductivity uncertainty percentages were calculated at some typical conditions of operation for both approaches (see Appendix B). The following figures plot the uncertainty percentage versus $\bar{T}_w - \bar{T}_f$. Figure 6.1 compares the results at T_i = 5°C and ΔT = 10°C ($\Delta T = T_o - T_i$), and Figure 6.2 compares the results at T_i = 5°C and ΔT = 20°C. From these two figures, the uncertainty of Approach 1 seems twice as large as the uncertainty in Approach 2. They show the same trends, and T_i and ΔT do not seem to be affected significantly. For other operating conditions, Figure 6.3 compares the results at T_i = 10°C and ΔT = 5°C, and Figure 6.4 compares the results at T_i = 10°C and ΔT = 20°C. Again, from these two figures, the trends are exactly the same as with the first two conditions. Therefore, these conclusions can be drawn:

- $\Delta\bar{T}_{wf}$ significantly affects the uncertainty of the measured thermal conductivity in both approaches.
- T_i and ΔT have less effect on the uncertainty of the measured thermal conductivity in both approaches.
- Approach 2 has less uncertainty than Approach 1.

SUMMARY OF APPROACHES

Two methods were discussed for the calculation of thermal conductivity: the Nusselt number calibration method and the Prandtl number method. In the Nusselt number calibration method, the uncertainty is caused by measured $\bar{h}$, $\dot{m}$, μ, Cp, and CF curve fittings. However, in the Prandtl number method, the uncertainty sources are only the Re_D (which depends on $\dot{m}$ and μ), the ΔT^*, and the Pr curve fits. The accuracy of the thermal conductivity measurement can be calculated from the uncertainty of each source. However, there are fewer variables used for the curve fits in the Prandtl number method than in the Nusselt number method. Therefore, the Prandtl number method is thought to be simpler and more convenient for obtaining thermal conductivity values.

Based upon the uncertainty analysis, the uncertainty of Approach 2 is only half of that for Approach 1. Approach 2 is therefore believed to be more accurate than Approach 1.

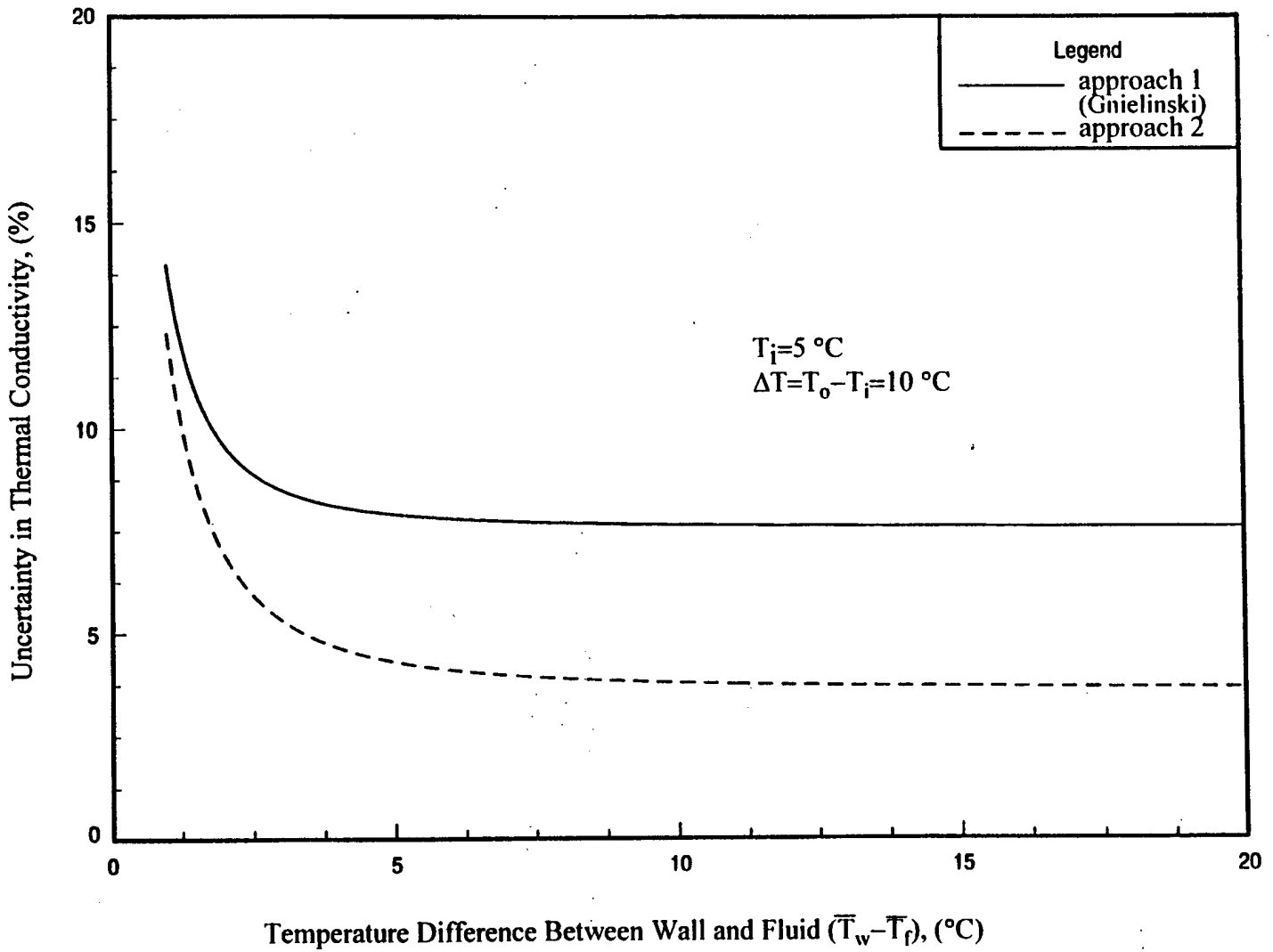

Figure 6.1: The uncertainty estimation at T_i = 5°C and ΔT = 10°C.

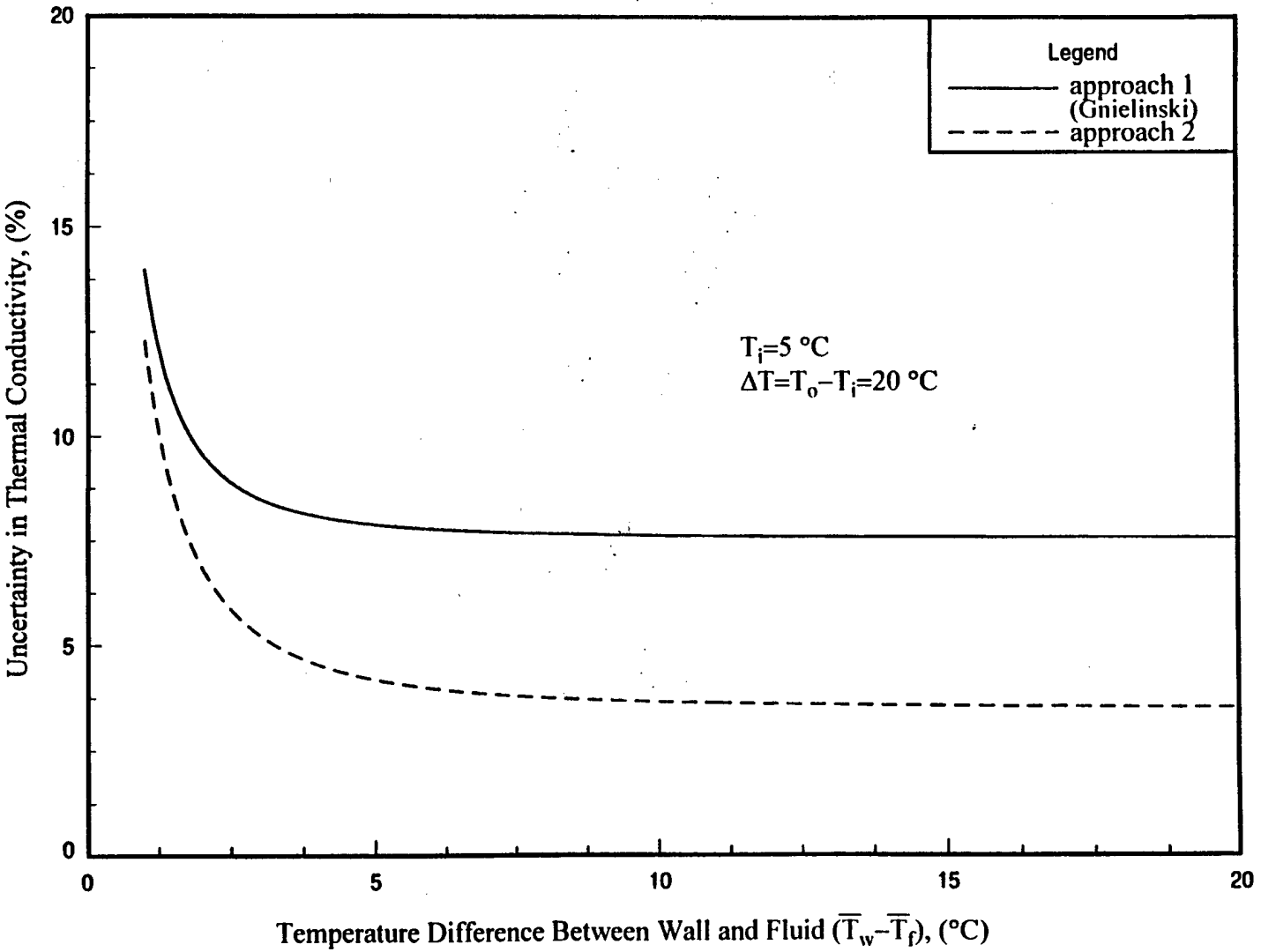

Figure 6.2: The uncertainty estimation at T_i = 5°C and ΔT = 20°C.

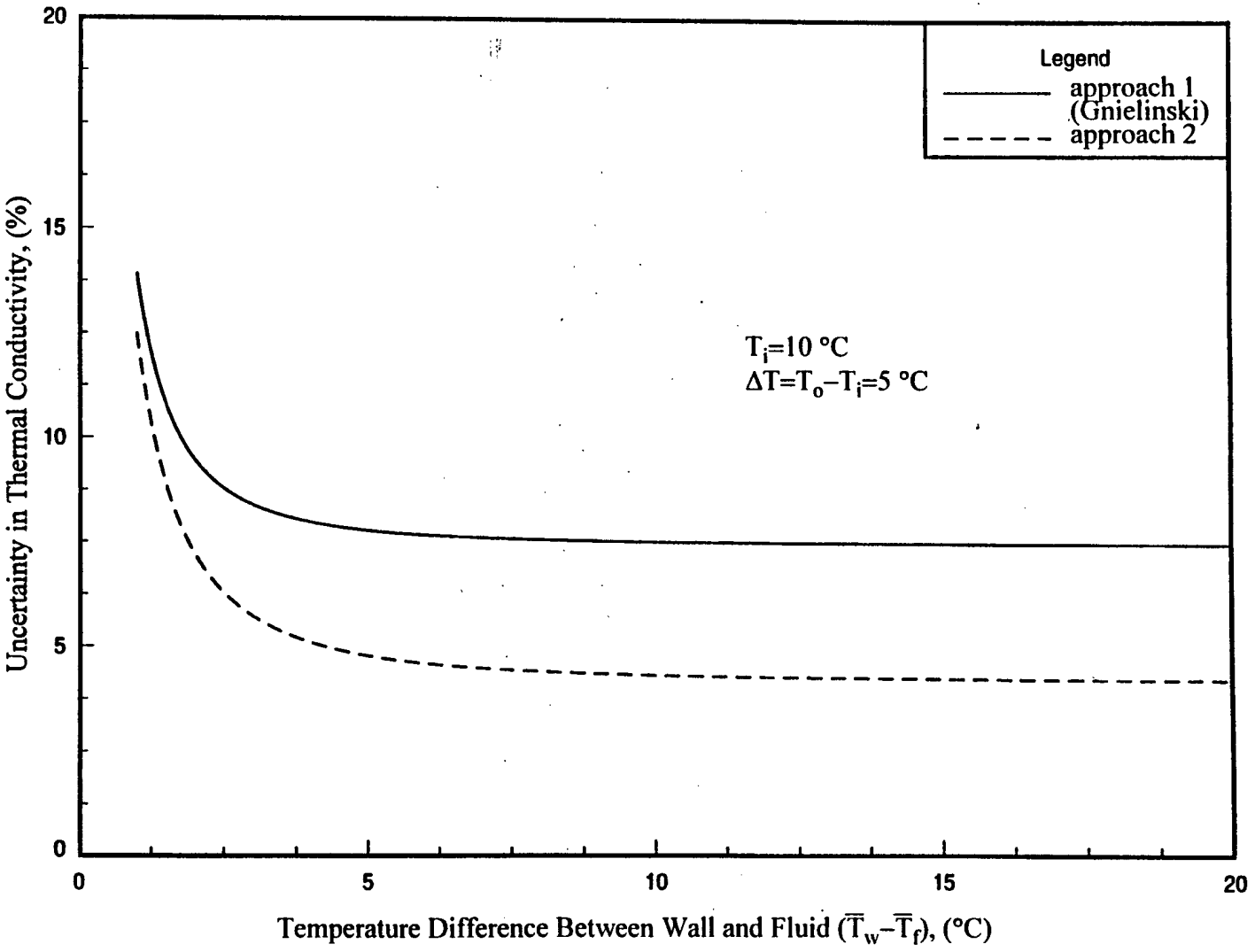

Figure 6.3: The uncertainty estimation at T_i = 10°C and ΔT = 5°C.

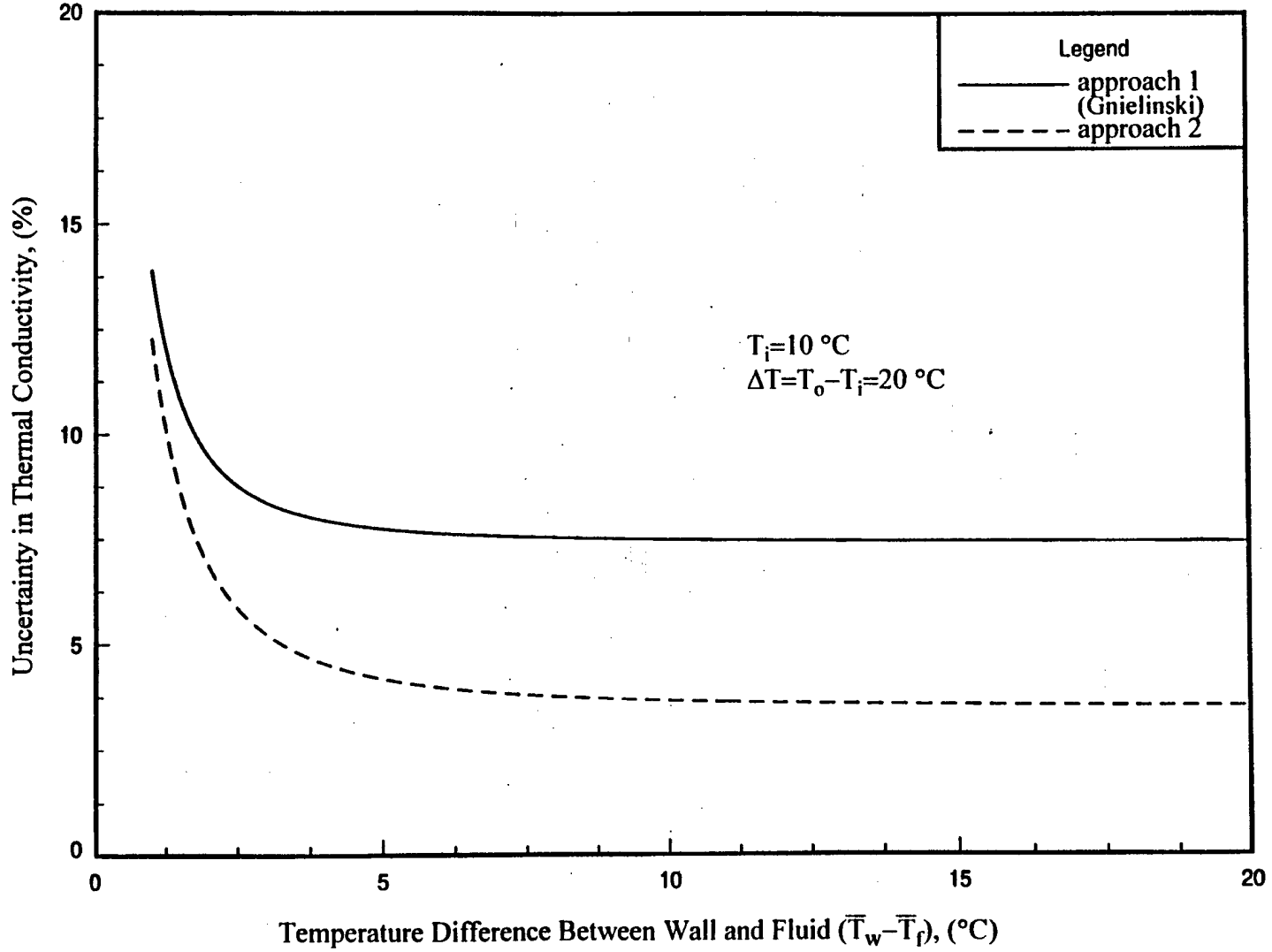

Figure 6.4: The uncertainty estimation at T_i = 10°C and ΔT = 20°C.

CHAPTER 7

EXPERIMENTAL DATA CALCULATIONS

In this chapter, the experimental analysis of the raw data is presented and the heat transfer coefficient calculation is described. Additionally, the thermal conductivity calculations from experimental data are also described. In the data analysis, each measured quantity was obtained by the average of 20 scans, and a FORTRAN program was then used to reduce the data. Appendix F contains a copy of the data analysis program. For regression of multiple variables, a SAS [80] program was also used for aiding in the correlation.

DATA REDUCTION

The data analysis procedure for the calibration refrigerants (HCFC-22, CFC-12, CFC-113, and/or CFC-114) and the measured refrigerant (HFC-236ea) is different for some treatments. However, for the raw data reduction, it follows the same procedure.

Inner Wall Temperature Corrections

In the test-tube used, the surface temperature is not measured on the actual inner tube wall surface because of the difficulty of installing thermocouple beads there. Instead of installment on the inner surface, all thermocouple beads for measuring wall surface temperature were buried midway into the wall. In order to obtain a more realistic surface temperature, a correction is required to obtain the real inner wall surface temperature. A correction equation was developed by a heat conduction model and is described as follows:

$$\dot{q}_{net} = \frac{2\pi L k_s (T_{r,2} - T_{r,1})}{ln\,(r_2/r_1)} \tag{7.1}$$

where $\dot{q}_{net}$ is net heat input rate, L is tube length (2 m in current test-tube), r_2 is the tube radius at the point where thermocouple beads are buried, r_1 is the inside radius of the tube, k_s is the thermal conductivity of solid tube (k_s = 401 $W/(m \cdot K)$ for pure copper), and $T_{r,1}$, and $T_{r,2}$ denote the temperature at r_1 and r_2, respectively. A correction temperature is then expressed as:

$$\Delta T_c = \frac{\dot{q}_{net} \ln (r_2/r_1)}{2\pi L k_s} \tag{7.2}$$

Therefore, the real inner wall temperature, $T_{r,1}$ is corrected by:

$$T_{r,1} = T_{r,2} - \Delta T_c \tag{7.3}$$

$T_{r,2}$ in this case is the measured temperature by a thermocouple.

Average Quantity Calculations

Average quantities include a timed average which indicates the average of measured quantities in a certain scanning time interval, and a location average which indicates the average of measured quantities in different positions. These average measured quantities are calculated as follows.

- Raw Data Average

In order to obtain a more average representation of the experimental data, 20 scans were taken for a steady-state situation, and these 20 values were then averaged for each representative quantity. These quantities include the following variables: T_i, T_o, T_{wi}, T_s, T_a, $\dot{m}$, $\dot{Q}$, and μ. Therefore:

$$average\ quantity = \frac{1}{n}\left[\sum_{i=1}^{n} (quantity)_i\right] \tag{7.4}$$

where n stands for the total number of scanning times ($n = 20$), and i represents the *i-th* scan.

- Average ΔT_{wf} Calculations

The average fluid temperature in the test-tube, $\bar{T}_f$, was therefore taken as the average temperature of the inlet and outlet temperature, $\bar{T}_i$ and $\bar{T}_o$, of the test-tube. However, in the average $\Delta \bar{T}_{wf}$ calculation, which is $\bar{T}_w - \bar{T}_f$, the finite control volume method was used which considers the local heat transfer characteristics (thermal entrance effect) rather than the all-points average method, Equation 7.5. The mathematical derivation is presented as follows. For the tube wall and fluid temperatures, the averages are calculated as the following:

$$\bar{T}_w = \left(\frac{1}{13}\right)(\bar{T}_{w1} + \bar{T}_{w2} + \cdots + \bar{T}_{w13}) \tag{7.5}$$

$$\bar{T}_f = \left(\frac{1}{2}\right)(T_i + T_o) \tag{7.6}$$

Equations 7.5 and 7.6 are used for obtaining an average wall temperature which assumes a linear wall temperature distribution. It is applicable for fully developed regions subjected to a constant heat flux. However,

the entrance effect, in some situations, is significant [29,76]. In those cases, the wall temperature distribution in that region is no longer linear. Therefore, if a linear average of the wall temperature is taken for the average wall temperature, that will affect the accuracy of the heat transfer coefficient calculation. Another approach, the finite control volume method mentioned above, is based on an energy balance which provides a better representation than the linear average method. This method is applied under the assumption of a constant heat flux situation. In this situation, the amount of heat added to a local section is everywhere equal as long as the surface area is equal. That means that an equal amount of heat is obtained for an equal length of heated section in a constant cross section area tube. An energy balance equation for a heated section can be expressed as:

$$\dot{Q} = \dot{q}_1 + \dot{q}_2 + \cdots + \dot{q}_i + \cdots + \dot{q}_n \tag{7.7}$$

where the subscript n represents the total number of subsections and i represents the *i-th* subsection.

Each $\dot{q}_i$ would be the same due to the constant heat flux, if each subsection has an equal surface area and the same property values. The above equation can also be written as:

$$\dot{Q} = q''(A_1 + A_2 + \cdots + A_i + \cdots + A_n) \tag{7.8}$$

However, since $\dot{Q}$ is equal to $\bar{h}A\Delta\bar{T}_{wf}$ the above equation can be rewritten as:

$$\Delta\bar{T}_{wf}\int_0^A h_x dA = q''(A_1 + A_2 + \cdots + A_i + \cdots + A_n) \tag{7.9}$$

or rewritten into the finite control volume form,

$$\Delta\bar{T}_{wf}\sum_{i=1}^{n} h_i A_i = q''(A_1 + A_2 + \cdots + A_i + \cdots + A_n) \tag{7.10}$$

Based upon the assumption of a constant heat flux in each subsection, h_i is equal to $q'' / \Delta T_{wfi}$. The ΔT_{wfi} is a locally averaged quantity, which is $\bar{T}_{w_i} - \bar{T}_{fi}$. Substituting h_i into above equation,

$$\Delta\bar{T}_{wf}\left[\sum_{i=1}^{n}\frac{q''A_i}{\Delta T_{wfi}}\right] = q''(A_1 + A_2 + \cdots + A_i + \cdots + A_n) \tag{7.11}$$

or,

$$\Delta\bar{T}_{wf}\left[\sum_{i=1}^{n}\frac{A_i}{\Delta T_{wfi}}\right] = A_1 + A_2 + \cdots + A_i + \cdots + A_n) = A \tag{7.12}$$

where A is the total heat transfer area.

Finally, the average temperature difference between the average wall temperature and fluid temperature can be expressed as:

$$\frac{1}{\Delta\bar{T}_{wf}} = \frac{1}{L}\sum_{i=1}^{n}\left(\frac{\Delta l_i}{\Delta T_{wfi}}\right) \tag{7.13}$$

Or, in another form,

$$\Delta\bar{T}_{wf} = \frac{L}{\sum_{i=1}^{n}\left(\frac{\Delta l_i}{\Delta T_{wfi}}\right)} \tag{7.14}$$

where Δl_i is the length of *i-th* section.

For the current test section, the wall temperature is measured at 13 locations. Finite control volumes, therefore, can be divided into 13 subsections. A typical wall temperature and average fluid temperature distribution is shown in Figure 7.1. Because of the entrance effect, the wall temperature at the inlet portion should reflect a non-linear distribution. For a better representation, smaller subsections were taken. Therefore, the determination of subsections at the inlet portion was based on the wall temperature at the measured points. Figure 7.2 shows the finite control volume configuration of the current test section. In this figure, the control volumes in the inlet and outlet portion were smaller than the middle portion because more temperatures were measured at the ends of the test section. This method for obtaining the average temperature difference was thought to be a better representation than average of the all-points method because it accounts for the thermal behavior of the entrance length. The subsection length distribution is listed in Table 7.1.

TABLE 7.1: SUBSECTION LENGTH DISTRIBUTION

subsection i	thermocouple point	distance from inlet, cm	Δl_i, cm
1	1	0	5
2	2	10	10
3	3	20	15
4	4	40	20
5	5	60	20
6	6	80	20
7	7	100	20
8	8	120	20
9	9	140	20
10	10	160	20
11	11	180	15
12	12	190	10
13	13	200	5

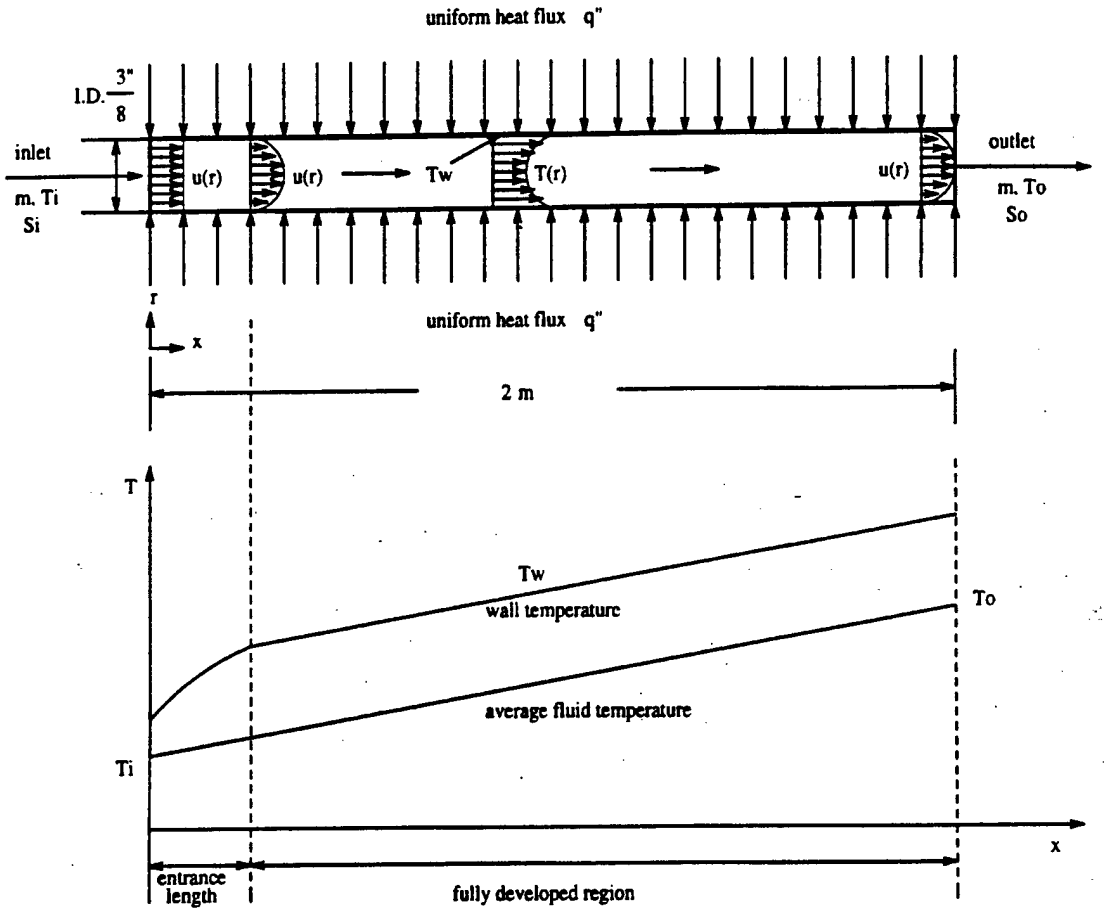

Figure 7.1: Typical temperature distribution along a heated test section.

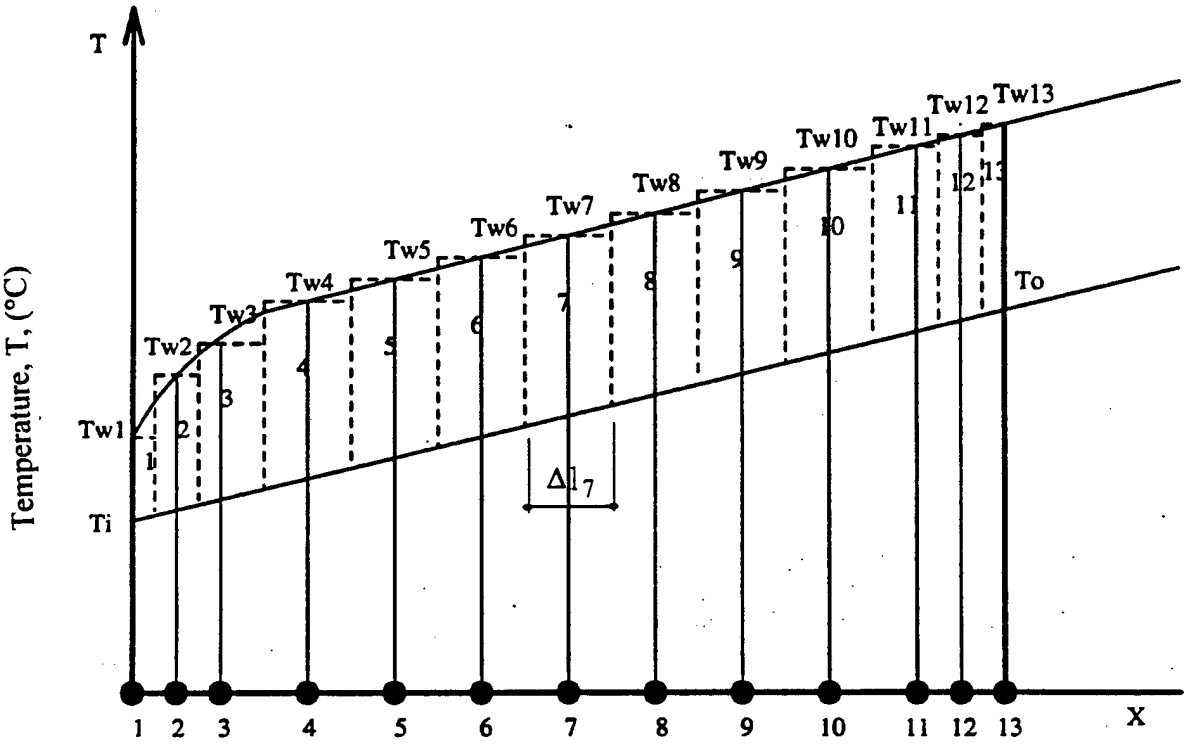

Figure 7.2: Finite control volume configuration of the test section.

Heat Transfer Calculations

One of the thermodynamic properties, specific heat (Cp), is used in calculating a single-phase heat transfer quantity, based upon the energy balance principle. This property, in general, is function of temperature and pressure. However, for a liquid at constant pressure, Cp is a function of temperature only. But, liquid Cp is not a strong function of temperature except above the reduced temperature, T_r, of 0.7 to 0.8. Detailed information on the description of Cp is given in thermodynamic and property textbooks [28,81].

The net heat input rate for refrigerants of known Cp was calculated directly from the energy equation for flow in the test-tube. That is, for refrigerants with known Cp:

$$\dot{Q}_{net} = \dot{m}\bar{C}p\,(\bar{T}_o - \bar{T}_i) \tag{7.15}$$

For refrigerants with unknown Cp, $\dot{Q}_{net}$ is calculated from the energy balance of the test section. That is, for refrigerants with unknown Cp, Equation 6.5 is applied. Then the $\dot{q}_{net}$ can be calculated from Equation 6.3.

$$\dot{Q}_{net} = \dot{Q}_{tot} - \dot{Q}_{loss} \tag{7.16}$$

In Equation 6.3, $\dot{q}_{loss}$ is the heat loss of the test section. A correlation for calculating $\dot{q}_{loss}$ was described in Equation 5.1 in Chapter 5. The heat transfer coefficients can be obtained by Equation 6.2. The parameters in this study, including $\bar{N}u_D$, Pr, $\bar{R}e_D$, and ΔT^*, were then calculated by their definitions presented earlier or defined in Chapter 6.

Viscosity and Thermal Conductivity Calculations

The product of viscosity and density is directly measured by the viscometer. The viscosity is then obtained by dividing it by density which is measured by a densimeter or obtained from reliable data sources, such as the ASHRAE Handbook [82] or REFPROP [83], which are shown in Appendix A.

There are two approaches proposed in this study. The thermal conductivity can be obtained using either one. However, except for thermal conductivity being directly calculated from the Dittus-Boelter correlation in Approach 1 (Equation 6.29) the other thermal conductivity correlations (Equations 6.30, 6.31, or 6.34) are developed from Pr. Therefore, Pr must be obtained before the thermal conductivity can be calculated.

CORRECTION OF THE PRESSURE EFFECT ON THERMAL CONDUCTIVITY AND VISCOSITY

Pressure has some effect on the thermal conductivity and viscosity of a liquid. However, these effects are usually significant only at high pressures. Thermal conductivity and viscosity are not only strong functions of temperature, but they are also strong functions of pressure when a liquid is subjected to a high pressure. The following discussion provides corrections for the pressure effects on thermal conductivity and viscosity.

Pressure Effect on Liquid Thermal Conductivity

In general, at moderate pressures, up to 5 or 6 MPa, the effect of pressure on the thermal conductivity of liquids is usually neglected, except near the critical point. Missenard has published a simple correlation for k which extends to high pressures [28]. The thermal conductivity ratio is subjected to two different pressures but at the same temperature. This ratio was found to correlate with reduced temperature and pressure as shown in the following equation:

$$\frac{k\,(P_r)}{k\,(low\ pressure)} = 1 + Q \cdot P_r^{0.7} \tag{7.17}$$

where P_r is reduced pressure and Q is a function of P_r and T_r. Q is given in Table 10-8 in R.C. Reid et al. [28]. A plot of thermal conductivity ratio against P_r is given by Figure 7.3.

Pressure Effect on Liquid Viscosity

Liquid viscosity will be affected by pressure, especially at high pressures. Increasing the pressure over a liquid results in an increased viscosity. However, at pressures less than the critical pressure, the pressure effect on viscosity is very weak. Lucas suggested that the change might be estimated from Equation 7.18 [28]:

$$\frac{\mu}{\mu_{sat}} = \frac{1 + D\,(\Delta P_r / 2.118)^A}{1 + C\omega\Delta P_r} \tag{7.18}$$

where

μ = viscosity of liquid at pressure of interest

μ_{sat} = viscosity of liquid at saturated state

ω = acentric factor

$\Delta P_r = (P - P_{vp}) / P_c$

P = liquid pressure

P_{vp} = vapor pressure

P_c = critical pressure

T_r = reduced temperature

$A = 0.9991 - [\,4.674 \cdot 10^{-4} / (1.0523\,T_r^{-0.03877} - 1.0513)\,]$

$D = [\,0.3257 / (\,1.0039 - T_r^{2.573}\,)^{0.2906} - 0.2086$

$C = -0.07921 + 2.1616\,T_r - 13.4040\,T_r^2 + 44.1706\,T_r^3 - 84.8291\,T_r^4 + 96.1209\,T_r^5 - 59.812\,T_r^6 + 15.6719\,T_r^7$

A plot of viscosity ratio versus ΔP_r is shown in Figures 7.4 and 7.5.

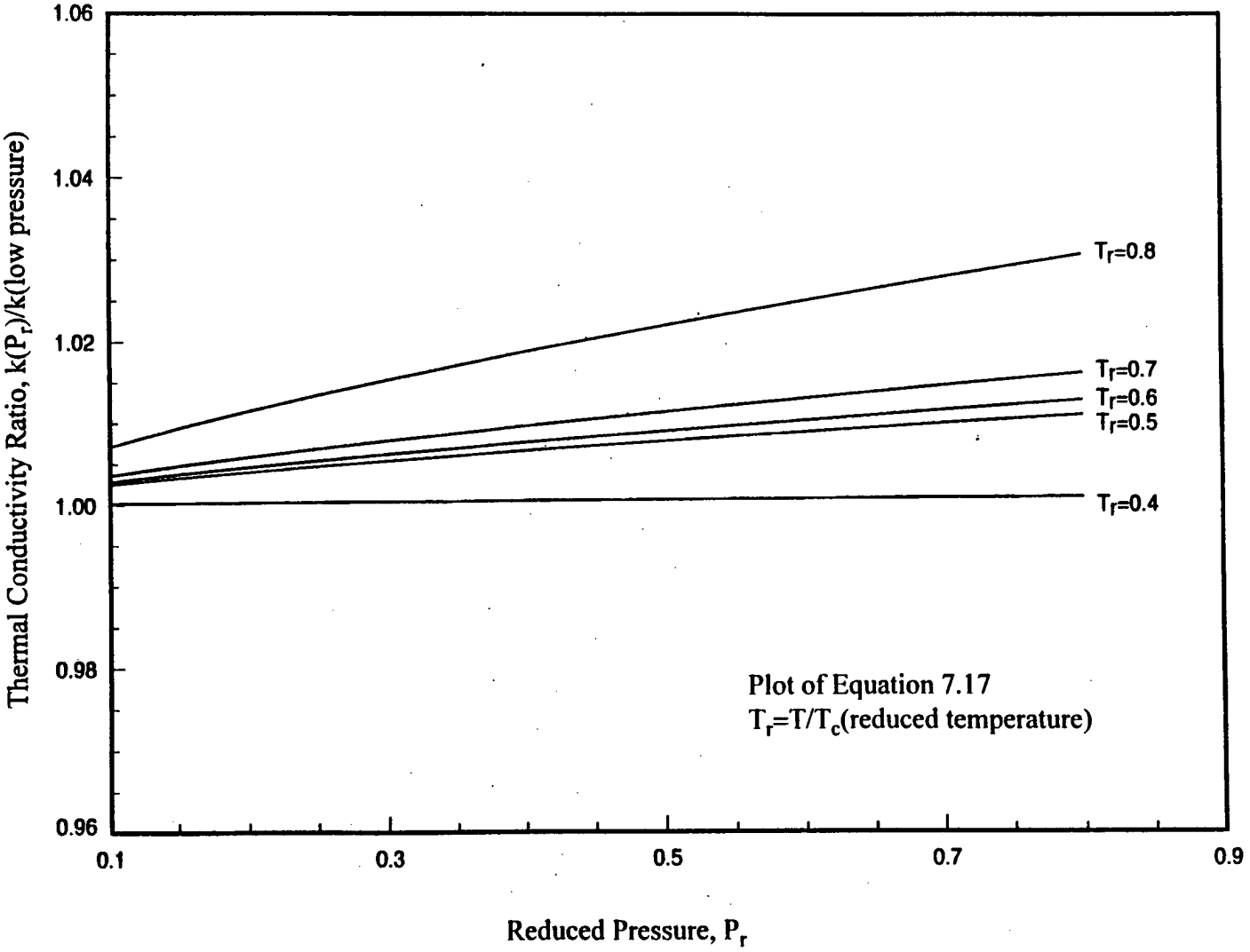

Figure 7.3: Pressure effect on liquid thermal conductivity.

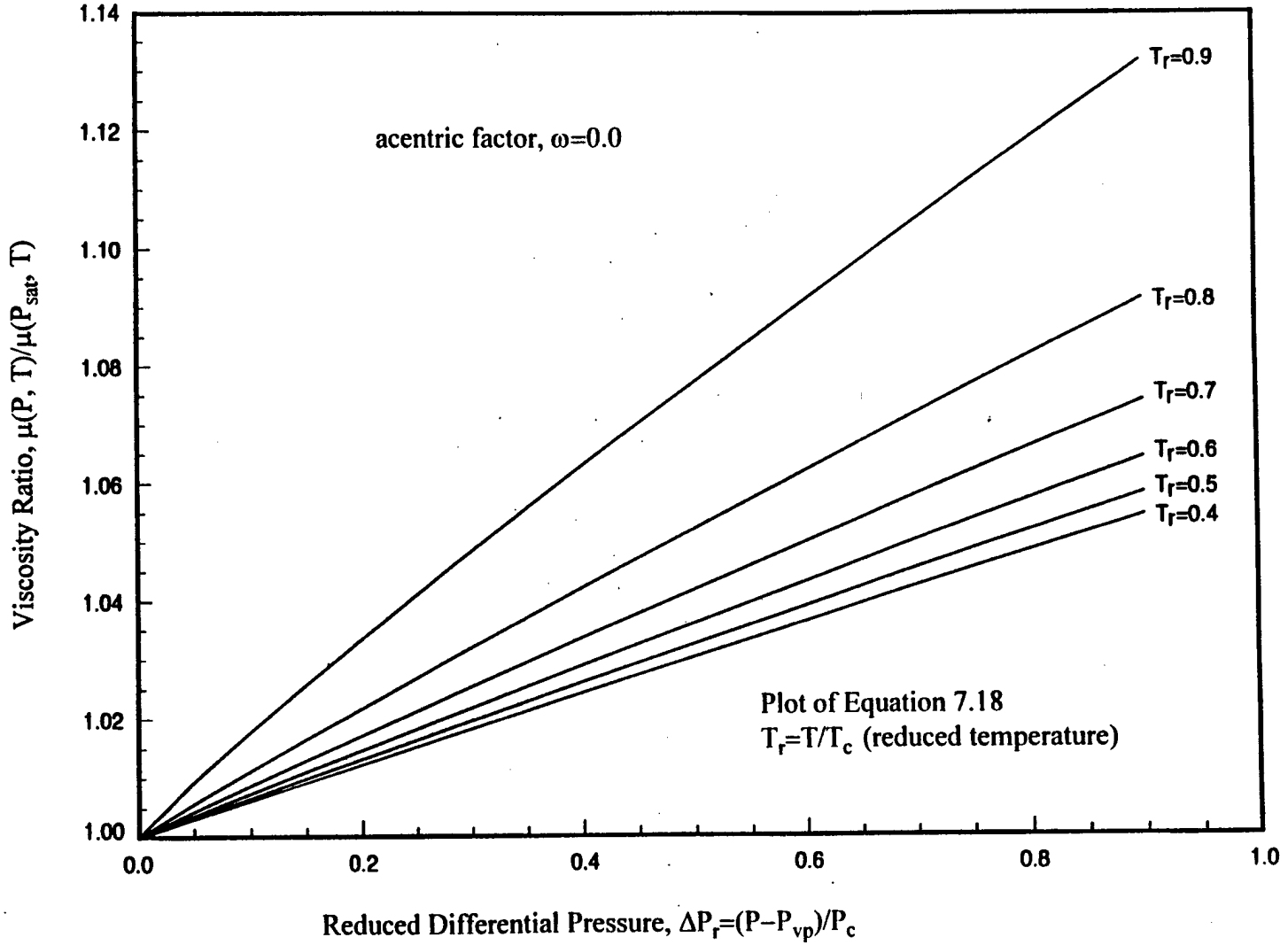

Figure 7.4: Pressure effect on liquid viscosity (ω = 0.0).

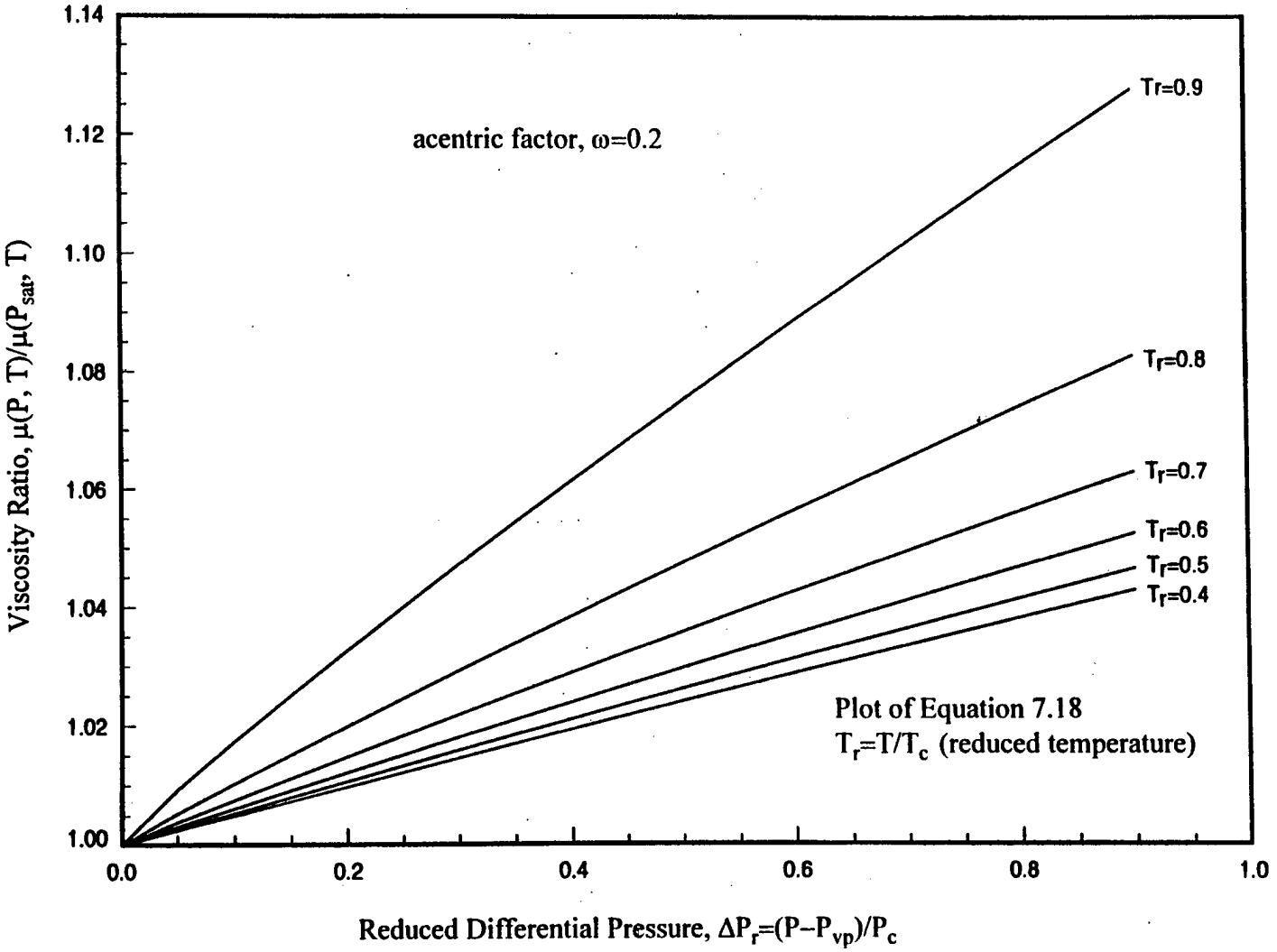

Figure 7.5: Pressure effect on liquid viscosity (ω = 0.2).

Thermal Conductivity and Viscosity Corrections for Pressure Effects

High pressure (higher than critical pressure) has a strong effect on viscosity and thermal conductivity, while low pressure has almost no effect or only a minor effect on them, as discussed in the above sections. In the current study, refrigerants were circulated in the low pressure range. Therefore, pressure had a very small effect on viscosity and thermal conductivity. However, to obtain accurate properties, pressure effects on both viscosity and thermal conductivity were still taken into account. The manner in which pressure effects were considered is outlined in Equations 7.17 and 7.18 for thermal conductivity and viscosity, respectively. Because the operating state must be controlled with limited subcooling at the outlet of the test section, the system pressure should also be greater than the saturation pressure to maintain a liquid phase throughout the test section. The viscosity and thermal conductivity at a selected pressure were obtained from those at the saturation pressure by using Equations 7.17 and 7.18. By reversing the usage of these equations and by knowing viscosity and thermal conductivity at a specific pressure, then the viscosity and thermal conductivity at the saturation pressure can also be obtained.

DATA PRESENTATION

This section describes the format used to present the data in order to identify trends for the purpose of data comparison. In general, the thermal conductivity and viscosity are strong functions of temperature and weak functions of pressure in a low pressure region. Therefore, the thermal conductivity and viscosity were presented only as a function of temperature. All the plots shown in this study were plotted as saturated liquid thermal conductivity and viscosity versus temperature. Measured data compared with the data in the ASHRAE Handbook and from REFPROP were also shown in the plots. The measured specific heat, Cp, and density, ρ, of interest versus temperature, T, were also plotted and compared with ASHRAE Handbook [82] or REFPROP [83] values.

CHAPTER 8

CALIBRATIONS OF THERMAL CONDUCTIVITY MEASUREMENT

In this chapter, calibration of the thermal conductivity measuring apparatus by using refrigerants of known properties will be shown and discussed for both approaches. The calibration function (*CF*) in Approach 1 and the correlation obtained by Approach 2 will be presented. In addition, the accuracy of the measured data by these approaches will also be presented.

CALIBRATION OF REFRIGERANTS AND OPERATING RANGES

Before measuring the thermal conductivity of HFC-236ea, the calibration functions should be obtained. The calibration functions have been obtained from several fluids with known properties by the method proposed in this study. Several refrigerants of known properties were selected in order to obtain the calibration functions. They were HCFC-22, CFC-12, CFC-113, and CFC-114. The properties used for these refrigerants are from ASHRAE data, and their curves are presented in Appendix A. Table 8.1 shows the operating ranges used to obtain the calibration functions of these selected refrigerants. The fluids (HFC-236ea, blends A and B) of unknown thermal conductivity must be tested within the *Pr* number ranges of the basic refrigerant data shown below. For HFC-236ea, as an example, with operating temperatures between 0°C and 50°C, the *Pr* number varies from 5.60 to 8.12, while Re_D can be controlled by regulating the mass flow rate within the ranges for the basic refrigerants listed above. Under most conditions, the mass flow rate varied from 3 kg/min. to 15 kg/min.

TABLE 8.1: PRANDTL NUMBER, REYNOLDS NUMBER, AND ΔT^* RANGES FOR SELECTED FLUIDS

refrigerant	Prandtl number (Pr)	Reynolds number (Re_D)	ΔT^*
HCFC-22	2.28 - 2.56	38360 - 184852	0.81 - 1.42
CFC-12	2.82 - 3.08	31031 - 168007	0.97 - 1.30
CFC-113	7.00 - 10.58	7970 - 64354	0.64 - 0.80
CFC-114	4.46 - 6.34	16296 - 99517	0.79 - 0.99
overall	2.28 - 10.58	7970 - 184852	0.64 - 1.42

CALIBRATION FUNCTIONS

The calibration functions were found for the three Nusselt correlations mentioned earlier. A linear regression between $ln(Nu / Pr^n)$ and $ln(Re_D)$ was performed for the experimental curve fits. In order to verify the current method for thermal conductivity measurement, the calibration refrigerants can be selected such that the calibration functions were obtained only for HCFC-22, CFC-12, and CFC-113, which covered the Pr number range from 2.28 to 10.58. These functions could then be applied to the calculation of unknown fluids such as CFC-114. Figures 8.1, 8.2, and 8.3 show the results for the three different Nusselt number correlations used for these calibration refrigerants.

The calibrated Nusselt number can be obtained from the curve-fitted equations such that:

$$\bar{N}u_{D_{experiment}} = CF \cdot \bar{N}u_{D_{correlation}} \tag{8.1}$$

where the calibration function, CF can be obtained from Equation 6.24.

As mentioned in Chapter 6, the Nusselt number can be obtained from the Dittus-Boelter correlation (Equation 6.6), the Petukhov and Popov correlation (Equation 6.7), and the Gnielinski correlation (Equation 6.8). Then, the Nusselt number can be expressed as the form of Re_D and Pr (Equations 6.22 and 6.23).

The coefficients from curves of the calibration functions are shown in Table 8.2 for $\bar{h}D/k$, in which $\bar{h}$ is experimentally measured, and for the three different Nusselt number correlations.

TABLE 8.2: CURVE-FIT COEFFICIENTS FOR NUSSELT NUMBER - THREE CALIBRATION REFRIGERANTS

coefficient	$\bar{h}D/k$	Dittus-Boelter	Petukhov	Gnielinski
C, C^e	0.006758	0.023	0.017266	0.012093
a, a^e	0.903770	0.8	0.827298	0.862783
b, b^e	0.502199	0.4	0.455283	0.441244

It should be noted that the calibration function, CF, is still expressed as function of Re_D and Pr. Therefore, like the $\bar{N}u_D$ expression in Equation 6.20, a linear relationship between $ln(CF/Pr^{b^e - b})$ and $ln(Re_D)$ holds true and can be described as follows:

$$ln(CF/Pr^{b^e - b}) = ln(C^e/C) + (a^e - a)\, ln(Re_D) \tag{8.2}$$

The plots of $ln(CF)$ versus $ln(Re_D)$ are shown in Figures 8.4, 8.5, and 8.6 for the CF obtained from the Dittus-Boelter, Petukhov and Popov, and Gnielinski equations, respectively. As indicated in these figures, the relationships are all linear with the various Pr.

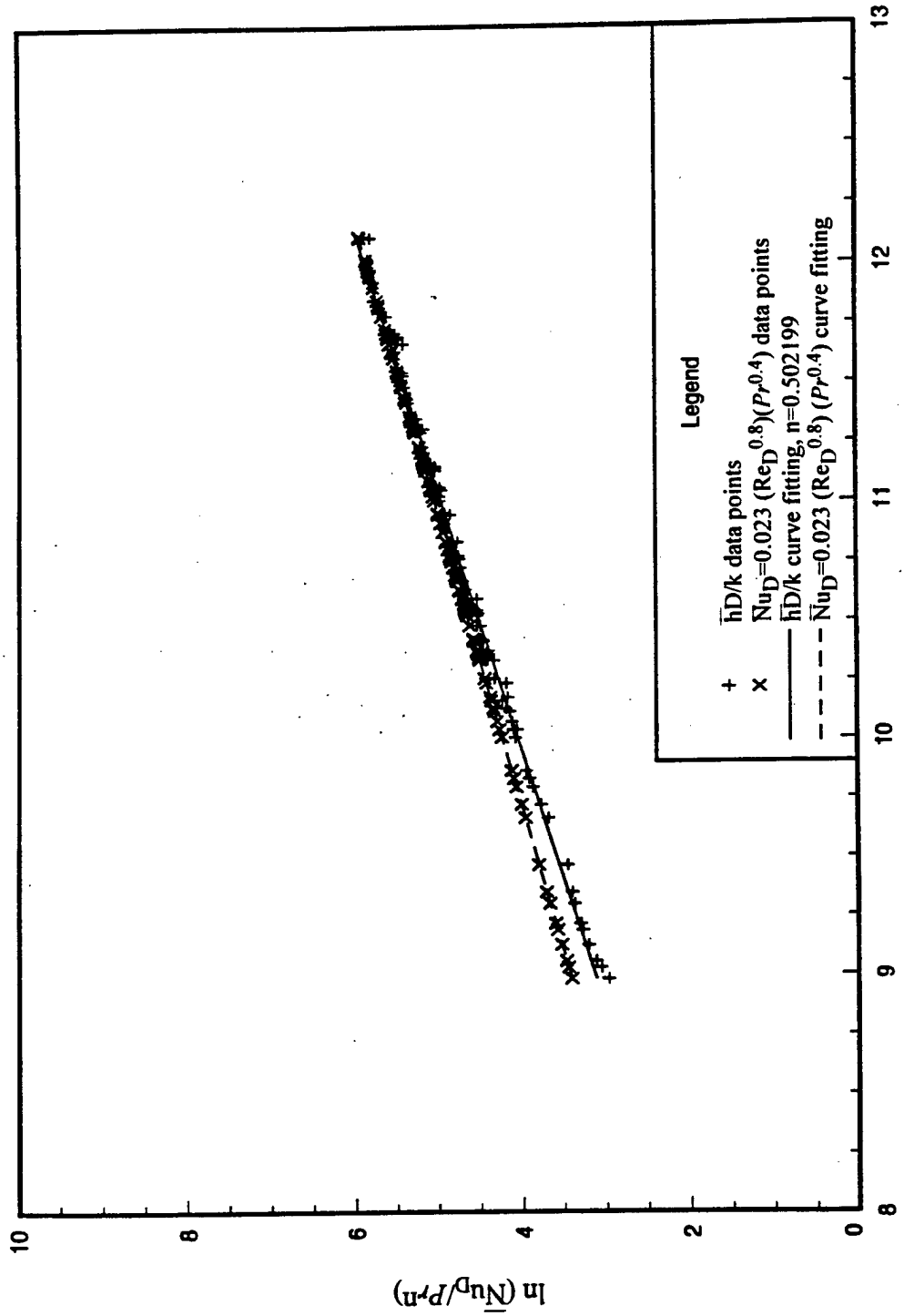

Figure 8.1: Nusselt number calculated from $\bar{h}D/k$ and Dittus-Boelter correlation for the calibration refrigerants.

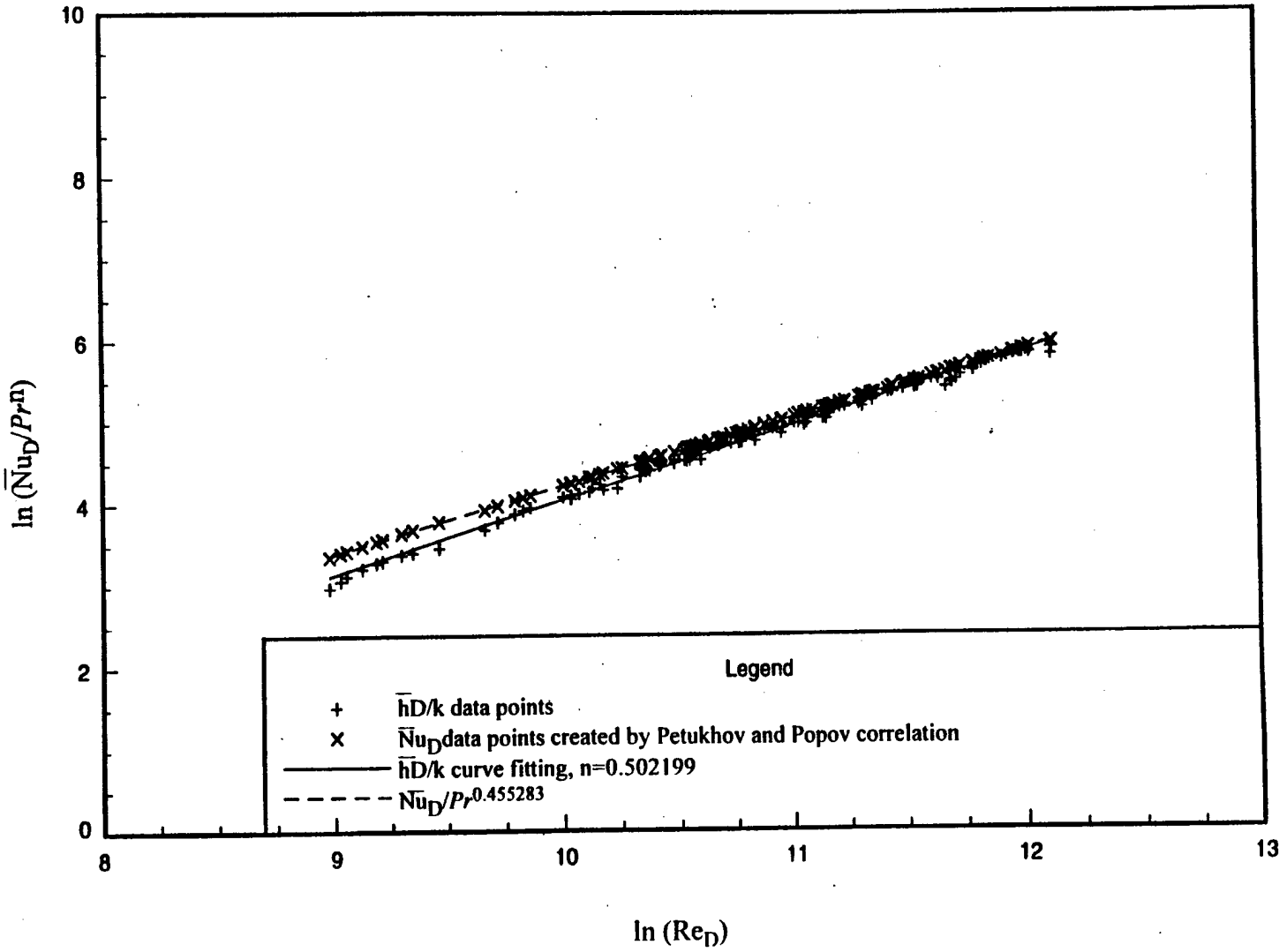

Figure 8.2: Nusselt number calculated from $\overline{h}D/k$ and Petukhov and Popov correlation for the calibration refrigerants.

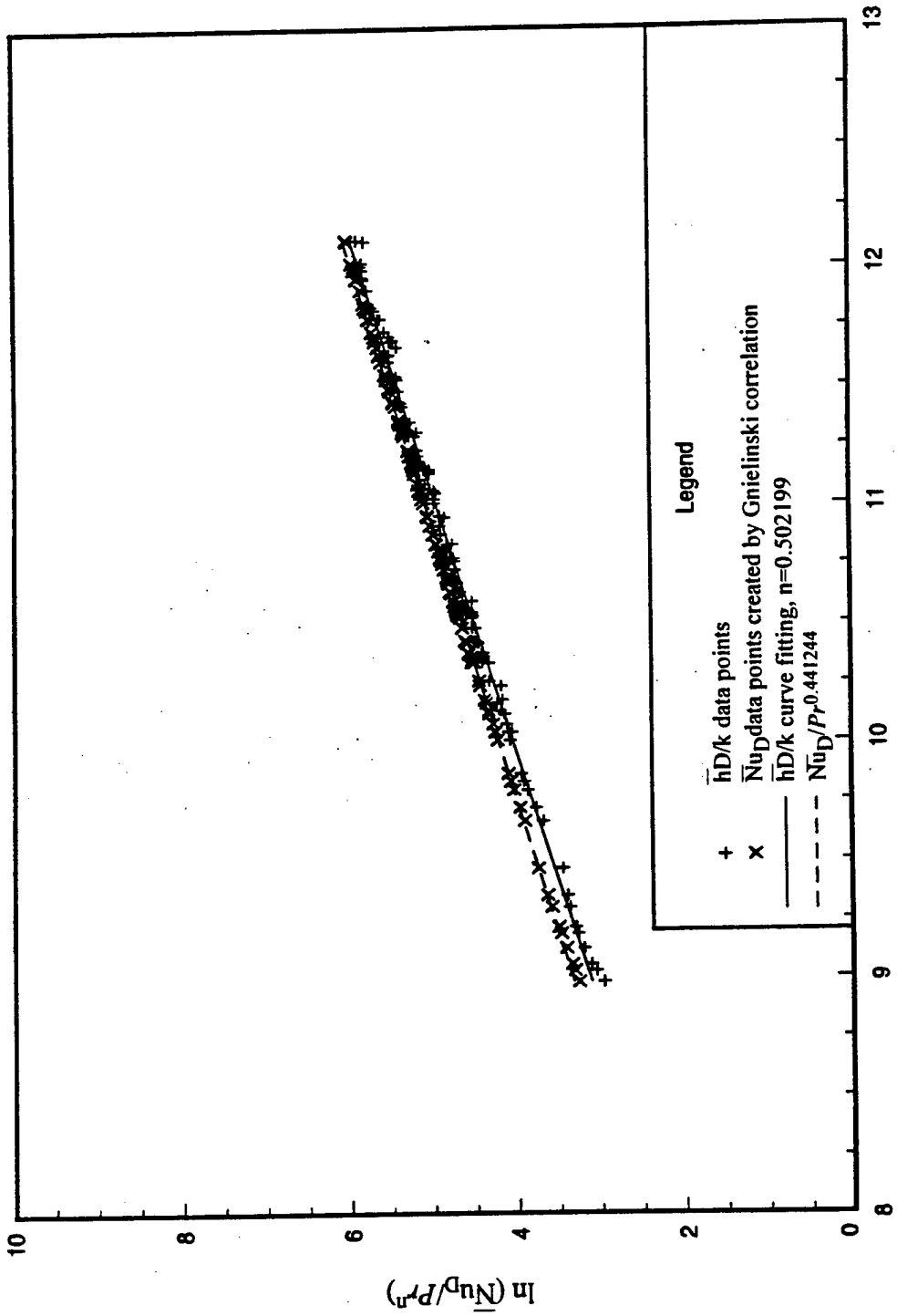

Figure 8.3: Nusselt number calculated from $\bar{h}D/k$ and Gnielinski correlation for the calibration refrigerants.

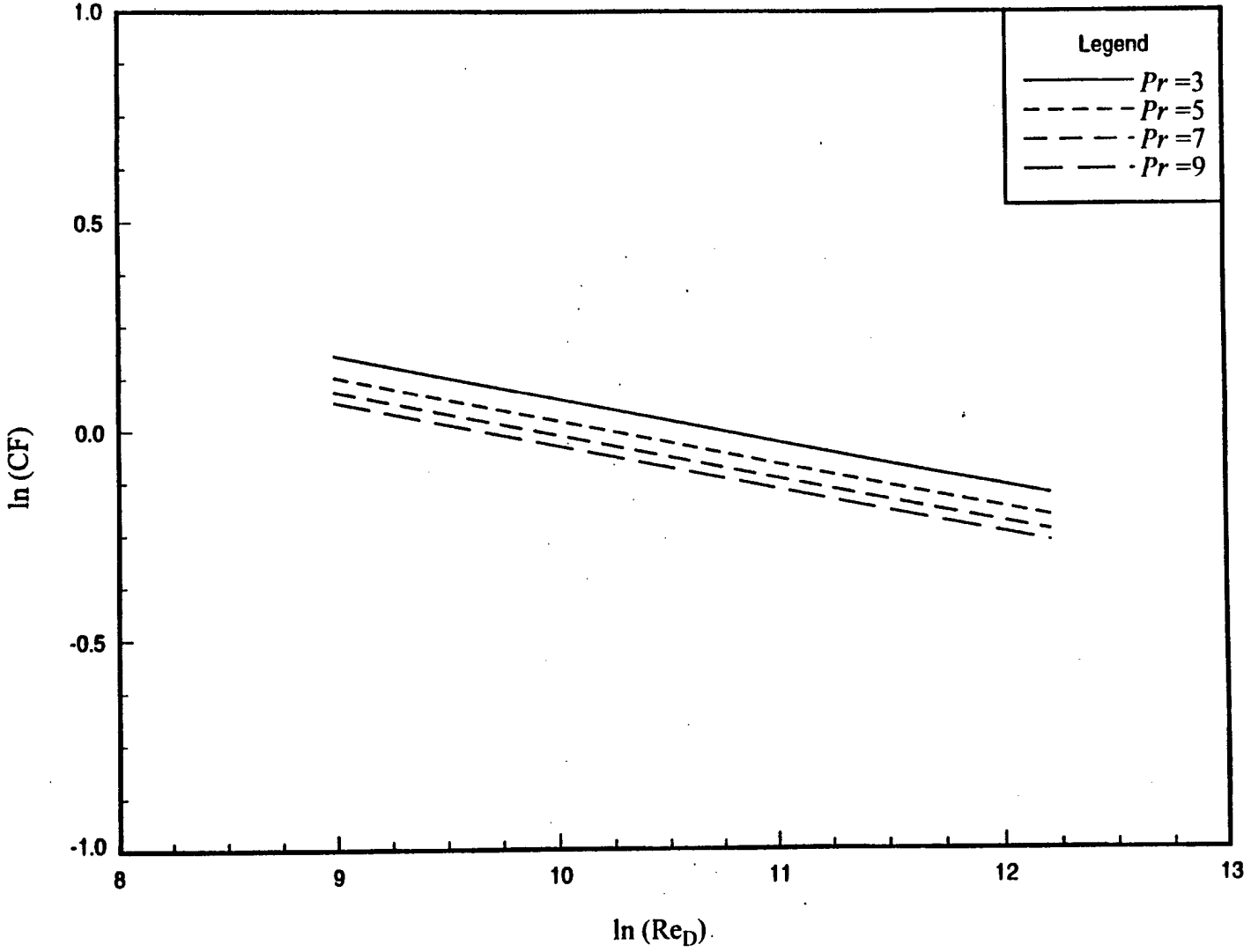

Figure 8.4: Calibration functions for the Dittus-Boelter correlation.

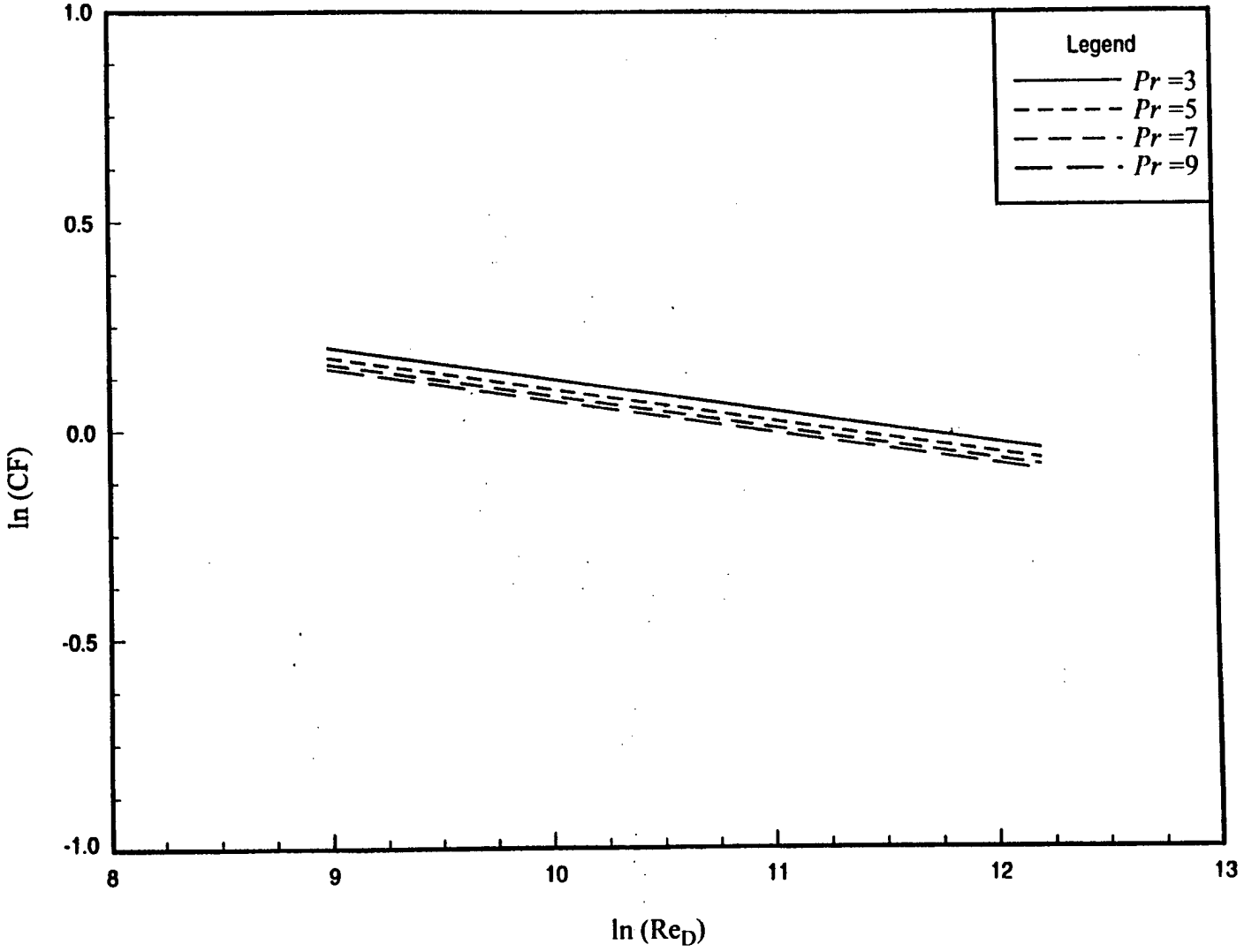

Figure 8.5: Calibration functions for the Petukhov and Popov correlation.

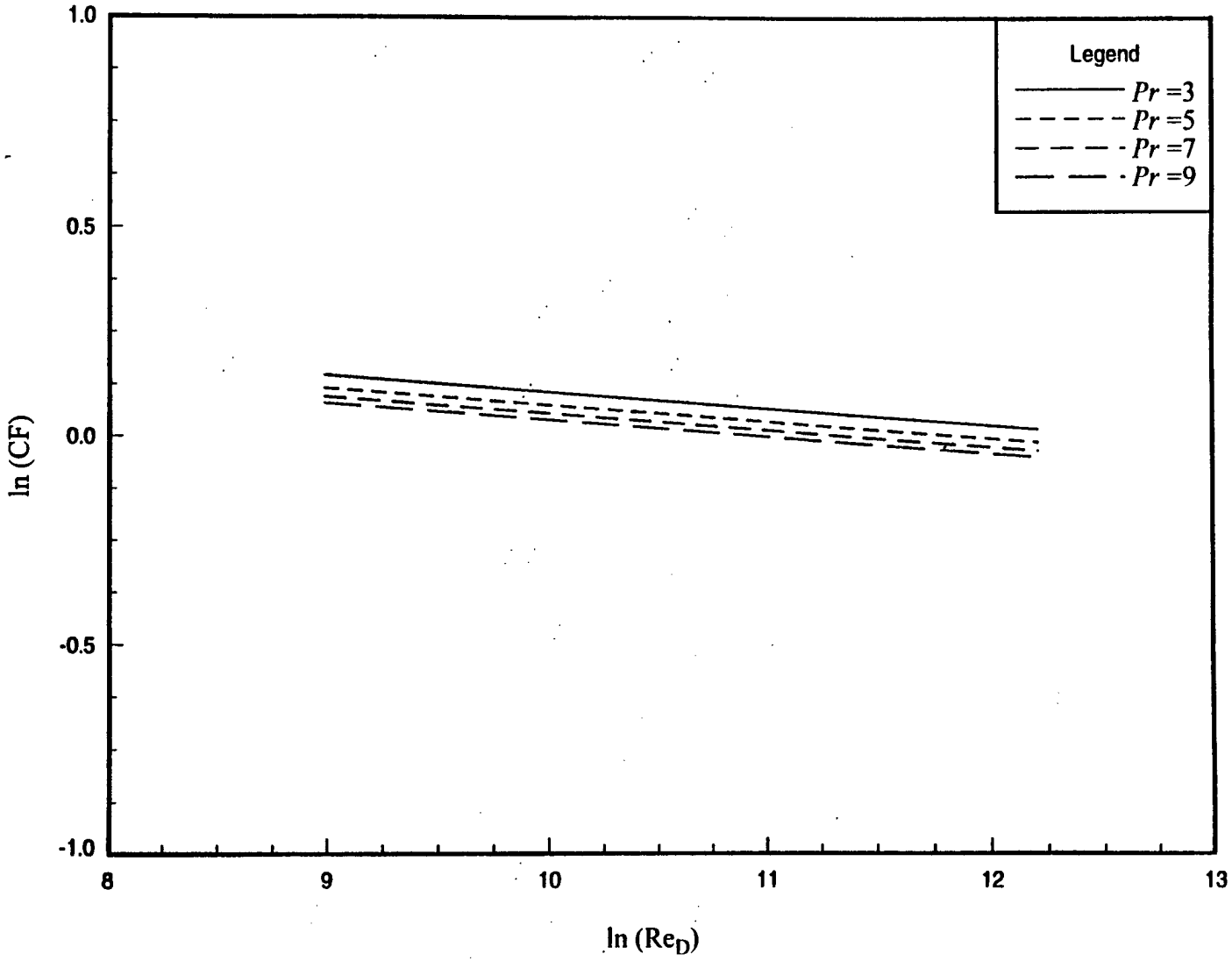

Figure 8.6: Calibration functions for the Gnielinski correlation.

If the four refrigerants, HCFC-22, CFC-12, CFC-113, and CFC-114, were used as the calibration refrigerants, the calibration function, *CF*, would be slightly different but very close to that obtained for the three calibration refrigerants. The *CF* coefficients are listed in Table 8.3.

TABLE 8.3: CURVE-FIT COEFFICIENTS FOR NUSSELT NUMBER - FOUR CALIBRATION REFRIGERANTS

coefficient	*hD/k*	Dittus-Boelter	Petukhov	Gnielinski
C, C^e	0.006633	0.023	0.017372	0.012381
a, a^e	0.905027	0.8	0.826843	0.860922
b, b^e	0.507640	0.4	0.457499	0.442776

THE PRANDTL NUMBER REGRESSION

As mentioned earlier, Approach 2 for calculating the thermal conductivity uses the Prandtl number, *Pr*. The *Pr* is determined as function of Re_D and ΔT^* as pointed out previously. For the three basic calibration refrigerants: HCFC-22, CFC-12, and CFC-113 and the four basic calibration refrigerants: HCFC-22, CFC-12, CFC-113, and CFC-114, the full term polynomial function regressions, based on Equation 8.3, for $ln(Pr)$ were fitted as shown in Table 8.4.

$$ln(Pr) = a_0 + a_1 ln(Re_D) + a_2 ln(\Delta T^*) + a_3 ln(Re_D^2) + a_4 ln(Re_D) \cdot ln(\Delta T^*) + a_5 ln(\Delta T^{*2}) + a_6 ln(Re_D^3) + a_7 ln(Re_D^2) \cdot ln(\Delta T^*) + a_8 ln(Re_D) \cdot ln(\Delta T^{*2}) + a_9 ln(\Delta T^{*3}) \quad (8.3)$$

TABLE 8.4: CURVE-FIT COEFFICIENTS FOR $ln(Pr)$

coefficient	3 refrigerants	4 refrigerants
a_0	96.908792	132.495075
a_1	-26.452258	-36.446721
a_2	83.304684	102.201609
a_3	2.459228	3.392931
a_4	-16.020859	-19.449363
a_5	8.088965	14.165714
a_6	-0.076756	-0.105753
a_7	0.750949	0.905506
a_8	-0.668378	-1.253316
a_9	2.213377	2.823725

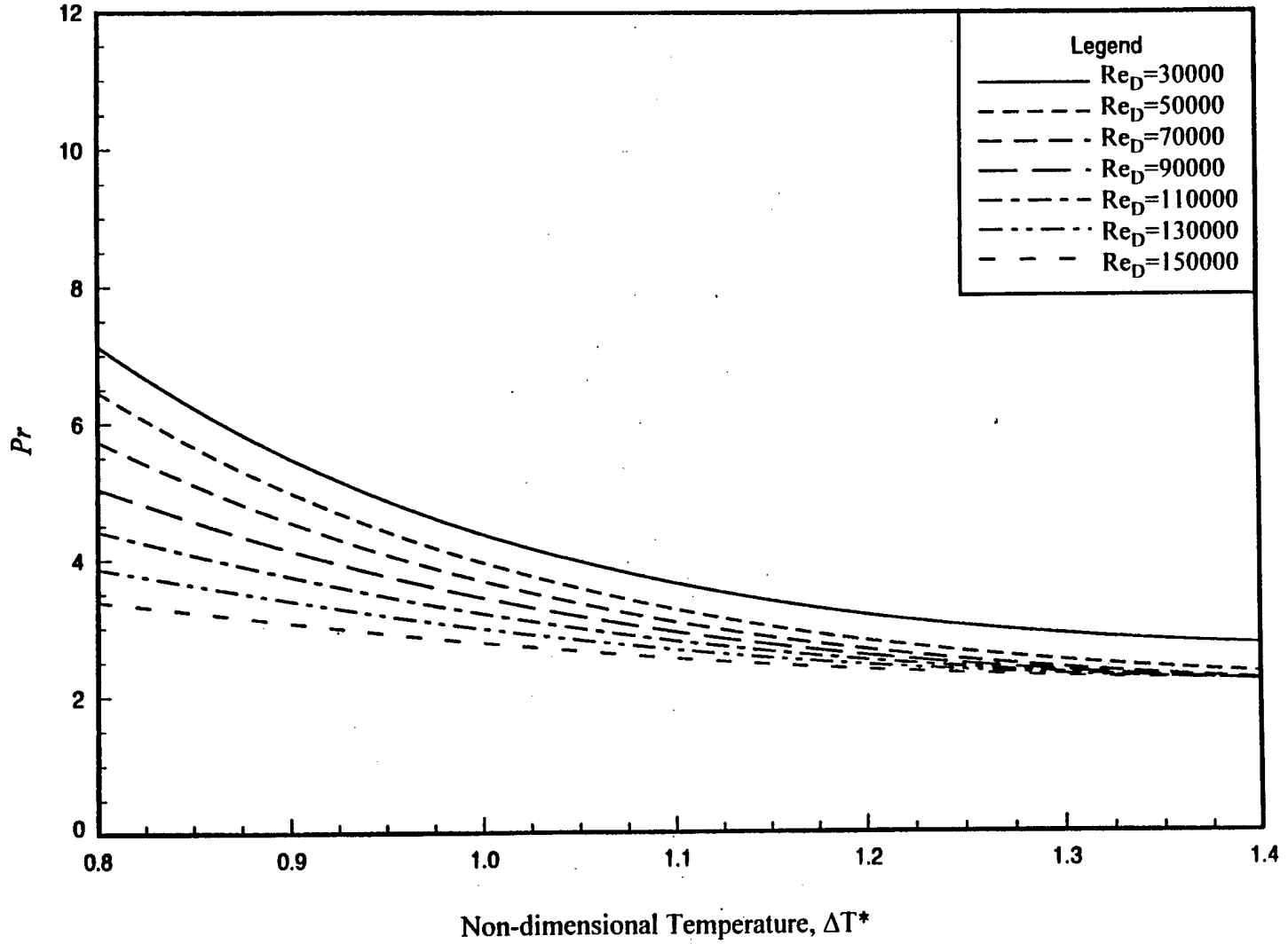

Figure 8.7: Plots of *Pr* versus ΔT^* (3-refrigerant base).

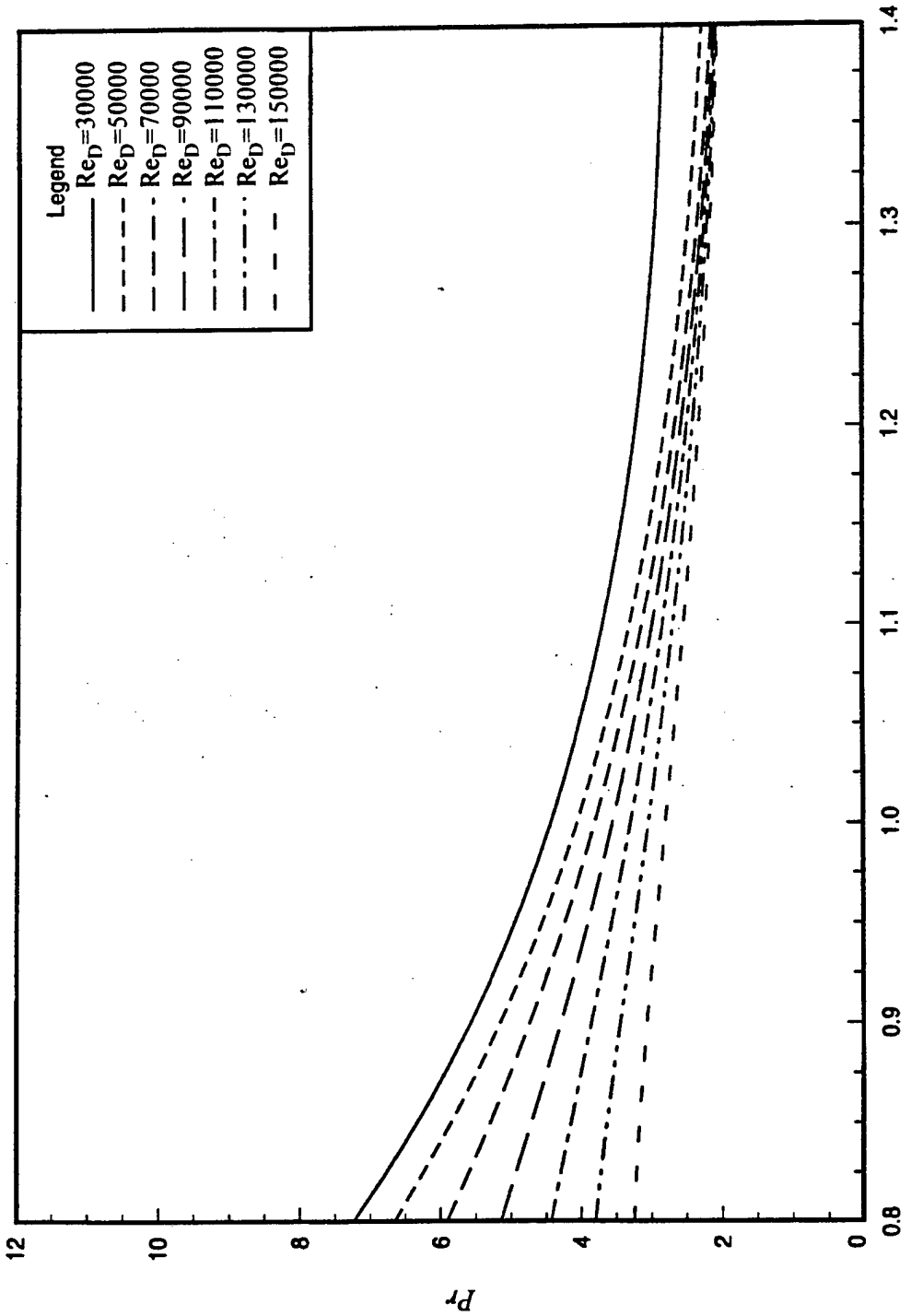

Figure 8.8: Plots of *Pr* versus *ΔT (4-refrigerant base).**

Plots of Pr versus ΔT^* are shown in Figures 8.7 and 8.8, for the three-refrigerant and four-refrigerant bases. As can be seen from these figures, the smaller the ΔT^*, the larger the Pr for a fixed Re_D. On the other hand, at a fixed ΔT^*, the smaller the Re_D, the larger is the Pr. These plots furnish the trends of the relationship between Pr, Re_D, and ΔT^* developed by Approach 2.

COMPARISON OF MEASURED THERMAL CONDUCTIVITY WITH REFERENCE DATA

It is of interest to compare the measured thermal conductivity with the ASHRAE handbook data [82] for the calibration refrigerants (following calibration). To do this comparison, the thermal conductivity of the four calibration refrigerants were plotted using Approaches 1 and 2. Figure 8.9 shows the measured thermal conductivity using Approach 1 and the ASHRAE handbook thermal conductivity plot, and Figure 8.10 shows the measured thermal conductivity by Approach 2 with the ASHRAE handbook thermal conductivity. Lines of ±5% were used to present an indication of the deviation in the measured data. As shown in these figures, most of the measured points were located inside the ±5% band except for some points scattered outside this band but within ±10%. This could be due to experimental errors, which are not included in the experimental uncertainty, such as unsteady-state or inaccurate property data. By comparing the distribution of the data points in these two figures, it is found that there seems to be more fluctuation in the results of Approach 1 than in the results of Approach 2. However, these results show that the experimental uncertainties were within ±5% as predicted by theoretical uncertainties which were pointed out earlier. These results provide more confidence in measuring other refrigerants by this method.

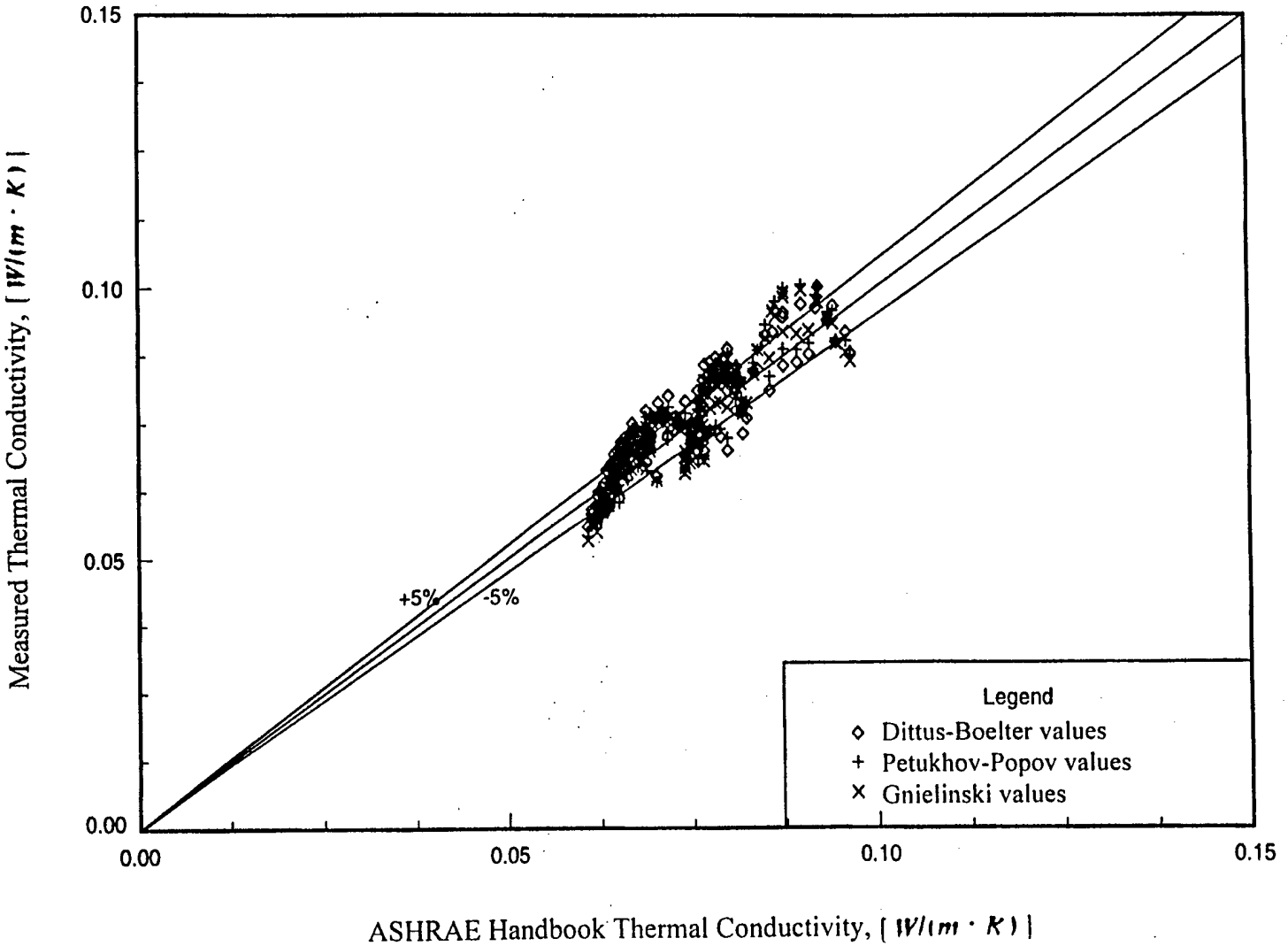

Figure 8.9: Measured thermal conductivity compared with ASHRAE data by Approach 1 (4-refrigerant base).

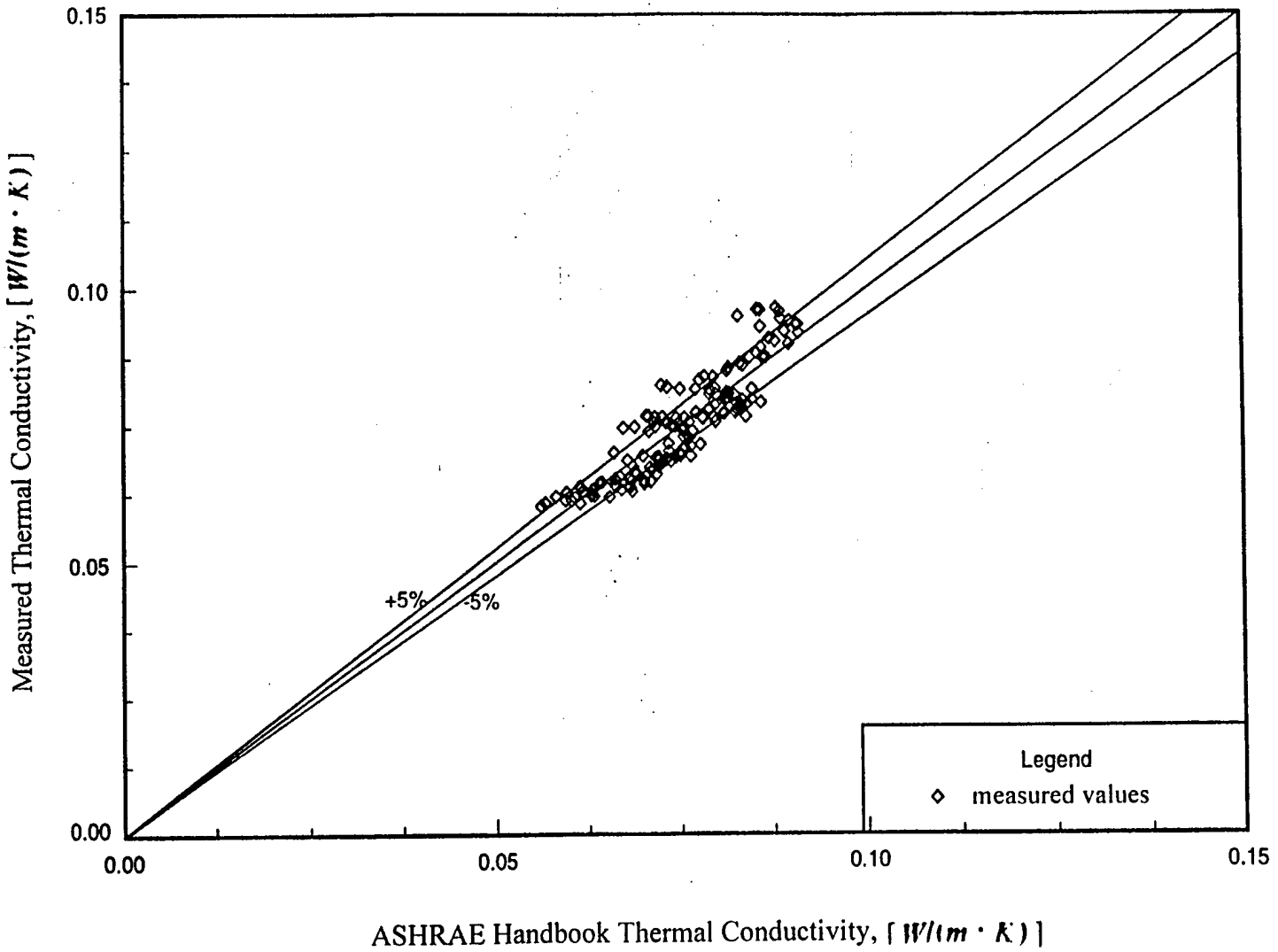

Figure 8.10: Measured thermal conductivity compared with ASHRAE data by Approach 2 (4-refrigerant base).

CHAPTER 9

VERIFICATION OF METHODOLOGY

The purpose of this study is to determine the selected properties of refrigerant alternatives. Because HFC-236ea is a proposed alternative for CFC-114, properties of CFC-114 were measured by the current approach and compared with the ASHRAE data in order to see whether this approach can be applied to fluids of unknown properties. The properties of CFC-114 being verified in this study are thermal conductivity, k, viscosity, μ, density, ρ, and specific heat, Cp. However, it is first interesting to compare these properties between REFPROP and ASHRAE data. Then, the measured results are presented and compared with the ASHRAE data. The comparisons are shown in the following sections.

CFC-114 PROPERTIES FROM REFPROP AND ASHRAE

REFPROP is a computer package for refrigerant properties recently developed by the National Institute of Standards and Technology (NIST), and REFPROP-4.0 is the most recent version. Because of the limited experimental data, theoretical predictions were thought to be the only method to obtain properties for this heat transfer study. In this section, interest is focused on a comparison of density, specific heat, viscosity, and thermal conductivity for CFC-114. Figures 9.1, 9.2, 9.3, and 9.4 show the plots of the ASHRAE data and REFPROP-4.0 data for these properties.

As shown in these comparison plots, some deviations exist. The deviations presented as percentages over a temperature range of -50°C to 120°C for each of the four properties discussed here are listed in Table 9.1. As shown in these figures (Figures 9.1 through 9.4) and Table 9.1, these properties deviate somewhat from each other over the temperature ranges under study. Therefore, the results obtained might be different if other data sources were used.

TABLE 9.1: CFC-114 PROPERTY COMPARISON BETWEEN ASHRAE AND REFPROP

property	dev.[a], % (low temp.)	dev., % (high temp.)
density, ρ, (kg/m^3)	+5.2	-0.02
specific heat, Cp, $[J/(kg \cdot K)]$	+6.8	-2.2
viscosity, μ, $(Pa \cdot s)$	+4.2	-7.1
thermal conductivity, k, $[W/(m \cdot K)]$	-2.7	-11.7

[a]dev., % = [(REFPROP value − ASHRAE value) / ASHRAE value] 100

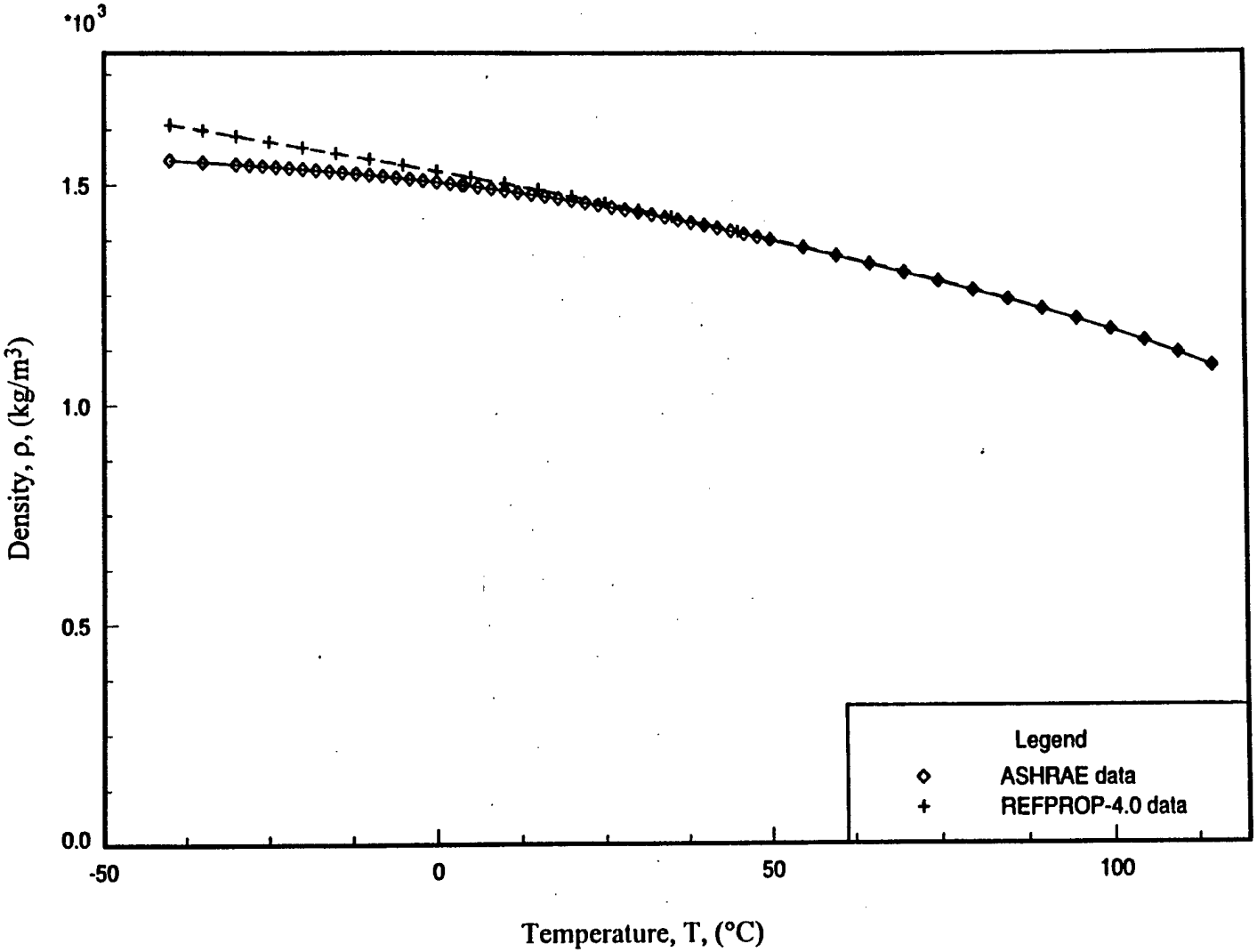

Figure 9.1: Comparison plot between ASHRAE and REFPROP data for CFC-114 density.

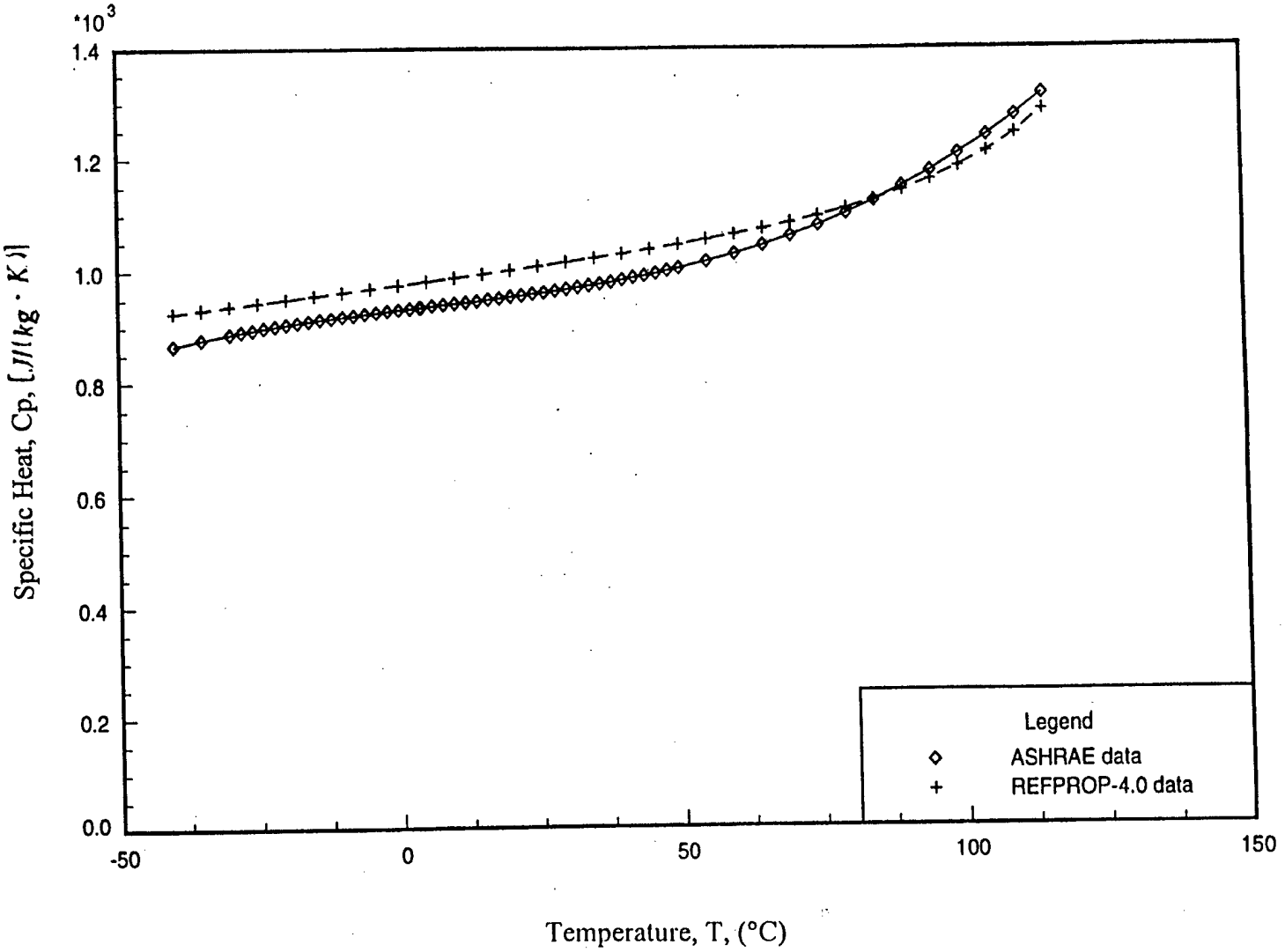

Figure 9.2: Comparison plot between ASHRAE and REFPROP data for CFC-114 specific heat.

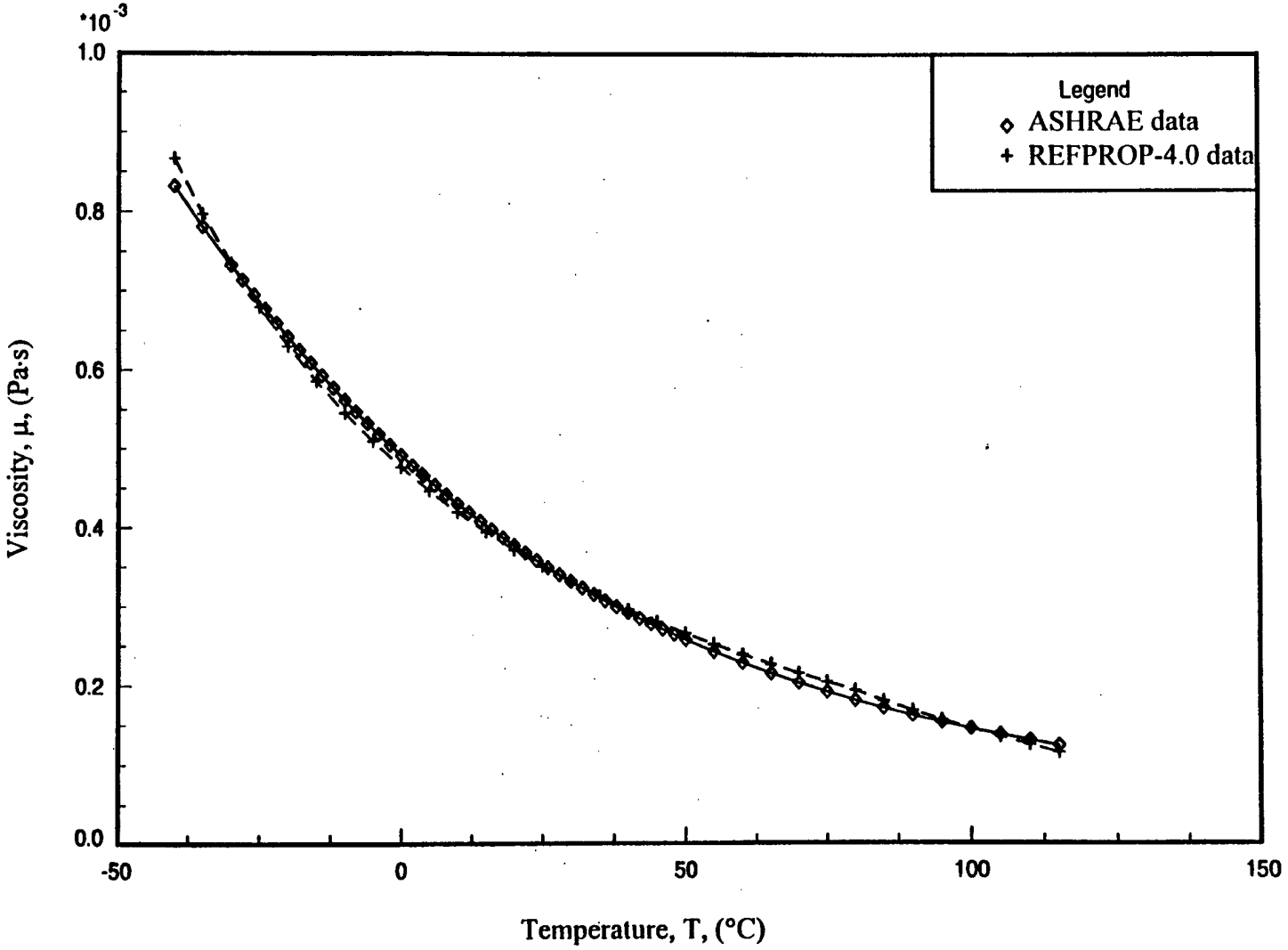

Figure 9.3: Comparison plot between ASHRAE and REFPROP data for CFC-114 viscosity.

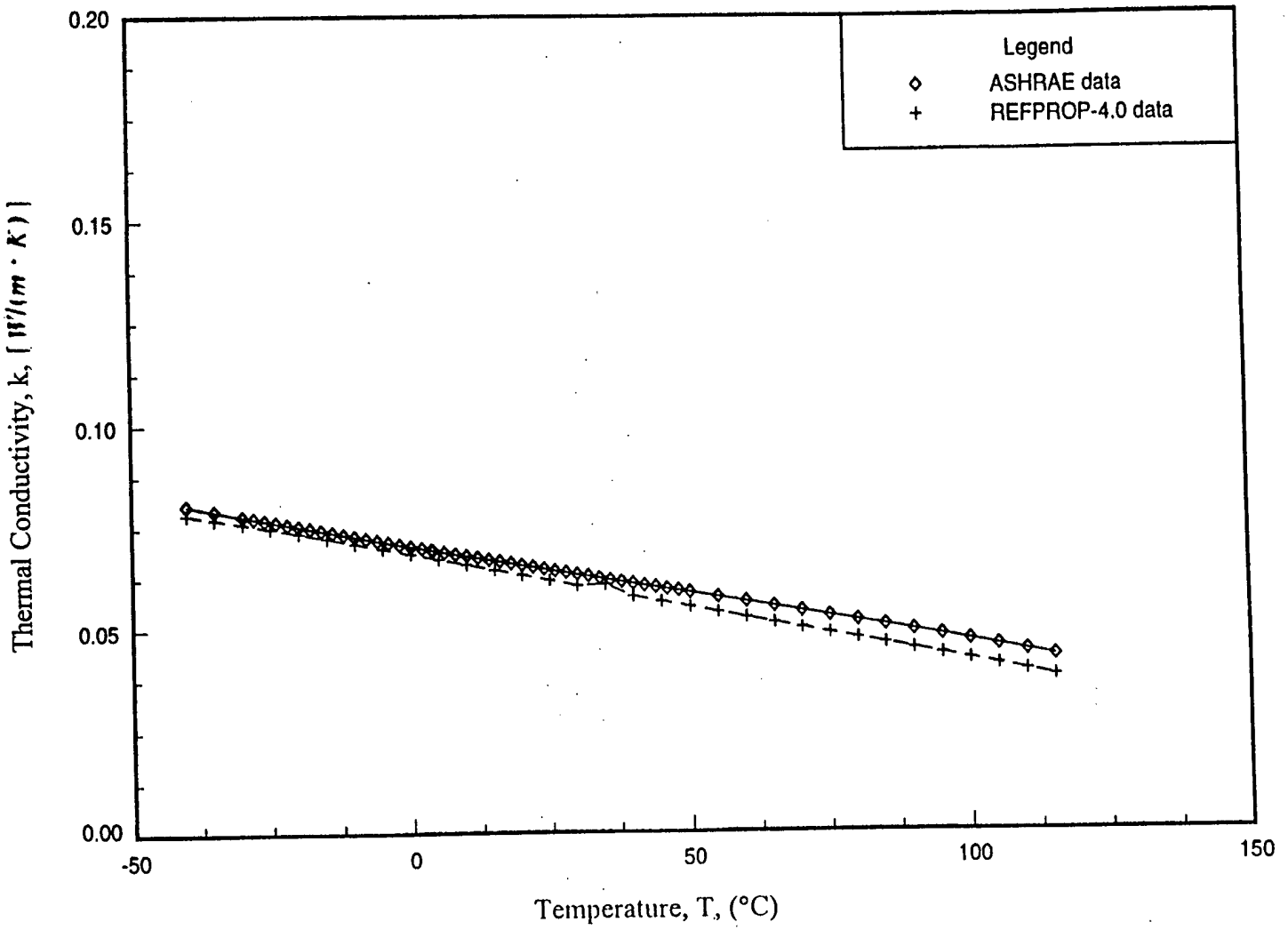

Figure 9.4: Comparison plot between ASHRAE and REFPROP data for CFC-114 thermal conductivity.

VERIFICATION OF CFC-114 PROPERTIES

In this section, the measured properties of CFC-114 which include thermal conductivity, viscosity, specific heat, and density will be presented and compared with ASHRAE data.

CFC-114 Thermal Conductivity

The CFC-114 thermal conductivities were obtained from experimental data operating from near 0°C to 50°C. Figure 9.5 shows the thermal conductivity of CFC-114 by Approach 1 as a function of temperature along with the ASHRAE data [82]. The deviations of thermal conductivity between measured and ASHRAE data are shown to be within ±5% over the measured temperature range. Figure 9.6 shows the thermal conductivity of CFC-114 by Approach 2 as a function of temperature along with the ASHRAE data. Again, the deviation is within ±5%. It is important to mention that the properties required in the thermal conductivity calculations, such as viscosity and specific heat, were all based on ASHRAE data. Deviations of thermal conductivity for measured and ASHRAE data are shown in Figures 9.7 and 9.8 for Approaches 1 and 2, respectively.

CFC-114 Viscosity

The CFC-114 viscosity was obtained from the product of viscosity and density, directly measured by the inline viscometer. The accuracy of the viscometer had already been verified for several fluids. Figure 5.11 shows the viscosity as a function of temperature for CFC-114. As can be seen from the figure, the measured viscosity and the ASHRAE viscosity were in very close agreement with the deviation being ±2%. Figure 5.12 shows the deviation plot over the measured temperature range.

CFC-114 Specific Heat

The measured specific heat was calculated from an energy balance of the test section. With the net heat transfer calculated, the specific heat was calculated from Equation 6.5. Figure 9.9 shows the specific heat of CFC-114 over a temperature range of 0°C to 50°C. As shown in this figure, the measured *Cp* closely matches the ASHRAE data. This suggests that the temperature and the net heat transfer to the refrigerant values are quite good and provide much confidence in measuring unknown fluids such as HFC-236ea.

It should be noted that the specific heat of CFC-114, *Cp*, was calculated by using the test section heat loss estimation described above. The resulting heat loss is shown in Figure 5.7, where Equation 5.1 was used. The measured *Cp* compared with the ASHRAE *Cp*, shown in Figure 9.9, is within ±3%.

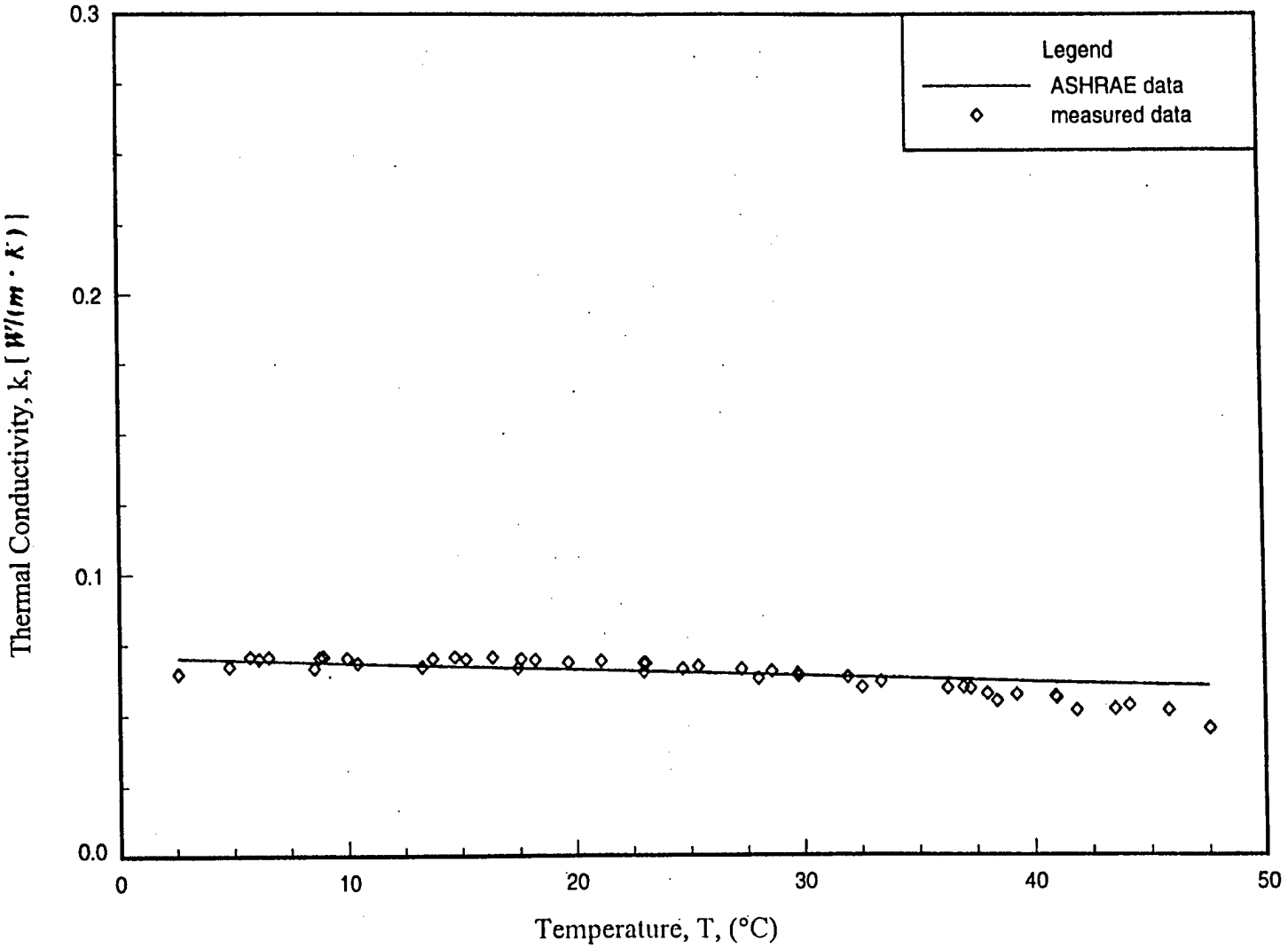

Figure 9.5: Comparison of measured thermal conductivity by Approach 1 and ASHRAE data for CFC-114.

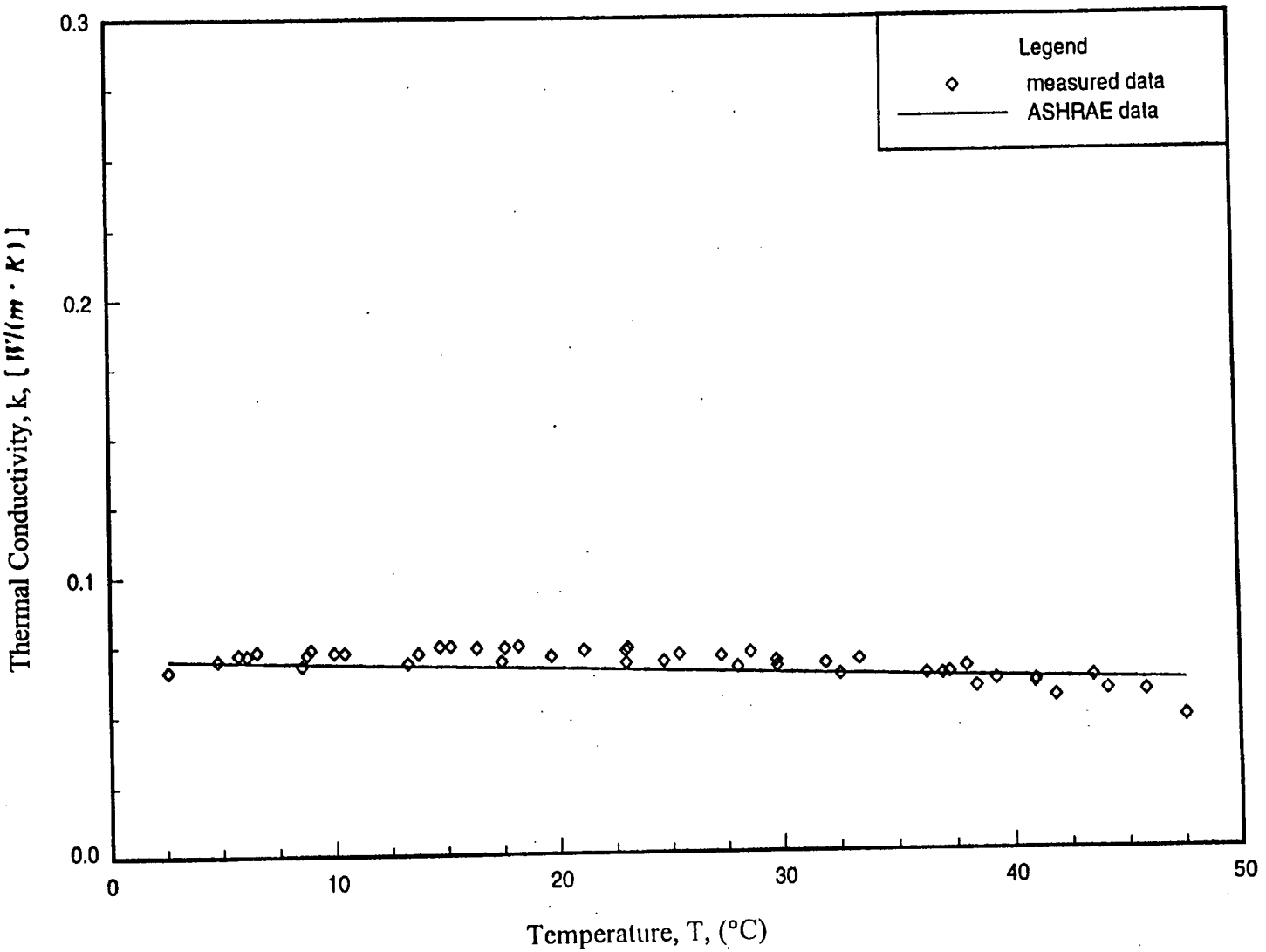

Figure 9.6: Comparison of measured thermal conductivity by Approach 2 and ASHRAE data for CFC-114.

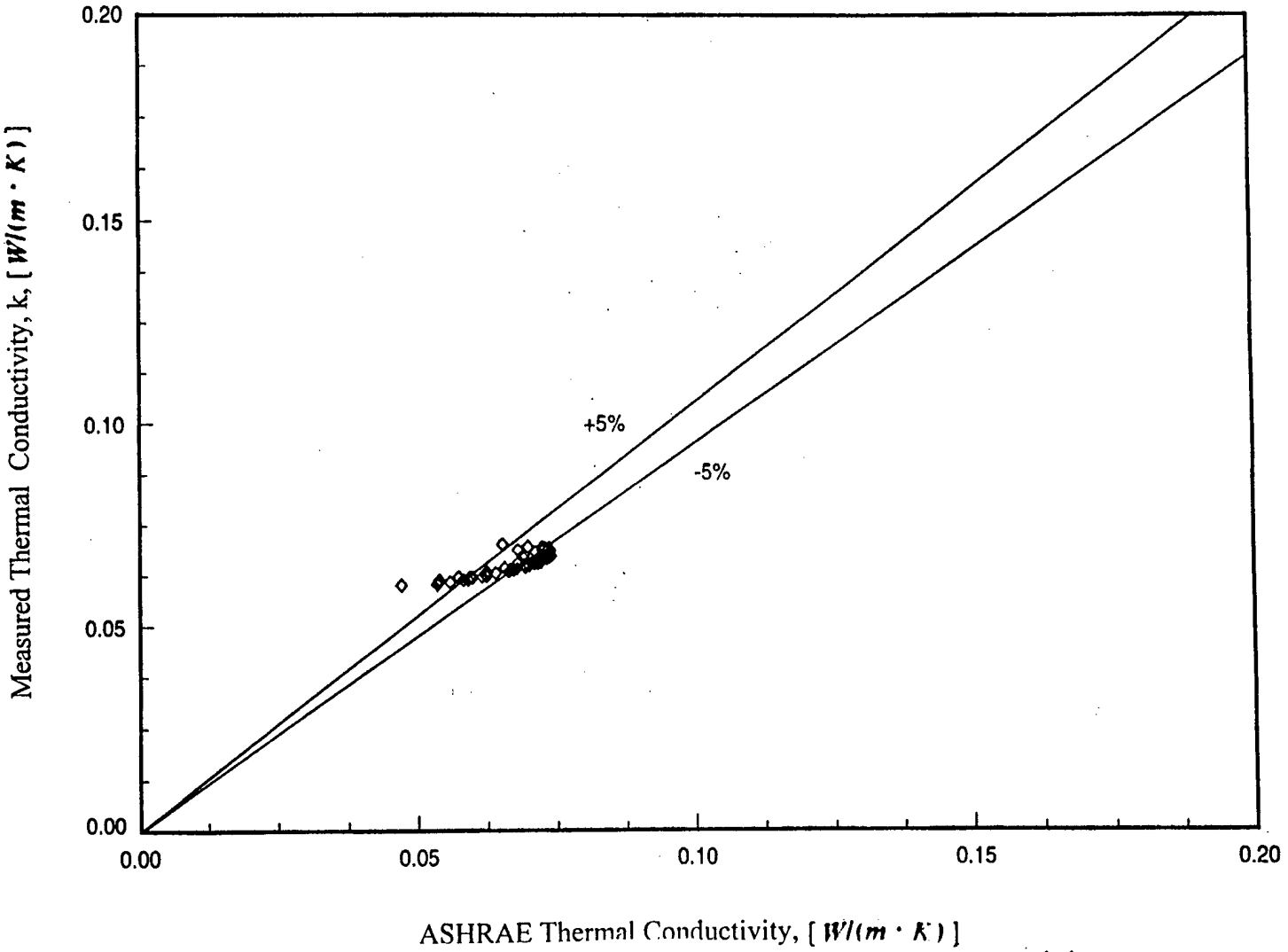

Figure 9.7: Comparison of measured thermal conductivity by Approach 1 and ASHRAE data for CFC-114.

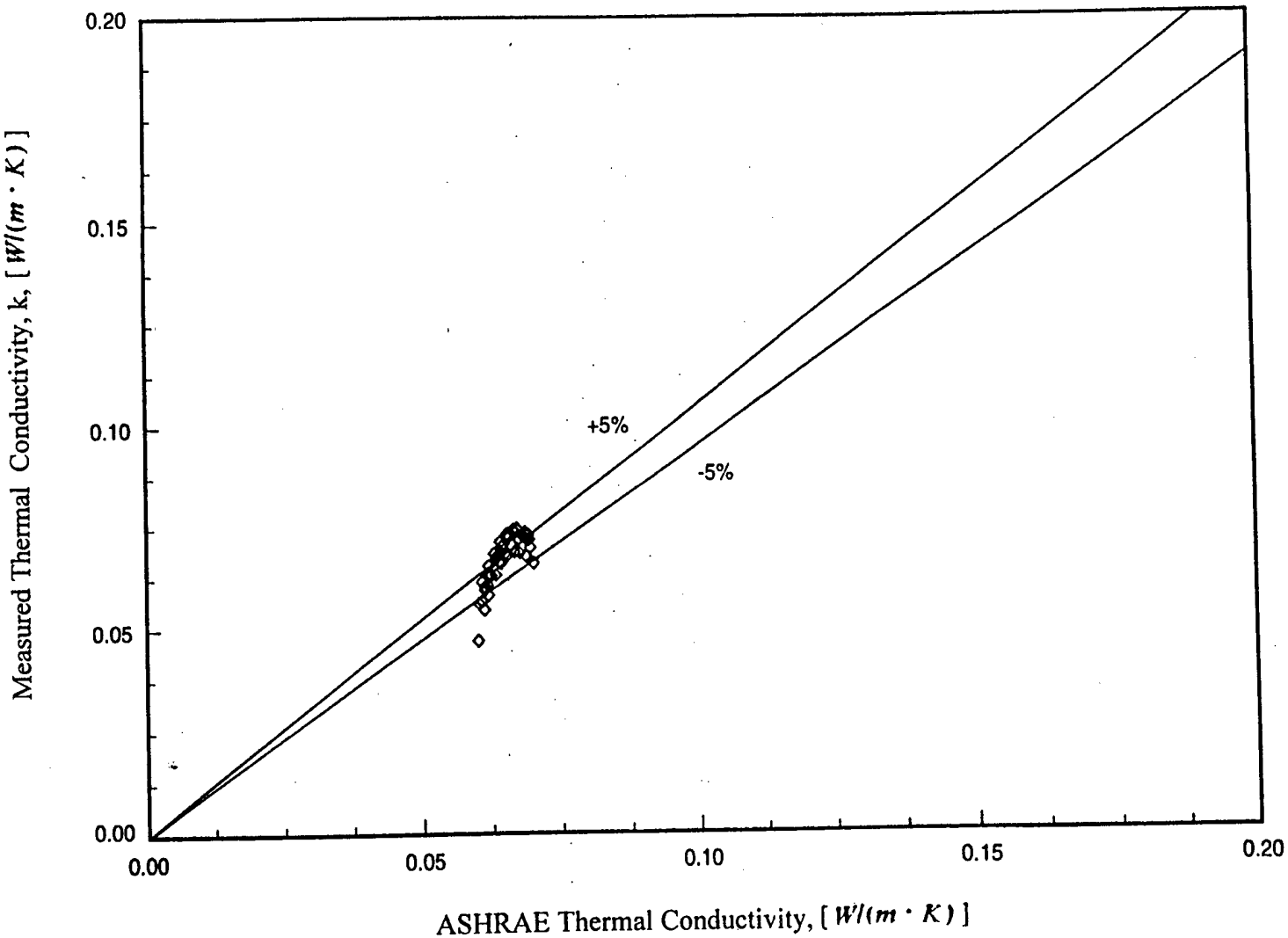

Figure 9.8: Comparison of measured thermal conductivity by Approach 2 and ASHRAE data for CFC-114.

CFC-114 Density

The density of CFC-114 was measured by a densimeter. The densimeter was verified using known refrigerant data, and the results were compared with the ASHRAE data as shown in Figure 5.8 (Chapter 5). The measured data are shown in Figure 9.10. The calculated deviation percentage was calculated to be within ±1.9% of the ASHRAE data for CFC-114.

SUMMARY

In this chapter, the measured properties of CFC-114 have been presented and compared with ASHRAE data. The purpose of the CFC-114 property measurements was to verify the methodologies used here. The main properties of interest are thermal conductivity and viscosity. However, other properties, such as specific heat and density, were also measured and compared. Since specific heat is a required property for determining the thermal conductivity for the methodologies of this study, the validity of the *Cp* data impacted the accuracy of the calculated *k*. In general, the measured properties closely matched the ASHRAE data. This supports the validity of the methodology developed in this study. A summary follows of this verification. Table 9.2 shows this summary of verified results for each property.

TABLE 9.2: SUMMARY OF MAXIMUM DEVIATION FOR CFC-114 PROPERTIES

property	Dev.$_1$[a] (-50 ~ 150°C)	Dev.$_2$[b] (0 ~ 50°C)
density, ρ	±5.2%	+1.9%
specific heat, *Cp*	±6.8%	±3%
viscosity, μ	±7.1%	±2%
thermal conductivity[c], *k*	±11.7%	±5%

[a] Dev.$_1$: [(REFPROP value − ASHRAE value) / ASHRAE value] · 100

[b] Dev.$_2$: [(Experiment value − ASHRAE value) / ASHRAE value] · 100

[c] for both Approaches 1 and 2

The deviations shown in Table 9.2 indicate that larger deviations exist between REFPROP and ASHRAE data for transport properties (viscosity and thermal conductivity), while smaller deviations were detected for thermodynamic properties (density and specific heat). For measured properties, it was shown that they deviate less from the ASHRAE data than from the REFPROP predictions. This indicates that the methodology worked adequately. However, to improve accuracy, more calibrations might be necessary. Other possible error sources, excluding experimental uncertainties such as operation errors (e.g. steady-state requirement), must be eliminated as much as possible during the experimental operation.

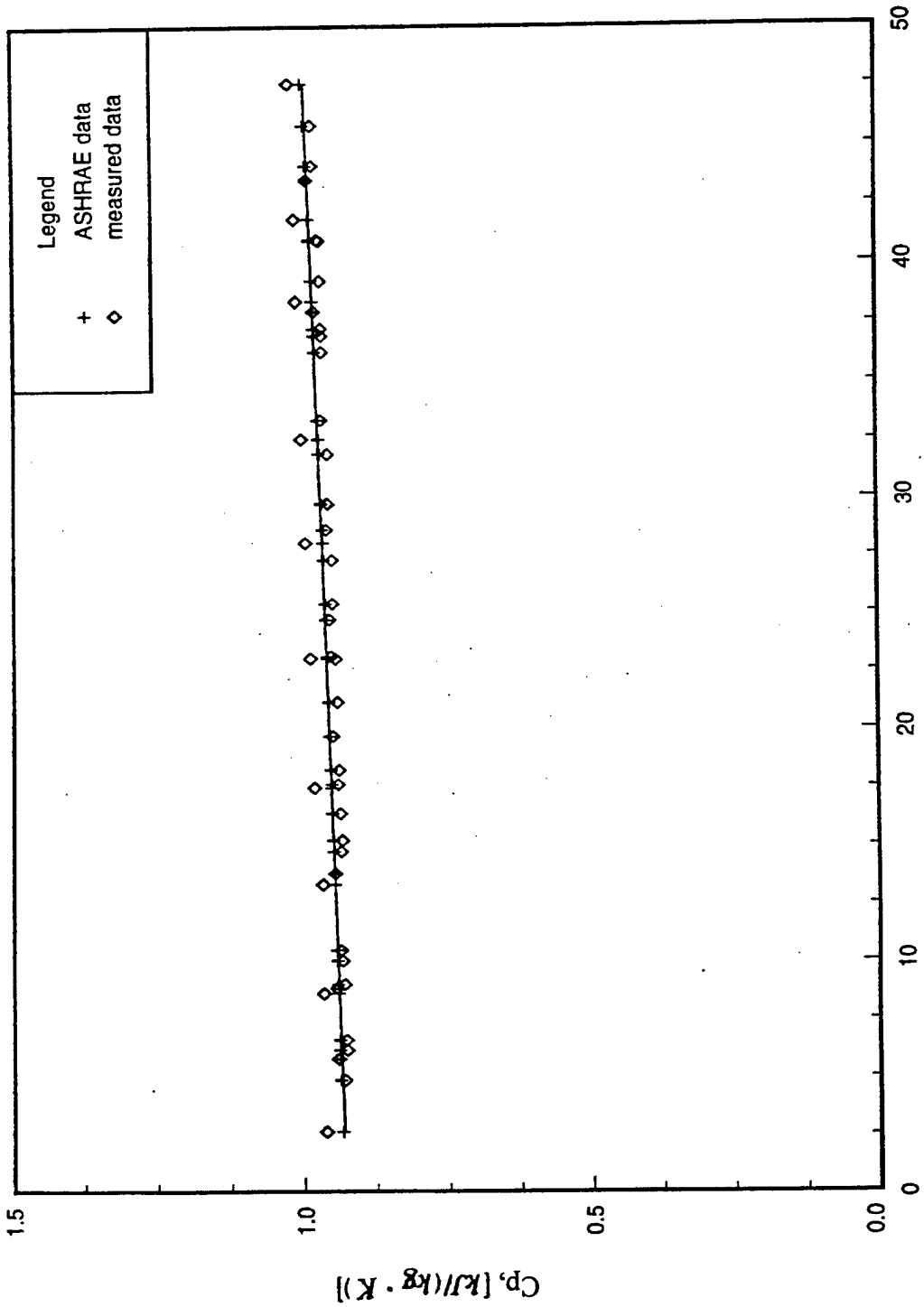

Figure 9.9: Comparison of measured specific heat for CFC-114.

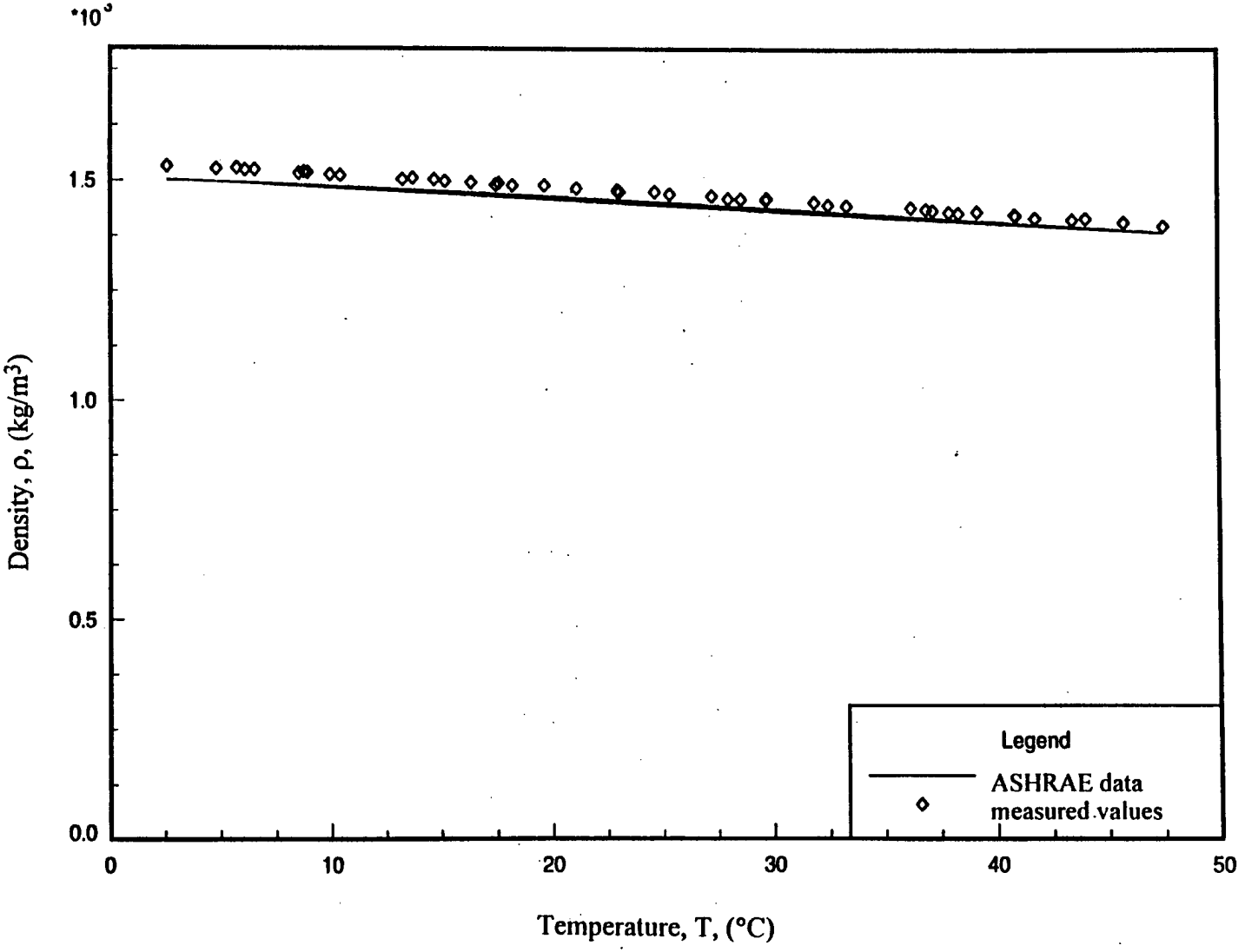

Figure 9.10: Comparison of measured density for CFC-114.

CHAPTER 10

PROPERTIES OF HFC-236ea

In the previous chapter, the measured properties of CFC-114 were compared with ASHRAE data. The small differences seen gave confidence for applying the current approach to measure refrigerant properties. Based on the thermal conductivity calibrations (both Approaches 1 and 2), same test section conditions and viscometer, the properties of HFC-236ea were measured. The results were also compared with REFPROP-4.0 data [83] and are presented below.

SPECIFIC HEAT

Based on the same test section heat loss estimation mentioned previously, the Cp of liquid HFC-236ea was determined. Figure 10.1 shows the Cp of HFC-236ea and compares it with the REFPROP-4.0 data. Because of the lack of the published experimental data, the REFPROP-4.0 data only are used for comparison. The measured data show the deviations from REFPROP-4.0 values are within +5%.

A linear curve fit equation is determined for the measured Cp [$kJ/(kg \cdot C)$] versus temperature (°C) and is shown below:

$$Cp = 1.2048 + 0.001925 \cdot T \tag{10.1}$$

VISCOSITY

HFC-236ea viscosity was measured by a viscometer with its accuracy verified with a number of fluids as shown in Chapter 5 to be ±2%. Figure 10.2 shows the measured viscosity of liquid HFC-236ea versus temperature over a temperature range from -5°C to nearly 60°C. The deviations from REFPROP values in Figure 10.3 indicate the deviations are within +5%.

In order to conveniently use the results, a curve fit equation expressed as a polynomial is given below:

$$\mu = \sum_{i=0}^{n} a_i \cdot T^i \tag{10.2}$$

where μ is in cp and T is in °C. The curve fit coefficients are listed in Table 10.1.

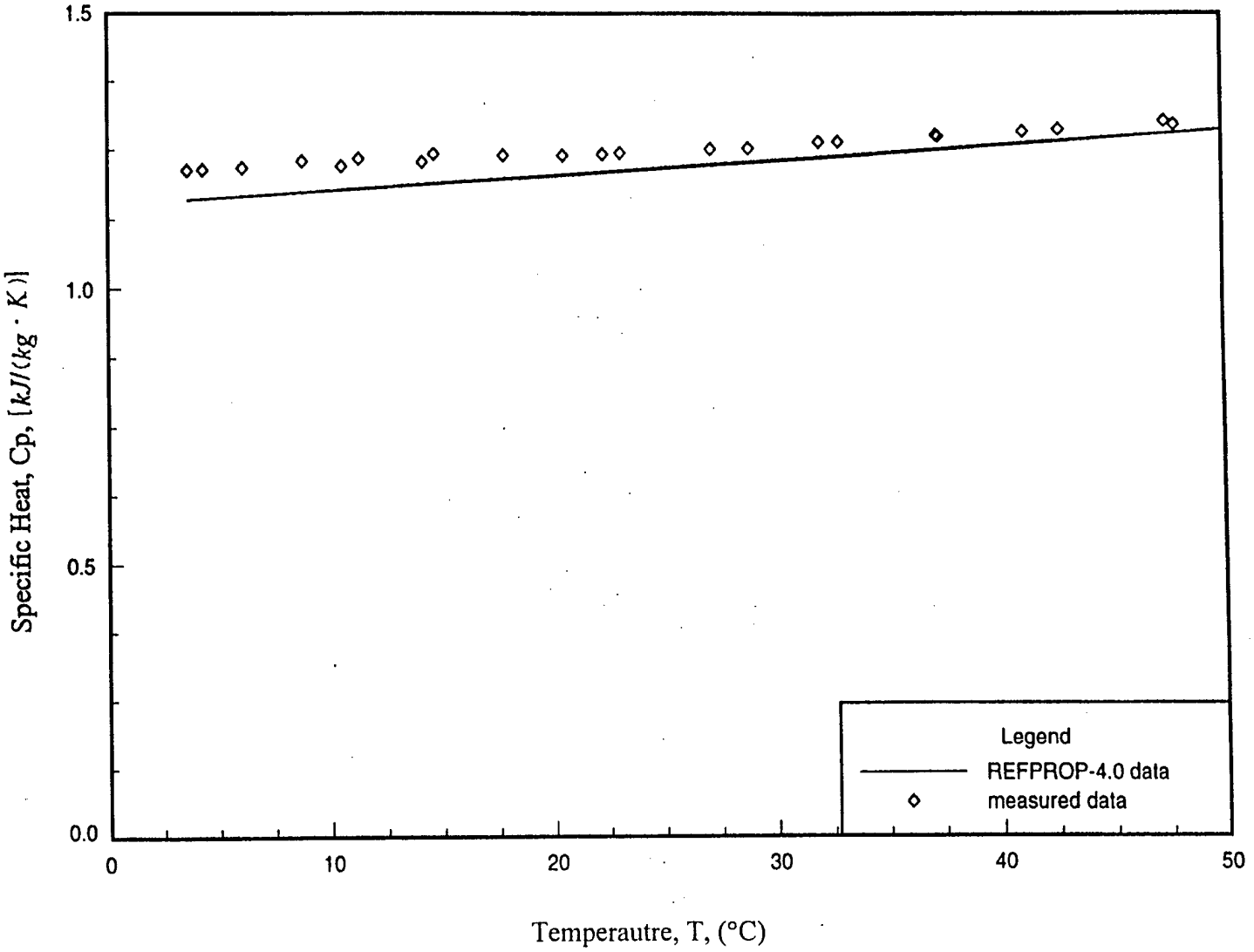

Figure 10.1: Comparison of measured specific heat and REFPROP data for HFC-236ea.

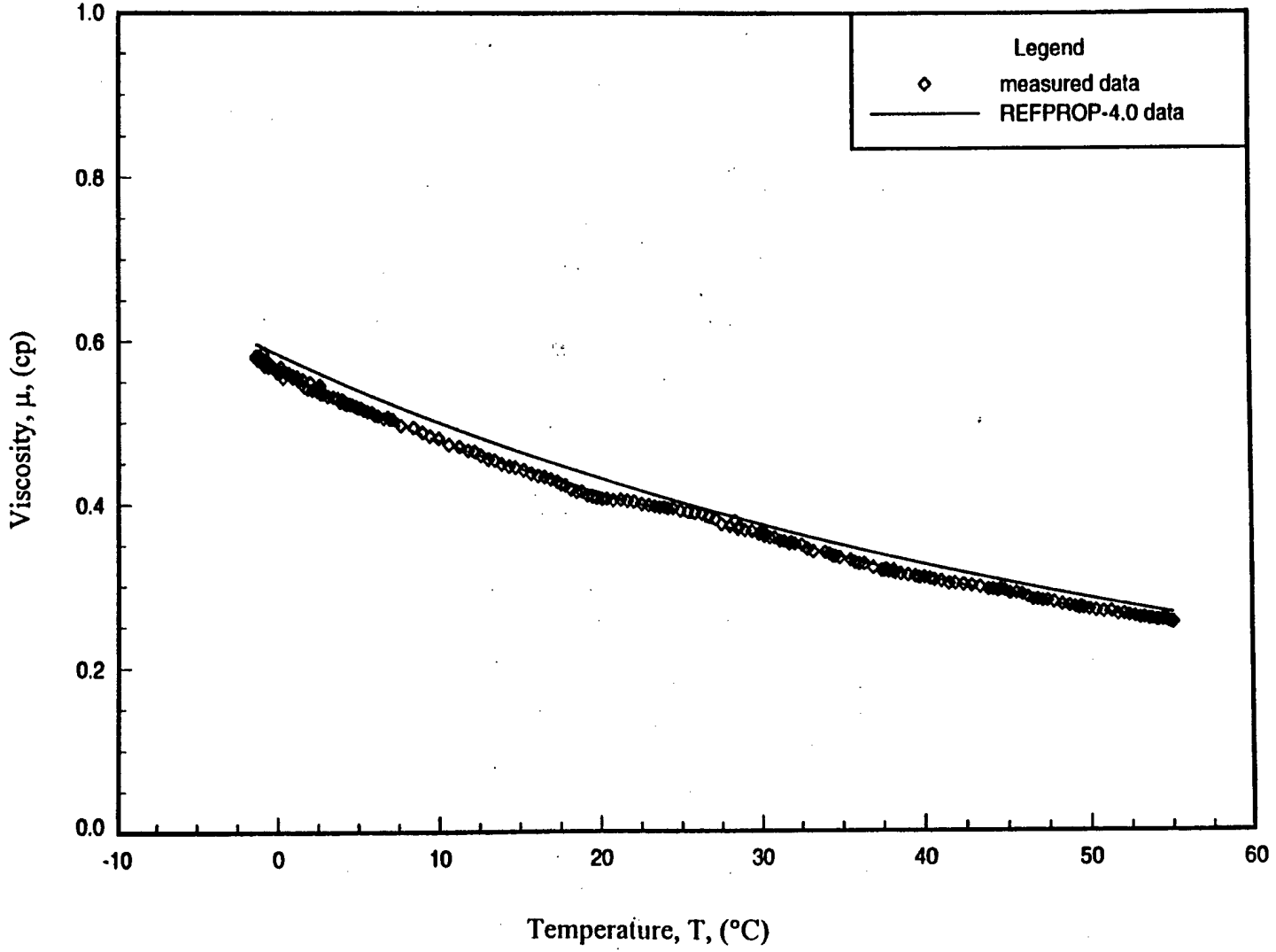

Figure 10.2: Comparison of measured viscosity and REFPROP data for HFC-236ea.

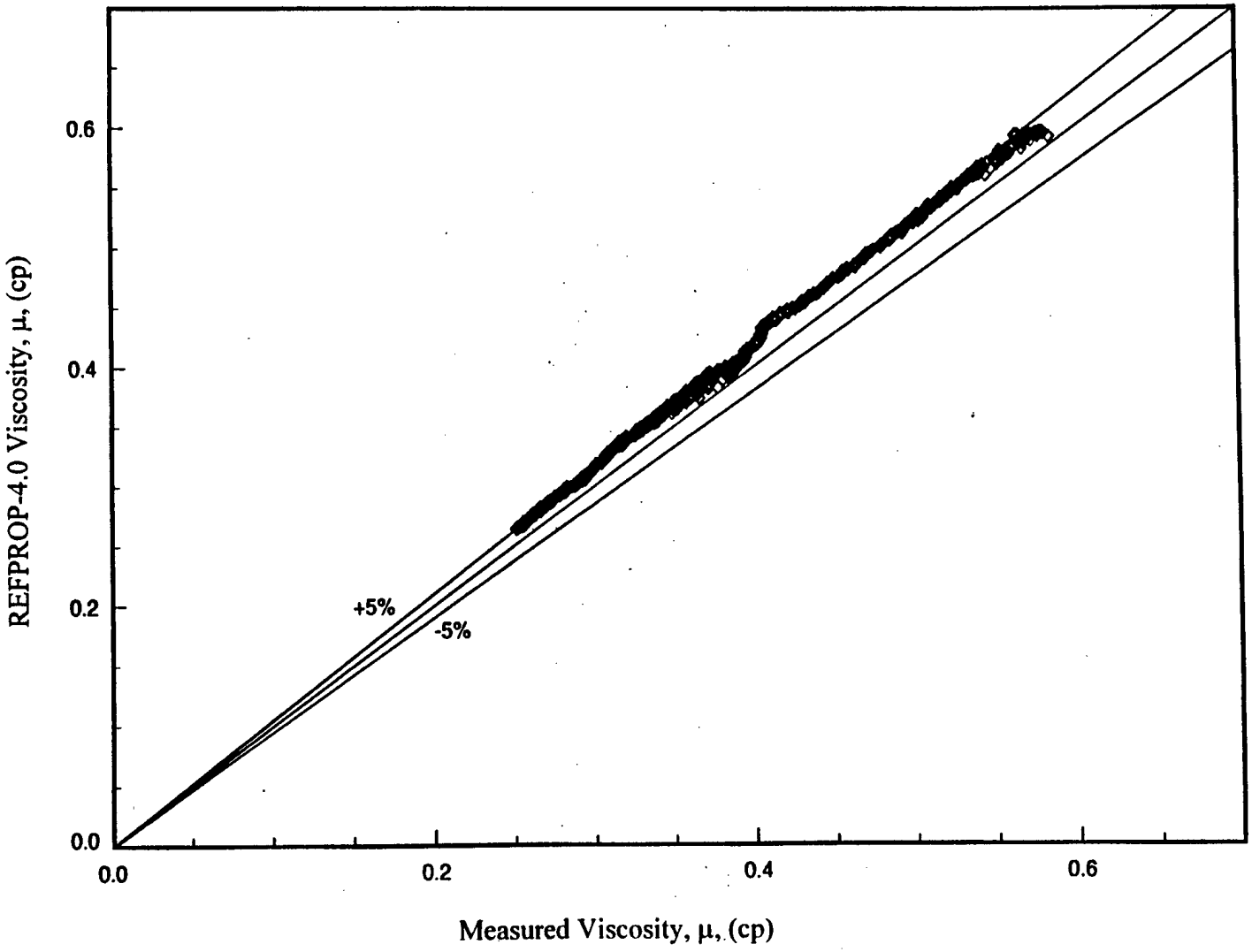

Figure 10.3: Comparison of measured viscosity deviation ranges and REFPROP data for HFC-236ea.

TABLE 10.1: POLYNOMIAL COEFFICIENTS FOR HFC-236ea VISCOSITY (Equation. 10.2)

coefficient	fifth degree polynomial	second degree polynomial
a_0	5.65237164E-01	5.62097609E-01
a_1	-1.06925368E-02	-8.41619726E-03
a_2	2.31479004E-04	5.20047470E-05
a_3	-4.57916803E-06	-
a_4	3.80020317E-08	-
a_5	-1.66399134E-11	-

DENSITY

The density of HFC-236ea was also measured by a densimeter. The accuracy of the densimeter has been verified with a number of refrigerants as discussed in Chapter 5. The resulting plot of density versus temperature is shown in Figure 10.4. The deviations were calculated to be within +1% compared with REFPROP-4.0 values.

The linear curve fit equation for the measured data is:

$$\rho = 1514.30969 - 3.13807 \cdot T \tag{10.3}$$

where ρ is in kg/m^3 and T is in °C.

THERMAL CONDUCTIVITY

The thermal conductivity of HFC-236ea over a temperature range of 0°C to 60°C was measured by Approaches 1 and 2 in this study. The resulting plot is shown in Figure 10.5 using Approach 1 and in Figure 10.6 using Approach 2. As shown in these two figures, the measured results average 15% higher than the REFPROP-4.0 values. Based on the verification data for CFC-114, the measured results imply that the REFPROP data are low for HFC-236ea for the measured temperature range. A linear curve fit equation is given for easy use below:

$$k = 0.097013 - 0.000277 \cdot T \quad \text{Approach 1 (Dittus-Boelter CF)} \tag{10.4}$$

$$k = 0.094944 - 0.000285 \cdot T \quad \text{Approach 1 (Petukhov-Popov CF)} \tag{10.5}$$

$$k = 0.093838 - 0.000282 \cdot T \quad \text{Approach 1 (Gnielinski CF)} \tag{10.6}$$

$$k = 0.0959604 - 0.000268 \cdot T \quad \text{Approach 2} \tag{10.7}$$

where k is in $W/(m \cdot K)$ and T is in °C.

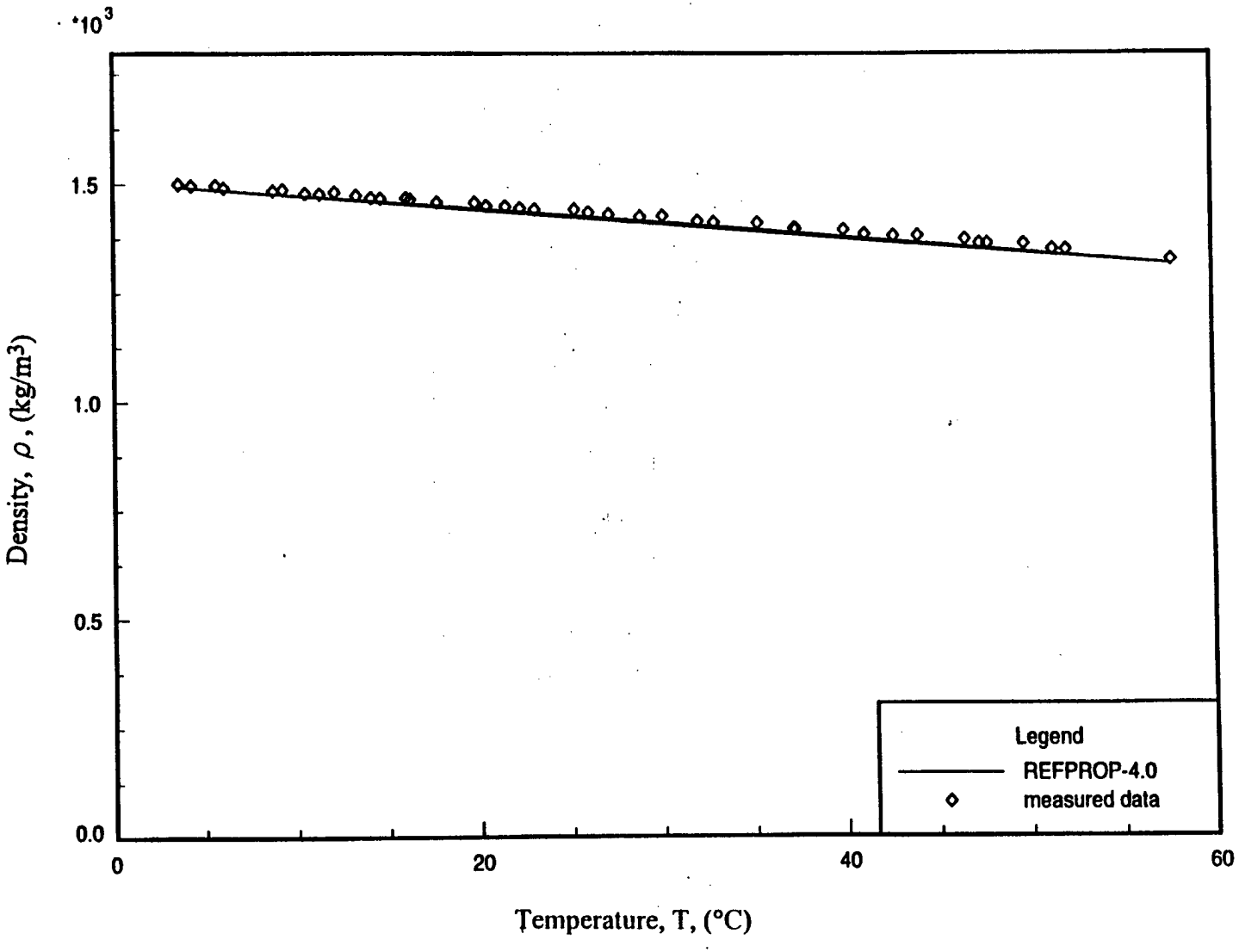

Figure 10.4: Comparison of measured density and REFPROP data for HFC-236ea.

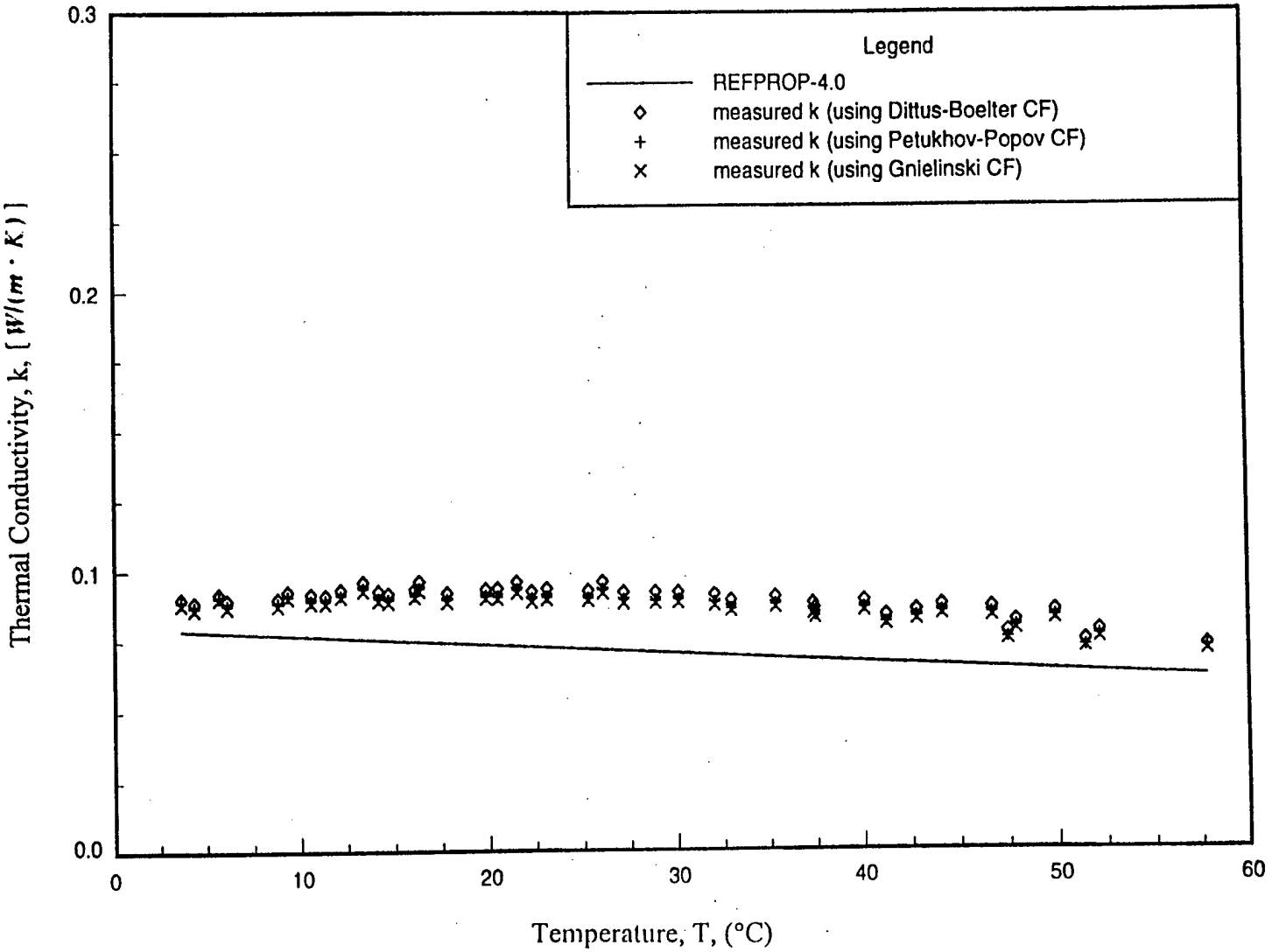

Figure 10.5: HFC-236ea thermal conductivity by Approach 1.

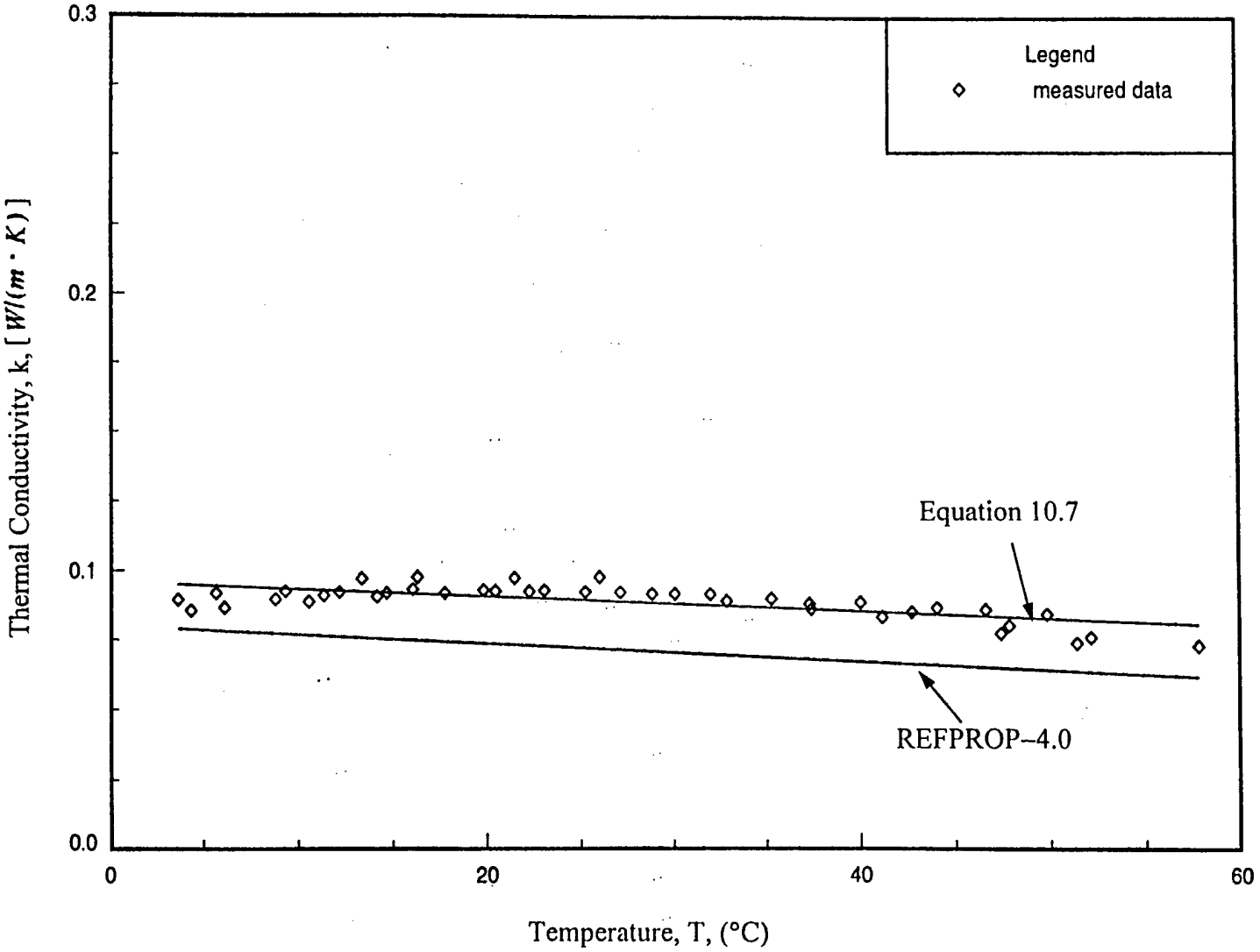

Figure 10.6: HFC-236ea thermal conductivity by Approach 2.

OTHER PROPERTIES

In the current study, there are liquid refrigerant properties which were measured or calculated. These include thermal conductivity, viscosity, specific heat, and density. However, other properties based on these four properties also can be calculated. These include thermal diffusivity and the Prandtl number. Thermal diffusivity is defined as $k / \rho Cp$, and Prandtl number is $\mu Cp / k$. Figures 10.7 and 10.8 show the thermal diffusivity and Pr of HFC-236ea versus temperature, respectively.

To produce the values of thermal diffusivity and Pr, Equation 10.7 was used for k and Equations 10.1 and 10.3 were used for Cp and ρ, respectively. For viscosity, μ, Equation 10.2 and the coefficients associated with the fifth degree in Table 10.1 were used.

SUMMARY

In this Chapter, HFC-236ea properties were measured by the current facility and methodology which were verified by the results of CFC-114 as discussed in the previous chapter. The thermodynamic properties of HFC-236ea (density and specific heat) showed good accuracy when compared with REFPROP. However, the transport properties (viscosity and thermal conductivity) showed larger deviations than the thermodynamic properties. A summary table of the deviations is shown in Table 10.2. As shown in this table, the deviations of density, specific heat, and viscosity are quite reasonable, while the thermal conductivity deviation is quite large. However, as shown in Figures 10.5 and 10.6, the trends of measured and REFPROP data were quite consistent. A modification between these two measures is necessary to achieve closer agreement.

TABLE 10.2: SUMMARY OF MAXIMUM DEVIATION FOR HFC-236ea PROPERTIES

properties	deviation[a] (0 ~ 50°C)
density, ρ	±1%
specific heat, Cp	+4.8%
viscosity, μ	-5%
thermal conductivity[b], k	+15%

[a] deviation = [(measured value − REFPROP value) / REFPROP value] 100

[b] for both Approaches 1 and 2

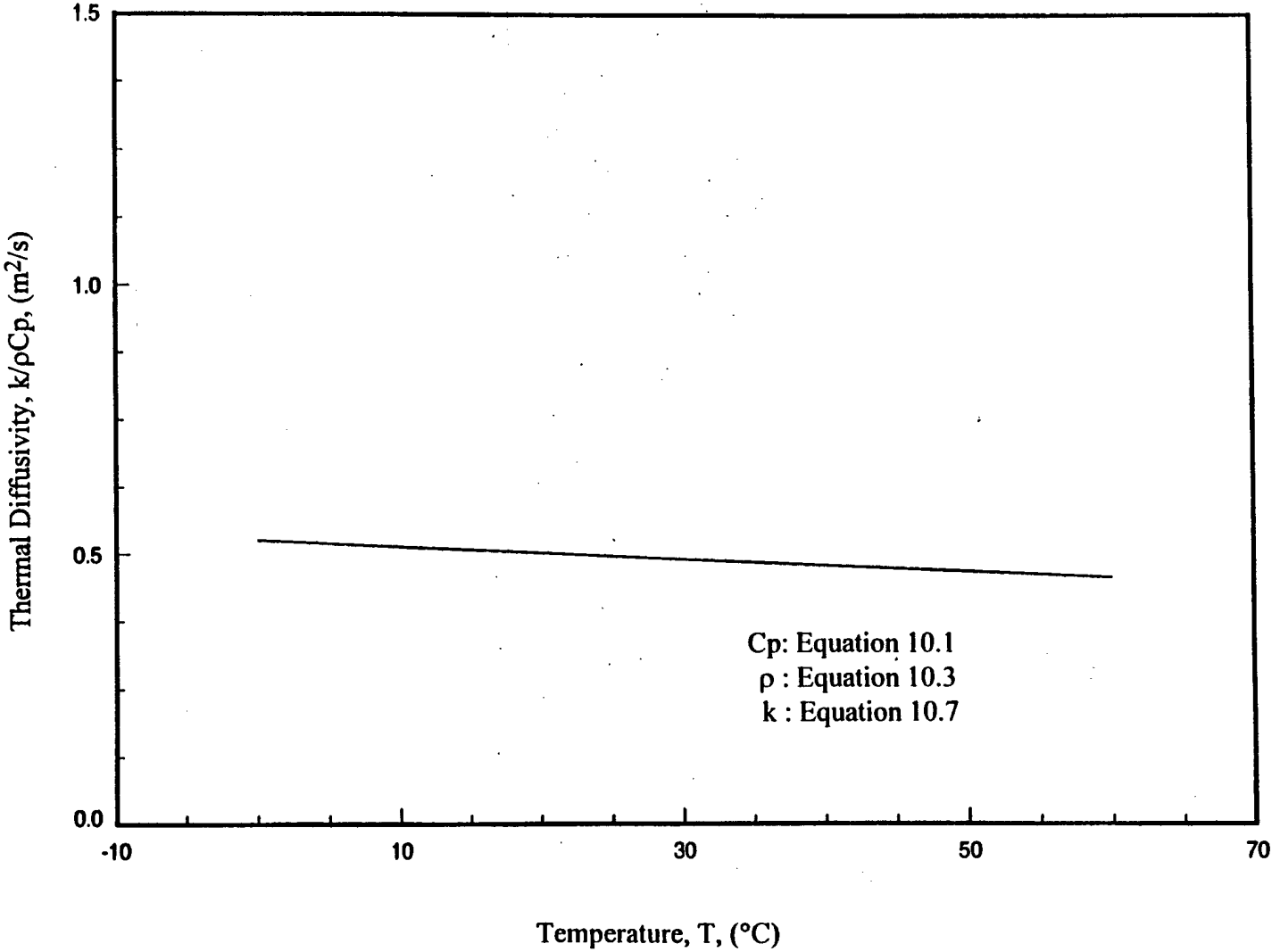

Figure 10.7: Variation of thermal diffusivity of HFC-236ea with temperature.

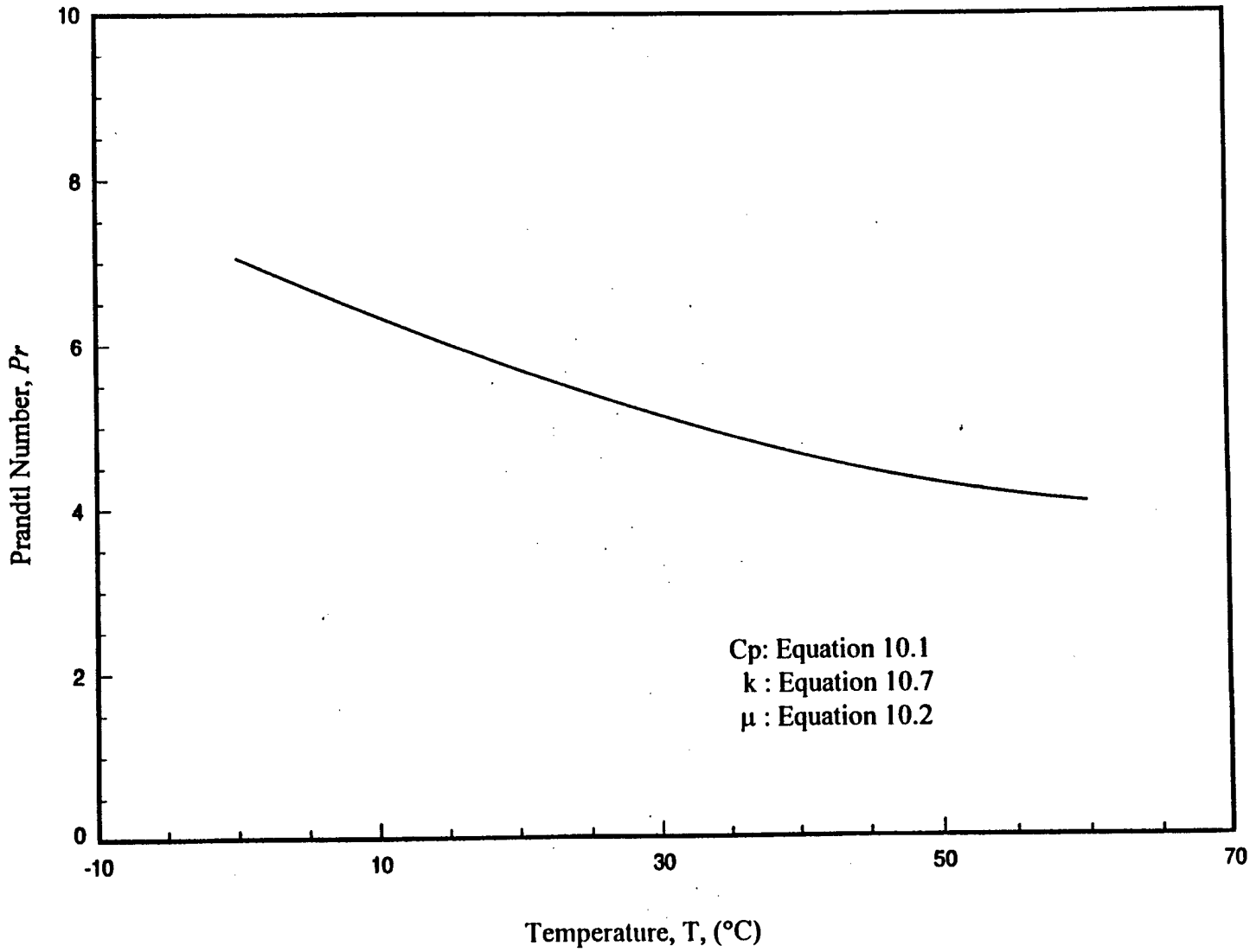

Figure 10.8: Variation of Prandtl number of HFC-236ea with temperature.

CHAPTER 11

PROPERTIES OF HFC-236ea AND LUBRICANT MIXTURES

Property characteristics of a HFC-236ea mixed with a polyol ester (POE) lubricant (Icematic Castrol oil SW68) were investigated. Properties studied included thermal conductivity and viscosity. However, specific heat and density were also determined in this study.

Procedures for lubricant injection and mass fraction sampling were described in Chapter 5. Four lubricant concentrations were studied in this work. Each concentration determination was taken after 10 hours of refrigerant circulation through the test loop following the injection of the lubricant. A summary table for lubricant concentrations is shown in Table 11.1.

TABLE 11.1: LIST OF HFC-236ea AND LUBRICANT CONCENTRATION SAMPLES

number of run	empty cell (g)	total cell (g)	net ref. + oil weight (g)	net oil + cell weight (g)	net oil weight (g)	net ref. weight (g)	oil mass percentage (%)
1	521.91	628.60	106.69	523.81	1.90	104.79	1.78
2	521.91	627.12	105.21	525.52	3.61	101.60	3.43
3	521.91	626.58	104.67	527.69	5.78	98.89	5.52
4	521.91	625.90	103.99	529.43	7.72	96.45	7.42

EFFECTS OF LUBRICANT CONCENTRATION ON THERMAL CONDUCTIVITY OF MIXTURE

Because of limited lubricant data sources, the thermal conductivity of the pure lubricant could not be obtained. So far, few papers have been published in this area. For refrigerant/lubricant mixtures, there have also been very limited data available for use in real refrigeration systems. In the current study, the thermal conductivity of HFC-236ea with a selected lubricant (Icematic Castrol oil SW68) mixture was determined. In this study, the thermal conductivity calculation was based on Approach 2 (Chapter 7) because it showed less uncertainty and was easier to apply (without *CF*) than Approach 1 as shown by previous results.

Figure 11.1 shows the HFC-236ea and the lubricant thermal conductivity versus temperature for various lubricant concentrations. As shown in this figure, at lower temperatures the thermal conductivity increases

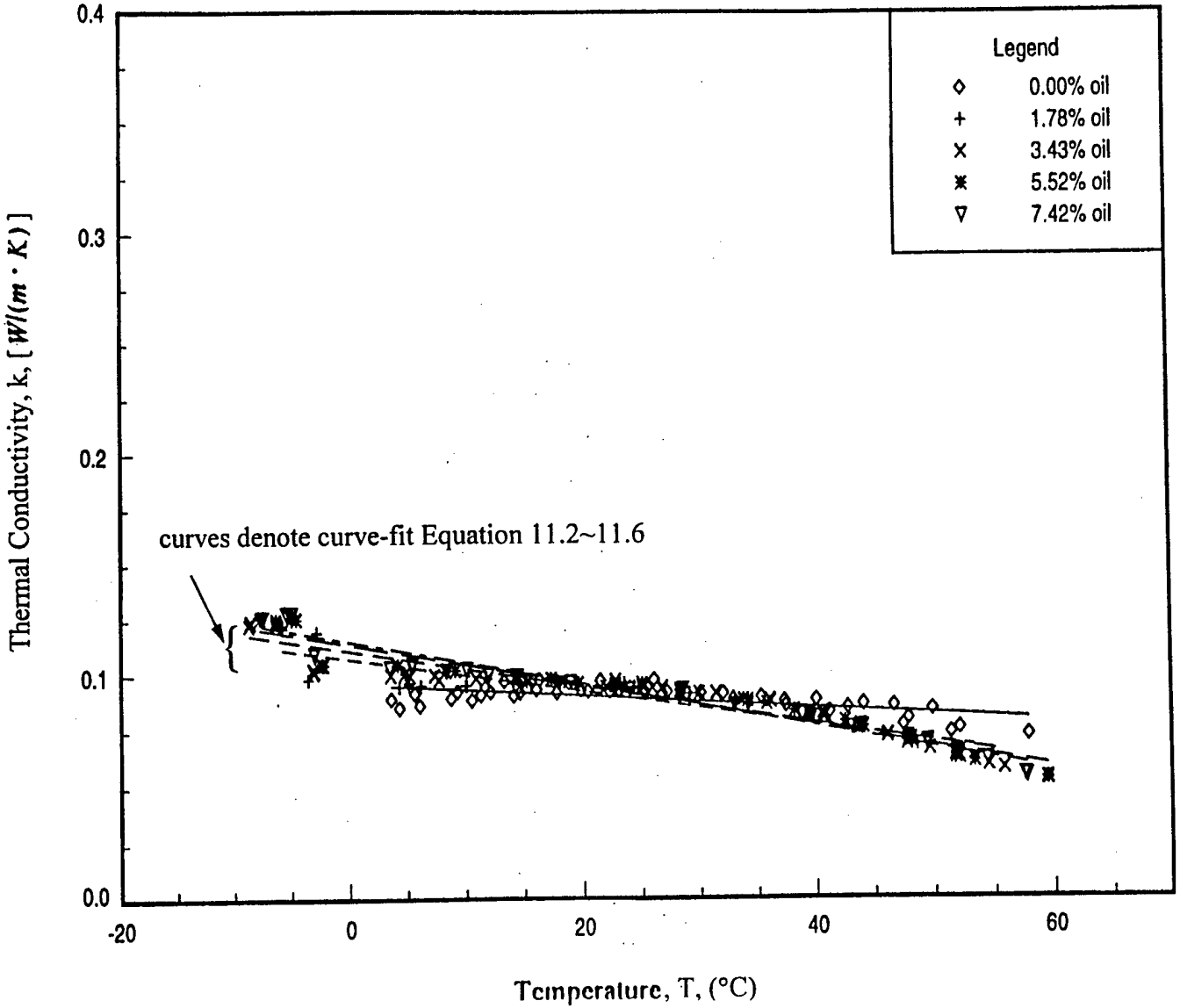

Figure 11.1: Dependence of liquid thermal conductivity of HFC-236ea and lubricant mixture on temperature.

somewhat with increasing lubricant concentration. It also shows the lubricant concentration's effect on the thermal conductivity. At higher temperatures, a minor effect of the lubricant concentration on the mixture's thermal conductivity was found. A slight decrease of thermal conductivity of the mixtures at higher temperatures and concentrations was detected. The curve fit equations are provided later in this discussion. It was found that the thermal conductivity of the mixture increased with lubricant concentration at the higher concentrations and lower temperatures. A nearly 40% thermal conductivity increase was found at -10°C and at the highest lubricant concentration tested (7.42%). At a high temperature (60°C), the thermal conductivity of the mixtures was found not to significantly change with lubricant concentration, at least for concentrations of less than 8% as used in the current study.

An alternative expression for the mixture's thermal conductivity plotted for thermal conductivity versus lubricant concentration is shown in Figure 11.2. In this figure, four constant temperature lines were plotted versus lubricant concentration. As shown, thermal conductivity increases with increasing lubricant concentrations at lower temperatures and decreases as the temperature increases. This is because the thermal conductivity of the lubricant is generally higher than that of the refrigerant, and thermal conductivity of liquids generally decreases with increasing temperature.

A two-variable correlation of temperature (T) and lubricant concentration (C_{oil}) for thermal conductivity of the lubricant and HFC-236ea mixture is developed by a curve-fitting scheme as shown below:

$$k_m = a_0 + a_1 T + a_2 C_{oil} + a_3 T^2 + a_4 T C_{oil} + a_5 C_{oil}^2 + a_6 T^3 + a_7 T^2 C_{oil} + a_8 T C_{oil}^2 + a_9 C_{oil}^3 \quad (11.1)$$

where k is in $W/m \cdot K$, T is in °C, and C_{oil} is the mass fraction of oil in the mixture. The a_i values are listed in Table 11.2.

TABLE 11.2: COEFFICIENTS OF THERMAL CONDUCTIVITY FOR LUBRICANT AND HFC-236ea MIXTURES

coefficient	value
a_0	0.095728
a_1	-0.000659
a_2	0.004704
a_3	3.4517E-05
a_4	-0.000218
a_5	-0.000273
a_6	-5.67E-07
a_7	8.44E-07
a_8	1.4516E-05
a_9	-7.671E-06

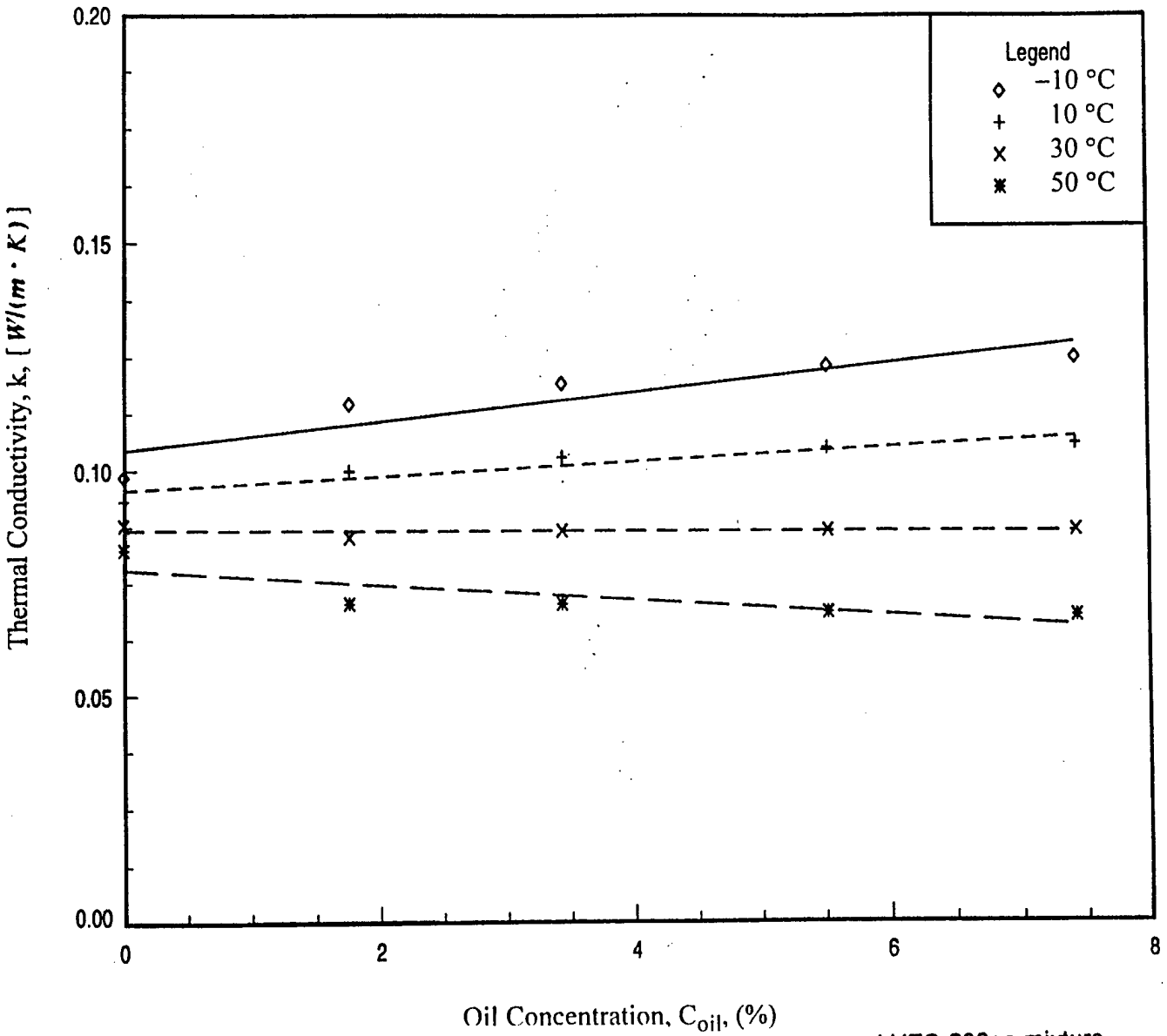

Figure 11.2: Dependence of thermal conductivity of lubricant and HFC-236ea mixture with lubricant mass fraction at four different temperatures.

A comparison of the deviation between experimental data and predicted values by the currently developed equation (Equation 11.1) is shown in Figure 11.3. As shown in this figure, the predicted values agree with the experimental data within ±5%.

An individual equation for the thermal conductivity of the lubricant and HFC-236ea mixture as a function of temperature is also provided for various lubricant mass concentrations over the temperature range from –10°C to 60°C and is shown below:

$$\text{0.0\% lubricant: } k_m = (9.59604010E-02) + (-2.68429925E-04)T \quad (11.2)$$

$$\text{1.78\% lubricant: } k_m = (1.07318327E-01) + (-7.35581270E-04)T \quad (11.3)$$

$$\text{3.43\% lubricant: } k_m = (1.10977404E-01) + (-8.13782855E-04)T \quad (11.4)$$

$$\text{5.52\% lubricant: } k_m = (1.13845766E-01) + (-9.09929338E-04)T \quad (11.5)$$

$$\text{7.42\% lubricant: } k_m = (1.15142770E-01) + (-9.53352253E-04)T \quad (11.6)$$

where k_m is in $W/(m \cdot K)$ and T is in °C.

EFFECTS OF LUBRICANT CONCENTRATION ON THE VISCOSITY OF MIXTURE

A lubricant (oil) usually has a very high viscosity compared with a refrigerant. In general, the lubricant's viscosity is several thousand times greater than most refrigerants at low temperatures. In general, the viscosity of a lubricant changes rapidly with temperature, especially in the low temperature range. However, the viscosity in the high temperature range, although not significantly changing with temperature, is still very high and could be several hundred times that of the refrigerant viscosity. As a lubricant is added to a refrigerant, the viscosity of the mixture rapidly increases due to the high viscosity of the lubricant added.

In the present study, the viscosity of the lubricant and HFC-236ea mixture was measured. Figure 11.4 shows the mixture viscosity versus temperature for various lubricant concentrations. As shown in this figure, the viscosity increases with a lubricant's increasing concentration and with a decreasing temperature. An interesting result was found that in the mixture viscosity rapidly increased with higher lubricant concentrations at lower temperatures. At low temperatures (below -10°C) and lubricant concentrations under 8%, it was found that the effect of lubricant concentration on the mixture viscosity was significant. At high temperature situations, the lubricant concentration was shown, not so obviously, to affect the mixture viscosity just as markedly as at low temperatures. An alternative plot for viscosity versus concentration for various temperatures is shown in Figure 11.5.

Equations developed for applying these results are useful and they are provided in the following discussion. Viscosity equations for various lubricant concentrations are listed below:

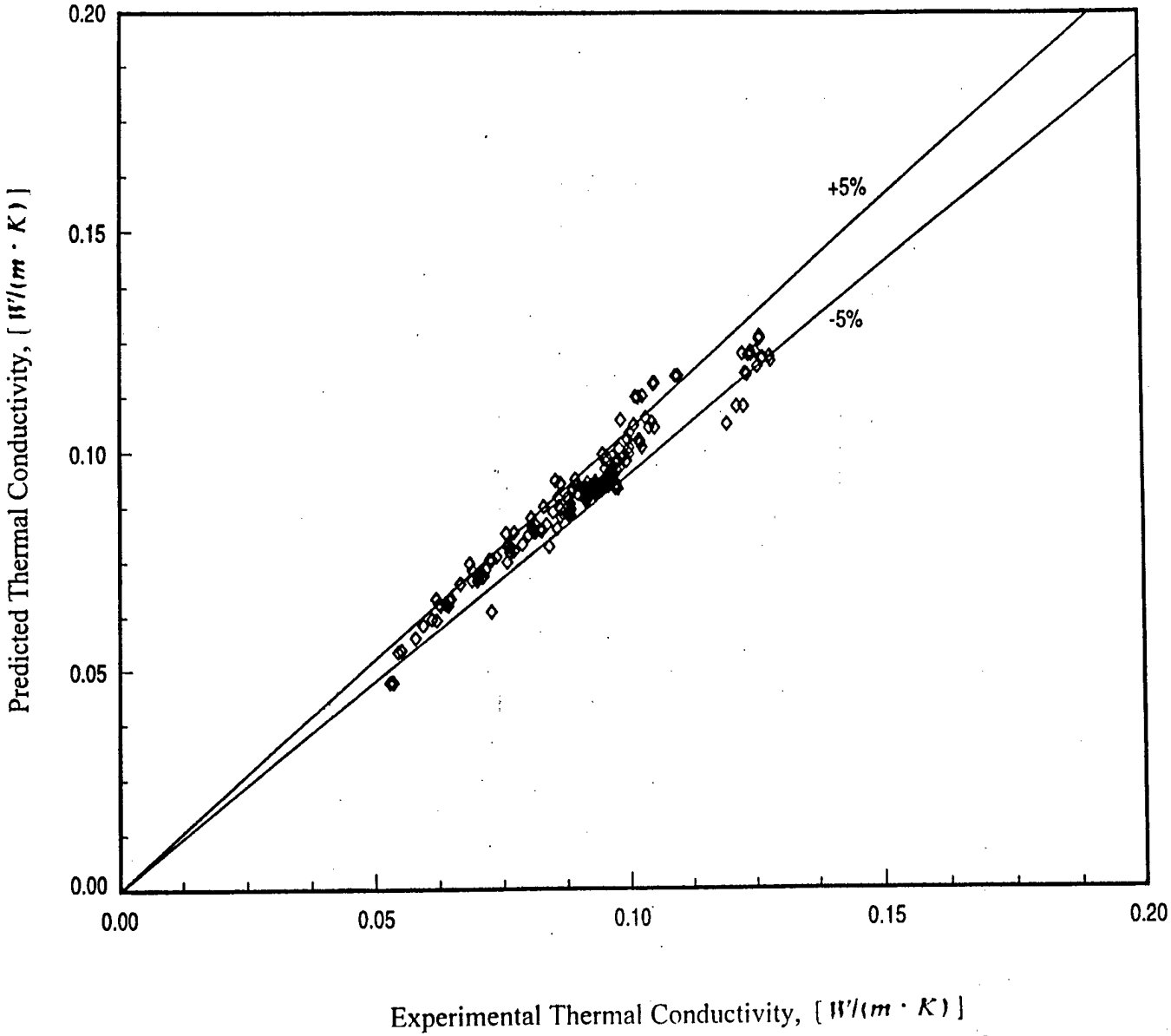

Figure 11.3: Predicted thermal conductivity versus experimental data of lubricant (Icematic Castrol SW68) and HFC-236ea mixtures.

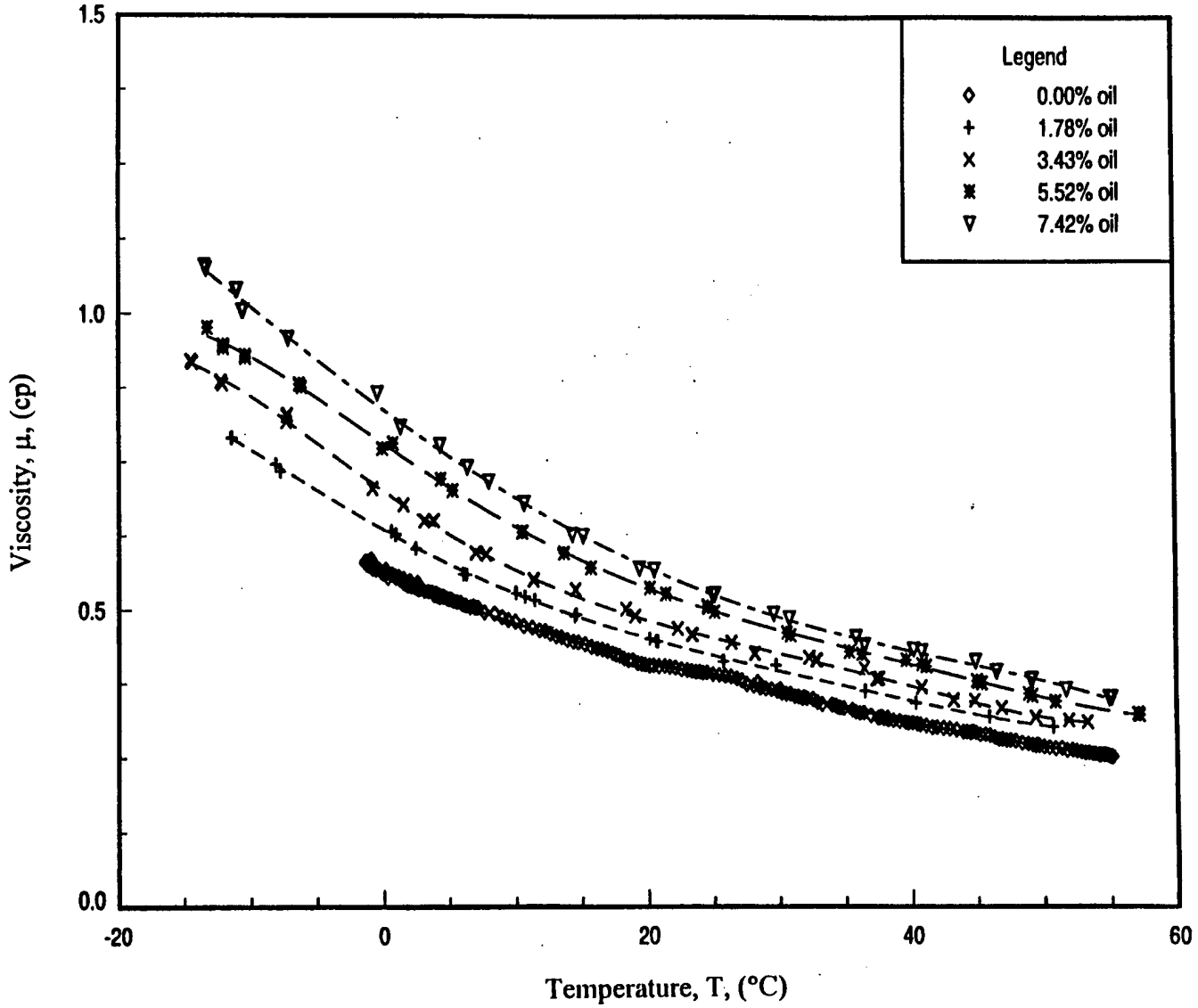

Figure 11.4: Viscosity versus temperature for lubricant and HFC-236ea mixture under various lubricant concentrations.

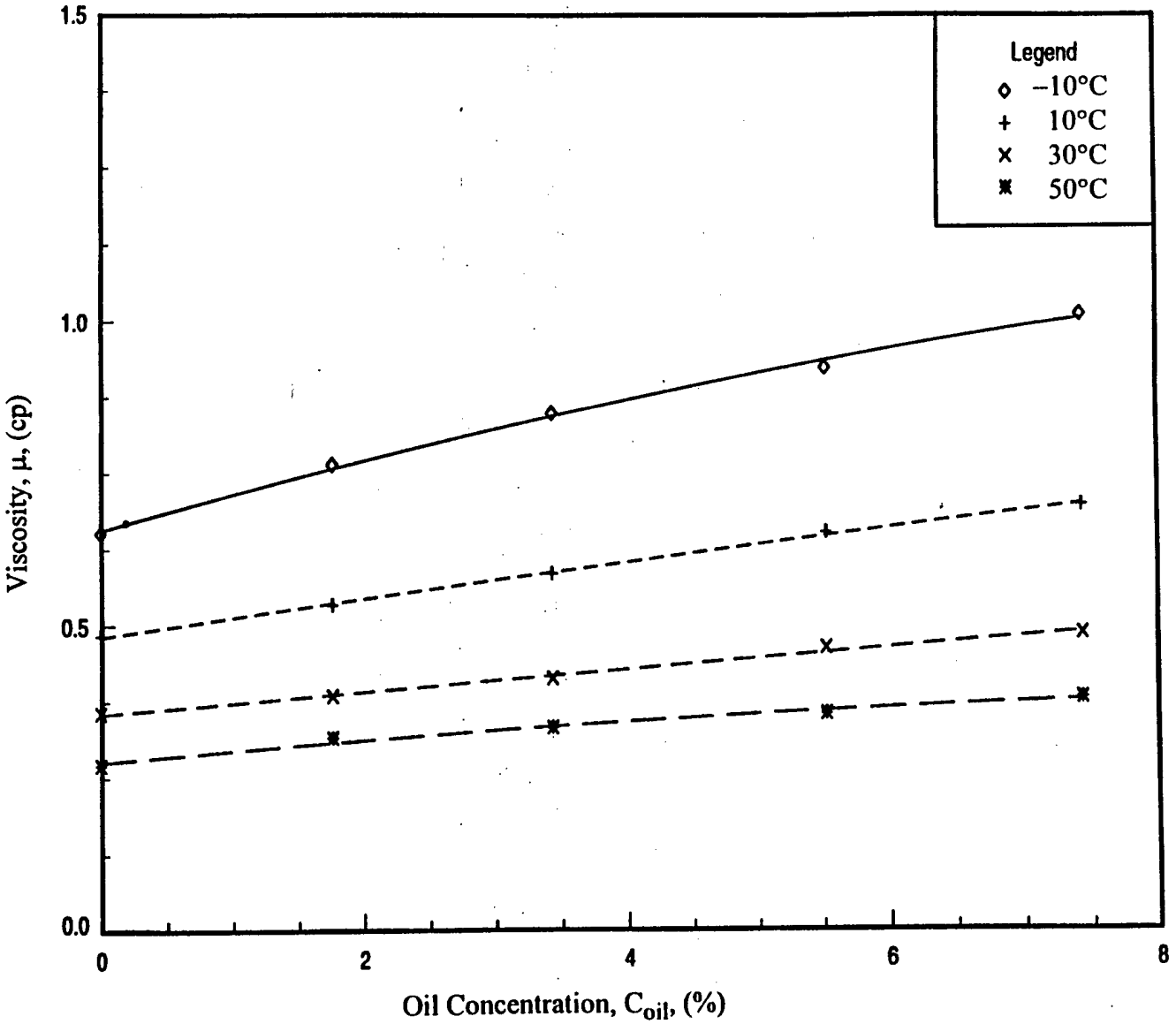

Figure 11.5: Viscosity versus lubricant mass fraction for lubricant and HFC-236ea mixture for various temperatures.

$$0.0\%\ \text{lubricant: } ln(\mu) = -52.355901 + 5796.690020\frac{1}{T} + 0.163335T - 0.000188T^2 \quad (11.7)$$

$$1.78\%\ \text{lubricant: } ln(\mu) = -0.457921 + 0.006319\frac{1}{T} - 0.018463T + 0.0000809067T^2 \quad (11.8)$$

$$3.43\%\ \text{lubricant: } ln(\mu) = -0.365710 - 0.008252\frac{1}{T} - 0.018990T + 0.0000752787T^2 \quad (11.9)$$

$$5.52\%\ \text{lubricant: } ln(\mu) = -0.265842 - 0.000275\frac{1}{T} - 0.018248T + 0.0000556867T^2 \quad (11.10)$$

$$7.42\%\ \text{lubricant: } ln(\mu) = -0.190103 - 0.010952\frac{1}{T} - 0.019339T + 0.0000719047T^2 \quad (11.11)$$

where T is in K and μ is in cp.

A two-variable correlation, temperature (T) and lubricant concentration (C_{oil}), for the viscosity of lubricant (Icematic Castrol oil SW68) and HFC-236ea mixture (μ_m) was also developed by the curve fit scheme as shown in Equation 11.12:

$$ln(\mu_m) = a_0 + a_1T + a_2C_{oil} + a_3T^2 + a_4TC_{oil} + a_5C_{oil}^2 + a_6T^3 + a_7T^2C_{oil} + a_8TC_{oil}^2 + a_9C_{oil}^3 \quad (11.12)$$

where μ_m is in cp, T is the temperature in °C, and C_{oil} is the mass fraction of lubricant in the mixture. The a_i are listed in Table 11.3. An accuracy test for using this equation was verified within ±2% with the experimental data covering a viscosity range of 0 to 1.2 cp. Figure 11.6 shows the predicted viscosity using Equation 11.12 versus experimental data. It shows that for the viscosity range of the experiments (0 to 1.2 cp), the values predicted by using Equation 11.12 agree with the experimental data.

TABLE 11.3: COEFFICIENTS OF VISCOSITY FOR LUBRICANT AND HFC-236ea MIXTURE

coefficient	value
a_0	0.567099
a_1	-0.010817
a_2	0.074007
a_3	0.000168
a_4	-0.001519
a_5	-0.005964
a_6	-1.4E-06
a_7	1.1996E-05
a_8	4.3801E-05
a_9	0.000302

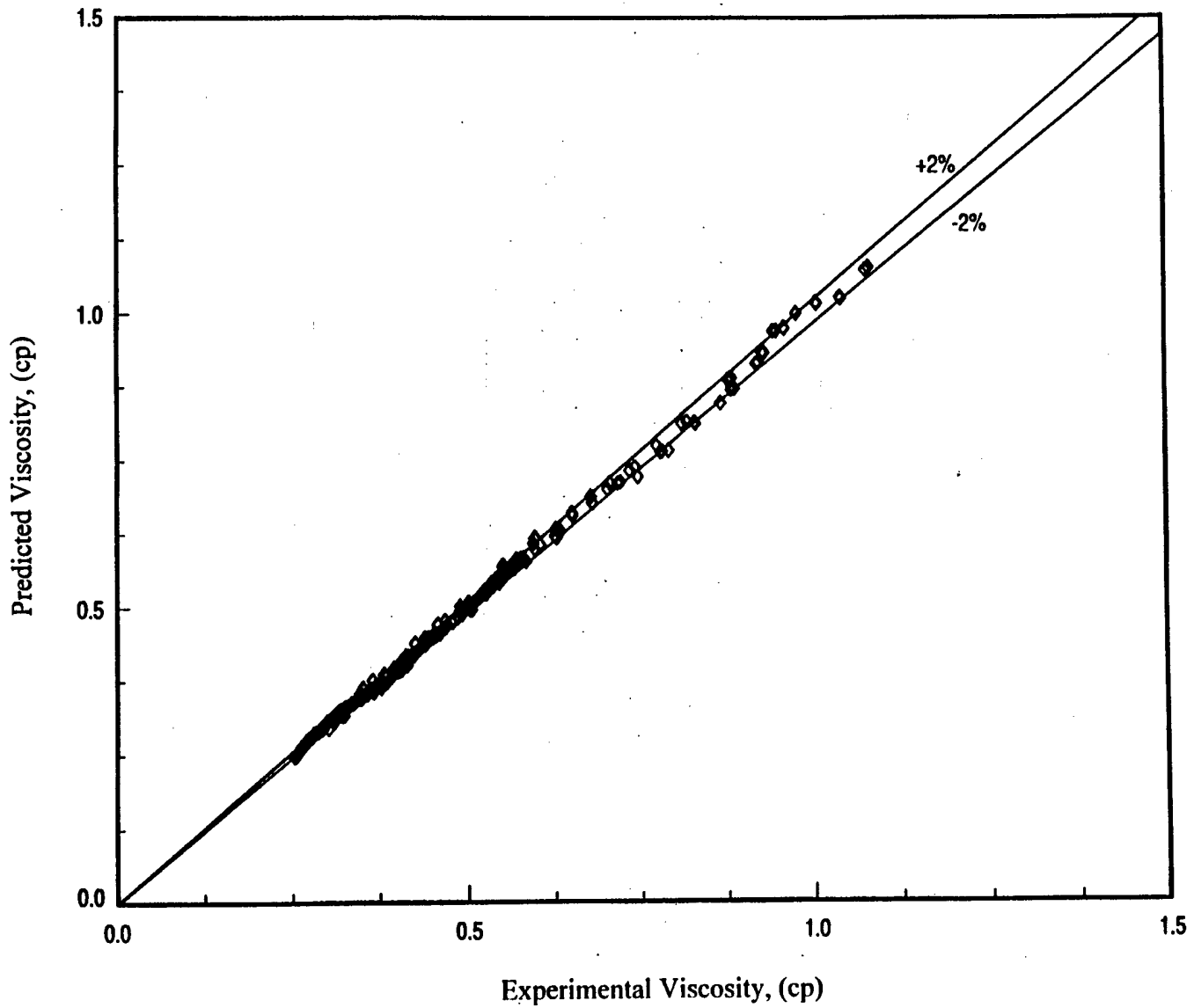

Figure 11.6: Predicted viscosity versus experimental data of the lubricant (Icematic Castrol SW68) and HFC-236ea mixture.

OTHER PROPERTIES OF LUBRICANT AND HFC-236ea MIXTURE

In this section, specific heat and density of HFC-236ea and Icematic Castrol SW68 oil are calculated and presented as curves. Figure 11.7 shows the specific heat of these mixtures. As shown, the specific heat is not significantly affected by lubricant concentrations except at high concentrations of lubricant in the lower temperature range. As the specific heat of a pure lubricant is difficult to obtain, it is assumed that the specific heat for both materials (HFC-236ea and lubricant) should be fairly close. However, further verification will be required when specific heat data of pure lubricants become available.

The density of the mixture is shown in Figure 11.8. As indicated, the density of the mixture decreases as the temperature increases. However, at a fixed temperature, the densities of the mixture with a low lubricant concentration are higher than those of high lubricant concentration. This implies that pure HFC-236ea has a higher density value than pure lubricant currently used.

SUMMARY

In this chapter, the transport properties of lubricant and HFC-236ea mixtures are presented. Lubricant concentration effects on both thermal conductivity and viscosity are discussed. However, viscosity is more significantly affected by lubricant concentration, especially in a lower temperature range. Thermal conductivity is affected by lubricant concentrations by 8 to 40% at -10°C and only by 1 to 10% at 40°C for a lubricant concentration varying from 2 to 7.4%.

Other properties, such as specific heat and density of the mixture of HFC-236ea and Icematic Castrol SW68 oil, were also calculated and discussed. The results showed that temperature and lubricant concentration have limited influence on these properties.

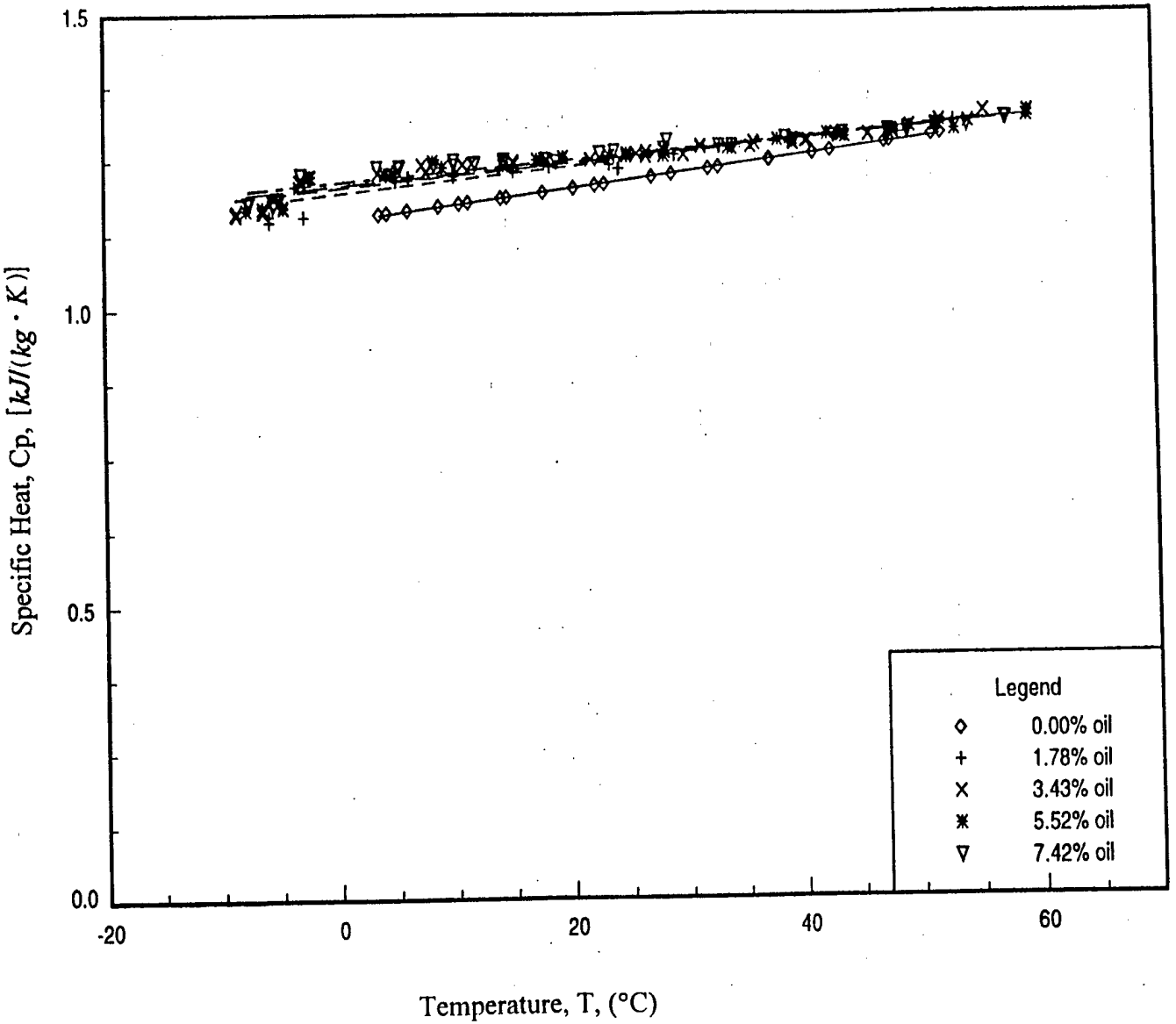

Figure 11.7: Comparison of predicted and measured viscosity for HFC-236ea/lubricant mixtures.

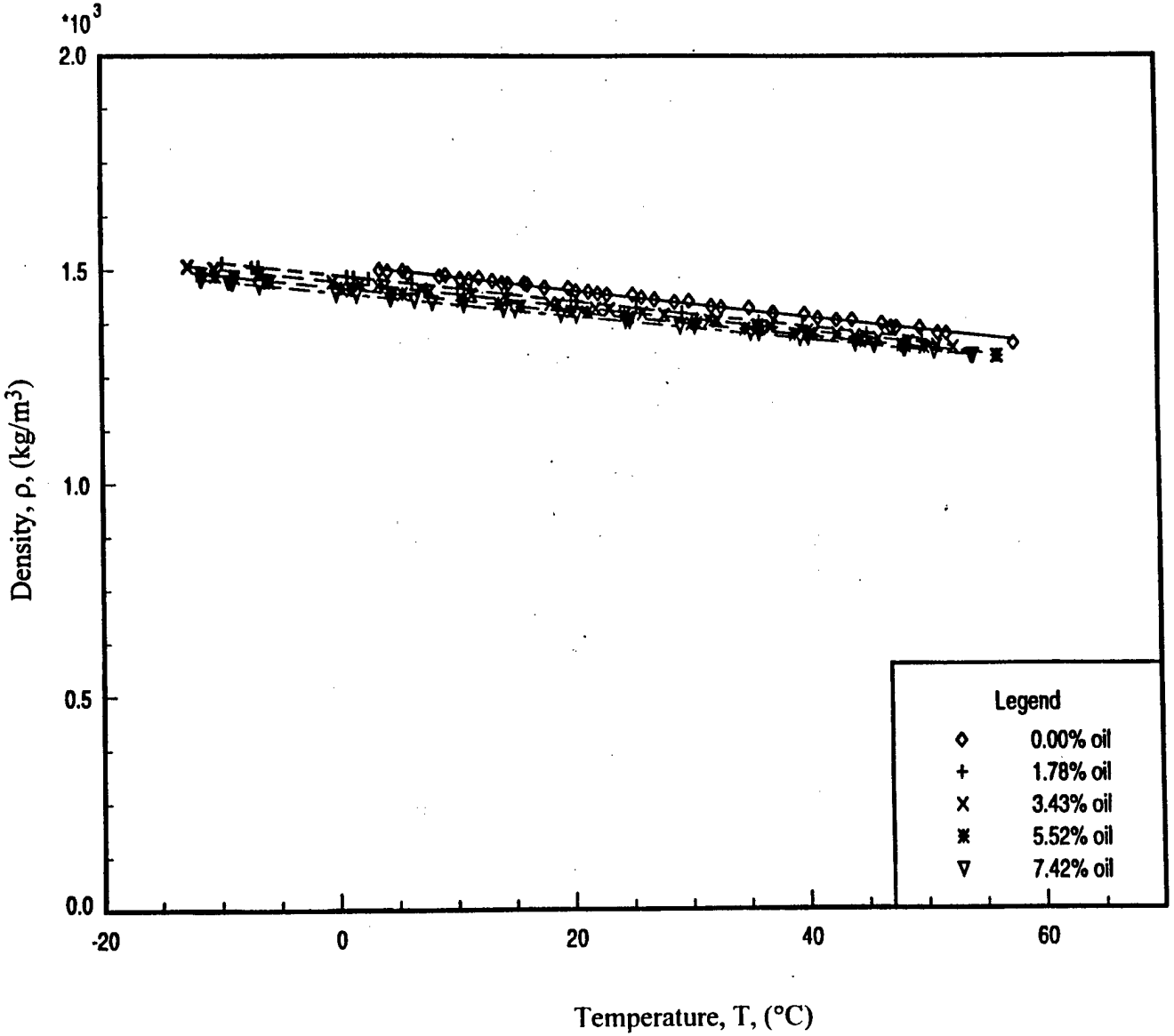

Figure 11.8: Density versus temperature of lubricant and HFC-236ea mixture.

REFERENCES

1. Cox, J.E. and Miro, C.R. "Rundown on CFC Legislation." ASHRAE Journal, p. 14, November 1989.

2. Cox, J.E. and Miro, C.R. "Montreal Protocol Assessment in Nairobi." ASHRAE Journal, p. 22, September 1994.

3. Bare, J.C. "Simulation of Performance of Chlorine-Free Fluorinated Ethers and Fluorinated Hydrocarbons to Replace CFC-11 and CFC-114 in Chillers." ASHRAE Transaction: Research, Vol. 99, No. 3661, Part 1, pp. 397-407, 1993.

4. Kazachki, G.S. and Hendriks, R.V. "Performance Testing of A Semi-Hermetic Compressor with HFC-236ea and CFC-114 at Chiller Conditions." Proceedings of the 1994 International Refrigeration Conference at Purdue, pp. 407-411, Purdue University, West Lafayette, IN, July 19-22, 1994.

5. Bell, K.L., Hewitt, G.F., and Morris, S.D. "Nucleate Pool Boiling of Refrigerant/Oil Mixtures." Experimental Heat Transfer, Vol. 1, pp. 71-86, 1987.

6. Guy, P.D., Tompsett, G., and Dekleva, T.W. "Compatibilities of Nonmetallic Materials with HFC-134A and Alternative Lubricants in Refrigeration Systems." ASHRAE Transactions: Symposia, Vol. 98, Pt. 1, No. AN-92-5-4, pp. 804-816, 1992.

7. Spauschus, H.O. and Speaker, L.M. "A Review of Viscosity Data for Oil-Refrigerant Solutions." ASHRAE Transaction, No. 3094 (RP-444), Vol. 93, Part 2, pp. 667-681, 1987.

8. Kruse, H.H. and Schroeder, M. "Fundamentals of Lubrication in Refrigerating Systems and Heat Pumps." ASHRAE Transaction, KC-84-14, Vol. 90, No. 1, Part 2B, pp. 763-783, 1984.

9. Zoz, S.C. "An Experimental Investigation of the Miscibility Characteristics of Alternative Refrigerant and Lubricant Mixtures." Ph.D. Diss., Iowa State University, Ames, IA, 1994.

10. Okubo, T. and Nagashima, A. "Measurement of The Viscosity of HCFC123 in The Temperature Range 233-418K and at Pressure up to 20 MPa." International Journal of Thermophysics, Vol. 13, No. 3, pp. 401-410, 1992.

11. Okubo, T., Hasuo, T., and Nagashima, A. "Measurement of the Viscosity of HFC134a in the Temperature Range 213-423K and at Pressure up to 30 MPa." International Journal of Thermophysics, Vol. 13, No. 6, pp. 931-942, 1992.

12. Assael, M.J., Oliveira, C.P., Papadaki, M., and Wakeham, W.A. "Vibrating-Wire Viscometers for Liquids at High Pressures", International Journal of Thermophysics, Vol. 13, No. 4, pp. 593-615, 1992.

13. Diller, D.E., Aragon, A. S., and Laesecke, A. "Measurements of The Viscosities of Saturated and Compressed Liquid 1,1,1,2 - Tetrafluoro-ethane (HFC-134a), 2,2 - dichloro - 1, 1 - Trifluoroethane (R123), and 1,1 - Dichloro - 1 - fluoroethane (R142b)." Fluid Phase Equilibria, Vol. 88, pp. 251-262, 1993.

14. Ferry, J.D. "Oscillation Viscometry - Effects of Shear Rate and Frequency." Measurements and Control, pp. 89-91, September-October 1977.

15. Fitzgerald, J.V., Matusik, F.J., and Walsh, T.M. "Inline Viscometry." Measurements and Control, pp. 118-123, December 1987.

16. Fitzgerald, J.V., Matusik, F.J., and Walsh, T.M. "Oscillation Viscometer." Measurements and Control, pp. 175-179, June 1986.

17. Sousa, A.T., Fialho, P.S., Neito De Castro, C.A., Tufeu, R., and Le Neindre, B. "The Thermal Conductivity of 1-Chloro-1,1-difluoroethane (HCFC-142b)." International Journal of Thermophysics, Vol. 13, No. 3, pp. 383-399, 1992.

18. Tanaka, Y., Nekata, M., and Makita, T. "Thermal Conductivity of Gaseous HFC-134a, HCFC-142b." International Journal of Thermophysics, Vol. 12, No. 6, pp. 947-963, 1992.

19. Neito de Castro, C.A., Perkins, R.A., and Roder, H.M. "Radiative Heat Transfer in Transient Hot-Wire Measurements of Thermal Conductivity." International Journal of Thermophysics, Vol. 12, No. 6, pp. 985-997, 1991.

20. Gross, U., Song, Y.W., and Hahne, E. "Thermal Conductivity of the New Refrigerants R134a, R152a, and R123 Measurement by the Transient Hot-Wire Method." International Journal of Thermophysics, Vol. 13, No. 6, pp. 957-983, 1992.

21. Assel, M.J., Karagiannidis, E., and Wakeham, W.A. "Measurements of Thermal Conductivity of R11 and R12 in the Temperature Range 250-340 K at Pressure up to 30 MPa." International Journal of Thermophysics, Vol. 13, No. 5, pp. 735-751, 1992.

22. Yata, J., Minamiyama, T., and Tanaka, S. "Measurement of Thermal Conductivity of Liquid Fluorocarbons." International Journal of Thermophysics, Vol. 5, No. 2, pp. 209-218, 1984.

23. Jung, D. and Radermacher, R. "Transport Properties and Surface Tension of Pure and Mixed Refrigerants." ASHRAE Transaction: Research, Vol. 97, Part 1, No. 3445, pp. 90-99, 1991.

24. Song, Y.W., Gross, U., and Hahne, E. "A New Method for Thermal Diffusivity and Thermal Conductivity Evaluation from Transient Hot-Strip Measurement." Fluid Phase Equilibria, Vol. 88, pp. 291-302, 1993.

25. Lin, J.Y. and Pate, M.B. "A Methodology for Simultaneously Measuring Thermal Conductivity and Viscosity of Refrigerant Mixtures." Proceedings of the 12th International Compressor Engineering and Refrigeration Conference at Purdue, Purdue University, West Lafayette, IN, pp. 43-48, July 19-22, 1994.

26. Lin, J.Y. "A New Methodology for the Determination of Transport Properties of Refrigerants." Ph.D. Diss., Iowa State University, Ames, IA, 1994.

27. McLinden, M.O. and Morrison, G. "NIST Thermodynamic Properties of Refrigerants and Refrigerant Mixtures Database." Version 4.0, U. S. Department of Commerce, Gaithersburg, MD, November 1993.

28. Reid, R.C., Prausnitz, J.M., and Poling, B.E. "The Properties of Gases and Liquids." the 4th Edition, Chapters 9 and 10, McGraw-Hill, Inc., New York City, NY, 1987.

29. Munson, B.R., Young, D.F., and Okiishi, T.H. "Fundamentals of Fluid Mechanics." John Wiley & Sons, Inc., New York City, NY, 1990.

30. White, F.M. "Viscous Fluid Flow", the 2nd Edition, McGraw-Hill, Inc., New York City, NY, 1991.

31. Bird, R.B., Stewart, W.E., and Lightfoot, E.N. "Transport Phenomena." John Wiley & Sons, Inc., New York City, NY, August 1978.

32. Baroncini, C., Filippo, P., DiLatini, G., and Pacetti, M. "Organic Liquid Thermal Conductivity: A Prediction Method in the Reduced Temperature Range 0.3 to 0.8." International Journal of Thermophysics, Vol. 2, No. 1, pp. 21-38, 1981.

33. Kandlikar, S.G., Bijlani, C.A., and Sukhatme, S.P. "Predicting the Properties of Mixtures of R22 and R12 Part II - Transport Properties." ASHRAE Transaction, Vol. 81, Part 1, No. 2343, pp. 285-294, 1975.

34. Levy, F.L. "A Modified Maxwell-Eucken Equation for Calculating the Thermal Conductivity of Two-Component Solutions or Mixtures." International Journal of Refrigeration, pp. 223-225, 1981.

35. Ely, J.F. and Hanley, H.J.M. "Prediction of Transport Properties 2. Thermal Conductivity of Pure Fluids and Mixtures." Industrial and Engineering Chemistry Fundamentals, Vol. 22, No. 1, pp. 89-97, 1983.

36. Jensen, M.K. and Jackman, D.L. "Prediction of Nucleate Pool Boiling Heat Transfer Coefficients of Refrigerant-Oil Mixtures." Transactions of the ASME: Journal of Heat Transfer, Vol. 106, pp. 184-190, 1984.

37. Baustian, J.J., Pate, M.B., and Bergles, A.E. "Properties of Oil-Refrigerant Liquid Mixtures with Applications to Oil Concentration Measurement: Part I - Thermophysical and Transport Properties." ASHRAE Transactions, No. 2937 (RP-356), Vol. 92, Part 1A, pp. 55-73, 1986.

38. Lin, J.Y. and Pate, M.B. "A Thermal Conductivity Predicting Method for Refrigerant Mixtures in Liquid Phase." Proceedings of the 1992 International Refrigeration Conference - Energy Efficiency and New Refrigerants, Vol. II, pp. 365-374, 1992.

39. Latini, G., Pierpaoli, P., and Polonara, F. "Dynamic Viscosity and Thermal Conductivity Prediction of Refrigerants and Refrigerant Mixtures." Proceedings of the 1992 International Refrigeration Conference - Energy Efficiency and New Refrigerants, Vol. II, pp. 489-499, 1992.

40. Watanabe, K., Sato, H., and Qian, Z.-Y. "Thermodynamic Properties of New Refrigerants -- HFC-32 and HFC-125." Proceedings of the 1992 International Refrigeration Conference - Energy Efficiency and New Refrigerants, Vol. II, pp. 443-452, 1992.

41. Stephan, K. and Heckenberger, T. "The Midas Data Base System for the Transport Properties of Pure Fluids and Mixtures." 17th International Congress of Refrigeration, pp. 1-6, 1987.

42. Ely, J.F. and Hanley, H.J.M. "Prediction of Transport Properties 1. Viscosity of Fluids and Mixtures." Industrial and Engineering Chemistry Fundamentals, Vol. 20, No. 4, pp. 323-332, 1981.

43. Kruse, H., Gerdsmeyer, K.D., Kuver, M., and Arnemann, M. "Measurements and Calculations of Thermodynamic Data for the Binary Refrigerant Mixture R22/R114." International Journal of Refrigeration, Vol. 12, pp. 62-70, March 1989.

44. "Thermal Conductivity." Edited by Tye, R.P., Vol. 2, Chapter 2, Academic Press Inc., (London) Ltd., New York City, NY, 1969.

45. Tsederberg, N.V. "Thermal Conductivity of Gases and Liquids", Chapter 1, Edited by Robert D. Cess, the M.I.T. Press, Cambridge, MA, 1965.

46. Bivens, D.B., Gorski, R.A., Wells, W.D., Yokozeki, A., Lindstrom, R.A., and Shimon, R.L. "Evaluation of Fluorocarbon Blends as Automotive Air Conditioning Refrigerants." SAE Paper No. 890306, 1989.

47. Grzyll, L.R. and Parrish, C.F. "An Innovative Approach for the Screening and Development of CFC Alternatives." Proceedings of the 1992 International Refrigeration Conference - Energy Efficiency and New Refrigerants, Vol. II, pp. 415-424, 1992.

48. Pannock, J., Didion, D.A. and Radermacher, R. "Performance Evaluation of Chlorine Free Zeotropic Refrigerant Mixtures in Heat Pumps - Computer Study and Tests." Proceedings of the 1992 International Refrigeration Conference - Energy Efficiency and New Refrigerants, Vol. II, pp. 25-34, 1992.

49. Radermacher, R. and Jung, D. "Theoretical Analysis of Replacement Refrigerants for HCFC-22 Residential Uses." ASHRAE Transactions: Research, Vol. 99, Part 2, No. 3654, pp. 333-343, 1993.

50. Shiflett, M.B., Yokozeki, A., and Bivens, D.B. "Refrigerant Mixtures as HCFC-22 Alternatives." Proceedings of the 1992 International Refrigeration Conference - Energy Efficiency and New Refrigerants, Vol. II, pp. 35-44, 1992.

51. Wakeham, W.A., Nagashima, A., and Sengers, J.V. "Experimental Thermodynamics - Vol. III, Measurement of the Transport Properties of Fluids." Blackwell Scientific, London, 1991.

52. Haarman, J.W. "A Contribution to the Theory of the Transient Hot-Wire Method." Physica, Vol. 52, pp. 605-619, 1971.

53. Leidenfrost, W. "An Attempt to Measure the Thermal Conductivity of Liquids, Gases, and Vapors with a High Degree of Accuracy over Wide Ranges of Temperature (-180 to 500°C) and Pressure (Vacuum to 500 atm)." Int. J. Heat Mass Transfer, Vol. 7, pp. 447-478, 1964.

54. Viskanta, R. and Grosh, R.J. "Heat Transfer by Simultaneous Conduction and Radiation in an Absorbing Medium." Transaction of the ASME, Journal of Heat Transfer, pp. 63-72, February 1962.

55. Nieto de Castro, C.A., Calado, J.C.G., and Wakeham, W.A. "Absolute Measurements of the Thermal Conductivity of Liquids Using a Transient Hot-Wire Technique." Proceedings of the Seventh Symposium on Thermophysical Properties, Edited by Ared Cezairliyan, pp. 730-738, Held at National Bureau of Standards, Gaithersburg, MD, May 10-12, 1977.

56. Menashe, J. and Wakeham, W.A. "Effect of Absorption of Radiation on Thermal Conductivity Measurements by the Transient Hot-Wire Technique." International Journal Heat Mass Transfer, Vol. 25, No. 5, pp. 661-673, 1982.

57. Saito, A. and Venart, J.E.S. "Radiation Effects with the Transient Line Source Measurement of Fluid Thermal Conductivity." Proceedings of the Sixth International Heat Transfer Conference, Hemisphere Publishing Corporation, Washington D. C., Vol. 3, pp. 79-84, Held at Toronto, Canada, August 7-11, 1978.

58. Nieto de Castro, C.A., Perkins, R.A., and Roder, H.M. "Radiative Heat Transfer in Transient Hot-Wire Measurements of Thermal Conductivity." International Journal of Thermophysics, Vol. 12, No. 6, pp. 985-997, 1991.

59. Nieto de Castro, C.A., Li, S.F.Y., Maitland, G.C., and Wakeham, W.A. "Thermal Conductivity of Toluene in the Temperature Range 35-90°C at Pressures up to 600 MPa." International Journal of Thermophysics, Vol. 4, No. 4, pp. 311-327, 1983.

60. Gross, U., Song, Y.W., and Hahne, E. "Thermal Conductivity of the New Refrigerants R134a, R152a, and R123 Measured by the Transient Hot-Wire Method." International Journal of Thermophysics, Vol. 13, No. 6, pp. 957-983, 1992.

61. Fodemesi, S.P. and Beck, A.E. "Induced Convection During Cylindrical Probe Conductivity Measurements on Permeable Media." Thermal Conductivity 17, Plenum Press, Edited by Hust, J. G., pp. 619-634, 1982.

62. Goldstein, R.J. and Briggs, D.G. "Transient Free Convection About Vertical Plates and Circular Cylinders." Transaction of the ASME, Journal of Heat Transfer, pp. 490-500, November 1964.

63. Gordon, D.T., Hamilton, J.F., and Fontaine, W.E. "An Empirical Equation for Predicting the Viscosity of Liquid Refrigerants." ASHRAE Transaction, Vol. 75, No. 2093, pp. 40-51, 1969.

64. Phillips, T.W. and Murphy, K.P. "Liquid Viscosity of Halogenated Refrigerants." ASHRAE Transactions, Vol. 76, pp. 146-156, 1970.

65. Kumagai, A. and Takahashi, S. "Viscosity of Saturated Liquid Fluorocarbon Refrigerants from 273 to 353 K." International Journal of Thermophysics, Vol. 12, No. 1, pp. 105-117, 1991.

66. Dymond, J.H., Robertson, J., and Isdale, J.D. "Transport Properties of Nonelectrolyte Liquid Mixture - IV. Viscosity Coefficients for Benzene, Perdeuterobenzene, Hexafluorobenzene, and an Equimolar Mixture of Benzene + Hexafluorobenzene from 25 to 100°C at Pressures up to the Freezing Pressure." International Journal of Thermophysics, Vol. 2, No. 3, pp. 223-236, 1981.

67. Dymond, J.H., Robertson, J., and Isdale, J.D. "Transport Properties of Nonelectrolyte Liquid Mixtures - III. Viscosity Coefficients for n-Octane, n-Dodecane, and Equimolar Mixtures of n-Octane + n-Dodecane and n-Hexane + n-Dodecane from 25 to 100°C at Pressures up to the Freezing Pressure or 500 MPa." International Journal of Thermophysics, Vol. 2, No. 2, pp. 133-154, 1981.

68. Benning, A.F. and Markwood, W.H. Jr. "The Viscosities of Liquid Freon Refrigerants." Refrigerating Engineering, Vol. 37, pp. 243-247, 1939.

69. Lilios, N. "The Viscosity of Several Liquid Refrigerants at Atmospheric Pressure." M.S. Thesis, Purdue University, West Lafayette, IN, 1957.

70. "Handbook of Chemistry and Physics," 67th Edition, Edited by Robert C. Weast, Melvin J. Astle, and William H. Beyer, CRC Press Inc., Boca Raton, FL, 1986-1987.

71. Suzuki, S., Fujisawa, Y., Nakazawa, S., and Matsuoka, M. "Measuring Method of Oil Circulation Ratio Using Light Absorption." ASHRAE Transactions: Research, No. 3663, Vol. 99, Part 1, pp. 413-421, 1993.

72. Baustian, J.J., Pate, M.B., and Bergles, A.E. "Properties of Oil-Refrigerant Liquid Mixtures with Applications to Oil Concentration Measurement: Part I - Thermophysical and Transport Properties." ASHRAE Transactions, No. 2937 (RP-356), Vol. 92, Part 1A, pp. 55-73, 1986.

73. Baustian, J.J., Pate, M.B., and Bergles, A.E. "Measuring the Concentration of a Flowing Oil-Refrigerant Mixture: Instrument Test Facility and Initial Results." ASHRAE Transactions, No. 3122 (RP-356), Vol. 94, Part 1, pp. 167-177, 1988.

74. Baustian, J.J., Pate, M.B., and Bergles, A.E. "Measuring the Concentration of a Flowing Oil-Refrigerant Mixture with a Bypass Viscometer." ASHRAE Transactions, No. 3180 (RP-356), Vol. 94, Part 2, pp. 588-601, 1988.

75. Kays, W.M. and Crawford, M.E. "Convective Heat and Mass Transfer." The Third Edition, Chapter 14, p. 319, McGraw-Hill, Inc., New York City, NY, 1993.

76. Incopera, F.P. and DeWitt, D.P. "Fundamentals of Heat and Mass Transfer", John Wiley & Sons, Inc., New York City, NY, The Third Edition, Chapter 8, pp. 496-497, 1990.

77. Petukhov, B.S., Kurganov, V.A., and Gladuntsov, A.I. "Heat Transfer in Turbulent Pipe Flow of Gases with Variable Properties." Heat Transfer - Soviet Research, Vol. 5, No. 4, pp. 109-116, July-August 1973.

78. Gnielinski, V. "New Equations for Heat and Mass Transfer in Turbulent Pipe and Channel Flow." International Chemical Engineering, Vol. 16, No. 2, pp. 359-368, 1976.

79. Kline, S.J. and McClintock, F.A. "Describing Uncertainties in Single Sample Experiments." Mechanical Engineering, Vol. 75, pp. 3-8, 1953.

80. "SAS Introductory Guide." Third Edition, SAS Institute Inc., Cary, NC, 1985.

81. Moran, M.J. and Shapiro, H.N. "Fundamentals of Engineering Thermodynamics." Chapters 3 and 11, John Wiley & Sons, Inc., New York City, NY, 1988.

82. "ASHRAE Handbook - Fundamentals." SI Edition, ASHRAE Inc., Atlanta, GA, 1993.

83. McLinden, M. O. and Morrison, G. "NIST Thermodynamic Properties of Refrigerants and Refrigerant Mixtures Database." NIST Standard Reference Database 23, Version 3.0, U. S. Department of Commerce, Gaithersburg, MD, December 1991.

APPENDIX A. THERMOPHYSICAL PROPERTIES

This appendix discusses the use of thermophysical properties such as saturated pressure (P_{sat}), density (ρ), specific heat (Cp), viscosity (μ), and thermal conductivity (k). Data sources of these properties are found in a number of references, such as ASHRAE, NIST (REFPROP), and Chemistry and Physics Handbook. However, for purposes of refrigerant study, ASHRAE data and REFPROP data are usually the preferred sources. It should be noted that REFPROP is a recently developed package which uses theoretical prediction methods. Because of limited experimental data for new refrigerants, such as HFC-236ea, REFP4.0 (REFPROP version 4.0) was employed as the reference data source for comparison. Although REFPROP data includes almost all of the refrigerants and their mixtures in any combination, it was discovered that the transport properties between these two data sources were sometimes quite different from each other. Therefore, proper care should be taken before using them. In this study, those properties used for thermal conductivity measurements are all based on the ASHRAE data source [82] while comparisons between measured properties and REFPROP [83] were made for the fluids of unknown properties.

In order to use property data conveniently, based on the ASHRAE or REFPROP data source, curve fit equations were developed by using polynomial functions described by:

$$property = \sum_{i=0}^{5} a_i \cdot T^i \qquad (A.1)$$

where temperature, T is in °C here and in the following discussions unless otherwise stated. The applied temperature range of regression for all properties is at the saturation temperature, and the pressure is also at the saturated condition. The curve fit temperature range, in °C, is listed in Table A.1.

TABLE A.1: CURVE-FIT TEMPERATURE RANGE IN °C FOR TEST REFRIGERANTS

refrigerant	P_{sat}	density	specific heat	viscosity	conductivity
CFC-12	-50 ~ 100	-50 ~ 100	-40 ~ 80	-70 ~ 68	-60 ~ 68
HCFC-22	-130 ~ 96.14	-130 ~ 96.14	-90 ~ 70	-20 ~ 40	-70 ~ 48
CFC-113	-30 ~ 214	-30 ~ 214	0 ~ 180	0 ~ 175	0 ~ 170
CFC-114	-40 ~ 115	-40 ~ 115	-40 ~ 115	-40 ~ 115	-40 ~ 115
HFC-236ea	-40 ~ 100	-40 ~ 100	-40 ~ 100	-40 ~ 100	-40 ~ 100
blend A	-40 ~ 85	-40 ~ 85	-40 ~ 85	-40 ~ 85	-40 ~ 85
blend B	-40 ~ 70	-40 ~ 70	-40 ~ 70	-40 ~ 70	-40 ~ 70

SATURATION PRESSURE

The P_{sat} versus temperature curve fit equations are provided in the following sections for the tested refrigerants. The unit for saturation pressure, P_{sat} is MPa for ASHRAE and psia for REFPROP data, while the temperature unit is °C.

P_{sat} for Calibration Refrigerants - ASHRAE

Table A.2 lists the curve fit coefficients of the saturation pressures of refrigerants based on the ASHRAE data. The form of the equation for each curve fit is a polynomial function as described by Equation A.1. These data were used to verify the subcooled conditions and to verify that all operating conditions were in the liquid phase.

TABLE A.2: SATURATION PRESSURE CURVE-FIT COEFFICIENTS FOR HCFC-22, CFC-12, CFC-113, AND CFC-114

polynomial coefficient	refrigerant			
	HCFC-22	CFC-12	CFC-113	CFC-114
a_0 , MPa	5.00005E-01	2.91020E-01	1.58554E-02	8.76786E-02
a_1 , MPa/°C	1.61909E-02	1.00845E-02	6.77690E-04	3.47903E-03
a_2 , MPa/(°C)^2	1.95017E-04	1.49920E-04	1.25848E-05	5.45875E-05
a_3 , MPa/(°C)^3	1.03242E-06	5.64051E-07	2.28213E-07	3.74883E-07
a_4 , MPa/(°C)^4	2.23206E-09	5.91877E-09	1.47081E-10	4.43447E-10
a_5 , MPa/(°C)^5	1.71047E-12	5.79095E-11	1.60668E-12	1.88150E-12
determinant	9.99996E-01	9.97749E-01	9.99998E-01	9.99999E-01

P_{sat} for HFC-236ea - REFPROP

Table A.3 lists the saturation pressure (psia) of refrigerants based on the REFPROP data.

TABLE A.3: SATURATION PRESSURE CURVE-FIT COEFFICIENTS FOR HFC-236ea

polynomial coefficient	HFC-236ea
a_0 , psia	1.13349352E+01
a_1 , psia/°C	4.84870791E-01
a_2 , psia/(°C)^2	8.30436591E-03
a_3 , psia/(°C)^3	6.78510114E-05
a_4 , psia/(°C)^4	2.04624143E-07
a_5 , psia/(°C)^5	-2.19035401E-10
determinant	1.00000000E+00

LIQUID DENSITY

The liquid density versus temperature curve fit equations are provided in the following sections for the tested refrigerants. The unit for density, ρ, is (kg/m^3) while the unit for temperature is °C.

Density for Calibration Refrigerants - ASHRAE

Because the type of viscometer used in this study measures the product of density (g/cm^3) and dynamic viscosity (cp), therefore, density is a property needed to be measured in the present study in order to obtain the viscosity. For the calibration of refrigerants of known properties, the ASHRAE data for density was used to verify both measured density and viscosity. Table A.4 lists the density curve fit equation coefficients at the saturated liquid state based on ASHRAE data.

TABLE A.4: LIQUID DENSITY CURVE-FIT COEFFICIENTS FOR HCFC-22, CFC-12, CFC-113, CFC-114

polynomial coefficient	refrigerant			
	HCFC-22	CFC-12	CFC-113	CFC-114
a_0 , kg/m^3	1.27397E+03	1.39594E+03	1.61316E+03	1.50572E+03
a_1 , $kg/m^3 \cdot °C$	-3.39602E+00	-3.22976E+00	-2.00082E+00	-1.76217E+00
a_2 , $kg/m^3 \cdot (°C)^2$	5.30874E-03	-7.53629E-03	1.26301E-02	-1.78123E-02
a_3 , $kg/m^3 \cdot (°C)^3$	1.21421E-05	-7.65376E-06	-4.93012E-04	-5.05889E-05
a_4 , $kg/m^3 \cdot (°C)^4$	-2.76909E-06	3.27685E-07	4.29266E-06	1.49907E-06
a_5 , $kg/m^3 \cdot (°C)^5$	-1.82476E-08	-1.14387E-08	9.94815E-01	-8.35448E-09
determinant	9.93922E-01	9.99988E-01	9.94815E-01	9.99996E-01

Liquid Density for HFC-236ea - REFPROP

The curve fitting coefficients of liquid density based on REFPROP are listed in Table A.5.

TABLE A.5: LIQUID DENSITY CURVE-FIT COEFFICIENTS FOR HFC-236ea

polynomial coefficient	HFC-236ea
a_0 , kg/m^3	1.50280E+03
a_1 , $kg/m^3 \cdot °C$	-2.84734E+00
a_2 , $kg/m^3 \cdot (°C)^2$	-5.44754E-03
a_3 , $kg/m^3 \cdot (°C)^3$	-2.65424E-05
a_4 , $kg/m^3 \cdot (°C)^4$	1.76196E-08
a_5 , $kg/m^3 \cdot (°C)^5$	-1.89195E-09
determinant	9.99996E-01

LIQUID SPECIFIC HEAT

The liquid specific heat versus temperature curve fit equations are provided in the following sections for the tested refrigerants. The unit for specific heat, Cp, is $kJ/(kg \cdot K)$, while the unit for temperature is °C.

Specific Heat for Calibration Refrigerants - ASHRAE

Table A.6 lists the specific heat curve fit equation coefficients for the saturated liquid state of HCFC-22, CFC-12, CFC-113, and CFC-114 based on the ASHRAE data.

TABLE A.6: LIQUID SPECIFIC HEAT CURVE-FIT COEFFICIENTS FOR HCFC-22, CFC-12, CFC-113, CFC-114

polynomial coefficient	refrigerant			
	HCFC-22	CFC-12	CFC-113	CFC-114
a_0 , $kJ/(kg \cdot K)$	1.17392E+00	9.27994E-01	9.21305E-01	9.30861E-01
a_1 , $kJ/(kg \cdot K) \cdot °C$	2.72938E-03	1.87657E-03	1.70157E-03	1.13601E-03
a_2 , $kJ/(kg \cdot K) \cdot (°C)^2$	1.46720E-05	1.52956E-05	-1.40780E-05	-3.84778E-06
a_3 , $kJ/(kg \cdot K) \cdot (°C)^3$	1.18154E-07	-1.12761E-08	9.15992E-08	1.96439E-07
a_4 , $kJ/(kg \cdot K) \cdot (°C)^4$	6.23786E-09	-5.42684E-10	6.44030E-11	8.34917E-11
a_5 , $kJ/(kg \cdot K) \cdot (°C)^5$	5.16438E-11	4.66421E-11	-1.80450E-13	-4.94558E-13
determinant	9.99485E-01	9.99954E-01	9.99994E-01	9.99993E-01

Specific Heat for HFC-236ea - REFPROP

The coefficients of specific heat curve fit based on REFPROP are listed in Table A.7.

TABLE A.7: LIQUID SPECIFIC HEAT CURVE-FIT COEFFICIENTS FOR HFC-236ea

polynomial coefficient	HFC-236ea
a_0 , $kJ/(kg \cdot K)$	1.15099E+03
a_1 , $kJ/(kg \cdot K) \cdot °C$	2.45936E+00
a_2 , $kJ/(kg \cdot K) \cdot (°C)^2$	4.03757E-03
a_3 , $kJ/(kg \cdot K) \cdot (°C)^3$	1.64306E-05
a_4 , $kJ/(kg \cdot K) \cdot (°C)^4$	-7.58220E-07
a_5 , $kJ/(kg \cdot K) \cdot (°C)^5$	1.53071E-08
determinant	9.99988E-01

LIQUID VISCOSITY

The liquid viscosity versus temperature curve fit equations are provided in the following sections for the tested refrigerants. The units for viscosity, μ, are $Pa \cdot s$ while the unit for temperature is °C.

Viscosity for Calibration Refrigerants - ASHRAE

Table A.8 lists the dynamic viscosity (in $Pa \cdot s$) curve fit equation coefficients at the saturated liquid state based on ASHRAE data.

TABLE A.8: LIQUID VISCOSITY CURVE FIT COEFFICIENTS FOR HCFC-22, CFC-12, CFC-113, AND CFC-114

polynomial coefficient	refrigerant			
	HCFC-22	CFC-12	CFC-113	CFC-114
a_0 , $Pa \cdot s$	2.10126E-04	2.57691E-04	9.54513E-04	4.91168E-04
a_1 , $Pa \cdot s$/°C	-2.27812E-06	-2.77653E-06	-1.31618E-05	-6.55940E-06
a_2 , $Pa \cdot s/(°C)^2$	1.14319E-08	1.89625E-08	1.11619E-07	4.48919E-08
a_3 , $Pa \cdot s/(°C)^3$	3.80621E-12	-8.65530E-11	-6.34269E-10	-1.26949E-10
a_4 , $Pa \cdot s/(°C)^4$	-7.75142E-13	-2.19818E-14	2.15999E-12	-4.40069E-13
a_5 , $Pa \cdot s/(°C)^5$	7.72755E-15	2.96471E-15	-3.23601E-15	3.18456E-15
determinant	9.99999E-01	9.99999E-01	9.99999E-01	9.99999E-01

Liquid Viscosity for HFC-236ea - REFPROP

The coefficients of dynamic viscosity curve fit equation based on REFPROP are listed in Table A.9.

TABLE A.9: LIQUID VISCOSITY CURVE-FIT COEFFICIENTS FOR HFC-236ea

polynomial coefficient	HFC-236ea
a_0 , $kJ/(kg \cdot K)$	5.83657E-04
a_1 , $kJ/(kg \cdot K) \cdot °C$	-9.32850E-06
a_2 , $kJ/(kg \cdot K) \cdot (°C)^2$	1.03792E-07
a_3 , $kJ/(kg \cdot K) \cdot (°C)^3$	-1.08120E-09
a_4 , $kJ/(kg \cdot K) \cdot (°C)^4$	8.20849E-12
a_5 , $kJ/(kg \cdot K) \cdot (°C)^5$	-2.86313E-14
determinant	9.99997E-01

LIQUID THERMAL CONDUCTIVITY

The liquid thermal conductivity versus temperature curve fit equations are provided in the following sections for the tested refrigerants. The units for thermal conductivity, k, are $W/(m \cdot K)$ while the unit for temperature is °C.

Thermal Conductivity for Calibration Refrigerants - ASHRAE

Thermal conductivity quoted for the calibration refrigerants was based on ASHRAE data. Table A.10 lists the thermal conductivity (in $W/(m \cdot K)$) curve fit equation coefficients at the saturated liquid state.

TABLE A.10: LIQUID THERMAL CONDUCTIVITY CURVE-FIT COEFFICIENTS FOR HCFC-22, CFC-12, CFC-113, AND CFC-114

polynomial coefficient	refrigerant			
	HCFC-22	CFC-12	CFC-113	CFC-114
a_0, $W/(m \cdot K)$	9.61623E-02	7.71084E-02	8.19249E-02	7.04566E-02
a_1, $W/(m \cdot K) \cdot °C$	-4.24513E-04	-3.66836E-04	-1.74554E-04	-2.41089E-04
a_2, $W/(m \cdot K) \cdot (°C)^2$	4.25538E-07	1.77984E-07	-6.07317E-08	2.54213E-07
a_3, $W/(m \cdot K) \cdot (°C)^3$	4.88343E-10	-4.95688E-10	1.01692E-09	-9.79673E-10
a_4, $W/(m \cdot K) \cdot (°C)^4$	-2.09592E-11	6.91404E-13	-6.47263E-12	-2.41232E-11
a_5, $W/(m \cdot K) \cdot (°C)^5$	-4.18749E-13	1.10221E-13	1.55361E-14	1.19913E-13
determinant	9.99996E-01	9.99996E-01	9.99989E-01	9.99994E-01

Thermal Conductivity for HFC-236ea - REFPROP

The coefficients of thermal conductivity curve fit equation based on REFPROP are shown in Table A.11.

TABLE A.11: LIQUID THERMAL CONDUCTIVITY CURVE-FIT COEFFICIENTS FOR HFC-236ea

polynomial coefficient	HFC-236ea
a_0 , $W/(m \cdot K)$	7.98508E-02
a_1 , $W/(m \cdot K) \cdot °C$	-3.22129E-04
a_2 , $W/(m \cdot K) \cdot (°C)^2$	-5.87303E-07
a_3 , $W/(m \cdot K) \cdot (°C)^3$	8.10775E-09
a_4 , $W/(m \cdot K) \cdot (°C)^4$	2.08164E-11
a_5 , $W/(m \cdot K) \cdot (°C)^5$	-4.47036E-13
determinant	9.99743E-01

APPENDIX B. UNCERTAINTY ANALYSIS FOR THERMAL CONDUCTIVITY MEASUREMENTS

This appendix analyzes the uncertainties of the thermal conductivity measurement for the methods of Approach 1: the Nusselt number method, and Approach 2: the Prandtl number method.

UNCERTAINTY ANALYSIS FOR APPROACH 1

Three different single-phase correlations employed in the thermal conductivity calculations will be analyzed for their uncertainties. The uncertainties of the measured thermal conductivity arise due to both sensor (or instrument) uncertainties and the Nusselt number correlation uncertainties. However, in this analysis, only the sensor uncertainties are included for the uncertainty calculation, while the Nusselt number uncertainty is discussed in this current analysis.

Uncertainty Analysis for Thermal Conductivity Calculated from the Dittus-Boelter Correlation

The thermal conductivity obtained from the Dittus-Boelter correlation is:

$$k_d = \left[\frac{\bar{h}D}{0.023} Re^{-0.8}\, \mu^{-0.4}\, Cp^{-0.4}\right]^{1.67} \tag{B.1}$$

$$= F(\bar{h}, D, Re_D, \mu, Cp) = F(\bar{h}, D, \dot{m}, \mu, Cp) \tag{B.2}$$

The thermal conductivity presented here is a function of $\bar{h}$, D, Re_D, μ, and C_p. Therefore, the uncertainty of the sum of ${}^{U_{k_d}} / k_d$ can be expressed as follows.

$$\left(\frac{U_{k_d}}{k_d}\right)^2 = \left(\frac{5}{3}\frac{U_{\bar{h}}}{\bar{h}}\right)^2 + \left(\frac{5}{3}\frac{U_D}{D}\right)^2 + \left(-\frac{4}{3}\frac{U_{Re_D}}{Re_D}\right)^2 + \left(-\frac{2}{3}\frac{U_\mu}{\mu}\right)^2 + \left(-\frac{2}{3}\frac{U_{C_p}}{C_p}\right)^2 \tag{B.3}$$

$$= SS_{k_d} \tag{B.4}$$

where ${}^{U_{\bar{h}}} / \bar{h}$, and ${}^{U_{Re_D}} / Re_D$, are discussed in the following sections. Then, the uncertainty ratio ${}^{U_{r_{dk}}} (= {}^{U_{k_d}} / k_d)$ is obtained by taking square root of the sum of squares of each uncertainty source, SS_{k_d}. That is,

$$\frac{U_{k_d}}{k_d} = \left(SS_{k_d}\right)^{1/2} \tag{B.5}$$

Uncertainty Analysis for Thermal Conductivity Calculated from the Petukhov and Popov Correlation

The thermal conductivity from the Petukhov and Popov correlation is found to be:

$$kp = \mu Cp \left[\frac{(8f)^{1/2} \mu Cp Re_D}{101.6 \bar{h} D} - \frac{1.07}{12.7} \left(\frac{f}{8}\right)^{-1/2} + 1 \right]^{-3/2} \tag{B.6}$$

$$= F(\mu, Cp, f, Re_D, \bar{h}, D) = F(\mu, Cp, f, \dot{m}, \bar{h}, D) \tag{B.7}$$

In this equation, kp is function of μ, Cp, f, Re_D, $\bar{h}$, and D. Therefore, the uncertainty of sum of square of U_{k_p} / k_p can be expressed as follows:

$$\left(\frac{U_{k_p}}{k_p}\right)^2 = \left(\frac{\partial k_p}{\partial \mu}\frac{U_\mu}{k_p}\right)^2 + \left(\frac{\partial k_p}{\partial C_p}\frac{U_{C_p}}{k_p}\right)^2 + \left(\frac{\partial k_p}{\partial f}\frac{U_f}{k_p}\right)^2 + \left(\frac{\partial k_p}{\partial Re_D}\frac{U_{Re_D}}{k_p}\right)^2 + \left(\frac{\partial k_p}{\partial \bar{h}}\frac{U_{\bar{h}}}{k_p}\right)^2 + \left(\frac{\partial k_p}{\partial_D}\frac{U_D}{k_p}\right)^2 \tag{B.8}$$

$$= SS_{k_p} \tag{B.9}$$

where each item in the above equation is derived as follows:

$$\frac{\partial k_p}{\partial \mu}\frac{U_\mu}{k_p} = \frac{U_\mu}{\mu} - \frac{3}{2}\left[\frac{(8f)^{1/2}}{101.6\bar{h}D} - \frac{1.07}{12.7}\left(\frac{f}{8}\right)^{-1/2} + 1 \right]^{-1} \cdot \left[\frac{f \mu Cp Re_D}{101.6 \bar{h} D (f/8)^{1/2}} \frac{U_\mu}{k_p} \right] \tag{B.10}$$

$$\frac{\partial k_p}{\partial Cp}\frac{U_{Cp}}{k_p} = \frac{U_{Cp}}{Cp} - \frac{3}{2}\left[\frac{(8f)^{1/2}}{101.6\bar{h}D} - \frac{1.07}{12.7}\left(\frac{f}{8}\right)^{-1/2} + 1 \right]^{-1} \cdot \left[\frac{f \mu Cp Re_D}{101.6 \bar{h} D (f/8)^{1/2}} \frac{U_{Cp}}{Cp} \right] \tag{B.11}$$

$$\frac{\partial k_p}{\partial f}\frac{U_f}{k_p} = -\frac{3}{2}\left[\frac{(8f)^{1/2}}{101.6\bar{h}D} - \frac{1.07}{12.7}\left(\frac{f}{8}\right)^{-1/2} + 1 \right]^{-1} \cdot \left[\frac{8^{1/2} f^{3/2} \mu Cp Re_D}{203.2 \bar{h} D} + \frac{8^{1/2}(1.07)}{25.4} f^{-1/2} \right] \frac{U_f}{f} \tag{B.12}$$

$$\frac{\partial k_p}{\partial Re_D}\frac{U_{Re_D}}{k_p} = -\frac{3}{2}\left[\frac{(8f)^{1/2}}{101.6\bar{h}D} - \frac{1.07}{12.7}\left(\frac{f}{8}\right)^{-1/2} + 1 \right]^{-1} \cdot \left[\frac{8^{1/2} f^{1/2} \mu Cp Re_D}{101.6 \bar{h} D} \right] \frac{U_{Re_D}}{Re_D} \tag{B.13}$$

$$\frac{\partial k_p}{\partial h}\frac{U_h}{k_p} = -\frac{3}{2}\left[\frac{(8f)^{1/2}}{101.6\bar{h}D} - \frac{1.07}{12.7}\left(\frac{f}{8}\right)^{-1/2} + 1 \right]^{-1} \cdot \left[-\frac{8^{1/2} f^{1/2} \mu Cp Re_D}{101.6 \bar{h} D} \right] \frac{U_h}{h} \tag{B.14}$$

$$\frac{\partial k_p}{\partial D}\frac{U_D}{k_p} = -\frac{3}{2}\left[\frac{(8f)^{1/2}}{101.6\bar{h}D} - \frac{1.07}{12.7}\left(\frac{f}{8}\right)^{-1/2} + 1\right]^{-1} \cdot \left[-\frac{8^{1/2}f^{1/2}\mu Cp Re_D}{101.6\bar{h}D}\right]\frac{U_D}{D} \tag{B.15}$$

Then, the uncertainty of $U_{r_{pk}}$ ($= U_{k_p} / k_p$) is obtained by taking square root of the sum of squares of each uncertainty source, SS_{k_p}. That is

$$\frac{U_{k_p}}{k_p} = \left(SS_{k_p}\right)^{1/2} \tag{B.16}$$

Uncertainty Analysis for Thermal Conductivity Calculated from the Gnielinski Correlation

The thermal conductivity from the Gnielinski correlation is found to be:

$$k_g = \mu Cp\left[\frac{(8f)^{1/2}\mu Cp\,(Re_D - 1000)}{101.6\bar{h}D} - \frac{1}{12.7}\left(\frac{f}{8}\right)^{-1/2} + 1\right]^{-3/2} \tag{B.17}$$

$$= F(\mu, Cp, f, Re_D, \bar{h}, D) = F(\mu, Cp, f, \dot{m}, \bar{h}, D) \tag{B.18}$$

In this equation, k_g is function of μ, Cp, f, Re_D, $\bar{h}$, and D. Therefore, the uncertainty of the sum of the squares of U_{k_g} / k_g can be expressed as follows:

$$\left(\frac{U_{k_g}}{k_g}\right)^2 = \left(\frac{\partial k_g}{\partial \mu}\frac{U_\mu}{k_g}\right)^2 + \left(\frac{\partial k_g}{\partial C_p}\frac{U_{C_p}}{k_g}\right)^2 + \left(\frac{\partial k_g}{\partial f}\frac{U_f}{k_g}\right)^2 + \left(\frac{\partial k_g}{\partial Re_D}\frac{U_{Re_D}}{k_g}\right)^2 + \left(\frac{\partial k_g}{\partial \bar{h}}\frac{U_{\bar{h}}}{k_g}\right)^2 + \left(\frac{\partial k_g}{\partial D}\frac{U_D}{k_g}\right)^2 \tag{B.19}$$

$$= SS_{kg} \tag{B.20}$$

where each term in the above equation is derived as follows:

$$\frac{\partial k_g}{\partial \mu}\frac{U_\mu}{k_g} = \frac{U_\mu}{\mu} - \frac{3}{2}\left[\frac{(8f)^{1/2}\mathrm{m}Cp\,(Re_D - 1000)}{101.6\bar{h}D} - \frac{1}{12.7}\left(\frac{f}{8}\right)^{-1/2} + 1\right]^{-1} \cdot \left[\frac{f\mu Cp\,(Re_D - 1000)}{101.6\bar{h}D\,(f/8)^{1/2}}\right]\frac{U_\mu}{\mu} \tag{B.21}$$

$$\frac{\partial k_g}{\partial Cp}\frac{U_{Cp}}{k_g} = \frac{U_{Cp}}{Cp} - \frac{3}{2}\left[\frac{(8f)^{1/2}\mathrm{m}Cp\,(Re_D - 1000)}{101.6\bar{h}D} - \frac{1}{12.7}\left(\frac{f}{8}\right)^{-1/2} + 1\right]^{-1} \cdot \left[\frac{f\mu Cp\,(Re_D - 1000)}{101.6\bar{h}D\,(f/8)^{1/2}}\right]\frac{U_{Cp}}{Cp} \tag{B.22}$$

$$\frac{\partial k_g}{\partial f}\frac{U_f}{k_g} = -\frac{3}{2}\left[\frac{(8f)^{1/2}\mathrm{m}Cp\,(Re_D - 1000)}{101.6\bar{h}D} - \frac{1}{12.7}\left(\frac{f}{8}\right)^{-1/2} + 1\right]^{-1} \cdot \left[\frac{8^{1/2}f^{3/2}\mu Cp\,(Re_D - 1000)}{203.2\bar{h}D} + \frac{8^{1/2}}{25.4}f^{1/2}\right]\frac{U_f}{f} \tag{B.23}$$

$$\frac{\partial k_g}{\partial Re_D}\frac{U_{Re_D}}{k_g} = -\frac{3}{2}\left[\frac{(8f)^{1/2}\mu Cp\,(Re_D-1000)}{101.6\bar{h}D} - \frac{1}{12.7}\left(\frac{f}{8}\right)^{-1/2}+1\right]^{-1}\cdot\left[\frac{8^{1/2}f^{1/2}\mu CpRe_D}{101.6\bar{h}D}\right]\frac{U_{Re_D}}{Re_D} \quad \text{(B.24)}$$

$$\frac{\partial k_g}{\partial \bar{h}}\frac{U_{\bar{h}}}{k_g} = -\frac{3}{2}\left[\frac{(8f)^{1/2}\mu Cp\,(Re_D-1000)}{101.6\bar{h}D} - \frac{1}{12.7}\left(\frac{f}{8}\right)^{-1/2}+1\right]^{-1}\cdot\left[-\frac{8^{1/2}f^{1/2}\mu Cp\,(Re_D-1000)}{101.6\bar{h}D}\right]\frac{U_{\bar{h}}}{h} \quad \text{(B.25)}$$

$$\frac{\partial k_g}{\partial D}\frac{U_D}{k_g} = -\frac{3}{2}\left[\frac{(8f)^{1/2}\mu Cp\,(Re_D-1000)}{101.6\bar{h}D} - \frac{1}{12.7}\left(\frac{f}{8}\right)^{-1/2}+1\right]^{-1}\cdot\left[-\frac{8^{1/2}f^{1/2}\mu Cp\,(Re_D-1000)}{101.6\bar{h}D}\right]\frac{U_D}{D} \quad \text{(B.26)}$$

Then, the uncertainty ratio of $U_{r_{gk}}$ ($= U_{k_g} / k_g$) is obtained by taking square root of sum of square of each uncertainty source, SS_{k_g}. That is

$$\frac{U_{k_g}}{k_g} = \left(SS_{k_g}\right)^{1/2} \quad \text{(B.27)}$$

Uncertainty Analysis for Heat and Flow Measurements

The uncertainty calculation in heat and flow measurements would contribute to those uncertainty quantities of the thermal conductivity uncertainties mentioned in the above three sections. In this section, analysis of these heat and flow uncertainties will be discussed. The uncertainties of the heat transfer measurements include those for the heat transfer rate, $\dot{Q}$, and heat transfer coefficient, $\bar{h}$, while the uncertainties of fluid flow measurements include those from the calculations of the Reynolds number, Re_D, and friction factor, f.

Uncertainty Analysis of Heat Transfer Measurement

The Uncertainty of $\dot{Q}$–

The net heat transfer rate is calculated from the following equation:

$$\dot{Q} = \bar{h}A\,(\bar{T}_w - \bar{T}_f) \quad \text{(B.28)}$$

$$= \dot{m}Cp\,(\bar{T}_o - \bar{T}_i) \quad \text{(B.29)}$$

$$= F\,(\dot{m}, Cp, \bar{T}_o, \bar{T}_i) \quad \text{(B.30)}$$

Therefore, the uncertainty of the sum of the squares of $U_{\dot{Q}} / \dot{Q}$ is given as:

$$\left(\frac{U_{\dot{Q}}}{\dot{Q}}\right)^2 = \left(\frac{U_{\dot{m}}}{\dot{m}}\right)^2 + \left(\frac{U_{Cp}}{Cp}\right)^2 + \left(\frac{U_{\bar{T}_o}}{\bar{T}_o}\right)^2 + \left(\frac{U_{\bar{T}_i}}{\bar{T}_i}\right)^2 \tag{B.31}$$

$$= SS_{\dot{Q}} \tag{B.32}$$

The resulting $U_{\dot{Q}} / \dot{Q}$ is given by:

$$\frac{U_{\dot{Q}}}{\dot{Q}} = \left(SS_{\dot{Q}}\right)^{1/2} \tag{B.33}$$

The Uncertainty of $\bar{h}$–

The average heat transfer coefficient is obtained from the following equation:

$$\bar{h} = \frac{\dot{Q}}{A\left(\bar{T}_w - \bar{T}_f\right)} \tag{B.34}$$

$$= \frac{\dot{Q}}{\pi DL\left(\bar{T}_w - \bar{T}_f\right)} \tag{B.35}$$

$$= F\left(\dot{Q}, D, L, \bar{T}_w, \bar{T}_f\right) \tag{B.36}$$

The uncertainty of the sum of the squares of $U_{\bar{h}} / \bar{h}$ is given by:

$$\left(\frac{U_{\bar{h}}}{\bar{h}}\right)^2 = \left(\frac{U_{\dot{Q}}}{\dot{Q}}\right)^2 + \left(-\frac{U_D}{D}\right)^2 + \left(-\frac{U_L}{L}\right)^2 + \left(-\frac{U_{T_w}}{\bar{T}_w - \bar{T}_f}\right)^2 + \left(-\frac{U_{T_f}}{\bar{T}_w - \bar{T}_f}\right)^2 \tag{B.37}$$

$$= SS_{\bar{h}} \tag{B.38}$$

Then, the uncertainty of $U_{\bar{h}} / \bar{h}$ is given by:

$$\frac{U_{\bar{h}}}{\bar{h}} = \left(SS_{\bar{h}}\right)^{1/2} \tag{B.39}$$

Uncertainty Analysis of Fluid Flow Measurement

The uncertainty of the fluid flow measurement includes the calculation of the Reynolds number, Re_D, and the friction factor, f. They are discussed as follows:

The Uncertainty of Re_D–

The Reynolds number is calculated from the following definition:

$$Re_D = \frac{4\dot{m}}{\pi D \mu} \tag{B.40}$$

$$= F(\dot{m}, D, \mu) \tag{B.41}$$

The uncertainty of the sum of the squares of U_{Re_D} / Re_D is given by:

$$\left(\frac{U_{Re_D}}{Re_D}\right)^2 = \left(\frac{U_{\dot{m}}}{\dot{m}}\right)^2 + \left(\frac{U_D}{D}\right)^2 + \left(\frac{U_\mu}{\mu}\right)^2 \tag{B.42}$$

$$= SS_{Re_D} \tag{B.43}$$

Therefore, the uncertainty of U_{Re_D} / Re_D is given by:

$$\frac{U_{Re_D}}{Re_D} = \left(SS_{Re_D}\right)^{1/2} \tag{B.44}$$

The Uncertainty of Friction Factor, f–

The friction factor is calculated from the following curve fitting equation:

$$f = [\,0.79 ln\,(Re_D) - 1.64\,]^{-2} \tag{B.45}$$

$$= F(Re_D) \tag{B.46}$$

Therefore, the uncertainty of the sum of the squares of friction factor, U_f / f, is given by:

$$\left(\frac{U_f}{f}\right)^2 = \left(\frac{\partial f}{\partial Re_D}\frac{U_{Re_D}}{f}\right)^2 \tag{B.47}$$

$$= SS_f \tag{B.48}$$

Or, the resulting uncertainty of U_f / f is derived as

$$\frac{U_f}{f} = \frac{1.58}{0.79ln\,(Re_D) - 1.64} \cdot \frac{U_{Re_D}}{Re_D} \tag{B.49}$$

UNCERTAINTY ANALYSIS FOR APPROACH 2

The Approach 2 for thermal conductivity is based on the Prandtl number, Pr, measurement. The Pr is expressed in Equation 6.34, which means

$$Pr = F(D, L, \bar{R}e_D, \Delta T^*) \tag{B.50}$$

Because $Pr = \mu Cp / k$, k is function of μ, Cp, and Pr. In other words,

$$k = \frac{\mu Cp}{Pr} = F(\mu, Cp, Pr) \tag{B.51}$$

The uncertainty of k is expressed as follows.

$$\frac{U_k}{k} = \left[\left(\frac{\partial k}{\partial \mu} \cdot \frac{U_\mu}{k}\right)^2 + \left(\frac{\partial k}{\partial Cp} \cdot \frac{U_{Cp}}{k}\right)^2 + \left(\frac{\partial k}{\partial Pr} \cdot \frac{U_{Pr}}{k}\right)^2 \right]^{1/2} \tag{B.52}$$

After taking the partial derivative of each term and rearranging, this equation can be written as

$$\frac{U_k}{k} = \left[\left(\frac{U_\mu}{\mu}\right)^2 + \left(\frac{U_{Cp}}{Cp}\right)^2 + \left(-\frac{U_{Pr}}{Pr}\right)^2 \right]^{1/2} \tag{B.53}$$

Uncertainty of *Pr*

The measured Pr is a function of D, L, $\bar{R}e_D$, and ΔT^*. Therefore, the uncertainty of Pr is expressed as

$$\frac{U_{Pr}}{Pr} = \left[\left(\frac{\partial Pr}{\partial D} \cdot \frac{U_D}{D}\right)^2 + \left(\frac{\partial Pr}{\partial L} \cdot \frac{U_L}{L}\right)^2 + \left(\frac{\partial Pr}{\partial Re_D} \cdot \frac{U_{Re_D}}{Re_D}\right)^2 + \left(\frac{\partial Pr}{\partial \Delta T^*} \cdot \frac{U_{\Delta T^*}}{\Delta T^*}\right)^2 \right]^{1/2} \tag{B.54}$$

where U_{Re_D} / Re_D is found from Equation B.42 and $U_{\Delta T^*} / \Delta T^*$ is given in the following section.

Uncertainty of ΔT^*

The ΔT^* is defined as $(T_o - T_i) / (T_w - T_f)$. The uncertainty of ΔT^* is expressed as the following equation:

$$\frac{U_{\Delta T^*}}{\Delta T^*} = \left[\left(\frac{U_{T_o}}{T_o - T_i}\right)^2 + \left(-\frac{U_{T_i}}{T_o - T_i}\right)^2 + \left(-\frac{U_{T_w}}{T_w - T_f}\right)^2 + \left(-\frac{U_{T_f}}{T_w - T_f}\right)^2 \right]^{1/2} \qquad \text{(B.55)}$$

APPENDIX C. SOME PHYSICAL PROPERTIES OF TEST REFRIGERANTS

TABLE C.1: SOME PHYSICAL PROPERTIES OF TEST REFRIGERANTS

test refrigerant	molecular weight, *g/mole*	acentric factor, ω	normal B.P. temp., °C	critical temp., °C	critical pressure, *kPa*
CFC-12	120.91	0.1814	-29.76	111.80	4113
HCFC-22	86.47	0.2211	-40.86	96.15	4974
HFC-32	52.02	0.2671	-51.75	78.21	5830
CFC-113	187.38	0.2563	47.65	214.35	3437
CFC-114	170.92	0.2511	3.65	145.65	3259
CFC-125	120.03	0.2953	-48.57	66.18	3571
HFC-134a	102.03	0.3235	-26.15	101.15	4067
HFC-143a	84.04	0.2566	-47.35	73.10	3811
HFC-152a	66.05	0.2573	-24.65	113.55	4492
HFC-236ea	152.05	0.3860	6.50	139.29	3533

In Table C.1, the acentric factor is a component constant, which is defined as:

$$\omega = -logP_{vp_r} \text{ (at } T_r = 0.7) - 1.000 \tag{C.1}$$

To obtain values of ω, the reduced vapor pressure ($P_{vp_r} = P_{vp} / P_c$) at $T_r = T / T_c = 0.7$ is required. One of the calculation methods was developed from the Lee-Kesler vapor pressure relation which was

$$\omega = \frac{\alpha}{\beta} \tag{C.2}$$

$$\alpha = -ln\,(P_c) - 5.92714 + 6.09648\theta^{-1} + 1.28862ln\,(\theta) - 0.169347\theta^6 \tag{C.3}$$

$$\beta = -15.2518 - 15.6875\theta^{-1} - 13.4721ln\,(\theta) + 0.43577\theta^6 \tag{C.4}$$

$$\theta = T_b / T_c \tag{C.5}$$

In the equation for α, the critical pressure, P_c, must be expressed in atmospheres.

APPENDIX D. EQUIPMENT AND INSTRUMENTATION SPECIFICATIONS

The manufacturer and model number of each component in the test apparatus are shown in Table D.1. Electronic instrumentation is listed in Table D.2.

TABLE D.1: COMPONENTS OF THE TEST RIG

component	manufacturer	description of type	model
refrigerant pump	Wanner Eng.	positive displ. diaphragm	D-10
motor	GE	1 hp, dc	58PB56SAA42A
motor controller	Dart Inc.	variable current	250G
filter drier	Sporlan	desiccant, 262 cm^3	C-164-S
auxiliary heater	Omega	heat tape, 627 W, 120V, 1.27 cm W x 244 cm L	STH051-080
teat-section heater	Omega	heat tape, 2 @ 627 W 120V, 1.27 cm W x 244 cm L	STH051-080
mixer	Omega	rugged static type 0.9525 cm I.D., 7.62 cm long	FMX 7301
sight glasses	Sporlan	1.27 cm, solder fit	-
condenser	Doucete	coaxial coil	CX-H 050
accumulator	Oil-Air Ind.	Bladder (butyl, Buna-N)	1-100-1
charging valve	Henry Co.	packed angle	9271
pres. relief valve	Nupro Co.	spring set type	SS-4R3A-A
chiller	Heat-X Inc.	CFC-12, 3 HP	PC-300
line conditioner	Tripp Lite Co.	spike, surge suppresser	LC1800
oil-injection cyl.	Clippard Inc.	pneumatic cylinder type	UDR-SS-32-6
sample cylinder	Swagelok Co.	closed-ends cylinder	304L-HDF4-75

TABLE D.2: DATA ACQUISITION AND INSTRUMENTATION COMPONENTS

component	manufacturer	description	model
computer	Zenith	386 PC	Z-386-20
multimeter	HP Inc.	digital multimeter	3457A
scanner	HP Inc.	digital control unit	3488A
meter board	HP Inc.	armature relay multiplexer, 10 channel	44491A
scanner board	Hewlett-Packard	multiplexer, 10 channel	44470A
interface card	National Instr.	AT-GPIB(FORTRAN)	776207-01
thermocouple	Omega	bare bead, teflon shield	T-type
cold junction	Omega	electric ice point	CJ-T
RTD probe	Hy-Cal Eng.	100 ohm platinum 0.00385/Ω/Ω/°C	RTS-36-T-100-A -5-2-36-X55
RTD transmitter	Hy-Cal Eng.	2-wire, 4-20 mA, 100 ohm	CT-801-A-S-X5
watts transducer	Jemtec Co.	2-element, 3-wire, 3-phase, accuracy: ±0.2%	XL31K5A2
mass flow meter	Micro Motion	0-1800 kg/hr accuracy: ±0.15%	RFT9739
densitometer	Micro Motion	0-1300 kg/m^3 accuracy: ±0.15%	RFT9739
viscometer	Nametre Co.	0.1-500 cp x g/cm^3 4-20 mA, accuracy: ±2%	1810-LV
abs. pressure	Setra Co.	0-250 psia, ±0.11% FS	C280E
diff. pressure	Setra Co.	0-1 psi, ±0.15% FS	C228-1
voltage regulator	Staco Energy Co.	120 V, 1.4 kVa	1010

APPENDIX E. SAS REGRESSION OUTPUTS

This appendix lists the output of the SAS program for three correlation regressions in the Nusselt number method (Approach 1) and two variable (Re_D and ΔT^*) regressions in the Prandtl number method (Approach 2) for three calibration refrigerants (HCFC-22, CFC-12, and CFC-113) and four calibration refrigerants (HCFC-22, CFC-12, CFC-113, and CFC-114). The SAS program (version 6.07) was accessed from the campus Vincent computer work station network. The first section in this appendix is the SAS output for three correlations discussed in Approach 1 whereas the second section is the SAS output for *ln* (*Pr*) regression with variables of *ln* (Re_D) and ΔT^* discussed in Approach 2. Both sections contain three- and four-calibration refrigerants cases.

NUSSELT NUMBER REGRESSION IN APPROACH 1

THREE CALIBRATION REFRIGERANTS

Model: MODEL 1
Dependent Variable: NUE

Analysis of Variance

Source	DF	Sum of Squares	Mean Square	F Value	Prob>F
Model	2	31.00300	15.50150	6419.126	0.0001
Error	120	0.28979	0.00241		
C Total	122	31.29279			

Root MSE	0.04914	R-square	0.9907
Dep Mean	5.53266	Adj R-sq	0.9906
C.V.	0.88821		

Parameter Estimates

Variable	DF	Parameter Estimate	Standard Error	T for H0: Parameter = 0	Prob > |T|
INTERCEP	1	-4.997045	0.10783630	-46.339	0.0001
LNRE	1	0.903770	0.00876542	103.106	0.0001
LNPR	1	0.502199	0.01131934	44.366	0.0001

Model: MODEL 2
Dependent Variable: NUD

Analysis of Variance

Source	DF	Sum of Squares	Mean Square	F Value	Prob>F
Model	2	25.54522	12.77261	.	.
Error	120	0	0		
C Total	122	25.54522			

Root MSE	0.00000	R-square	1.0000
Dep Mean	5.48384	Adj R-sq	1.0000
C.V.	0.00000		

Parameter Estimates

Variable	DF	Parameter Estimate	Standard Error	T for H0: Parameter = 0	Prob > |T|
INTERCEP	1	-3.772261	0.00000000	.	.
LNRE	1	0.800000	0.00000000	.	.
LNPR	1	0.400000	0.00000000	.	.

Model: MODEL 3
Dependent Variable: NUP

Analysis of Variance

Source	DF	Sum of Squares	Mean Square	F Value	Prob>F
Model	2	26.09945	13.04973	189914.474	0.0001
Error	120	0.00825	0.00007		
C Total	122	26.10770			

Root MSE	0.00829	R-square	0.9997
Dep Mean	5.57329	Adj R-sq	0.9997
C.V.	0.14873		

Parameter Estimates

Variable	DF	Parameter Estimate	Standard Error	T for H0: Parameter = 0	Prob > |T|
INTERCEP	1	-4.059037	0.01819021	-223.144	0.0001
LNRE	1	0.827298	0.00147858	559.521	0.0001
LNPR	1	0.455283	0.00190939	238.445	0.0001

Model: MODEL 4
Dependent Variable: NUG

Analysis of Variance

Source	DF	Sum of Squares	Mean Square	F Value	Prob>F

Model	2	29.39758	14.69879	51780.573	0.0001
Error	120	0.03406	0.00028		
C Total	122	29.43164			

Root MSE	0.01685	R-square	0.9988
Dep Mean	5.58170	Adj R-sq	0.9988
C.V.	0.30185		

Parameter Estimates

Variable	DF	Parameter Estimate	Standard Error	T for H0: Parameter = 0	Prob > |T|
INTERCEP	1	-4.415096	0.03697204	-119.417	0.0001
LNRE	1	0.862783	0.00300526	287.091	0.0001
LNPR	1	0.441244	0.00388087	113.697	0.0001

FOUR CALIBRATION REFRIGERANTS

Model: MODEL 1
Dependent Variable: NUE

Analysis of Variance

Source	DF	Sum of Squares	Mean Square	F Value	Prob>F
Model	2	42.89045	21.44522	10119.359	0.0001
Error	166	0.35179	0.00212		
C Total	168	43.24224			

Root MSE	0.04604	R-square	0.9919
Dep Mean	5.48795	Adj R-sq	0.9918
C.V.	0.83884		

Parameter Estimates

Variable	DF	Parameter Estimate	Standard Error	T for H0: Parameter = 0	Prob > |T|
INTERCEP	1	-5.015673	0.08491757	-59.065	0.0001
LNRE	1	0.905027	0.00687972	131.550	0.0001
LNPR	1	0.507640	0.00970171	52.325	0.0001

Model: MODEL 2
Dependent Variable: NUD

Analysis of Variance

Source	DF	Sum of Squares	Mean Square	F Value	Prob>F
Model	2	35.03234	17.51617	.	.
Error	166	0	0		
C Total	168	35.03234			

Root MSE	0.00000	R-square	1.0000
Dep Mean	5.43887	Adj R-sq	1.0000
C.V.	0.00000		

Parameter Estimates

Variable	DF	Parameter Estimate	Standard Error	T for H0: Parameter = 0	Prob > |T|
INTERCEP	1	-3.772261	0.00000000	.	.
LNRE	1	0.800000	0.00000000	.	.
LNPR	1	0.400000	0.00000000	.	.

Model: MODEL 3
Dependent Variable: NUP

Analysis of Variance

Source	DF	Sum of Squares	Mean Square	F Value	Prob>F
Model	2	35.99052	17.99526	167377.653	0.0001
Error	166	0.01785	0.00011		
C Total	168	36.00837			

Root MSE	0.01037	R-square	0.9995
Dep Mean	5.53387	Adj R-sq	0.9995
C.V.	0.18737		

Parameter Estimates

Variable	DF	Parameter Estimate	Standard Error	T for H0: Parameter = 0	Prob > |T|
INTERCEP	1	-4.052869	0.01912666	-211.896	0.0001
LNRE	1	0.826843	0.00154957	533.594	0.0001
LNPR	1	0.457499	0.00218519	209.363	0.0001

Model: MODEL 4
Dependent Variable: NUG

Analysis of Variance

Source	DF	Sum of Squares	Mean Square	F Value	Prob>F
Model	2	40.13652	20.06826	67855.395	0.0001
Error	166	0.04909	0.00030		
C Total	168	40.18562			

Root MSE	0.01720	R-square	0.9988

Dep Mean	5.53955	Adj R-sq	0.9988
C.V.	0.31045		

Parameter Estimates

Variable	DF	Parameter Estimate	Standard Error	T for H0: Parameter = 0	Prob > |T|
INTERCEP	1	-4.391624	0.03172280	-138.437	0.0001
LNRE	1	0.860922	0.00257007	334.980	0.0001
LNPR	1	0.442776	0.00362428	122.169	0.0001

PRANDTL NUMBER REGRESSION IN APPROACH 2

THREE CALIBRATION REFRIGERANTS

Model: MODEL 1
Dependent Variable: PR

Analysis of Variance

Source	DF	Sum of Squares	Mean Square	F Value	Prob>F
Model	9	40.84252	4.53806	969.099	0.0001
Error	113	0.52915	0.00468		
C Total	122	41.37167			

Root MSE	0.06843	R-square	0.9872
Dep Mean	1.45033	Adj R-sq	0.9862
C.V.	4.71827		

Parameter Estimates

Variable	DF	Parameter Estimate	Standard Error	T for H0: Parameter = 0	Prob > |T|
INTERCEP	1	96.908792	38.77678932	2.499	0.0139
X	1	-26.452258	10.79544008	-2.450	0.0158
Y	1	83.304684	26.64656684	3.126	0.0023
X2	1	2.459228	0.99959736	2.460	0.0154
XY	1	-16.020859	4.93940149	-3.243	0.0016
Y2	1	8.088965	7.10238635	1.139	0.2572
X3	1	-0.076756	0.03078419	-2.493	0.0141
X2Y	1	0.750949	0.22852190	3.286	0.0014
XY2	1	-0.668378	0.65967019	-1.013	0.3131
Y3	1	2.213377	1.01672374	2.177	0.0316

FOUR CALIBRATION REFRIGERANTS

Model: MODEL 1
Dependent Variable: PR

Analysis of Variance

Source	DF	Sum of Squares	Mean Square	F Value	Prob>F
Model	9	42.70508	4.74501	1012.626	0.0001
Error	159	0.74505	0.00469		
C Total	168	43.45013			

Root MSE	0.06845	R-square	0.9829
Dep Mean	1.50972	Adj R-sq	0.9819
C.V.	4.53416		

Parameter Estimates

Variable	DF	Parameter Estimate	Standard Error	T for H0: Parameter = 0	Prob > |T|
INTERCEP	1	132.495075	34.02680322	3.894	0.0001
X	1	-36.446721	9.44835075	-3.857	0.0002
Y	1	102.201609	23.81121972	4.292	0.0001
X2	1	3.392931	0.87286660	3.887	0.0001
XY	1	-19.449363	4.40931003	-4.411	0.0001
Y2	1	14.165714	6.12753638	2.312	0.0221
X3	1	-0.105753	0.02682882	-3.942	0.0001
X2Y	1	0.905506	0.20379577	4.443	0.0001
XY2	1	-1.253316	0.57134480	-2.194	0.0297
Y3	1	2.823725	0.81305846	3.473	0.0007

APPENDIX F. DATA ANALYSIS PROGRAM

This appendix contains a copy of the FORTRAN program used to reduce the raw data from the transport property tests. This program opened the raw data files which were collected from the data acquisition system used to collect all of the property and heat transfer information. Two approaches, the Nusselt number method and Prandtl number method, were also used to analyze the thermal conductivity in this program. All the equations referred to in this program were mentioned and discussed in the previous chapters.

Properties needed were obtained from the ASHRAE Handbook or REFPROP (version 4.0), which were mentioned in the Appendix A, and written in subroutine form. Calculated or measured properties (including thermal conductivity, viscosity, specific heat, and density, etc.) are available to execute this computer program.

```
      program analysis
      implicit real*8(a-h,o-z)
      common/acp/acp0,acp1,acp2,acp3,acp4,acp5
      common/av/av0,av1,av2,av3,av4,av5
      common/ak/ak0,ak1,ak2,ak3,ak4,ak5
      common/gpda/ga,pa,da
      common/gpdb/gb,pb,db
      common/gpdc/gc,pc,dc
      common/cc/ccs,ccg,ccp,ccd
      dimension tw(15),ttw(13),two(13),twi(13)
      real*8 kt,ktt,nu
      data di,dl,pai/0.009525,2.0,3.141592654/
c     toamp=(ti+81.4854431)/1.00110283e+04  !to amp(current)
c     toamp=(ti+81.4854431)/1.00110283e+04
c.....open output files
      open(unit=9,file='pr.dat',status='unknown')
      open(unit=10,file='lognu.dat',status='unknown')
      open(unit=11,file='ynu.dat',status='unknown')
      open(unit=12,file='cfh.h',status='unknown')
      open(unit=13,file='yynu.dat',status='unknown')
      open(unit=14,file='raw1.dat',status='unknown')
      open(unit=15,file='raw2.dat',status='unknown')
      open(unit=16,file='refined.dat',status='unknown')
      open(unit=17,file='sf.dat',status='unknown')
      open(unit=18,file='loss.dat',status='unknown')
      open(unit=19,file='cp.dat',status='unknown')
      open(unit=21,file='ycf.dat',status='unknown')
      open(unit=8,file='ypgnu.dat',status='unknown')
      open(unit=7,file='modified.k.dat',status='unknown')
      open(unit=23,file='new.k.dat',status='unknown')
      open(unit=22,file='hk.dat',status='unknown')
      open(unit=24,file='viscp.dat',status='unknown')
c-----------------------------------------------------
c.....Cp, viscosity, K curve fitting coefficient from ASHRAE or REFPROP
c.....nr=1 for r22; nr=2 for r12; nr=3 for r113; nr=4 for r114;
c.....nr=5 for r236ea(REFPROP);
c-----------------------------------------------------
      write(*,*)'input refrigerant number, nr=?',
     &'nr=1(r22);nr=2(r12);nr=3(r113);nr=4(r114);',
     &'nr=5(r236ea);nr=6(90% E.G.);nr=7(80% E.G.);',
     &'nr=8(70% E.G.);nr=9(60% E.G.);nr=10(50% E.G.)'
      read(*,*)nr0
      write(*,*)'input ending refrigerant number, nend=?'
      read(*,*)nend
      nr=nr0
      write(*,*)'input number of data set, NTDATA=?'
      read(*,*)ntdata
      ndata=1
   90 if(nr.eq.1)then
c.....r22 transport properties data
c.....r22 Cp, viscosity, K curve fitting coefficient from ASHRAE
    1 tc=96.15+273.33
```

```
      tb=-40.86+273.33
      pc=733.02
      wm=86.47
      w=0.2211
      call prop(nr)        !call prop(nr) to properties coefficients
      open(unit=5,file='r22.dat',status='old')
      go to 50
c
c.....r12 transport properties data
c.....r12 Cp, viscosity, K curve fitting coefficient from ASHRAE
c
      else if(nr.eq.2)then
    2 tc=111.8+273.33
      tb=-29.76+273.33
      pc=606.26
      wm=120.91
      w=0.1814
      call prop(nr)        !call prop(nr) to properties coefficients
      open(unit=5,file='r12.dat',status='old')
      go to 50
c
c.....r113 transport properties data
c.....r113 Cp, viscosity, K curve fitting coefficient from ASHRAE
c
      else if(nr.eq.3)then
    3 tc=214.35+273.33
      tb=47.65+273.33
      wm=187.38
      w=0.2563
      call prop(nr)        !call prop(nr) to properties coefficients
      open(unit=5,file='r113.dat',status='old')
      go to 50
c
c.....r114 transport properties data
c.....r114 Cp, viscosity, K curve fitting coefficient from ASHRAE
c
      else if(nr.eq.4)then
    4 tc=145.65+273.33
      tb=3.65+273.33
      pc=471.08
      wm=170.92
      w=0.2511
      call prop(nr)        !call prop(nr) to properties coefficients
      open(unit=5,file='r114.dat',status='old')
      go to 50
c
c.....r236ea transport properties data
c.....r236ea Cp, viscosity, K curve fitting coefficient from REFPROP-4.0
c
      else if(nr.eq.5)then
    5 tc=139.29+273.33
      tb=6.5+273.33
```

```
      pc=512.42
      wm=152.05
      w=0.3860
      call prop(nr)        !call prop(nr) to properties coefficients
      open(unit=5,file='r236ea.dat',status='old')
c     open(unit=5,file='/home/yuan/viscometer/r236eat1.dat',
c     &status='old')
      go to 50
      end if
c-------------------------------------------------------
c.....output head lines
   50 write(*,*)'Tave(C)  mass(kg/s) heat(W)  h(W/m^2.C)    Nu'
      write(*,*)'  T(C)   Kg(W/m.C) Kp(W/m.C) Kd(W/m.C) Kt(W/m.C)  E(%
     &)-G  E(%)-P  E(%)-D'
      write(*,*)'-------------------------------------
     &-------------'
      write(*,*)
      area=pai*di*dl
      nexp=20
      do 1000 i=ndata,ntdata
c
c.....reading data over nexp(=20) times
c
      do 200 k=1,nexp
      read(5,*,end=1001)(tw(j),j=1,15)
      read(5,*,end=1001)power,ti,to,pd,pi,den,tsen,rmass
c.....rtd anti-calibration for checking accuracy purpose
c     tiamp=(ti+81.2238617)/1.00184971e+04
c     ti=-80.0+(1.0e+04)*tiamp
c     toamp=(ti+81.4854431)/1.00110283e+04
c     to=-80.0+(1.0e+04)*toamp
      tf=0.5*(ti+to)
c
c.....fluid transport properties at Tsat: Cp, vis, and K
c.....(ASHRAE data from curve fitting)
c.....coefficients obtained from calling prop(nr) previously
c
      fcp=acp0+acp1*tf+acp2*(tf**2)+acp3*(tf**3)+acp4*(tf**4)+
     &acp5*(tf**5)                    !Cp
      fvis=av0+av1*tf+av2*(tf**2)+av3*(tf**3)+av4*(tf**4)+
     &av5*(tf**5)                     !viscosity
      fkt=ak0+ak1*tf+ak2*(tf**2)+ak3*(tf**3)+ak4*(tf**4)+
     &ak5*(tf**5)                     !thermal conductivity
c.....net heat input to the test section
      heat=rmass*fcp*(to-ti)       !real heat input to the test section
      hflux=heat/area              !heat flux of the test section
c
c.....inner wall temperature correction by heat conduction through wall
c
      r1=(3.0/16.0)*0.0254         !tube inside diameter
      r2=(4.0/16.0)*0.0254         !tube outside diameter
      twc=hflux*r1*log(r2/r1)/401.0  !wall temp. correction(wall conduction)
```

```
      do 300 n=1,13
      twi(n)=tw(n)-twc            !inner wall temp.
  300 continue
c     twi(10)=0.5*(twi(9)+twi(11))  !bad tw(10), so use 9,11 for average
      call dtwf(twi,ti,to,dt)     !call dtwf to get dt
      h=heat/(area*dt)            !heat transfer coefficient
c
c.....total quantities for wall temp., fluid, power, insulation surface,
c.....and air temperature
c
      ht=ht+h
      tti=tti+ti
      tto=tto+to
      do 180 n=1,13
      ttw(n)=ttw(n)+tw(n)     !each outer wall temp. total quantities
  180 continue
      ttwa=ttwa+twa           !twa=average wall temp.
      ttfa=ttfa+tf            !tfa=average fluid temp.
      tts=tts+tw(14)          !tw(14)=insulation surfeace temp.
      tta=tta+tw(15)          !tw(15)=ambient temp.
c     tt=tt+t                 !t=viscometer temperature(C)
      tpi=tpi+pi              !pi=inlet pressure(psia)
      tpower=tpower+power     !power=power input(I*V)
c     tvismm=tvismm+vismm     !vismm=viscosity measured by viscometer(cp)
      trmass=trmass+rmass     !rmass=mass flow rate
      tden=tden+den           !den=density
      cpt=cpt+cp              !cp=specific heat capacity
      vist=vist+vis           !vis=viscosity
      ktt=ktt+kt              !kt=thermal conductivity
  200 continue
c
c.....average quantities for nexp(=20) times
c
      do 190 n=1,13
      two(n)=ttw(n)/nexp      !each average outer wall temp. of nexp times
      twi(n)=two(n)-twc
  190 continue
      tiave=tti/nexp                !average inlet temp.
      toave=tto/nexp                !average outlet temp.
      twa=ttwa/nexp                 !average wall temp.
      tfa=ttfa/nexp                 !average fluid temp.
c     t=tt/nexp                     !average sample cell temperature(viscometer)
      pi=tpi/nexp                   !average inlet pressure
      tsave=tts/nexp                !average insulation surface temp.
      taave=tta/nexp                !average ambient temp.
      powera=tpower/nexp            !average power input
c     vismm=tvismm/nexp             !average viscosity(cp) measured
      rmass=trmass/nexp             !average mass flow rate
      den=tden/nexp                 !average density
      have=ht/nexp                  !average heat transfer coefficient
c     cpave=cpt/nexp                !average cp
c     visave=vist/nexp              !average viscosity
```

```
c     ktave=ktt/nexp                !average thermal conductivity
c
c.....Psat
      if(nr.eq.1)then
      w=0.2211
      pc=733.02
      psat=((5.00004649E-01)+(1.61909014E-02)*tfa+
     &     (1.95017230E-04)*tfa**2+
     &     (1.03241905E-06)*tfa**3+(2.23205832E-09)*tfa**4+
     &     (1.71046532E-12)*tfa**5)*1.0E+06*1.45038E-04
      else if(nr.eq.2)then
      w=0.1814
      pc=606.26
      psat=((2.91020423E-01)+(1.00844698E-02)*tfa+
     &     (1.49919608E-04)*tfa**2+
     &     (5.64050538E-07)*tfa**3+(-5.91876770E-09)*tfa**4+
     &     (5.79094585E-11)*tfa**5)*1.0E+06*1.45038E-04
      else if(nr.eq.3)then
      w=0.2563
      pc=501.25
      psat=((1.58554465E-02)+(6.77690492E-04)*tfa+
     &     (1.25848301E-05)*tfa**2+
     &     (2.28212969E-07)*tfa**3+(-1.47080736E-10)*tfa**4+
     &     (1.60667465E-12)*tfa**5)*1.0E+06*1.45038E-04
      else if(nr.eq.4)then
      w=0.2511
      pc=471.08
      psat=((8.76785517E-02)+(3.47902835E-03)*tfa+
     &     (5.45874973E-05)*tfa**2+
     &     (3.74883115E-07)*tfa**3+(4.43446752E-10)*tfa**4+
     &     (1.88150016E-12)*tfa**5)*1.0E+06*1.45038E-04
      else if(nr.eq.5)then
      w=0.3860
      pc=512.42
      psat=(1.13349352E+01)+(4.84870791E-01)*tfa+
     &     (8.30436591E-03)*tfa**2+
     &     (6.78510114E-05)*tfa**3+(2.04624143E-07)*tfa**4+
     &     (-2.19035401E-10)*tfa**5
      end if
c.....fluid saturated transport properties based on temperature at tfa:Cp, vis, and K
c.....(ASHRAE data from curve fitting)
c.....coefficients obtained from calling prop(nr) previously
c
      cp=acp0+acp1*tfa+acp2*(tfa**2)+acp3*(tfa**3)+acp4*(tfa**4)+
     &acp5*(tfa**5)                 !Cp
      vis=av0+av1*tfa+av2*(tfa**2)+av3*(tfa**3)+av4*(tfa**4)+
     &av5*(tfa**5)                  !viscosity
      kt=ak0+ak1*tfa+ak2*(tfa**2)+ak3*(tfa**3)+ak4*(tfa**4)+
     &ak5*(tfa**5)                  !thermal conductivity
c.....non-dimensionized temperature and pressure
c
      tr=(tfa+273.33)/tc                !tc is critical Temp.
```

```
      ppr=pi/pc                              !pc is critical pressure
      dpr=(pi-psat)/pc                       !psat is saturated pressure
      call kfactor(tr,ppr,ratiok)            !k midified factor based on current pressure pi
      call vfactor(w,tr,dpr,ratiov)          !viscosity modified factor based on pi
      write(*,*)'ratiok=',ratiok,'ratiov=',ratiov
c
      vis=vis*ratiov   !modifying viscosity from saturated state to pi state
      viscp=vis*cp
      kt=kt*ratiok     !modifying k from saturated state to pi state
      call dtwf(twi,tiave,toave,dt)          !call dtwf to get dt
      dtn=(toave-tiave)/dt                   !non-dimensionized dt
      twave=tfa+dt
      h=rmass*cp*(toave-tiave)/(area*dt)     !heat transfer coefficient
c.....write aveaged data
      write(14,3000)i,tfa,rmass,tiave,toave,twave,dt,taave,tsave,powera
 3000 format(1x,i3,1x,f6.3,1x,f8.5,1x,6(f7.3,1x),f10.4)
c
c.....heat loss calculations and calibrations
c
      tak=taave+273.33
      call airprop(tak,dena,cpa,visa,tka)   !call airprop to get prop.
c
c.....heat loss calculations
c
      pra=visa*cpa/tka              !air Prantdl number
      beta=1.0/taave                !air expansion coefficient
      g=9.8              !gravitional accleration
      dvisa=visa/dena               !air kinermatic viscosity
      alpha=tka/(dena*cpa)          !air thermal diffusivity
      dia=2.5*2.54/100.0            !outer insulation diameter
      ao=pai*dia*dl                 !outer insulation surface area
      dtsa=tsave-taave              !temp. difference between surf/air
      dtwa=twave-taave              !temp. difference between wall/air
      rdtswa=dtsa/dtwa              !temp. diff. ratio between suf-wall-air
      rada=(g*beta*dtsa*dia**3.0)/(dvisa*alpha)          !Ra number
c
c.....churchill free convection's Nusselt number calculations
c
      heat=rmass*cp*(toave-tiave)           !real heat input to the test section
      hflux=heat/area                       !heat flux of the test section
      prn=(1.0+((0.559/pra)**(9.0/16.0)))**(8.0/27.0)
      anuic=(0.6+(0.387*(rada**(1.0/6.0))/prn))**2.0  !air Nu(unmodify)
      yanuic=log(anuic)                     !log(anuic)
      anu=1.2*anuic                         !modified Nu number, update 1.2
      ha=anu*tka/dia                        !air heat loss cofficient, ha
      qloss=ha*ao*(tsave-taave)             !heat loss calculated from C.C. eq.
      qlossx=powera-heat                    !true heat loss
      hac=qlossx/ao/(tsave-taave)           !true ha
      anuc=hac*dia/tka                      !true Nuair
      yanuc=log(anuc)                       !log(anuc)
      cf=qlossx/qloss                       !heat loss ratio
      ylncf=log(cf)                         !log of heat loss ratio
```

```
      xlnra=log(rada)                    !log of Ra
      write(18,2250)log(dtsa),log(qlossx)  !write to loss.dat
 2250 format(1x,3(f15.6,2x))
c
c.....net heat input
c.....heat loss prediction by measured Ts-Ta
      qloss=(exp(0.612001419))*(dtsa)**1.33022535          !heat loss prediction
      qnet=powera-qloss                  !net heat to the test section
      qlratio=(qloss/powera)*100.0       !heat loss percentage ratio
      cpc=qnet/(rmass*(toave-tiave))     !calculated Cp
      rcp=((cpc-cp)/cp)*100.0            !Cp deviation percentage
      write(19,2260)tfa,cp,cpc,rcp       !write to cp.dat
 2260 format(1x,f10.5,2x,2f12.6,2x,f7.3)
c.....Re and Pr number
      re=(4.0*rmass)/(pai*di*vis)        !Reynolds numbers
      xre=log(re)                        !logarithm Re transformation
      pr=vis*cp/kt                       !fluid Prantdl number
      ec=rmass**2/(den**2*di**2*cpc*dt)
      write(24,1013)tfa,kt,rmass,vis,cpc
      write(23,*)log(pr),log(re),log(dtn)
c     write(23,1013)kt,rmass,vis*1.0E+03,cp/1000.0,dtn
c     write(*,*)'vis=',vis,'cp=',cp,'rmass=',rmass
      call newk(pr,re,dtn)
      if(nr.eq.5)then
      hk=vis*cpc/pr
      else
      hk=vis*cp/pr
      end if
      hk=hk/ratiok
      rhk=((hk-kt)/kt)*100.0
      write(22,1014)tfa,hk,kt,rhk
 1014 format(1x,f9.6,2(f12.6,1x),f10.6)
c
c.....parameter logarithm transformation for corrected Nusselt number
c
      pr=vis*cp/kt                 !fluid Prantdl number
      xpr=log(pr)                  !log Prandtl
      nu=h*di/kt                   !corrected Nu number
      ynu=log(nu)                  !log Nu
      yynu=log(nu/(pr**0.507056))
      write(15,3001)i,tfa,tr,re,pr,cp
 3001 format(1x,i3,1x,2(f6.3,1x),1x,f10.2,1x,f8.4,1x,f10.5)
c
c.....correlation Nusselt number calibration functions
c.....call subroutine cnucf(re,gcf,pcf,dcf)
c
      call cfnu(pr,re,enu,cfg,cfp,cfd,cfh)
c
c
c.....modified h values from enu(curve fitting equation) values
c
      hstar=(enu*kt)/di
```

```
      cfh=hstar/h
      yhstar=log(hstar)
      yh=log(h)
      h1=h*cfh
      yyh=log(h/pr**(-0.477820))
      yyhstar=log(hstar/pr**(-0.477820))
c
c.....Dittus Boelter correlation
c
c     h=have
      a1=0.905027
      b1=0.507640
      c1=exp(-5.015673)
      a2=0.800013840
      b2=0.4
      c2=exp(-3.772261)
      em1=a1-a2+0.8
      em2=b1-b2+0.4
      en=1.0/(0.6-b1+b2)
      dks=((c2*h*di)/(0.023*c1*re**em1*(vis*cp)**em2))**en
      dks=dks/ratiok
      dnustar=h*di/kt
      dnu=0.023*re**0.8*pr**0.4   !Dittus-Boelter eq. Nu
      ydnu=log(dnu)               !ln(Nud)
      ydcf=ynu-ydnu
      dcf=nu/dnu
      dk=((h*di)/(0.023*re**0.8*(vis*cp)**0.4))**(5.0/3.0)
      dk=dk/ratiok
 1980 format(1x,f9.5,1x,f9.5,1x,4(f12.6,1x))
      prd=vis*cp/dk
c     prstar=7.41372108e-2+9.85503972e-1*prd
c     dk=vis*cp/prstar
      rdk=((dks-kt)/kt)*100.0                    !deviation ratio
      if(abs(rdk).le.5.0)then
      write(16,1800)powera,rmass,den,
     &tfa,tiave,toave,twave,dt,taave,tsave
      else if(abs(rdk).gt.5.0)then
      go to 800
      end if
 1800 format(1x,f9.4,1x,f8.5,1x,f10.3,1x,7(f8.5,1x))
  800 write(*,*)re,pr,xre,xpr,nu,dnu
      write(10,2010)re,pr,xre,xpr,nu,dnu
 2010 format(1x,f15.6,1x,f8.4,1x,4(f12.6,2x))
      write(*,900)tr,tfa,pr,kt,dk,rdk
      write(9,900)tr,tfa,pr,kt,dk,rdk,dens,den          !write to pr.dat
  900 format(1x,f5.2,2x,f5.2,2x,f8.4,2x,2(f8.5,2x),f8.4,2x,2(f8.3,2x))
c.....Petukhov Popov correlation
      f=(1.82*log10(re)-1.64)**-2
      pnu1=(f/8)*re*pr
      pnu2=1.07+12.7*((f/8)**(0.5))*(pr**(2./3.)-1.0)
      pnu=pnu1/pnu2
      ypnu=log(pnu)
```

```
      ypcf=ynu-ypnu
      pcf=nu/pnu
      cstar=c1
      astar=a1
      bstar=b1
      cpe=exp(-4.052869)
      ape=0.826843
      bpe=0.457499
      prpold=pr
  850 fp1=(cstar*(f/8.)**0.5*vis*cp*re**(astar-ape+1))/
     &(12.7*cpe*h*di)
      fp2=(1.07/(12.7*(f/8.)**0.5))
      fp=prpold**(2./3.)-fp1*prpold**(bstar-bpe)+fp2-1
      fpp=(2./3.)*prpold**(-1./3.)-(bstar-bpe)*fp1*
     &prpold**(bstar-bpe-1)
      prpnew=prpold-(fp/fpp)
      epsp=prpnew-prpold
      if(abs(epsp).le.1.0e-12)go to 920
      prpold=prpnew
      go to 850
  920 pk=vis*cp/prpnew
      pk=pk/ratiok
      rpk=((pk-kt)/kt)*100.0
c.....Gnielinski correlation
      fg=(0.79*log(re)-1.64)**-2
      gnu1=(fg/8)*(re-1000.0)*pr
      gnu2=1.0+12.7*((fg/8)**0.5)*(pr**(2./3.)-1.0)
      gnu=gnu1/gnu2          !Gnielinski Nu
      gkc=vis*cp*((gnu1/(12.7*(fg/8)**(0.5)*h*di))-
     &(1/(12.7*(fg/8)**0.5))+1)**(-1.5)
      ygnu=log(gnu)          !ln(Nug)
      ygcf=ynu-ygnu
      gcf=nu/gnu
      cge=exp(-4.391624)
      age=0.860922
      bge=0.442776
      prgold=pr
  860 fg1=(cstar*(fg/8.)**0.5*vis*cp*(re-1000.)**(astar-age+1))/
     &(12.7*cge*h*di)
      fg2=(1.0/(12.7*(fg/8.)**0.5))
      ffg=prgold**(2./3.)-fg1*prgold**(bstar-bge)+fg2-1
      ffgp=(2./3.)*prgold**(-1./3.)-(bstar-bge)*fg1*prgold**
     &(bstar-bge-1)
      prgnew=prgold-(ffg/ffgp)
      epsg=prgnew-prgold
      if(abs(epsg).le.1.0e-12)go to 930
      prgold=prgnew
      go to 860
  930 gk=vis*cp/prgnew
      gk=gk/ratiok
      rgk=((gk-kt)/kt)*100.0
c.....write to output
```

```
c     gkcc=((gkc-kt)/kt)*100.0   !k deviation from Gnielinski eq.
c     if(gkcc.gt.10.0)go to 990 !based on gkc to throw away bad points
      write(8,2500)i,xre,xpr,ynu,ydnu,ypnu,ygnu     !write to file ypgnu.dat
  990 write(7,2510)tfa,kt,dks,pk,gk,rdk,rpk,rgk  !write to file modified.k.dat
      write(21,2520)xre,xpr,ydcf,ypcf,ygcf   !write to file ycf.dat
 2500 format(1x,i4,1x,6(f15.6,1x))
 2510 format(1x,f6.3,2x,4(f8.6,2x),2x,3(f7.3,2x))
 2520 format(1x,2x,5(f12.6,2x))
c.....Nusselt number curve fittings
c.....n for Pr^n in 3 and 4 calibration fluids(R22,R12,R113, add R114) are:
c.....expriment:0.498730;0.504359
c.....Dittus:0.4;0.4
c.....Petukhov:0.455420;0.457575
c.....Gnielinki:0.441340;0.442798
      yenu=log(nu/pr**0.523086)
      ydnu=log(dnu/pr**0.4)
      ypnu=log(pnu/pr**0.457575)
      ygnu=log(gnu/pr**0.442798)
      write(11,2600)xre,yenu,ydnu,ypnu,ygnu        !write to ynu.dat
 2600 format(2x,5(f12.8,2x))
c
c.....read another set of data at different temp. level
c.....set total quantity equal to 0.0
c
  600 do 601 n=1,13
      ttw(n)=0.0                    !total quantity of each wall temp.
  601 continue
      ht=0.0              !total quantity of heat transfer coef.
      tti=0.0             !total quantity of inlet temp.
      tto=0.0             !total quantity of outlet temp.
      ttwa=0.0            !total quantity of average wall temp.
      ttfa=0.0            !total quantity of average fluid temp.
      tts=0.0             !total quantity of insulation surface temp.
      tta=0.0             !total quantity of ambient air temp.
c     tt=0.0              !total quantity of sample cell temperature
      tpi=0.0             !total quantity of inlet pressure
c     tvismm=0.0          !total quantity of viscosity
      tpower=0.0          !total quantity of power input
      trmass=0.0          !total quantity of mass flow rate
      tden=0.0            !total quantity of density
      ndata=i+1           !number of data set(each set has nexp times)
 1000 continue
c.....read another working fluid data set
 1001 if(nr.eq.nend)go to 2000              !end of data file detected come here and check nr
      close(unit=5)                         !temporary close 5 and ready open 5 for another fluid
      ndata=i                               !set data number continuously
      nr=nr+1                               !number of refrigerant increased by 1
      go to 90                              !back to very beginning of data reading
 1010 format(1x,i2,2x,6(f15.8))
 1011 format(1x,f6.3,7(f10.5,1x))
 1012 format(1x,i2,2x,6(f15.8))
 1013 format(1x,5(f15.8,1x))
```

```
 2000 close(unit=5)
      stop
      end
C*****************************************************************************
C     This subroutine calculates the refrigerant properties, such as specific  *
C     heat capacity, viscosity, and thermal conductivity, by curve fittings.   *
C     The source data are based upon ASHRAE except R236ea based on REFPROP4.0  *
C*****************************************************************************
      subroutine prop(nr)                !input number of refrigerant
      implicit real*8(a-h,o-z)
      common/acp/acp0,acp1,acp2,acp3,acp4,acp5  !Cp coefficients
      common/av/av0,av1,av2,av3,av4,av5         !Viscosity coef.
      common/ak/ak0,ak1,ak2,ak3,ak4,ak5         !K coef.
      if(nr.eq.1)then
      open(unit=20,file='prop.22',status='old') !coef. file for HCFC-22
c.....coefficients for HCFC-22 Cp
      read(20,*)acp0,acp1,acp2,acp3,acp4,acp5
c.....coefficients for HCFC-22 viscosity
      read(20,*)av0,av1,av2,av3,av4,av5
c.....coefficients for HCFC-22 K
      read(20,*)ak0,ak1,ak2,ak3,ak4,ak5
      close(unit=20)
      return
      else if(nr.eq.2)then
      open(unit=20,file='prop.12',status='old') !coef. file for CFC-12
c.....coefficients for CFC-12 Cp
      read(20,*)acp0,acp1,acp2,acp3,acp4,acp5
c.....coefficients for CFC-12 viscosity
      read(20,*)av0,av1,av2,av3,av4,av5
c.....coefficients for CFC-12 K
      read(20,*)ak0,ak1,ak2,ak3,ak4,ak5
      close(unit=20)
      return
      else if(nr.eq.3)then
      open(unit=20,file='prop.113',status='old') !coef. file for CFC-113
c.....coefficients for CFC-113 Cp
      read(20,*)acp0,acp1,acp2,acp3,acp4,acp5
c.....coefficients for CFC-113 viscosity
      read(20,*)av0,av1,av2,av3,av4,av5
c.....coefficients for CFC-113 K
      read(20,*)ak0,ak1,ak2,ak3,ak4,ak5
      close(unit=20)
      return
      else if(nr.eq.4)then
      open(unit=20,file='prop.114',status='old') !coef. file for CFC-114
c.....coefficients for CFC-114 Cp
      read(20,*)acp0,acp1,acp2,acp3,acp4,acp5
c.....coefficients for CFC-114 viscosity
      read(20,*)av0,av1,av2,av3,av4,av5
c.....coefficients for CFC-114 K
      read(20,*)ak0,ak1,ak2,ak3,ak4,ak5
      close(unit=20)
```

```
      return
      else if(nr.eq.5)then
      open(unit=20,file='prop.236',status='old') !coef. file for HFC-236ea
c.....coefficients for HFC-236ea Cp
      read(20,*)acp0,acp1,acp2,acp3,acp4,acp5
      acp0= 1.19340710E+03
      acp1= 6.33325863E+00
      acp2=-4.13577229E-01
      acp3= 1.47026302E-02
      acp4=-2.22029586E-04
      acp5= 1.21074845E-06
c     acp0=1.20477688E+03
c     acp1=1.92495738E-00
c     acp2=0.0
c     acp3=0.0
c     acp4=0.0
c     acp5=0.0
c.....coefficients for HFC-236ea viscosity
      read(20,*)av0,av1,av2,av3,av4,av5
      av0=( 5.63759208E-01)*1.0e-3
      av1=(-1.03053898E-02)*1.0e-3
      av2=( 2.14341562E-04)*1.2e-3
      av3=(-5.06344441E-06)*1.0e-3
      av4=( 6.69040219E-08)*1.0e-3
      av5=(-3.19661297E-10)*1.0e-3
c.....coefficients for HFC-236ea K
      read(20,*)ak0,ak1,ak2,ak3,ak4,ak5
      close(unit=20)
      return
      end if
      end
C*******************************************************************************
C     This subroutine calculates the air properties, such as density, Cp,     *
C     viscosity, and thermal conductivity, by curve fittings. The source data *
C     are based on back tables in Appendix of the book by Incoporea and DeWitt.*
C*******************************************************************************
      subroutine airprop(tak,dena,cpa,visa,tka)
      implicit real*8(a-h,o-z)
      data d0,d1,d2,d3,d4,d5/8.40219021e+00,-7.31001496e-02,
     &3.01471766e-04,-6.34908758e-07,6.58567756e-10,-2.66433143e-13/
      data c0,c1,c2,c3,c4,c5/1.11507312e+03,-1.31544113e+00,
     &5.91507275e-03,-1.29040736e-05,1.44722101e-08,-6.33937087e-12/
      data v0,v1,v2,v3,v4,v5/-3.79514205e-07,+8.36939549e-08,
     &-9.95046476e-11,1.33037244e-13,-1.27004888e-16,5.52250075e-20/
      data t0,t1,t2,t3,t4,t5/-4.19377378e-04,1.03869352e-04,
     &-7.47035287e-08,1.22800797e-10,-1.55568361e-13,7.10215355e-17/
c.....getting density, specific heat, viscosity, and thermal
c.....conductivity of air at temperature tak(in K)
      dena=d0+d1*tak+d2*tak**2+d3*tak**3+d4*tak**4+d5*tak**5
      cpa=c0+c1*tak+c2*tak**2+c3*tak**3+c4*tak**4+c5*tak**5
      visa=v0+v1*tak+v2*tak**2+v3*tak**3+v4*tak**4+v5*tak**5
      tka=t0+t1*tak+t2*tak**2+t3*tak**3+t4*tak**4+t5*tak**5
```

```
      return
      end
C*****************************************************************************
C     This subroutine calculates the average wall and fluid temperature      *
C     difference by using finite control volume method                       *
C*****************************************************************************
      subroutine dtwf(twi,tiave,toave,dt)
      implicit real*8(a-h,o-z)
      dimension twi(13),tfi(13),dx(13),x(13)
c
c.....finite control volume grid increament and coodinates
c
      dx(1)=0.05
      x(1)=0.0
      dx(2)=0.1
      x(2)=0.1
      dx(3)=0.15
      x(3)=0.2
      do 10 i=4,10
      dx(i)=0.2
      x(i)=x(i-1)+0.2
   10 continue
      dx(11)=0.15
      x(11)=0.18
      dx(12)=0.1
      x(12)=0.19
      dx(13)=0.05
      x(13)=2.0
      dl=2.0
c
c.....fluid temperature distribution(assume linear)
c
      tfi(1)=tiave
      tfi(13)=toave
      do 20 i=2,12
      tfi(i)=tfi(i-1)+(x(i)-x(i-1))*((tfi(13)-tfi(1))/dl)
   20 continue
c
c.....dt calculations
c
      dtt=0.0
      do 30 i=1,13
      dtt=dtt+(dx(i)/(twi(i)-tfi(i)))
   30 continue
      dt=dl/dtt
      return
      end
C*****************************************************************************
C     This subroutine calculates the calibration functions for the Nusselt   *
C     number's equations, such as Gnielinski, Petukhov, and Dittus-Boelter   *
C     equations. Also, the experimental data forms the Nusselt number        *
C     correlation, Nue. Those are obtained by curve fittings from SAS.       *
```

```
C*****************************************************************************
      subroutine cfnu(pr,re,enu,cfg,cfp,cfd,cfh)
      implicit real*8(a-h,o-z)
      common/gpda/ga,pa,da
      common/gpdb/gb,pb,db
      common/gpdc/gc,pc,dc
      common/cc/ccs,ccg,ccp,ccd
      data ae,be,ce/0.850544751,0.507056,-4.39778757/
      data ag,bg,cg/0.835702658,0.495804,-4.16347694/
      data ap,bp,cp/0.819511116,0.516636,-4.03165674/
      data ad,bd,cd/0.799977124,0.400000,-3.77200365/
      data ha,hb,hc/0.746661,-0.477820,-0.159677/
      data ha1,hb1,hc1/0.746638,-0.477820,-0.159415/
      ga=ae-ag
      pa=ae-ap
      da=ae-ad
      gb=be-bg
      pb=be-bp
      db=be-bd
      ccs=exp(ce)
      ccg=exp(cg)
      ccp=exp(cp)
      ccd=exp(cd)
      gc=ce-cg
      pc=ce-cp
      dc=ce-cd
      enu=pr**ae*re**be*exp(ce)
      cfg=(pr**(be-bg))*(re**(ae-ag))*(exp(ce-cg))
      cfp=(pr**(be-bp))*(re**(ae-ap))*(exp(ce-cp))
      cfd=(pr**(be-bd))*(re**(ae-ad))*(exp(ce-cd))
      cfh=(pr**(hb-hb1))*(re**(ha-ha1))*(exp(hc-hc1))
      return
      end
c*****************************************************************************
c     The following subroutine calculates the thermal conductivity    *
c     ratio at different pressure but at the same temperature. This is*
c     so called pressure effects on thermal conductivity. The equation*
c     used here is Missenard correlation(1970)                  *
c*****************************************************************************
      subroutine kfactor(tr,pr,ratiok)
      implicit real*8(a-h,o-z)
      dimension a(21)
      data a(1),a(2),a(3),a(4),a(5),a(6),a(7),a(8),
     &    a(9),a(10),a(11),a(12),a(13),a(14),a(15),a(16),
     &    a(17),a(18),a(19),a(20),a(21)
     &    /-0.376480,1.998078,0.007849,-3.419245,-0.053279,
     &     0.000131,1.956588,0.115588,-0.000281,-0.000001554,
     &     0.0,-0.075644,-0.000291,0.000005608,-5.59027E-10,
     &     0.0,0.0,0.000517,-0.000004349,9.446296E-11,2.460594E-13/
      q=a(1)+a(2)*tr+a(3)*pr+a(4)*tr**2+a(5)*tr*pr+a(6)*pr**2+
     & a(7)*tr**3+a(8)*tr**2*pr+a(9)*tr*pr**2+a(10)*pr**3+
     & a(11)*tr**4+a(12)*tr**3*pr+a(13)*tr**2*pr**2+a(14)*tr*pr**3+
```

```
     & a(15)*pr**4+a(16)*tr**5+a(17)*tr**4*pr+a(18)*tr**3*pr**2+
     & a(19)*tr**2*pr**3+a(20)*tr*pr**4+a(21)*pr**5
      ratiok=1.0+q*pr**0.7
      return
      end
c*************************************************************************
c    The following subroutine calculates the liquid viscosity       *
c    ratio at different pressure but at the same temperature. This is*
c    so called pressure effects on liquid viscosity. The equation    *
c    used here is Lucas correlation(1981)                            *
c*************************************************************************
      subroutine vfactor(w,tr,dpr,ratiov)
      implicit real*8(a-h,o-z)
      a=0.9991-(4.674E-04/(1.0523*tr**(-0.03877)-1.0513))
      d=(0.3257/(1.0039-tr**2.573)**0.2960)-0.2086
      c=-0.07921+2.1616*tr-13.4040*tr**2+44.1706*tr**3-
     & 84.8291*tr**4+96.1209*tr**5-59.8127*tr**6+15.6719*tr**7
      ratiov=(1.0+d*(dpr/2.118)**a)/(1.0+c*w*dpr)
      return
      end
c*************************************************************************
c    The following program is used to calculate k by directly curve  *
c    fitting by function log(h), log(vis*cp), and log(re)            *
c*************************************************************************
      subroutine newk(pr,re,dtn)
      implicit real*8(a-h,o-z)
      data a0,a1,a2,a3,a4,a5,a6,a7,a8,a9
     &   /96.908792,-26.452258,83.304684,2.459228,
     &    -16.020859,8.088965,-0.076756,0.750949,
     &    -0.668378,2.213377/
      x=log(re)
      y=log(dtn)
      pr=a0+a1*x+a2*y+a3*x**2+a4*x*y+a5*y**2+
     & a6*x**3+a7*x**2*y+a8*x*y**2+a9*y**3
      pr=exp(pr)
      return
      end
```

TECHNICAL REPORT DATA
(Please read Instructions on the reverse before completing)

1. REPORT NO. EPA-600/R-98-037	2.
3. RECIPIENT'S ACCESSION NO.	
4. TITLE AND SUBTITLE Transport Property Measurements of HFC-236ea	5. REPORT DATE April 1998
	6. PERFORMING ORGANIZATION CODE
7. AUTHOR(S) J.-Y. Lin and M. B. Pate	8. PERFORMING ORGANIZATION REPORT NO.
9. PERFORMING ORGANIZATION NAME AND ADDRESS Iowa State University, 2088 H. M. Black Engineering Building, Ames, Iowa 50011-2160	10. PROGRAM ELEMENT NO.
	11. CONTRACT/GRANT NO. CR820755-01-4
12. SPONSORING AGENCY NAME AND ADDRESS **EPA, Office of Research and Development, Air Pollution Prevention and Control Division, Research Triangle Park, NC 27711**	13. TYPE OF REPORT AND PERIOD COVERED Final; 10/92-3/95
	14. SPONSORING AGENCY CODE **EPA/600/13**

15. SUPPLEMENTARY NOTES APPCD project officer is Theodore G. Brna, Mail Drop 63, 919/541-2683.

16. ABSTRACT The report gives results of an evaluation of transport properties of 1,1,1,2,3,3-hexafluoropropane (HFC-236ea), with liquid viscosity and thermal conductivity being the two main transport properties of interest. In addition, the specific heat and density of refrigerant/lubricant mixtures are also provided in this study. (NOTE: HFC-236ea is currently a candidate to replace 1,2-dichloro-tetrafluoroethane--CFC-114--in surface craft and submarine chiller units.) The study used a novel method for simultaneously measuring viscosity and thermal conductivity, using inline property sensors in series with a heat transfer measurement system. Specifically, viscosity was measured with an inline torsional oscillation viscometer, and thermal conductivity was measured from the knowledge of single-phase heat transfer characteristics of a heated test section. The viscosity and thermal conductivity measurements for CFC-114 were compared with ASHRAE (American Society of Heating, Refrigerating and Air-Conditioning Engineers) data: agreement was within +/-5% for thermal conductivity and +/-2% for viscosity. For HFC-236ea, the measured data were compared with REFPROP, a theoretical prediction package developed by the NIST (National Institute of Standards and Technology): average deviations were within +15% in thermal conductivity, and -5% in viscosity.

17. KEY WORDS AND DOCUMENT ANALYSIS

a. DESCRIPTORS	b. IDENTIFIERS/OPEN ENDED TERMS	c. COSATI Field/Group
Pollution	Pollution Prevention	13B
Refrigerants	Stationary Sources	13A
Viscosity	Shipboard Chillers	20D
Thermal Conductivity	Hydrofluorocarbons	20M
Halohydrocarbons	Chlorofluorocarbons	07C

18. DISTRIBUTION STATEMENT **Release to Public**	19. SECURITY CLASS *(This Report)* **Unclassified**	21. NO. OF PAGES 199
	20. SECURITY CLASS *(This page)* **Unclassified**	22. PRICE

EPA Form 2220-1 (9-73)